Performance degradation and recovery of YSZ membrane under the sulphuric acid thermal decomposition

Guanghu He (MEng, BEng)

Submitted for the degree of Doctor of Philosophy

Department of Chemical and Biological Engineering

June 2013

Supervisors: Prof RWK Allen, Dr Rachael Elder

ACKNOWLEDGEMENTS

I emphatically express my deep gratitude to my supervisors: Prof. Ray Allen and Dr Rachael Elder for accepting me as a PhD student and for giving me the opportunity to study with them. I would also like to thank them for all the constructive guidance they offered throughout my PhD studies. They always made time to discuss research projects with me. Not only did these discussions make my research more interesting, they also made my PhD study both enjoyable and rewarding. In particular, I would to thank Dr Rachael elder for reading most of my reports and articles, giving valuable comments and improving the language.

I would like to thank Dr Ming Li, who helped me with the preparation of YSZ tubular membrane and laboratory analysis such as SEM-EDS, electrical impedance spectroscopy; Dr Denis Cumming for processed my documents and helped me to set up the *in-situ* impedance measurement; Stuart Richards and Clifton Wray, for help with design and building of my experimental facilities; Adrian Lumby and Keith Penny, who supplied gas cylinders and materials; Mark Mcintosh, who solved all my computer problems; and Oz McFarlane, for help with making the dc voltage pulse generator.

I would like to thank my colleagues in the group of process fluidics group and friends in Sheffield, including Moises Romero, Nicolas Romero-Gonzales, Thomas Butterworth, Najwa Elbakhbakhi, Kayode Omojola, Mohamed Zambri, Chern Yean Sim, Junying Liu, Dr Hanning Li, Dr Yang Liu, Dr Xi Yu and the many others whom I have not mentioned here. Life at Sheffield was much easier with you all.

I'd also like to deeply thank my parents, my sister and my girlfriend for their support during my PhD study. I truly appreciate their love, tolerance and understanding that I could not be with them during my study in the UK.

Finally I would like to thank the Engineering and Physical Sciences Research Council

ABSTRACT

The effect of sulphur dioxide (SO_2) present in the cathode feed stream on the performance of a 8 mole% yttria-stabilized zirconia/platinum (8YSZ/Pt) cell was studied. SO_2 concentration of 30% in oxygen (5ml/min) and helium (30ml/min) was exposed to the cell applying an external dc voltage of 1.5V at 850°C. Experiments showed that the cell performance had a sharp degradation (type I degradation) followed by a gradual degradation (type II degradation) inferred from current and oxygen permeate flux changes. Type II degradation may be related to formation of sulphide on cathode of membrane cell during the SO_2 exposure period. Strong but short dc voltage pulses could reduce significantly membrane performance degradation impacting upon both charge transfer and mass transfer properties. In this work, the optimum voltage pulse for achieving the most stable membrane performance in SO_2 exposure time was 10V, 0.08s length. High pulse frequency was helpful for achieving a high and stable membrane performance SO_2 exposure tests lasting up to 2 hours. An oxygen separation process based on a YSZ tubular membrane was constructed and initial proof of concept experiments performed. Performance degradation by sulphur poisoning and recovery by voltage pulse of YSZ tubular membrane were also observed with this system. However, the oxygen permeation flux of the YSZ tubular membrane was lower than that of YSZ planar membrane, which may be related to YSZ thickness and the gas flow pattern. Initial experiments to integrate the membrane system into the thermal decomposition of H_2SO_4 to produce SO_2 and O_2 were carried out in a quartz tube reactor filled with an alumina supported Pt catalyst. A promising and feasible method of monitoring oxygen in-situ to determine acid conversion was proposed. Future work should concentrate on improvement of YSZ tubular membrane configuration and deeper integration of membrane operation and acid decomposition.

Contents

List of Figures

List of Tables

Chapter 1

1 Introduction

1.1 Hydrogen energy systems

The need for clean and sustainable energy sources is quite evident, because fossil fuels have a number of drawbacks: 1) fossil fuels are a non-renewable resource. The production of fluid fossil fuels will reach peak point in about 15 years and begin to decrease (Veziroglu and Sahin 2008). They cannot meet the global energy demand with the development of the world economy and the growth of the world population. 2) the production and utilization of fossil fuels lead to an unpredictable climate including acid rain and greenhouse effects. 3) fossil fuels are dependent on a few oil-exporting regions in the world. Therefore, searching the alternative energy sources of fossil fuel for Sustainable Development (Von Wolfersdorff et al.) is becoming more and more important and urgent as time goes on.

A suitable candidate fuel should satisfy the following necessary conditions (Veziroglu and Sahin 2008):

- It must be a convenient fuel for transportation.
- It must be versatile or convert with ease to other energy forms at the user end.
- It must have high utilization efficiency.
- It must be safe to use.
- It must be environmental friendly.
- It must be economical.

Hydrogen stands out as the best fuel alternative after comparing hydrogen with other conventional and unconventional fuels (Veziroglu and Barbir 1992). It has been

viewed as the energy source for the 21st century (Dunn 2002)   (Edwards et al. 2008) (Veziroglu and Sahin 2008) (Jain 2009) (Zuttel et al. 2010). Johnston et al. predicted that we could be well into the migration to a hydrogen environment within 10 years if government and industry were really motivated to make it happen (Johnston et al. 2005).

Today, research and development into hydrogen as an energy carrier is moving forward in every way including production, storage, transportation, distribution and utilization of hydrogen energy. In the world, there are many scholars (Bockris, Veziroglu, et. al), nations and regions (USA, European, Brazil, Iceland, Japan, China, Indian, Hawaii, et. al), periodicals on hydrogen (*Int. J. Hydrogen Energy, The Hydrogen & Fuel Cell Letter, Fuel cells Bulletin, Hydrogen Today, et. al*), famous books and TV programs, international conferences and associations (CEA, Westinghouse, General Atomics, Sandia National Laboratory, Idaho National Laboratory, University of Sheffield, et. al) making contributions to the transition from fossil fuel to hydrogen energy system.

1.2   Sulphur-iodine thermal cycle (S-I cycle)

Hydrogen production is the first stage for any hydrogen energy system. The mature processes for hydrogen production are water electrolysis, steam reforming of natural gas, catalytic decomposition of natural gas, partial oxidation of heavy oil and coal gasification (Momirlan and Veziroglu 2002). However, they are not ideal technologies for hydrogen production due to being low efficiency, not environmental-friendly or difficult to industrialize. A significant potential technology to obtain hydrogen at high efficiency without greenhouse gas emission is thermochemical process. A thermochemical hydrogen production process is one which requires only water as a material input and mainly thermal energy, or heat, as an energy input. The output of the process is hydrogen and oxygen. There are hundreds of thermochemical cycles. After many years of research and comparison, the sulphur-iodine thermochemical cycle has been emerged as one of the most promising solutions and has been researched the most at present (Brown et al. 2003).

The S-I cycle can be simplified into three common sections: Bunsen reaction (Eq.(1.1)) where two acids are formed, hydrogen iodine (HI) decomposition reaction (Eq.(1.2)) where hydrogen is produced, and sulphuric acid (H_2SO_4) decomposition reaction (Eq.(1.3)) where sulphur dioxide is recycled to Bunsen reaction [Figure 1.1].

$$SO_2 + I_2 + 2H_2O \rightarrow 2HI + H_2SO_4 \tag{1.1}$$

$$2HI \rightarrow H_2 + I_2 \tag{1.2}$$

$$H_2SO_4 \rightarrow H_2O + SO_2 + 0.5O_2 \tag{1.3}$$
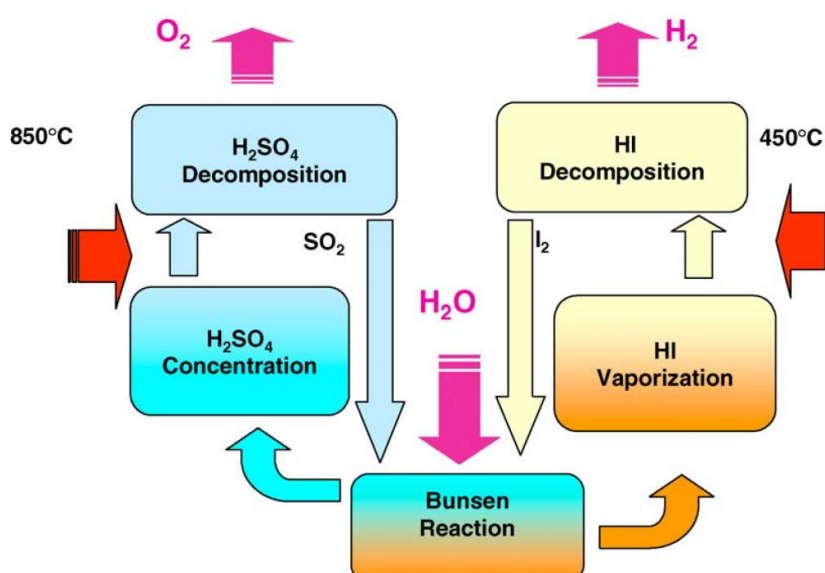
Figure 1.1: *Schematic representation of the S–I cycle (Vitart et al. 2006)*

In the S-I thermal cycle, water is the only raw material and is decomposed into hydrogen and oxygen. The sulphur and iodine compounds are recovered and reused. The energy used in this process is only heat (e.g. nuclear or solar) which doesn't have to be converted to electricity as in other hydrogen production technologies. Accordingly, it should have a higher efficiency than water electrolysis and achieve the commercial production of hydrogen without byproducts or effluents. It is well suited for continuous operation because of all fluid process in this cycle, and suitable for application with solar, nuclear, and hybrid sources of heat. After the recent closed-loop demonstration achieved in Japan (Kubo et al. 2004), research on the S-I

cycle is now mainly focused on engineering issues regarding the coupling with the heat source, the equipment design and the efficiency improvements.

1.3 Sulphuric acid thermal decomposition

H_2SO_4 thermal decomposition needs two stages: sulphuric acid dissociation and sulphur trioxide decomposition.

$$H_2SO_4 \rightarrow SO_3 + H_2O \tag{1.4}$$

$$SO_3 \rightarrow SO_2 + 0.5O_2 \tag{1.5}$$
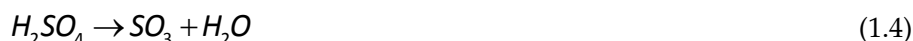
As shown in Figure 1.1, the high temperature required in the S-I cycle is for the sulphuric acid thermal decomposition reaction. Lowering this temperature is a critical step in terms of process management, kinetics, energy losses, corrosion, cost and efficiency of S-I cycle. With the goal of lowering the operating temperature, it has been proposed in our research group that an oxygen ion conducting electrolysis cell could be used to separate O_2 from SO_2 in sulphuric acid decomposition.

Due to thermodynamic limitations, the SO_3 to SO_2 conversion reaction reaches an equilibrium point that inhibits the conversion of 100% of the SO_3 to SO_2. The equilibrium can be altered by removing oxygen from the system. Once oxygen is removed, the temperature at which complete conversion can be achieved is lowered. The effect of the oxygen removal on the SO_3/SO_2 equilibrium is shown in Figure 1.2, calculated by HSC Chemistry for the reaction Eq.(1.5).
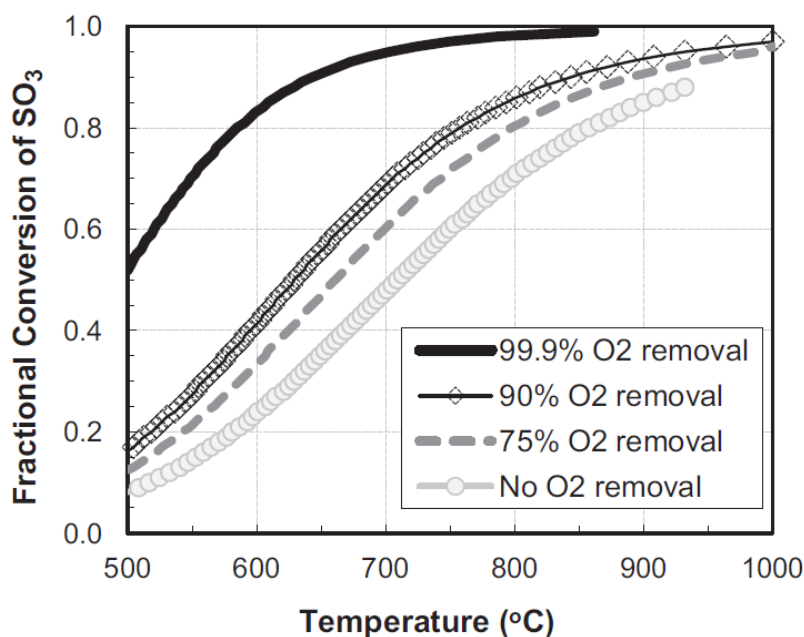
Figure 1.2: *Effect of O$_2$ removal on the fractional conversion of SO$_3$ to SO$_2$ as a function of temperature (Mawdsley et al. 2012)*

When no oxygen is removed from the system, an 80% conversion of SO$_3$ to SO$_2$ is obtained at 850°C theoretically. However, if 90% of the oxygen is removed, the temperature of 80% conversion reduces to about 750°C. This same 80% conversion can be achieved at around 590°C if 99.9% of the oxygen is removed. 99.9% removal of oxygen is possible in principle if an oxygen membrane is used. An oxygen ceramic membrane for removing oxygen will overcome the thermodynamic limitation of sulphur trioxide decomposition and reduce the operating temperature for a given SO$_2$ yield. It is also capable of being integrated into the S-I process.

In the case of removing oxygen from the products of H$_2$SO$_4$ decomposition at high temperature, it is natural to consider well known types of fuel cells as a starting point for oxygen membranes.

1.4 Yttria-stabilized zirconia (YSZ) membrane

Yttria-stabilized zirconia (YSZ) as a kind of electrolyte is well known for high oxygen ion conductivity and good mechanical strength at a wide temperature range, and is used widely in many technologically important devices such as solid oxide fuel cells (SOFCs), solid oxide electrolyzer cells (SOECs), oxygen sensors and so on. In previous work, YSZ was selected as the electrolyte of a membrane in combination with platinum as the electrode material. Oxygen permeation processes using Pt/YSZ pellets were demonstrated at the temperature range of 700 - 900°C, with the gas components of He-O_2-SO_2 in the cathode side and He in the anode side. Sulphur poisoning behaviour was demonstrated similar in nature to that previously observed in SOFCs. The performance of the Pt/YSZ membrane showed severe degradation during O_2-SO_2 exposure period which was not reversible after SO_2 was removed from the feed. This sulphur poisoning effect has been a big problem for YSZ membranes at high performance levels for a long time (Jing et al. 2007) (Fu et al. 2009) (Zhai et al. 2010) (Matsuzaki and Yasuda 2000) (Nagahara et al. 2008). So far, the mechanism of membrane degradation because of the sulphur-containing gas poisoning effect has not been known clearly, even though some work has been undertaken by (Lussier et al. 2008) (Li et al. 2010). There is a significant challenge of understanding the degradation mechanism at severe operating conditions including high temperature and a corrosive environment with a limited range of analysis techniques for electrochemical and surface research. One of objectives in this research is to understand the mechanism of membrane performance degradation because of sulphur poisoning at high temperatures. There have been many efforts to reduce such membrane performance degradation. One possible solution is applying to the membrane cell a high current density or high voltage pulse (Li et al. 2010) (Fu et al. 2009) (Nagahara et al. 2008) (Baumann et al. 2005). This was confirmed experimentally in our research group who found a partial performance recovery of Pt/8YSZ/Pt after a 2-minute 3V pulse treatment, exposed to 15ml/min of SO_2 in 5ml/min O_2 and 30ml/min helium in feed (Atkin 2009). In other words, an external high voltage pulse across membrane cell may be helpful to keep the membrane at a relatively high performance level for a long

SO$_2$ exposure time by partial recovery cycles. If this can be shown to be effective, this could be an energy efficient method of performing gas separation using a YSZ electrolyte. For the first time, the effect of high dc voltage pulse on membrane performance recovery in SO$_2$ poisoning period has been studied to reduce membrane performance degradation and extend the life-span of membrane.

1.5 Objectives of this thesis

By removing oxygen from sulphuric acid thermal decomposition using membrane processes, the operating temperature of acid decomposition could, in principle, be lower for a given acid conversion. If so, it would permit the use of lower temperature heat sources with the sulphur family thermochemical cycles. Alternatively, it would allow decomposer throughput to be increased for a given heating duty.

Like SOFCs and SOECs, however, an importance challenge to achieve a wide application of membrane processes in sulphur-iodine and hybrid sulphur cycles is sulphur poisoning effects which can cause severe membrane performance degradation. The mechanism of sulphur poisoning effect is still unclear at present, and approaches to reduce this membrane performance degradation have yet to be developed.

The objectives of this research were to:

- Study the Pt/8YSZ/Pt pellet performance degradation during SO$_2$ exposure by analysis techniques such as x-ray diffraction (XRD), SEM (scan electron microscope), EDS (energy-dispersive x-ray spectroscopy), Raman Spectroscopy and impedance spectroscopy (IS);
- Investigate the effect of strong but short dc voltage pules on membrane performance recovery, and optimise voltage pulse to achieve a significant rate of performance recovery whilst maintaining membrane performance for a long SO$_2$ exposure period;

- Examine the oxygen permeation performance of a YSZ tubular membrane instead of the more common YSZ planar membrane;

- Carry out sulphur acid thermal decomposition in the presence of Pt/Al_2O_3 catalyst at a scale which would allow it to be integrated with membrane separation process.

1.6   Thesis structure and presentation

This thesis consists of seven individual chapters. Following a literature review, Chapters three and four study membrane performance degradation after SO_2 injection into the feed stream and its recovery after high voltage pulse treatment. Chapter five investigates the oxygen permeate flux of a YSZ tube operating under the same conditions as a YSZ planar membrane system, whilst Chapter six develops a small scale approach to the decomposition of sulphuric acid in laboratory for the integration with the membrane separation processes. The final chapter is the overall conclusions and future work. Each chapter has an introduction describing the more detailed background to the investigation in order to present a logical progression of the thesis as a whole together with a final conclusion to capture the essential findings. Figure 1.3 shows the overall structure of the thesis.
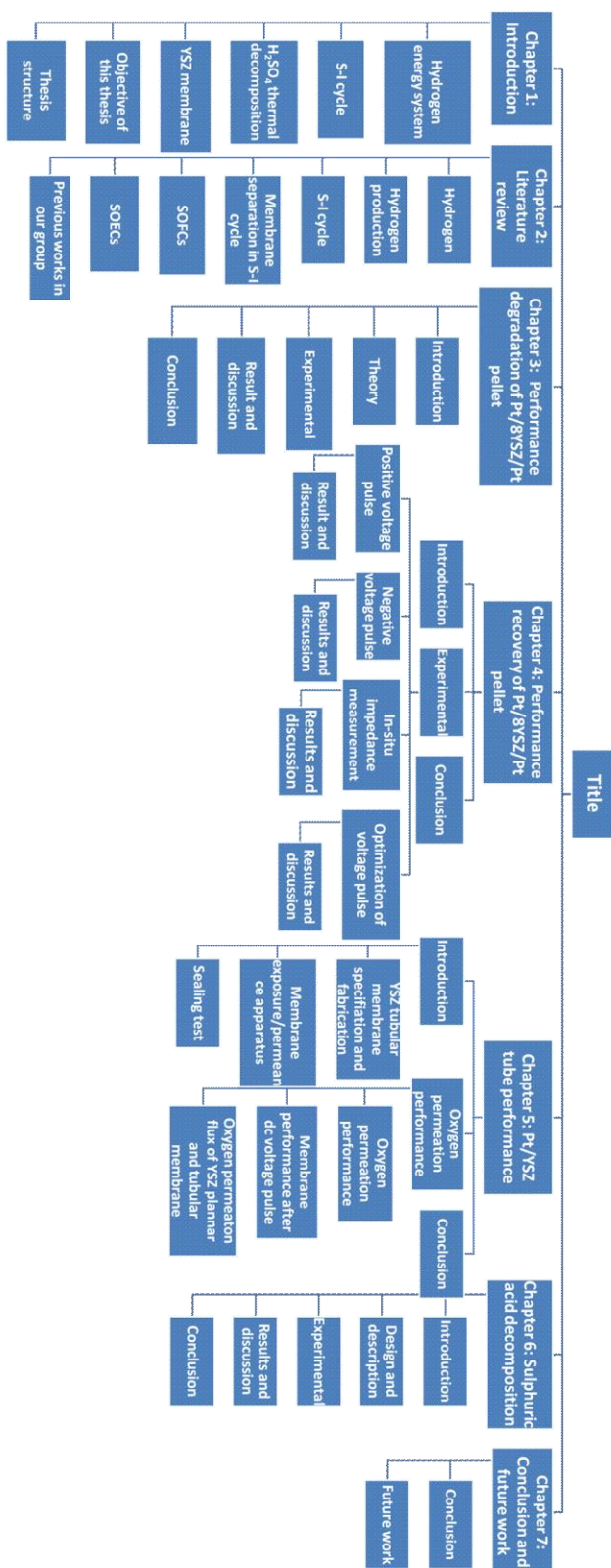
Figure 1.3: *The overall structure of the thesis*

Chapter 2

2 Literature review

In this chapter, the significance and urgency of research and development of hydrogen as an energy carrier is outlined by considering the environment problems and the deterioration of humans' life quality resulting from the utilization of fossil fuel and the energy crisis. A series of hydrogen production routes, especially the Sulphur-Iodine thermochemical cycle (S-I cycle), are presented. The research and development of sulphuric acid (H_2SO_4) thermal decomposition in S-I cycle are reviewed. Application of membrane separation processes in S-I cycle is also reported. As an important reference to my research, solid oxide fuel cells (SOFCs) and solid oxide electrolyser cells (SOECs) are reviewed. Finally, previous work in our research group on membrane separation processes applying to H_2SO_4 thermal decomposition is summarized in brief.

2.1 Hydrogen

2.1.1 Energy crisis

Up to now, human society has derived great benefits from fossil fuels in form of petroleum, natural gas and coal. Humans' and beasts' toil were replaced by machines driven by nature's energy sources. Production efficiency was improved greatly, which also resulted in mass production of goods, with corresponding reduction of commodity prices and rising living standards. As a result, people's demands became greater and increasingly diversified. This led to the emergence of factories, railroads, highways, airports and seaports; it meant more jobs, more income, more goods and more services. According to this mode, society, economy

and human living standards improved continuously. Therefore, the prosperous scene at present is in large part because of fossil fuels.

The supply of primary energy all over the world from 1971 to 2008 is presented in Figure 2.1. Fossil fuels (coal, oil and natural gas) always make up most of the energy supply in these decades. Without fossil fuels, advanced economies may not sustain the level and speed of economic development. Without fossil fuels, developing and emerging economies may never attain the growth and quality of life to which they aspire. Therefore, fossil fuels make the greatest contribution to human energy demand in the world so far. Currently, fossil fuels provide almost 80% of world energy supply (Sims and Schock 2007). However, fossil fuels are not an ideal energy source. They are non-renewable resources because they take millions of years to form, and reserves are being depleted much faster than new ones are being made.
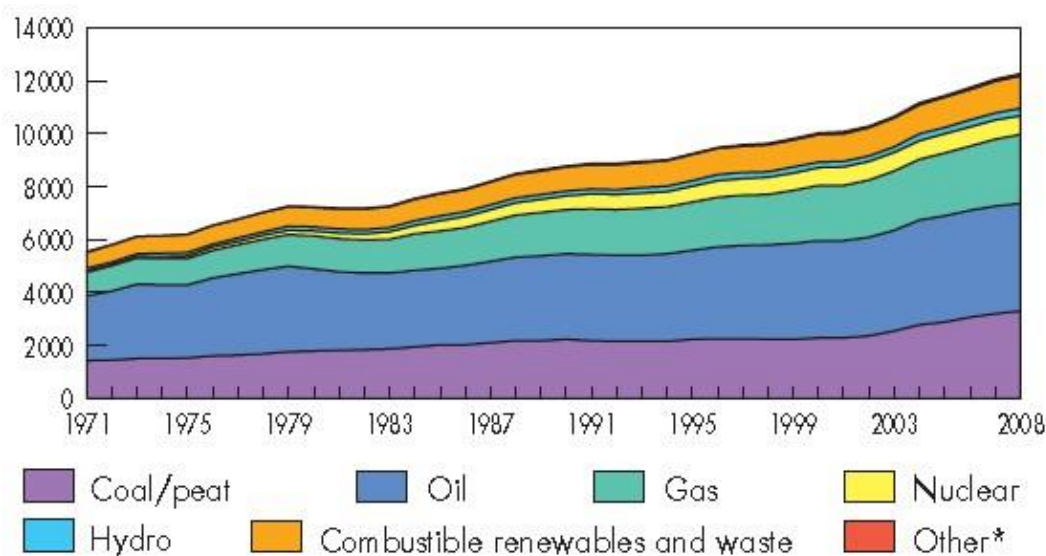
Figure 2.1: *Evolution from 1971 to 2008 of world total primary energy supply by fuel (Mtoe)*
*Other includes geothermal, solar, wind, heat, etc.
Data source: International Energy Agency (IEA) - Key World Energy Statistics 2010

Worse, the continuing exponential increase in world population and growing demand by the developing countries for improving their living standards leads to rapid rises in energy demand for fossil fuels. Accordingly, they accelerate fossil fuels depletion. World population estimates, based on UN 2010 projections and US Census Bureau historical figures, may rise up to a maximum of 16 billion by 2100

(Cohen 2002). The annual production of fluid fossil fuels will soon peak, and thereafter begin to decrease. For example, the coal production decreases faster and will be run out around 2030 by projection [Figure 2.2](Veziroglu and Sahin 2008).

Even worse, with the increasing development of the economy and the increasing consumption of fossil fuels, a lot of problems appear and are becoming more and more serious. Firstly, the uneven geographical distribution of fossil fuel in the world is more and more obvious with the decrease of energy reserves and the increase of transportation cost. The supply of energy will become more and more unstable. Secondly, the environmental damage is caused by fossil fuels and by their combustion products. Technologies for fossil fuel extraction, transportation, processing and particularly their end use, have harmful impacts on the
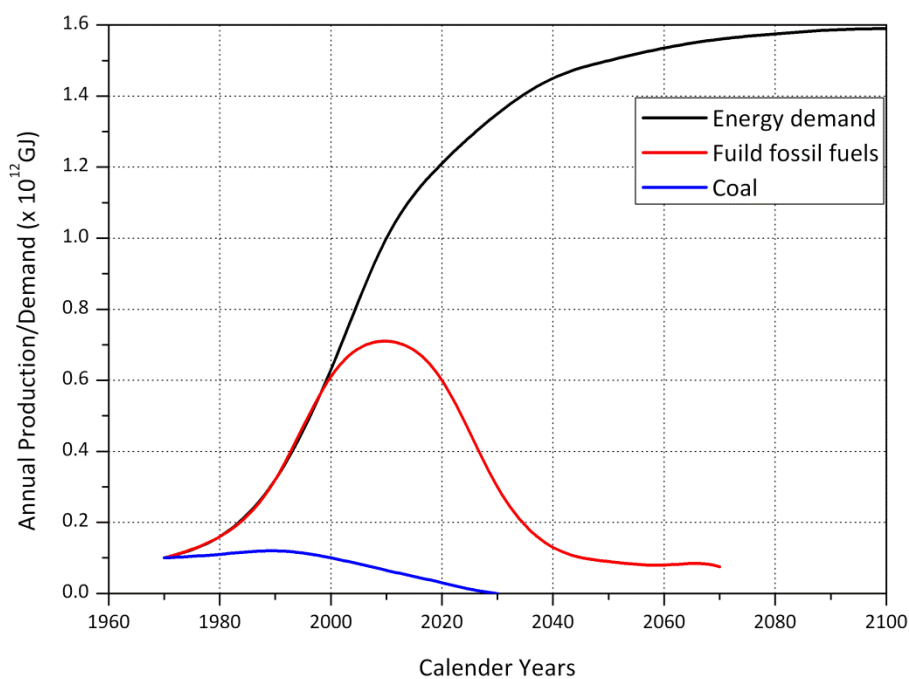
Figure 2.2: *Estimates of world fossil fuel production*

environment, which cause direct and indirect negative effects on the economy. For example, burning of fossil fuels (oil, gas, petrol, etc.) emits a lot of carbon dioxide into the environment and leads to global warming. There are two major effects of global warming: increase of temperatures on the earth by about 0.4 to 0.8 degrees C since the late 1800's (World book at NASA) and rise of sea levels by 18 to 59 cm during 21st century projected by the Intergovernmental Panel on Climate Change

(IPCC) in 2007. These make the climate become unpredictable (e.g. floods, droughts, heat waves, and tornadoes). Other effects of global warming include higher or lower agricultural yields and species extinctions. Figure 2.3 illustrates the relationships between fossil fuels and society, environmental, ecology problems.

Because of the foregoing, people have to find an alternative energy source to replace fossil fuels. Basically, there are quite a number of primary energy sources available such as solar, water, wind, geothermal, biomass, tides and waves and so on.
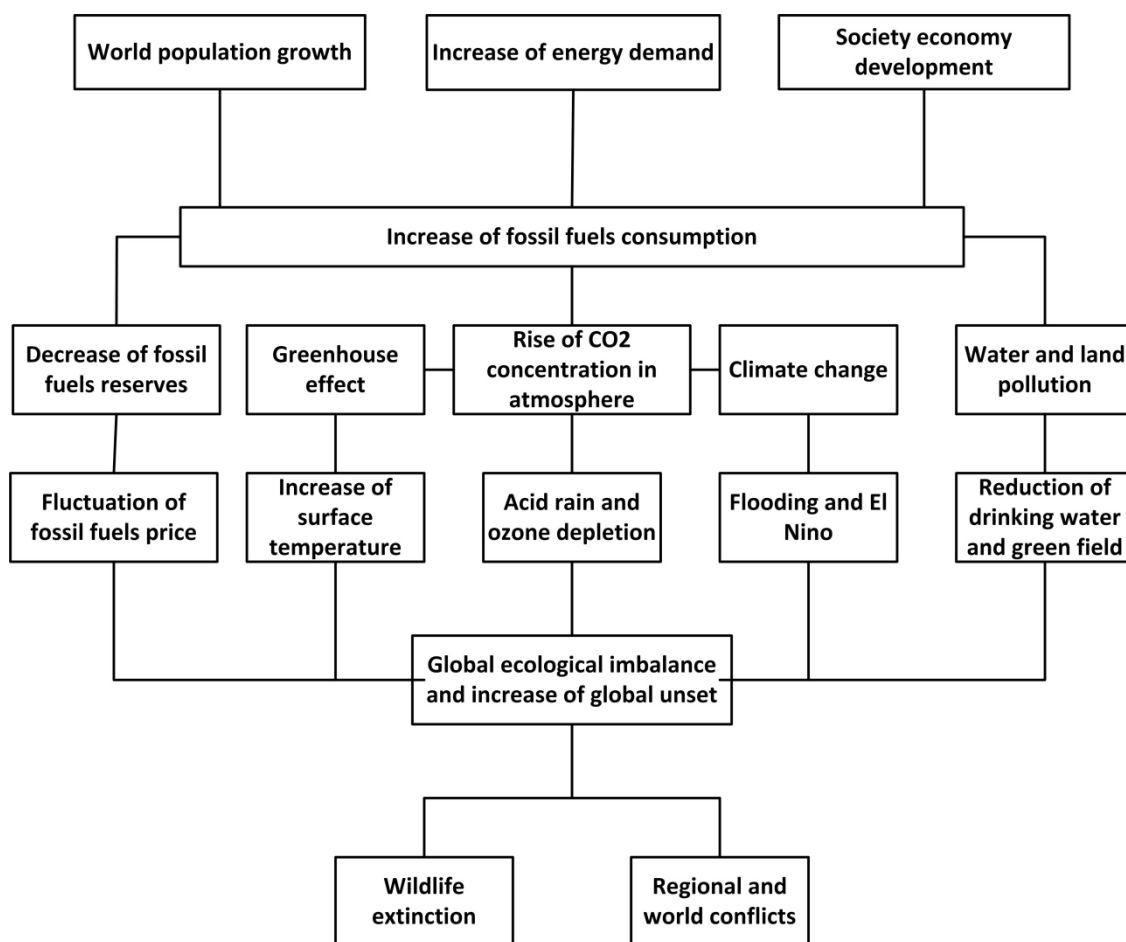
Figure 2.3: *Illustration of possible global problems from increasing use of fossil fuels*

2.1.2   Hydrogen

For end users of primary energy, as the prime requirements are either a fuels or electricity. Therefore, the primary energy sources mentioned above must be firstly converted to these two energy carriers for the consumer. There are many candidates

for such alternative energy carriers, including synthetic gasoline, synthetic natural gas, methanol, ethanol and hydrogen.   Like fossil fuels, these can be used directly or allow easy storage. (Veziroglu and Sahin 2008). A suitable candidate should satisfy the following necessary requirements (Veziroglu and Barbir 1992).

- It must be convenient fuel for transportation.
- It must be versatile or convert with ease to other energy forms at the user end.
- It must have high utilization efficiency.
- It must be safe to use.
- It must be environmental friendly.

Hydrogen as an energy carrier is given the highest marks and viewed as the ideal alternative of fossil fuels. The reasons include (Jain 2009):

- Clean Energy
- Most abundant element in the universe
- Lightest fuel
- Richest in energy per unit mass [Table 2.1]
- Can be stored easily
- Can be produced by water
- Direct conversion into thermal, mechanical and electrical energy

Fuel	Energy (Kcal/g)
Hydrogen	34.0
Petroleum	10.3 – 8.4
Paraffin	10.3 – 9.8
Graphite (Coal)	7.8
Castor oil	9.4
Wood	4.2

Table 2.1: *Heat of combustion of various fuels (Jain 2009)*

2.1.3   Hydrogen safety

So far, the security of hydrogen is viewed as the biggest obstacle, to the adoption of hydrogen, in public perception, The Hindenburg disaster in 1937 (Johnston et al. 2005) made a very strong impression on the public. People always think that this disaster resulted from the ignition of the hydrogen gas which is flammable over a

wide range of concentrations. However, the results of Johnston's study indicated that the explosion was due to the ignition of iron oxides and aluminium rather than hydrogen (http://www.cleancaroptions.com/html/hydrogen_safety.html). Experience of industrial hydrogen use has shown that its safety record is good and hydrogen is no more or less dangerous than other flammable fuels, including gasoline and natural gas. In fact, some of hydrogen's differences actually provide safety benefits compared to gasoline or other fuels (http://www.fchea.org/index.php?id=50).

- Hydrogen is lighter than air and diffuses rapidly. Hydrogen has a rapid diffusivity, some 3.8 times faster than natural gas. Hydrogen rises 2 times faster than helium and 6 times faster than natural gas at a speed of around 45 mph (20m/s). Therefore, the laws of physics prevent hydrogen from building up in a room unless a roof, or some other poorly ventilated structure contains the rising gas.

- Hydrogen is odourless, colourless and tasteless. Industry often uses hydrogen sensors to help detect hydrogen leaks and has maintained a high safety record using them for decades. By comparison, natural gas is also odourless, colourless and tasteless, but industry adds a sulphur-containing odorant, called mercaptan, to make it detectable by people.

- Hydrogen flames have low radiant heat. The flame emit low levels of heat near the flame, the risk of secondary fires is lower. This fact has a significant impact for public and rescue workers.

- Hydrogen's buoyancy, diffusivity and small molecular size make it difficult to contain and create a combustible situation.

- Hydrogen can be explosive at concentrations of 18.3-59% with an oxidizer such as oxygen. Although the range is wide, it is important to remember that gasoline presents a more dangerous potential than hydrogen since the potential for explosion occurs with gasoline at much lower concentration, 1.1-3.3%.

Overall, hydrogen safety problems can be viewed the best by comparison with fossil fuels. Like gasoline and natural gas, hydrogen is flammable and can behave dangerously under specific conditions. Hydrogen can be handled safely when following simple guidelines based on an understanding of the behaviour of hydrogen.

2.1.4   Hydrogen research and development

Today, research and development on hydrogen as an energy carrier is moving forward in every way including production, storage, transportation, distribution, utilization of hydrogen energy. In the world, there are many scholars (Bockris, Veziroglu, et al), nations and regions (USA, European, Brazil, Iceland, Japan, China, Indian, Hawaii, et. al), periodicals on hydrogen (Int. J. Hydrogen Energy, The Hydrogen & Fuel Cell Letter, Fuel cells Bulletin, Hydrogen Today, et. al), famous books and TV programs, international conferences and associations making contributions to the transition from fossil fuels to hydrogen energy systems.

With the continuing efforts of researchers and engineers all over the world as well as strong support from governments and regions, a new era based on hydrogen energy system will come one day [Figure 2.4]. In this system, hydrogen is produced in large industrial plants where the primary energy source (solar, nuclear, and even fossil) and water (H_2O), the raw material, are available. Hydrogen is then transported by means of pipelines or super tankers to energy consumption sectors. Subsequently, it is used in electricity, transportation, industrial, residential and commercial sectors as a fuel and/or an energy carrier. The by-product is water or water vapour which are recycled back through rain, rivers, lakes and oceans to make up for the water used in the first place to manufacture hydrogen (Veziroglu and Sahin 2008).
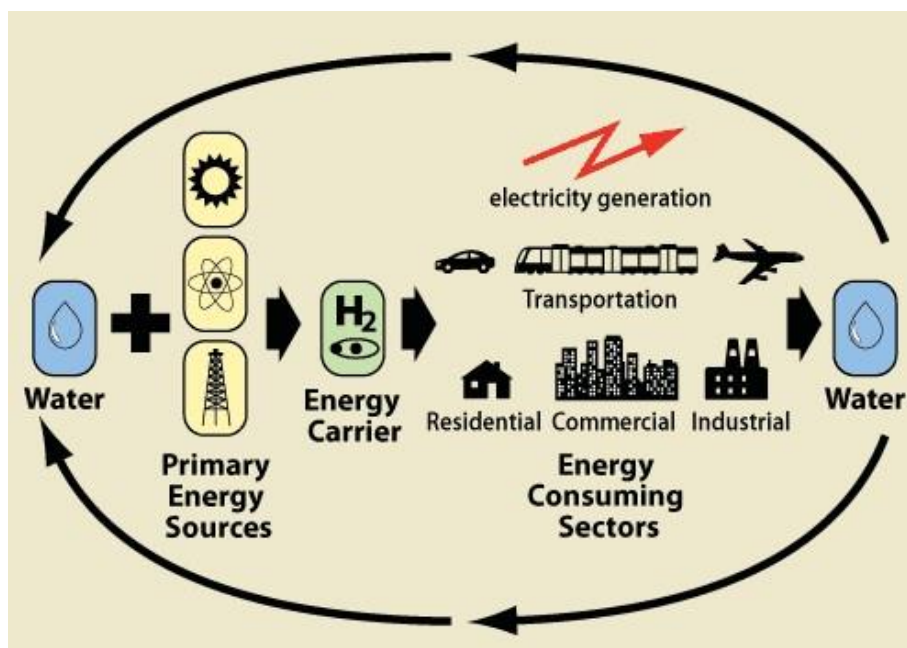
Figure 2.4: *Hydrogen energy system*

Source: United Nations Industrial Development Organization

2.2 Methods of hydrogen production

Hydrogen production is the first stage in this hydrogen energy system. In general, hydrogen can be generated in a number of ways such as electrochemical processes, thermochemical processes, photochemical processes, photocatalytical processes, photoelectrochemical processes and photobiological processes. Some of these technologies are mature and commercially available, while others are still under research in the laboratory or under development from laboratory to industry

2.2.1 Electrochemical processes

An electrochemical process is a chemical reaction that either causes or is caused by the movement of electrical current. These processes are a type of oxidation-reduction reaction in which one atom or molecule loses an electron to another atom or molecule.

Hydrogen production by an electrochemical process, is well known as water electrolysis in which water decomposes into oxygen and hydrogen due to an electric current being passed through the water [Figure 2.5].
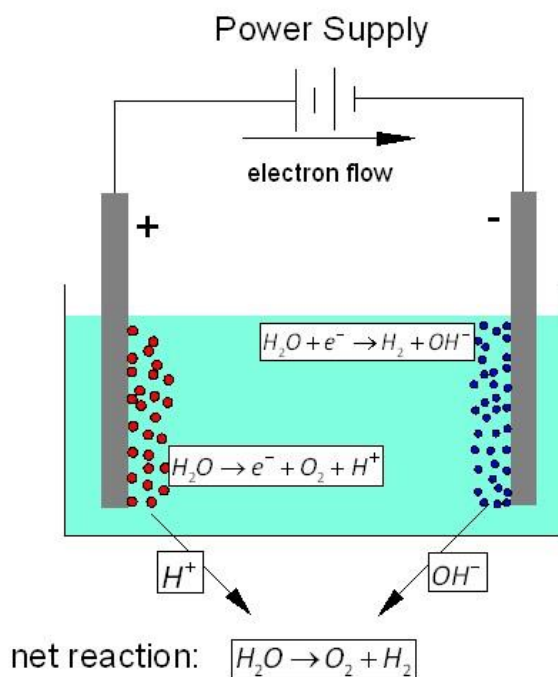
Figure 2.5: *Schematic of water electrolysis process*

Actually, water electrolysis for hydrogen production has been well known for more than 200 years (Stojic et al. 2003) and is a mature technology today. It is even used widely for some special situations such as rocket fuel. It is a promising method of deriving hydrogen in a long-term; cost-effective in small amounts; but, it is the most expensive process at larger scales today, about three to five times as much as a fossil fuel feedstock (Dunn 2001). As a result, water electrolysis only accounts for around 4% of world hydrogen production (De Souza et al. 2007). Cost declines are expected with improvements in research and technology. Some promising research has been applied into water electrolysis to reduce the cost of hydrogen production at a large scale. For example, solar and wind-power-based electrolysis systems have been demonstrated in Finland, Germany, Italy, Saudi Arabia, Spain, Switzerland, and the United States, and Geothermal power electrolysis in Iceland, Vanuatu, and Hawaii. Also, a lot of research on improving the efficiency of electrolysis facilities has been undertaken (Dunn 2002) (Stojic et al. 2003) (Utgikar and Thiesen 2006). Some new technologies based on water electrolysis like solid oxide electrolyte cells (SOECs) which are attracting much interest recently as a highly efficient electrolyser for

production of hydrogen at high temperature. SOECs are introduced in detail in section 2.6.

2.2.2   Thermochemical Processes

Thermochemical processes for hydrogen production involve thermally assisted chemical reactions which release hydrogen. Basically, they are usually conducted at high temperature with a heat source such as nuclear energy, solar and geothermal. Up to now, there are more than 200 thermochemical processes reported, most of which are at experimental or bench-scale stage because of the technical problems such as separation of products, the facilities development for industrialization as well as possible pollution problem (Momirlan and Veziroglu 2002). Thermochemical processes can be classified by their feedstocks such as hydrocarbon, biomass and water.

2.2.2.1   Hydrocarbon

Steam Methane Reforming (SMR)

At present, SMR is the most popular method of hydrogen production at an industrial scale. It accounts for 95% and 48% of all hydrogen production in the U.S. and in the world, respectively (Park et al. 2008). SMR consists of two reactions: 1) stream-reforming reaction, a process which high temperature steam is used to produce hydrogen from the methane source, such as natural gas. Specifically, methane reacts with water at high temperature in the presence of a catalyst to produce hydrogen, carbon monoxide and a small amount of carbon dioxide. This reaction is endothermic, which means that a heat source is required to make the reaction proceed. 2) water-shift reaction, the carbon monoxide coming from the reforming reaction and steam produce catalytically carbon dioxide and more hydrogen. Subsequently, carbon dioxide and other impurities are removed from steam to form pure hydrogen.

Stream-Reforming reaction:

$$CH_4 + H_2O \xleftarrow{\quad heat \quad} CO + 3H_2$$

(2.1)

Water- Shift reaction:

$$CO + H_2O \leftrightarrow CO_2 + H_2 \qquad (2.2)$$

Since a process for the conversion of hydrocarbon into hydrogen in the presence of steam was first described by Tessies du Motay and Marechal in 1868 (Adris et al. 1996), the SMR process to produce hydrogen has been developed and used for many decades. SMR of natural gas is a mature technology. It can be operated at or near the theoretical energy efficiency limits of the process (Barelli et al. 2008). Natural gas is a convenient, easy to handle, methane feedstock with a high hydrogen-to-carbon ratio. The cost of hydrogen produced by SMR is dependant mainly on natural gas prices and is currently the least expensive compared with other approaches of hydrogen production(Padro and Putsche 1999). A well-developed infrastructure system for natural gas already exists all over the world, which is another attractive advantage to achieve hydrogen economy by SMR technology.

However, the drawbacks and challenges of SMR are also very important. Firstly, its feedstock, mainly natural gas, is a non-renewable energy source like oil and coal. It cannot solve the energy crisis fundamentally because natural gas will be depleted one day. Secondly, SMR has a large carbon footprint in the form of carbon dioxide and carbon monoxide which account for around 78% of global greenhouse gas contribution (Dunn 2002). Thirdly, to avoid the emission of carbon dioxide into the atmosphere, CO_2 needs to be concentrated, captured or sequestered. But the technologies of the concentration, capture and sequestration of CO_2 are not developed yet at present for industrial application.

Coal Gasification

The same as SMR, coal gasification is also a commercial process for hydrogen production. It is very complex and involves many chemical reactions. The feedstock firstly takes physical and chemical changes at high temperature, yields tars, oils, phenols, and hydrocarbon gas. These products react further to form majority of CO_2, H_2, CO and minority of CH_4, HCl, HCN, H_2S and others components (Stiegel and Ramezan 2006). Afterwards, the synthesis gas (Lin et al. 2002) must be separated and

cleaned. Then, CO is converted to CO_2 and H_2 in water-gas shift reactor. In a simple form, coal gasification can be shown

$$C_nH_m(coal) + 2nH_2O \rightarrow nCO_2 + (2n + m/2)H_2 \tag{2.3}$$

Nearly 20% of hydrogen produced worldwide is derived from coal gasification (Stiegel and Ramezan 2006). Gasification-based systems are the most efficient and environmentally friendly technologies for the production of low-cost electricity and other products (Ratafia-Brown et al. 2002). However, of all fossil fuels coal has the lowest hydrogen to carbon ratio, so more CO_2 is produced per mole of H_2. Thus coal is viewed as a dirty fuel due to its high greenhouse emissions when combusted. The requirement for pure oxygen feeding in coal gasification is another main disadvantage (Lin et al. 2002). At present, some technologies associated with coal gasification are developing. 1) The gasifier, it plays the most important role on the process of coal gasification; 2) Synthesis gas cleaning technologies; 3) Gas separation technologies. If these technologies can achieve their goals, the cost of hydrogen production by this approach will be reduced by 25-50% from current values (Stiegel and Ramezan 2006).

Partial Oxidation (POX)

Partial oxidation of hydrocarbon is a type of chemical reaction with fuel and oxygen, producing a hydrogen-rich syngas which can be put to further use, for example in a fuel cell. Partial oxidation is a technically mature process in which a heavy hydrocarbon is mixed in an exothermic process with oxygen. The general PO_X reaction is

$$C_nH_m + \frac{n}{2}O_2 \xrightarrow{\text{Catalyst}} nCO + \frac{m}{2}H_2 \tag{2.4}$$

$$C_nH_m + \frac{2n+m}{4}O_2 \xrightarrow{\text{Without catalyst}} nCO + \frac{m}{2}H_2O \tag{2.5}$$
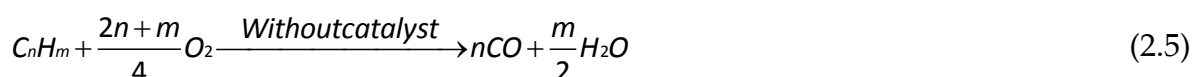
The feedstock (C_nH_m) is often fossil fuel such as methane (natural gas), heating oil, methanol, ethanol and their derivatives. A distinction is made between thermal partial oxidation and catalytic partial oxidation. The thermal partial oxidation in the

presence of oxygen is often conducted at high temperature in order to ensure high conversation and to reduce the carbon that may be produced. Once a catalyst is employed, POX may be conducted at relative low temperatures, but actually it is hard to control the temperature because partial oxidation is exothermic(Holladay et al. 2009).

For partial oxidation of methane, the catalysts are typically based on Ni or noble metals. Noble metals seem to be more active for POM and ATR reactions, as proposed by (Ashcroft et al. 1990) and (Vernon et al. 1990), but they are a hundred times more expensive. Among the different noble metals, Rh has been widely investigated (Grunwaldt et al. 2001) (Freni et al. 2000). On the whole, the high operating temperatures and safety concerns may make their use for practical, compact, portable devices difficult (Holladay et al. 2009).

2.2.2.2   Biomass

Biomass, mainly in the form of wood, is the oldest form of energy used by humans. The most important biomass energy sources are wood and wood wastes, agricultural crops and their waste by-products, municipal solid waste, animal wastes, waste from food processing, and aquatic plants and algae. Currently, much research has been focused on sustainable and environmental friendly energy from biomass to replace conventional fossil fuels (Balat and Kirtay 2010). Biomass as a major feedstock for hydrogen production has received considerable attention in recent years. Hydrogen from biomass has many advantages: 1) independence from oil imports, 2) net product remains within the country, 3) stable pricing level, 4) peace keeping, 5) the CO_2 balance can be improved by around 30% (Demirbas 2008). On the contrary, the seasonality and type of the feedstock and the transportation in distance are the three restriction factors for biomass process of hydrogen production (Dincer 2002).

Usually, to obtain hydrogen from biomass, gasification or pyrolysis is needed. Biomass gasification is a thermochemical process operated at high temperature and low pressure. Through gasification, biomass is converted into a gaseous mixture of hydrogen, carbon monoxide, carbon dioxide, methane, and other compounds such

as ethane (Ji et al. 2009). Gasification of biomass is generally observed to follow the reaction:

$$Biomass + O_2\,(or\;H_2O) \rightarrow CO, CO_2, H_2O, H_2, CH_4 + other\;CHs + tar + char + ash \qquad (2.6)$$
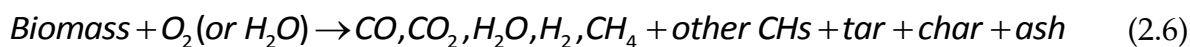
Pyrolysis of biomass involves the thermal decomposition of biomass in the absence of air or oxygen. This is a slow heating process, with temperatures ranging from 300 to 900°C, which results mostly in charcoal formation. Therefore, this process is not attractive for producing hydrogen (Tanksale et al. 2010).

2.2.2.3   Water

Decomposition of pure water into hydrogen and oxygen at standard temperature and pressure is not favourable in thermodynamic terms. Increasing the reaction temperature or pressure will make the reaction occur. Water can decompose to oxygen and hydrogen at around 2500°C, this heat could be provided by nuclear energy or a solar energy or concentrating device. The problem is that the material which can withstand the high temperature is not available today. Therefore chemical reagent is introduced into the water splitting process to lower the decomposition temperature.

There are more than 300 water splitting processes referenced in literature. In choosing the thermochemical water splitting process there are five criteria: 1) In the temperature considered, the Gibbs free energy (ΔG) of each reactions should approach zero. This is the most important criterion. 2) The number of the steps in the cycle should be minimal. 3) Each reaction must have fast reaction rate and this rate is also similar to the rates of other reactions in the process. 4) Each reaction should produce minimum chemical-by- product, and the products should be easily separated in terms of cost and energy consumption. 5) Intermediate products should be easily handled. Currently, there are several processes which meet these five criteria, such as the sulphur-iodine thermal cycle and the UT-3 cycle (Holladay et al. 2009).

Sulphur-Iodine Thermochemical Cycle (S-I cycle)

The sulphur-iodine(S-I) cycle is a basic thermochemical cycle, which consists of two oxidation-reduction cycles based on sulphur and iodine. This cycle involves seven chemical reactions, as shown in Eqs. (2.7)- (2.13)

$$(9I_2)_l + (SO_2)_g + (16H_2O)_l \rightarrow (2HI + 10H_2O + 8I_2)_l + (H_2SO_4 + 4H_2O)_l \tag{2.7}$$

$$L_2 = (2HI + 10H_2O + 8I_2)_l \rightarrow (2HI)_g + (10H_2O + 8I_2)_l \tag{2.8}$$

$$(2HI)_g \rightarrow H_2 + (I_2)_l \tag{2.9}$$

$$L_1 = (H_2SO_4 + 4H_2O)_l \rightarrow (H_2SO_4)_l + (4H_2O)_l \tag{2.10}$$

$$(H_2SO_4)_l \rightarrow (H_2SO_4)_g \tag{2.11}$$

$$(H_2SO_4)_g \rightarrow (SO_3)_g + (H_2O)_g \tag{2.12}$$

$$(SO_3)_g \rightarrow (SO_2)_g + 0.5O_2 \tag{2.13}$$
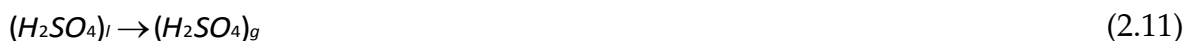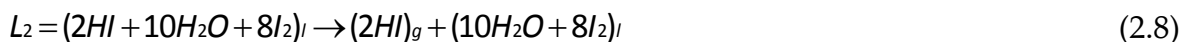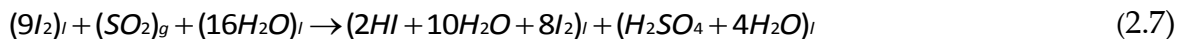
In this cycle, hydrogen can be produced from Eq. (2.9) of which the other product (I_2) will be recycled. Sulphuric acid decomposition consists of two steps: sulphuric acid dissociation and sulphur trioxide decomposition. Sulphur dioxide is also recycled to the Bunsen reaction Eq. (2.7). Overall, the feedstock consumed in this cycle is only water, and the products are oxygen and hydrogen.

The whole cycle can be often simplified into three common sections: Bunsen Reaction, Hydrogen Iodide Decomposition (Eqs. 2.8-2.9), and Sulphuric Acid Decomposition (Eqs. 2.10-2.13). A sketch of the cycle is shown on Figure 2.6:
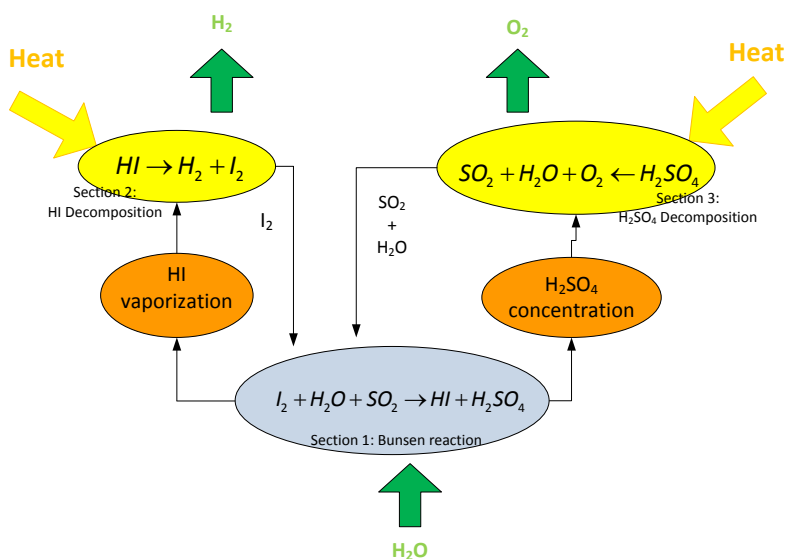
Figure 2.6: *Schematic representation of the S–I cycle*

The main challenges of S-I cycle are to improve the efficiency and reduce the energy

requirement. The "standard sulphur-iodine cycle" (Goldstein et al. 2005) has an efficiency of 36% based on calculation and reasonable assumptions. The expected efficiency of sulphur-iodine cycle is around 50%. 20% of input energy is expected to be recovered compared to classical S-I cycle. At present, there are many arguments which are incomplete in five questions about S-I cycle (Vitart et al. 2008).

- High temperature (above 1000K) is necessary which needs a heat source,
- The holdup of material, especially iodine, is high,
- Reactants are corrosive and dangerous in an industrial scale.
- Iodine losses may be high
- An efficiency of 50% cannot be yet reached.

The sulphur-iodine cycle is a very versatile cycle, which means that it allows lot of variants for each section which can be adjusted in synergy for optimising the whole process. Catalysts are being developed for operating the cycle at relatively low temperature. New unit operations such as membrane separation, reaction distillation are being introduced to optimise the cycle for obtaining high efficiency. New materials are being researched and developed for use in the corrosion resisting reactors used in the S-I cycle. Therefore, with the contributions of optimum process conditions, suitable catalyst, and corrosive resisting material, the efficiency and energy consumption per hydrogen production of S-I cycle will be achieved. The research and development of S-I cycle is introduced in detail in section 2.3.

Thermochemical hybrid Process

The thermochemical hybrid process is a combined cycle process with both thermochemical and electrolytic reactions for water splitting. The hybrid process provides the possibility to run low-temperature reactions on electricity. One of popular examples is hybrid sulphur process [Figure 2.7].
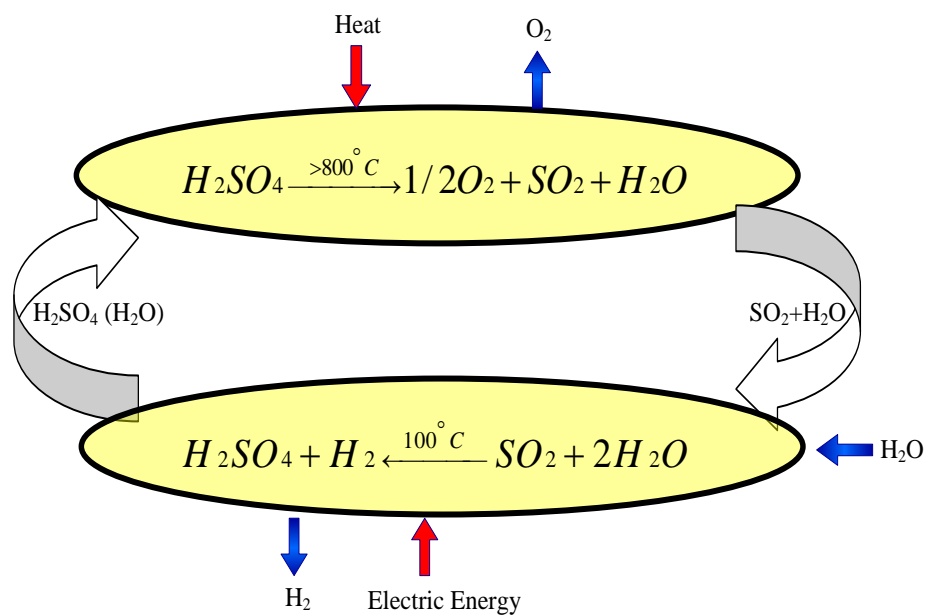
Figure 2.7: *The hybrid sulphur process scheme*

This is one of the advanced and promising thermochemical processes to produce hydrogen at large scale. It consists of two steps and is an all fluid process. The first step is sulphuric acid decomposition at elevated temperature with sustainable nuclear or solar heat sources. Oxygen, as one final product, will be separated from sulphur dioxide and water stream which will be the feedstock for the second step. Usually, the sulphuric acid is injected into the decomposer after a concentration and vaporization process in order to obtain high acid conversion and less heat consumption. Afterward, the mixture of SO_2, SO_3, H_2O and O_2, and the un-reacted sulphuric acid will be injected into an SO_2 depolarized electrolyser (SDE) after removing oxygen, producing sulphuric acid and hydrogen. SDE is the essential component of the second step (SO_2 oxidation section) of the hybrid sulphur cycle.

Hybrid cycles have always attracted considerable interest in that typically they are simpler than pure thermochemical cycles. Never-the-less, they have one characteristic that tends to make them uneconomic at large scale. Energy efficient electrochemical processes require parallel electrodes, small gaps between electrodes and minimal mixing of the anodic and cathodic products – in short they require a thin membrane between the anode and cathode. This basically limits efficient electrochemical processes to the small electrode areas that are consistent with thin membrane manufacture (Brown et al. 2003).

Ca-Br-Fe (UT-3 cycle)

UT-3 cycle is a kind of water splitting thermochemical cycles used to produce hydrogen, which was developed by (Aochi et al. 1989) in the University of Tokyo. Nowadays UT-3 cycle is one of the two cycles of the best cycles in 115 unique thermochemical cycles (Brown et al. 2003). UT-3 cycle includes five compounds and four chemical reactions:

$$CaBr_2(s) + H_2O(g) \rightarrow CaO(s) + 2HBr(g) \qquad 700\text{-}760°C \qquad (2.14)$$

$$CaO(s) + Br_2(g) \rightarrow CaBr_2(s) + 0.5O_2(g) \qquad 500\text{-}600°C \qquad (2.15)$$

$$Fe_3O_4(s) + 8HBr(g) \rightarrow 3FeBr_2(s) + 4H_2O(g) + Br_2(g) \qquad 200\text{-}300°C \qquad (2.16)$$

$$3FeBr_2(s) + 4H_2O(g) \rightarrow Fe_3O_4(s) + 6HBr(g) + H_2(g) \qquad 550\text{-}650°C \qquad (2.17)$$
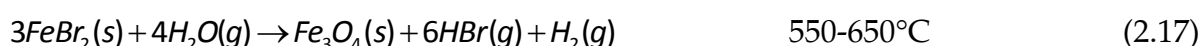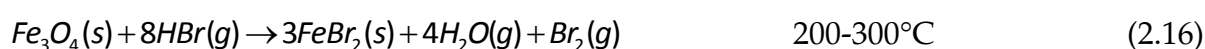
Reaction 2.14 and 2.17 are the endothermic reactions which require a continuous and stable energy source such as solar or nuclear. All of the reactions in UT-3 are solid-gas reactions.

Figure 2.8 is one example of UT-3 cycle. The four chemical reactions take place in four adiabatic fixed, packed bed chemical reactors that contain the solid reactants and products. The chemical reactors occur in pairs — one pair contains the calcium compounds and the other pair the iron compounds. The nuclear reactor transfers heat through a secondary heat exchanger into the gas stream which traverses through the four chemical reactors, three process heat exchangers, two membrane separators and the recycle compressor in sequence before the gases are recycled to the reactor secondary heat exchanger.

The three main advantages of UT-3 cycle are 1) all gas-solid reactions which make the separation easy; 2) circulation of gas only which reduces operating cost; 3) the theoretical efficiency is high, around 50%. However, the main challenges include 1) it is possibly difficult for membranes to separate H_2 and O_2 when scaling-up the system; 2) there is limited potential for improvement: already at melting point of $CaBr_2$; 3) necessary to compress H_2 and O_2 produced at sub-atmospheric pressures. However, this cycle cannot be operated in steady-state mode without moving solids. Beds of solid material must be periodically changed from one temperature to

another. The high temperature endothermic steps are operated under conditions in which the free energy of the reaction is positive. These reactions are forced to proceed by sweeping the reaction products out of the reaction zone. These reactions are operated very near the melting point of the bromides and, if melting occurs, transport of the molten bromides could lead to blockage of the beds.

This cycle has been extensive studied in Japan. It is the only thermochemical cycle presently being studied at large scale. There appear to be some parts of this reaction that are not discussed in the open literature, indicating that there may be some surprises that make this cycle more favourable than it appears.
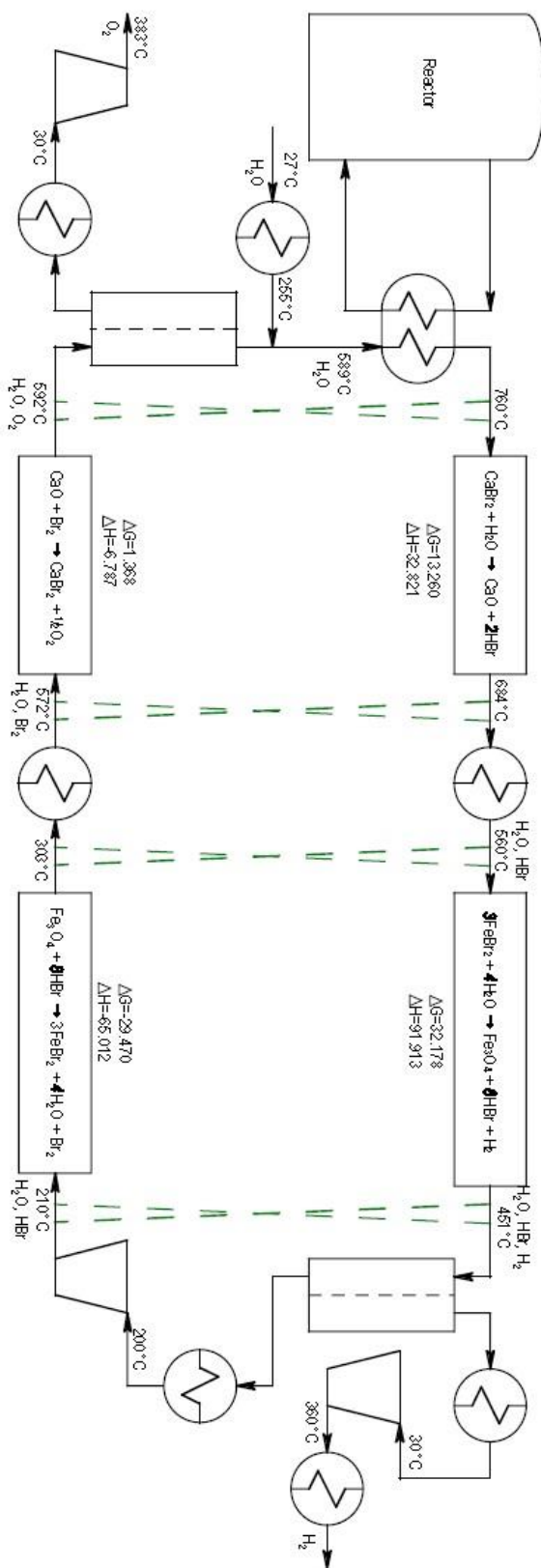
Figure 2.8: *UT-3 process flow diagram [Source: Sandia National Laboratory Report: GA-A24285]*

2.2.3   Photochemical process

Photochemical processes use solar light to produce the hydrolysis of water. Nowadays two procedures are known widely: photoelectrochemical and photobiological (Suárez-González et al. 2011).

In the photoelectrochemical process, water is split into hydrogen and oxygen in a single step and on a single device. On this device, the photovoltaic cell receives the solar energy and is also used as one of the electrodes. The photovoltaic device has to generate enough voltage to split water and its surface has to conduct the electricity, resist the corrosion produced by the electrolyte and catalyze the electrochemical reactions.

Photobiological processes are based in the capacity of some organisms, such as green algae, cyanobacteria, photosynthetic bacteria, and dark fermentation bacteria, to act as biological catalysts in the production of hydrogen from water and different enzymes. The great variety of organisms that are capable of being used, allows hybridising approaches with photoreactors and fermentors.

The main advantage of both processes is the ability of using sunlight to produce hydrogen. It may decrease dramatically the capital of hydrogen production processes. However, a lot of challenges have not been solved at present. For example, the distribution of solar radiation is non-uniform. Suitable catalysts are required for many reactions, but this catalyst is still under developed. The design of reactors also has a lot of problems. At present, the status of these processes is still early in research and development (Momirlan and Veziroglu 2002).

2.2.4   Summary on method of hydrogen production

Overall, water electrolysis and steam methane reforming are two mature technologies for hydrogen production, which have been used widely for small scale and industry scale respectively. Due to the disadvantages of low efficiency or non-environmental friendly, other promising hydrogen production processes are emerging and developing promptly such as UT-3 cycle, thermochemical hybrid

process, sulphur-iodine thermal cycle, and photochemical process.

2.3 Sulphur-iodine cycle

As mentioned above, sulphur-iodine (S-I) thermochemical cycle for hydrogen production conceived by General Atomics in 1972 consists of three main chemical reactions: Bunsen reaction, hydrogen iodine (HI) decomposition, and sulphur acid (H_2SO_4) decomposition. Water is the only raw material and is decomposed into hydrogen and oxygen. The energy used in this process is only heat which does not need to be converted to electricity. In order to commercially viable, the efficiency of a thermochemical cycle should be better than that of water electrolysis.

2.3.1   Bunsen reaction

Bunsen main reaction is the following (Hadj-Kali et al. 2009)

$$2H_2O + SO_2 + I_2 \rightarrow H_2SO_4 + 2HI \quad \Delta G^{\circ}(400K) = 82 kJ/mol$$

(2.18)

ΔG° is the standard Gibbs free energy. This reaction produces two acids: hydriodic acid (HI in water) and sulphuric acid. Water, sulphur dioxide and iodine as raw materials in an aqueous solutions. The mixed acids are separated into two types of acid, the upper and light H_2SO_4 solution phase, and lower and heavy iodine/iodide-water phase. The acid, which is rich in HI, is HI_x phases; while the acid, which is rich in H_2SO_4, is H_2SO_4 phase (H_2SO_4 solution). The understanding of Bunsen reaction is very well developed and the remaining problems are about the separation of HI_x mixtures and concentration of HI and H_2SO_4 before decomposition.

Generally water and iodine are in excess to make the Bunsen reaction spontaneous and induce the acid phase separation, which is the key point of the process. However, such excesses are quite unfavourable for the following HI_x separation section which contains HI, H_2O, high concentrations of I_2, plus small amount of hydrogen sulphide and sulphur because of side reactions (Sakurai et al. 2000):

$$6HI + H_2SO_4 \leftrightarrow S + 3I_2 + 4H_2O$$

(2.19)

$$8HI + H_2SO_4 \leftrightarrow H_2S + 4I_2 + 4H_2O$$

(2.20)

Hence, research and development efforts are devoted to finding new operation points for the Bunsen reaction with lower amounts of I_2 and H_2O, or develop new processes to separate HI_x and concentrate HI.

2.3.2   HI decomposition

HI decomposition is the reaction of hydrogen generation. According to Eqs. 2.8-2.9, HI decomposition must be achieved in the form of HI_x mixture produced in the Bunsen reaction. In this stage, there are four main challenges (Vitart et al. 2006):

- The removal of HI from the HI_x mixture is difficult because of the presence of an azeotrope in the mixture [Figure 2.9].
- The separation process of HI from the HI_x mixture requires a large amount of heat exchanges because of the presence of water which has a large heat capacity.
- The decomposition reaction is incomplete. The HI decomposition degree is limited by the chemical equilibrium and the conversion at 723K does not exceed 22.4% (Belaissaoui et al. 2008).
- The decomposition reaction is slow.

The main options are current being considered for the HI decomposition challenges [Figure 2.10]

Extractive distillation was proposed by General Atomics (Besenbruch et al. 2000): the introduction of phosphoric acid induces the separation of iodine firstly, and then allows simple distillation of HI. HI is decomposed in gaseous phase around 800K to yield hydrogen, which has to be separated from the gaseous mixture using membranes.

The present Japanese scheme favours electrodialysis (Onuki et al. 2000), which removes some water of HI_x mixture to concentrate it beyond the azeotropic limit. Excess HI is then removed by simple distillation. Membrane technology is always associated with electrodialysis for HI concentration (Caputo et al. 2007) (Hwang et al. 2003) (Tanaka et al. 2010) (Elder et al. 2009).
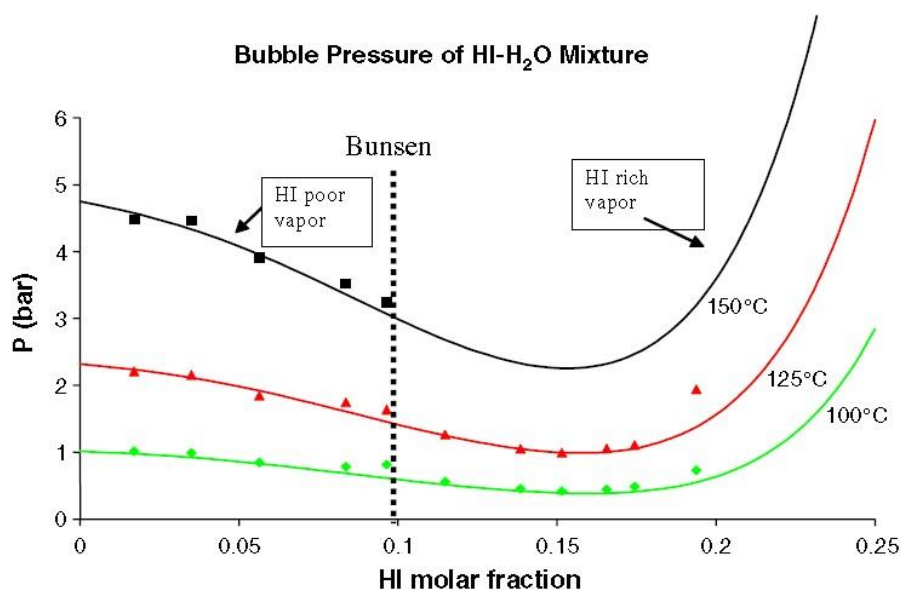
Figure 2.9: *Azeotropic lines of HIx mixture*
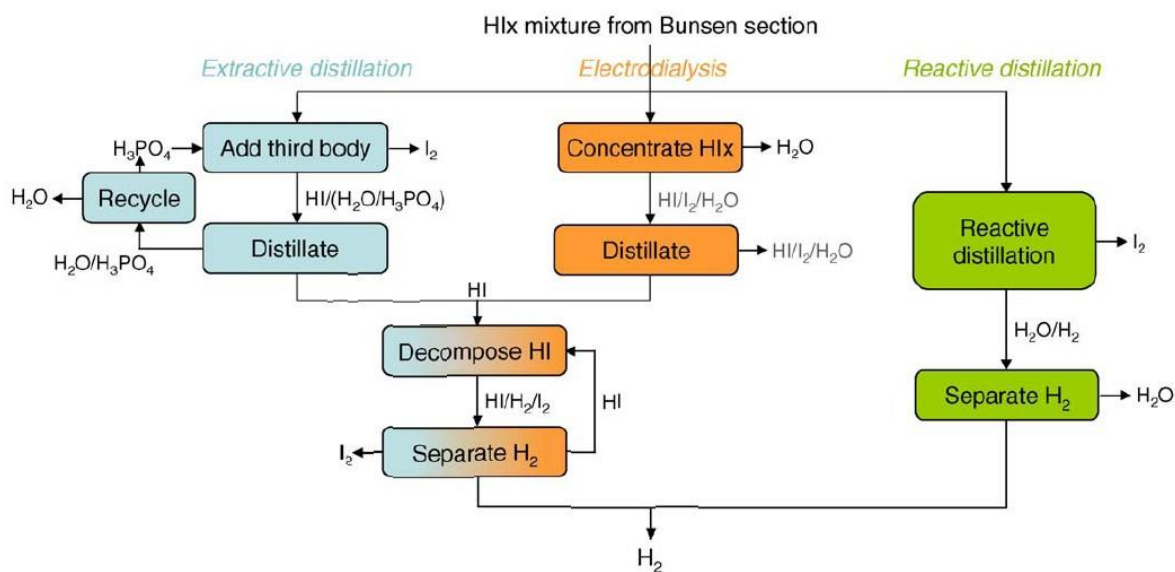
Figure 2.10: *Schematic representation of the main options for the HI section(Vitart et al. 2006)*

For reactive distillation, HI_x distillation and HI decomposition are performed in the same reactor at 350°C. Liquid-gas equilibrium is obtained in the middle of the column. I_2 is solubilised in the lower liquid phase. Gaseous H_2 and water are recovered at the top of the column. Belaissaoui et al. (Belaissaoui et al. 2008) researched the feasibility, synthesis and design of reactive distillation column involving vapour phase chemical reaction using an extended global design approach for vapour phase HI decomposition. The influence of the reactive distillation column

pressure on operation condition was investigated by (Kane and Revankar 2008) who simulated HI decomposition section with Aspen plus based on General Atomics work. At the same time, its thermodynamic analysis was first carried out in order to check the accuracy by comparing the bubble pressure of the HI–H_2O mixture of the current analysis with the theoretical analysis of GA. Lanchi et al. (Lanchi et al. 2009) studied thermodynamic analysis of the HI-H_2O-I_2 system and designed the HI_x decomposition section. Equilibrium data for the HI_x mixture is very important for the correct evaluation of the actual efficiency of reactive distillation. Because the amount of hydrogen produced during the process depends closely on the I_2 and HI concentrations in the vapour. The research on liquid-vapour equilibrium data involves experimental devices as well as the development of suitable analytical methods such as FTIR spectrometry, UV-visible spectrophotometer, spontaneous Raman scattering.

2.3.3   Sulphuric acid decomposition

In the sulphur-iodine (S-I) cycle, H_2SO_4 decomposition is the most complicated and technologically demanding part because of the rigorous operation conditions (i.e. extreme temperature of the highly corrosive reactants and the substantial energy requirements of the endothermic reaction) (Barbarossa et al. 2006). Sulphuric acid decomposition occurs in a series of three steps. The first step is the vaporization of the acid. The second step is the dissociation of sulphuric acid vapour to water and sulphur trioxide. Finally, the most challenging step is the highly endothermic decomposition of the sulphur trioxide to sulphur dioxide and oxygen. Explicitly, these steps are:

$$H_2SO_4(l) = H_2SO_4(g) \tag{2.21}$$

$$H_2SO_4(g) = SO_3(g) + H_2O(g) \tag{2.22}$$

$$SO_3(g) = SO_2(g) + 0.5O_2(g) \tag{2.23}$$

In last few decades, the research on sulphuric acid decomposition in S-I thermal cycle is related to catalyst, identification of the materials and flowsheet design in order to reduce the operating decomposition temperature (exceed 800°C in the gas

phase and >200°C for the liquid handing components) and increase the overall efficiency of S-I cycle.

2.3.3.1   Catalyst

Catalyst plays an important role on H_2SO_4 decomposition. Basically, the requirements of the catalysts used in this reaction are (Ginosar et al. 2007):

- High activity,
- robust with temperature,
- stable activity over many hours of operation (high temperatures, harsh chemicals),
- physical stability

Various catalysts have been studied before. The effectiveness of a number of potential catalysts (Ru, Pt, V_2O_4, CuO, Cr_2O_3, Fe_2O_3, NiO, Mn_3O_4, CoO, ZnO) for sulphur trioxide decomposition was studied by admitting gaseous SO_3 to an alumina reactor containing the material and monitoring the exit gas composition by mass spectrometry (Brittain and Hildenbrand 1983). At the same percentage decomposition of SO_3 as a function of temperature for each catalyst, the lowest threshold temperatures for catalysis were exhibited by Pt and Ru comparing to a blank run with no catalyst present and to the equilibrium composition at 1×10^{-6}atm. But metal oxides had less degradation of catalytic activity changing the operating pressure to 4×10^{-6}atm, compared to Ru catalyst.

The activity and stability of Al_2O_3, ZrO_2, TiO_2 supported platinum catalysts were explored for the sulphuric acid decomposition reaction (Ginosar et al. 2007). They found that the higher surface area Pt/Al_2O_3 and Pt/ZrO_2 catalysts had the higher activity but deactivated rapidly. A low surface area Pt/TiO_2 catalyst had good stability in short term tests, but slowly lost activity for over 200h of continuous operation. Attempting to decrease the cost of catalyst, Ginosar et al. also investigated the activity and stability of $FeTiO_3$, $MnTiO_3$, $NiFe_2O_4$, $CuFe_2O_4$, $NiCr_2O_4$, $2CuO \cdot Cr_2O_3$, CuO and Fe_2O_3 for the atmospheric decomposition of concentrated sulphuric acid (Ginosar et al. 2009). Catalyst activity was determined at

temperatures from 725 to 900°C. Catalyst stability was examined at 850°C for up to 1 week of continuous operation. The results were compared to a 1.0wt% Pt/TiO_2 catalyst. The conclusion was that at temperatures lower 800°C, the 1.0 wt% Pt/TiO_2 catalyst had higher activity than the complex oxide, but at temperatures above 850°C, the $2CuO \cdot Cr_2O_3$ and $CuFe_2O_4$ samples had the highest activity. However, these catalysts all displayed shortcomings including material sintering, phase changes, low activity and moderate temperatures due to sulphate formation, and decomposition to their individual oxides.

Specially, Barbarossa et al. (Barbarossa et al. 2006) studied the poisoning effects on an iron oxide (Fe_2O_3) catalyst, supported on quartz wool and alumina pellets, used for H_2SO_4 to SO_2 decomposition in the temperature range 873-1073K. The alumina supported catalyst presented better catalyst activity in the case of the presence of I_2/I^-. It was noted that the decrease of the catalyst activity was observed to be reversible for Fe_2O_3/Al_2O_3 and irreversible for Fe_2O_3/SiO_2. Because of catalyst, the temperature of H_2SO_4 decomposition could be decreased by around 300K, to 1150K. Similarly, a satisfactory catalyst activity of $Fe_2O_3-Al_2O_3$ (0.3 wt% Fe_2O_3) was observed in sulphuric acid decomposition by using a solar furnace, compared to the predicted conversion rates for the reaction without catalyst (Brutti et al. 2007).

Overall, Pt-based catalysts have the highest activity among the noble metal-based catalysts. Sulphuric acid decomposition rate on a metal particle was mainly defined by the removal rate of the reaction products from the particle. The catalysts made of "harder" metals (Rh, Ir, Ru, and Os), with the higher melting temperatures and sublimation enthalpy, experienced low catalytic activity because they bind the reaction products stronger than the "softer" metal (Pd and Pt) particles (Rashkeev et al. 2009). However, in the long-term noble metals suffer significant decrease in catalytic activity. Metal oxides are promising candidates, but at low temperatures and high pressures are subject to rapid loss due to sulphate formation. The decomposition temperature of the corresponding metal sulphate dictates the catalytic activity of a given transition metal oxide (Brown and Revankar 2011).

2.3.3.2 Process intensification of sulphuric acid decomposition

Besides developing higher activity and better stability of catalyst, the process intensification for sulphuric acid thermal decomposition is also an approach to achieve the decomposition proceeding with lower temperature or high efficiency.

One of the most critical components of sulphuric acid decomposition is the high-temperature heat exchangers such as the preheater and the decomposer. An acid decomposer made from ceramic material such as silicon carbide or alumina overcomes the challenges presented by both the high temperatures and the corrosive nature of the H_2SO_4. However, the use of ceramics then presents the problem of creating seals between the low-temperature metal components and the high-temperature ceramic components of the reactor. Plastic materials, such as Teflon, are only allowable at temperatures up to 300°C. The use of metal gaskets would create issue of corrosion and possible loosening under cyclic operating conditions. A ceramic high-temperature heat exchanger as a sulphur acid decomposer made of silicon carbide (Jiang et al.) was proposed by Ponyavin et al.(Ponyavin et al. 2008). The inner wall of decomposer was coated by a catalyst to decompose sulphur trioxide into sulphur dioxide and oxygen. Three alternative geometries of the decomposer channel were investigated ribbed ground channel, hexagonal channel, and diamond channel. Relative low decomposition rates were achieved for SO_3 using this design. Similarly, Westinghouse Electric Company also designed a compact decomposer that preheats, concentrates, and decomposes sulphuric acid for use in the production of hydrogen (Connolly et al. 2009).

The flowsheets for sulphuric acid decomposition were developed using Aspen Technologies's HYSYS chemical process simulator (CPS) to study the beneficial effect of high temperature solar heat for decomposition of sulphuric acid in the S-I cycle (Huang and T-Raissi 2005). Based on the HYSYS analyses, two new process flowsheets were developed and compared with Bilgen's flowsheet whose thermal efficiency is about 77% for sulphuric acid decomposition. However, Bilgen's flowsheet is complex resulting in potentially higher capital and operating costs. In addition, the temperature stability of the Bilgen's process is low at reaction

temperature below 750°C. The improved processes are simple and stable at acid decomposition temperatures down to 500°C, yet offer process efficiencies comparable to that of Bilgen's flowsheet.

2.3.3.3   Kinetic and thermodynamic study of acid decomposition

Beside the research on catalysts and design of a flowsheet for sulphuric acid decomposition, the kinetics and thermodynamics of the decomposition reaction of SO_3 to SO_2 also has been the subject of some studies because it is still scarce and very significant for further understanding the reaction mechanism, determination of the optimum operation conditions and reactor design at large scale. Only a few papers have presented kinetic data on decomposition reactions. The most recent thermodynamic modeling of the decomposition of H_2SO_4 (g) was performed considering the effect of temperature, pressure and initial composition of the gas (Brutti et al. 2006). Sulphur trioxide decomposition was believed to be a rate-limiting step in the conversion of spent sulphuric acid to SO_2 (Yilmaz et al. 2006). The rate constant for the thermal dissociation of SO_3 to SO_2 at 1269K and atmosphere pressure was estimated to be 6.9×10^{10} cm^3/mol· s with an uncertainty factor of 3.

2.4 Membrane separation processes in S-I cycle

Separation process plays a very important part in the S-I cycle. After the Bunsen reaction, HI should be separated from HI_x consisting of HI, H_2O and I_2, in order to be decomposed into hydrogen as the objective product of S-I cycle and to recycle I_2 into Bunsen reaction. After HI decomposition, hydrogen is needed to be separated from iodine which is reused in Bunsen reaction. Also sulphur dioxide is required to be separated from the products of H_2SO_4 decomposition, again in order to be recycled. Membrane operation offers distinct advantages over existing separation technologies such as: high separation efficiency with high quality products, energy saving, operation easily, greater flexibility in designing systems, environmental friendly and so on.

2.4.1   Membrane processes in the Bunsen reaction

In the traditional way of carrying out the Bunsen reaction, SO_2 was directly contacted with aqueous iodine, and required excess amount of water to make the reaction spontaneous (Leybros et al. 2009). Also an excess amount of iodine was added to reduce the side reaction and to induce the separation of products into two immiscible phases by means of density difference (Sakurai et al. 2000). In this way, there are two problems created: the concentration of H_2SO_4 and separation of HI_x mixtures containing HI, I_2 and H_2O. Pervaporation of water from sulphuric acid was demonstrated using both Nafion® and SPEEK membranes (Orme et al. 2009). Measured fluxes of water and separation factors are commercially competitive. Further, this work was extended successfully to HI. Nafion®-117 membranes were successfully used to remove water from aqueous hydriodic acid (HI) by pervaporation at the temperatures of 22, 50, 70 and 100°C (Orme et al. 2005). The separation factor is of magnitude 10^3. The activation energy was calculated from initial flux data to be 14.8 kJ/mol. Fluxes of water increased with temperature reaching a maximum of 1.50 kg/m^2 h at 100°C without significant reduction of the separation factor. Similarly, Stewart et al. studied the removal of water from HI by pervaporation using the same membrane at the similar temperature range (Stewart et al. 2007). Separation factors were measured between 200 and 700, which are commercially attractive with industrial prevaporation processes. Beside Nafion® 117 membrane, Nafion® 212 was also investigated using both a batch and a continuous flow arrangement operating with a range of HI-H_2O and HI-H_2O-I_2 solution concentrations (Elder et al. 2009). Permeates of almost pure water and reasonable fluxes were seen, and good correspondence was observed between the results from the two rigs. Consideration of the solution-diffusion model suggested that sorption and desorption, as well as diffusion, played a limiting role in the permeate flux. Sulfonated poly (ether ether ketone) (SPEEK) membranes was used to concentrate HI at 134°C without any significant degradation of transport behaviour.

2.4.2   Membrane processes in HI decomposition

The application of membrane operation for this phase is mainly in H_2 separation

after HI decomposition. A membrane reactor was proposed and designed for completing HI decomposition and hydrogen separation at the same time (Tosti et al. 2008). A dense membrane tube made from niobium and tantalum was designed for selective separation of hydrogen from an azeotropic H_2O-HI mixture in the temperature range of 700 – 800K. By a finite element method for the membrane reactor, the effect of temperature and pressure on the HI conversion and hydrogen yield was evaluated.

The reactor consisted of zirconia-silica composite membranes coated on porous ceramic tubing was characterised, afterwards the separation experiments for gaseous mixtures of HI-H_2O was carried out at 423-773K (Ohya et al. 1994). It was found that the permeation flux of H_2 increased with an increase in temperature. The permeation mechanism of H_2 is mainly due to the mechanism of activated diffusion and Knudsen diffusion. In the separation experiments of the H_2O-HI gaseous mixture, it was found that HI was concentrated in the permeated gases. The separation factors were in the range of 5 to 26. The zirconia composite membrane separated H_2 from the thermochemical decomposed gaseous mixture successfully.

2.4.3   Membrane processes in H_2SO_4 decomposition

No literature reports the application of membrane separation process in H_2SO_4 decomposition. H_2SO_4 decomposition is required for recycling sulphur dioxide. In this part of S-I cycle, membrane operation should be an opportunity to separate the products of H_2SO_4 decomposition, which can recycle SO_2 and increase the acid conversion as well. Because H_2SO_4 decomposition proceeds only at high temperature in presence of catalyst (above 800°C) and   the products are gaseous mixtures before cooling down, any membrane used in products separation process after acid decomposition should be made from inorganic substance because of its characteristics (Hwang 2001):

- Enjoy much high thermal stabilities and can stand high temperatures for a long time,

- Resistance to rigorous environments such as extreme acidity or alkalinity,

- High mechanical strength (stable at high operating pressure),

- Resistance to microbial attacks,

- High flux

- Easy cleaning

- Long operating life

- Easy to be modified by adding catalyst

The requirement of the membrane used for SO_2-O_2 separation in sulphuric acid decomposition and the working conditions of membrane are associated easily to solid oxide fuel cell (SOFC) or solid oxide electrolyser cell (SOEC) which are both electrochemical conversation devices that produce electricity or hydrogen directly from electrochemical reactions at high temperature, typically between 500 and 1000°C. The electrolyte in SOFCs and SOECs has high oxygen ionic conductivity at high temperature, which only allows oxygen ions diffusing through to achieve the charge balance with electrochemical reactions on electrode surface.

2.5 Solid oxide fuel cells (SOFCs)

SOFCs have recently emerged as a serious high temperature fuel cell technology. They promise to be extremely useful in large, high-power applications such as full-scale industrial stations and large-scale electricity-generating stations. Some fuel cell developers see SOFCs being used in motor vehicles. A SOFC system usually utilizes a solid ceramic as the electrolyte and operates at extremely high temperatures (600-1000°C). This high operating temperature allows internal reforming, promotes rapid electro-catalysis with non-precious metals, and produces high quality byproduct heat for co-generation. Efficiencies for this type of fuel cell can reach up to 70% with an additional 20% as heat recovery. SOFCs are the best suited for provision of power in utility applications due to the significant time required to reach operating temperatures.

2.5.1 Solid oxide fuel cell history

Emil Baur and his colleague H. Preis experimented with solid oxide electrolytes in the late 1930s, using such materials as zirconium, yttrium, cerium, lanthanum, and tungsten oxide (Stambouli and Traversa 2002). The operation of the first ceramic fuel cell at 1000°C, by Bayr and Preis, was achieved in 1937 (Baur and Preis 1937). Since then, great efforts have been devoted to the research and development of SOFCs focusing on many problems including relatively high internal electrical resistance, melting, and short-circuiting due to semi-conductivity. In 2000, a world record for SOFC operation has demonstrated two critical successes: the ability to withstand more than 100 thermal cycles, and voltage degradation of less than 0.1% per thousand hours. (Stambouli and Traversa 2002) Moreover, a 140 kW peak power SOFC cogeneration system, supplied by Siemens Westinghouse, is presently operating in the Netherlands. This system has operated for over 16,600 h, becoming the longest running fuel cell in the world.

2.5.2 Principle of solid oxide fuel cell

A SOFC consists of two electrodes sandwiched around a hard ceramic electrolyte.

Hydrogen fuel is fed into the anode of the fuel cell and oxygen, from the air, enters the cell through the cathode. By burning fuel containing hydrogen on one side of the electrolyte, the concentration of oxygen is dramatically reduced. The electrode on this surface will allow oxygen ions to leave the electrolyte and react with the fuel which is oxidized, thereby releasing electrons. On the other side of the plate, which is exposed to air, an oxygen concentration gradient is created across the electrolyte, which attracts oxygen ions from the air side, or cathode, to the fuel side, or anode. If there is an electrical connection between the cathode and the anode, this allows electrons to flow from the anode to the cathode, where a continuous supply of oxygen ions (O^{2-}) for the electrolyte is maintained, and oxygen ions from cathode to anode, maintaining overall electrical charge balance, thereby generating useful electrical power from the combustion of the fuel. The only byproduct of this process is a pure water molecule (H_2O) and heat, as shown in Figure 2.11.
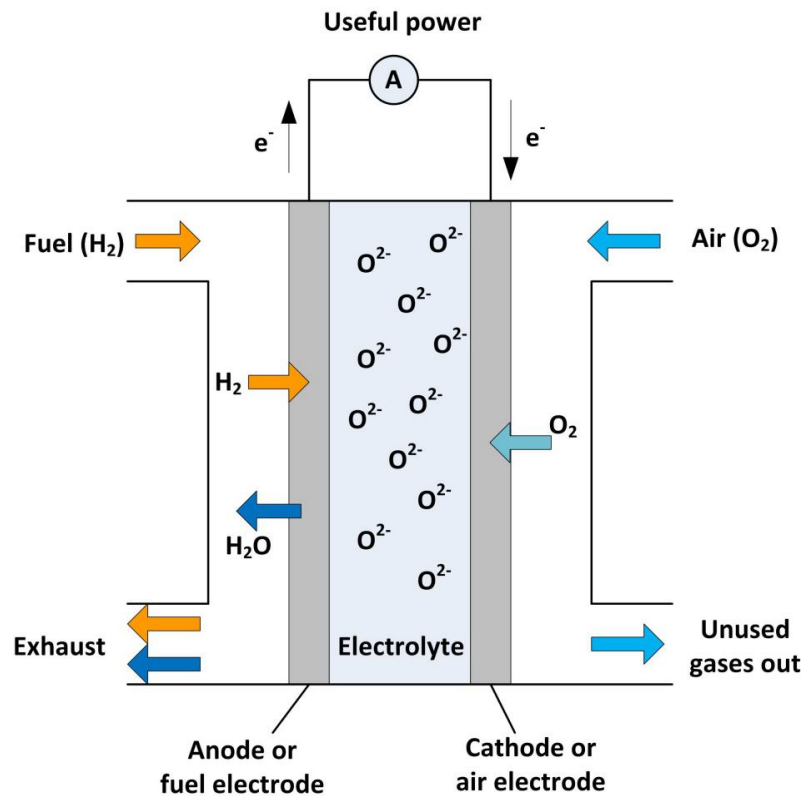
Figure 2.11: *Concept diagram of SOFC based on oxygen-ion conductors*

The SOFC reactions include: anode side

$$H_2 + O^{2-} \rightarrow H_2O + 2e^- \tag{2.24}$$

$$CO + O^{2-} \rightarrow CO_2 + 2e^- \tag{2.25}$$

$$CH_4 + 4O^{2-} \rightarrow 2H_2O + CO_2 + 8e^- \quad \text{(Fuel containing hydrogen)} \tag{2.26}$$

Cathode side

$$O_2 + 4e^- \rightarrow 2O^{2-} \tag{2.27}$$
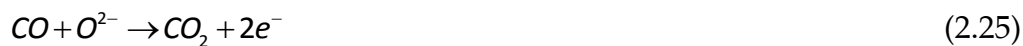
2.5.3   Components of SOFCs

A SOFC is mainly composed of two electrodes (the cathode and the anode), and a solid electrolyte. The main function of the electrode is to induce reaction between the reactant (fuel or oxygen) and the electrolyte, without itself being consumed or corroded. It must also bring into contact the three phases, i.e., the gaseous fuel, the solid electrolyte and the electrode.

The anode, used as the negative post of the fuel cell, disperses the hydrogen gas

equally over its whole surface and conducts the electrons, which are freed from hydrogen molecule, to be used as a useful power in the external circuit. Metals can be used as SOFC anode materials because of the reducing conditions of the fuel gases. Moreover, these metals must be non-oxidised since the composition of the fuel changes during the operation of the cell. Generally, SOFC anodes are fabricated from nickel oxide (NiO) and composite powder mixtures of electrolyte material such as YSZ, GDC or SDC (Zhu and Deevi 2003).

The cathode, the positive post of the fuel cell, distributes the oxygen fed to it onto its surface and conducts the electrons back from the external circuit where they can recombine with oxygen ions, passed across the electrolyte, and hydrogen to form water. Because of the high operating temperature of the SOFC, only noble metals or electron conducting oxides can be used as cathode materials. Noble metals are unsuitable for practical application because of their prohibitive cost. The state of the art of cathode development in SOFCs was reviewed with the main focus being the advantages and existing constrains of various cathode materials (Sun et al. 2010).

The electrolyte determines the operating temperature of the fuel cell and is used to prevent the two electrodes coming into electronic contact by blocking the electrons. It also allows the flow of charged ions from one electrode to the other to maintain the overall electrical charge balance. Current technology employs several ceramic materials for the active SOFC components. Although a variety of oxide combinations has been used for solid non-porous electrolytes, the most common to date has been the stabilised zirconia with conductivity based on oxygen ions (O^{2-}), especially yttria-stabilized zirconia (YSZ) which is the major reference within the former family of solid electrolytes, with ionic conductivity around 0.1 S cm^{-1} at 1000°C for solid solutions with 8 mol% yttria   (Figueiredo and Marques 2013).

2.5.4   Advantages and limitations of SOFCs

SOFCs have many advantages: they can be modular, be distributed to eliminate the need for transmission lines, they operate quietly and are vibration free. SOFCs could provide higher system efficiency not restricted by the Carnot Cycle, higher power

density, and simpler designs than fuel cells based on liquid electrolytes. Thus SOFCs may be helpful to ease energy crisis because of oil depletion in the near future. The fuel of SOFC may be produced from natural gas, propane, butane, methanol and diesel fuel.

However, the operating temperature of SOFCs decreases the cell lifetime and increases the cost of materials. Oxygen ion conduction through the YSZ electrolyte membrane is a highly active process, thus resulting in high voltage losses across the layer at lower temperatures (Badwal and Foger 1996). In addition, leakage in SOFCs is generally a possibility, which affects cell performance significantly (Lessing 2007).

2.5.5   The future of SOFCs

Solid oxide fuel cells have the potential to revolutionize electric power generation in the next century, and developments to date look promising. Areas which need innovative solutions involve (Badwal and Foger 1996):

- Improved interconnect material and seals,
- Cost competitive fabrication, and
- Long term stability

2.6 Solid oxide electrolyser cells (SOECs)

A solid oxide electrolyser cell (SOEC) is a solid oxide fuel cell that is running in regenerative mode to achieve the electrolysis of water and which uses a solid oxide, or ceramic, electrolyte to produce oxygen and hydrogen gas (Hauch et al.). High temperature solid oxide electrolyser cells (SOECs) have a great potential for hydrogen production in a very efficient and economical way, as SOECs can split H_2O into H_2 and O_2 with a low quantity of electrical energy at high temperature. When coupled to an external heat source like solar, geothermal or nuclear, a very high efficiency could be achieved without any greenhouse gas emissions.

2.6.1   Principle of SOECs

The key components of a SOEC are a dense ionic conducting electrolyte and two porous electrodes. The fundamental mechanisms involved in SOEC operation are

shown in Figure 2.12. Steam is fed to the porous cathode. When the required electrical potential is applied to the SOEC, water molecules diffuse to the reaction sites and are dissociated to form hydrogen gas and oxygen ions at the cathode-electrolyte interface. The hydrogen gas diffuses to the cathode surface and gets collected. The oxygen ions are transported through the dense electrolyte to the anode. On the anode side, the oxygen ions are oxidized to oxygen gas and the produced oxygen is transported through the pores of the anode to the anode surface.
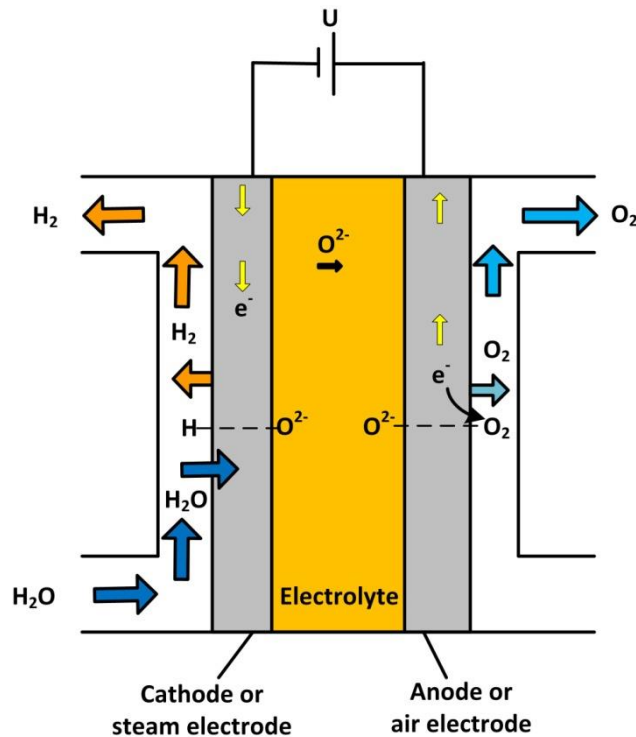
Figure 2.12: *Schematics of SOEC hydrogen production (Ulrich Vogt et al.)*

The cathode reaction:

$$H_2O + 2e^- \rightarrow H_2 + O^{2-} \tag{2.28}$$

The anode reaction:

$$O^{2-} \rightarrow 0.5O_2 + 2e^- \tag{2.29}$$

The overall reaction (endothermic reaction)

$$H_2O \rightarrow H_2 + 0.5O_2 \tag{2.30}$$

2.6.2 Components of SOECs

The same as SOFCs, a SOEC consists of three parts: cathode, electrolyte and anode. The typical materials used in SOEC are similar to those discussed in the previous section.

The dense electrolyte should be chemically stable and have good ionic conductivity with low electronic conduction to achieve high energy conversion efficiency in a wide temperature range. The most common electrolyte material is a dense ionic conductor consisting of ZrO_2 doped with 8 mol% of Y_2O_3 (YSZ) (Hauch et al. 2008). This material presents high ionic conductivity as well as thermal and chemical stability at the operation temperatures (800 – 1000°C). Other materials are also considered, such as Scandia stabilized zirconia (ScSZ) (O'brien et al. 2006) (Laguna-Bercero et al. 2009), ceria-based electrolytes (Eguchi et al. 1996) (Zhu et al. 2006), or the lanthanum strontium magnesium gallate (LSGM) materials (Ishihara et al. 2010) (Ishihara and Kannou 2011).

Both electrodes should be chemically stable in the highly reducing/oxidizing environments and have good electronic conductivity. Also they should have suitable porosity and pore size in order to not only support gas transportation between the electrode surface and the electrode-electrolyte interface but also to provide sufficient electrolyte-electrode-gas triple phase area (reaction sites). The thermal expansion coefficients of both electrodes should be close to that of the electrolyte to prevent gas leakage because of electrodes and electrolyte having different thermal expansion at the high temperature. For the steam electrode, the most commonly used material is a porous cermet composed of YSZ and metallic nickel (Hauch et al. 2008). Other alternative materials also used for the steam electrode including samaria doped ceria (SDC) with nickel dispersed nanoparticles (Uchida et al. 2004), titanate/ceria composites (Marina et al. 2007), or the perovskite material lanthanum strontium chromium manganite (LSCM) (Yang and Irvine 2008). For the oxygen electrode the most common material used to date is the lanthanum strontium manganite (LSM)/YSZ composite (Hauch et al. 2008). Different electrode materials have also been proposed, including $La_{0.8}Sr_{0.2}FeO_3$ (LSF), and $La_{0.8}Sr_{0.2}CoO_3$ (LSCo) (Wang et al.

2006); lanthanum strontium cobalt ferrite (LSCF) and lanthanum strontium copper ferrite (LSCuF) (Marina et al. 2007); nickelate based materials such as $Nd_2NiO_{4+\delta}$ (Chauveau et al. 2010) or the $Sr_2Fe_{1.5}Mo_{0.5}O_{6-\delta}$ (SFM) perovskite (Liu et al. 2010). Overall, the materials typically employed for SOEC until now have been basically the same as those used for SOFC.

2.6.3 Advantages and challenges of SOECs

Comparing to others technologies for hydrogen production, the advantages of SOEC are as following (Ulrich Vogt et al.)

- Low overall energy demand
- High efficiency, increasing with temperature
- Use of several high temperature steam sources
- Splitting of CO_2 into CO and O_2 for syngas production
- Broad know-how from SOFC technology available

Due to the high operation temperature of 700 or 800°C to 1000°C, the SOEC components have to meet specific requirements for a cost effective hydrogen production:

- Electrolyte: chemically stable and gastight with high ionic and low electronic conductivity
- Electrodes: porous, chemically stable in highly reducing/oxidizing environments with good electronic conduction and CTE (coefficient of thermal expansion) close to the electrolyte
- Interconnects: chemically stable in reducing/oxidizing environments

2.6.4 The future of SOECs

SOECs offer a practical solution for clean hydrogen production from renewable resources. In the future, more research work is required to study

- The electrode-electrolyte compatibility and the long-term stability of the SOEC
- The fundamental mechanisms of electrochemical reaction at the electrodes.
- The effect of impurity on electrode long-term stability

- Novel configurations designed for SOEC having high mechanical strength, better manufacturability and high electrochemical performance.

2.7   Previous work in our research group

In order to increase SO_2 yield of sulphuric acid decomposition in S-I cycle by membrane separation process, the selection of electrolyte, cathode and anode as three components of a membrane was undertaken previously. The membrane performance exposed to gas mixtures of He-O_2-SO_2 was demonstrated at the temperature range of 700 - 900°C. The main conclusions according to the results of experiments and analysis were that oxygen permeation through YSZ membrane occurred in the presence of SO_2 at high temperature, and the oxygen permeate flux decreased with time once SO_2 was introduced into the feed side. It may be due to the adsorption of SO_2 on the cathode surface of the membrane, which decreased the length of the triple-phase boundary (TPB).

2.7.1   Yttria-stabilized zirconia (YSZ)

YSZ is a kind of popular electrolytes used in many technical devices such as solid oxide fuel cells (SOFCs) and oxygen sensors. YSZ has a high oxygen ionic conductivity and good mechanical strength at a wide temperature range. It is chemically stable at high temperatures.   The oxygen ionic conductivity arises from the oxygen vacancy in YSZ. Figure 2.13 shows how the oxygen vacancy is formed. The addition of yttria to the pure zirconia replaces some of the Zr^{4+} ions in the zirconia lattice structure with the Y^{3+} ions. This produces the oxygen vacancy because four oxygen ions are replaced by three oxygen ions.
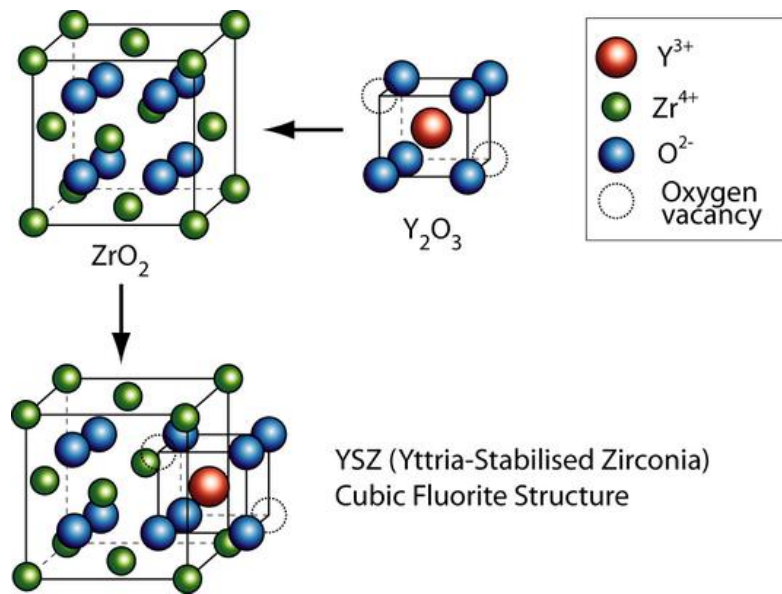
Figure 2.13: *How the oxygen vacancy produces*
(Source from: http://www.doitpoms.ac.uk/tlplib/fuel-cells/sofc_electrolyte.php)

The oxygen conductivity of YSZ means that the oxygen ion in the YSZ hops from one occupied site to another oxygen vacancy in the yttria-zirconia lattice. The oxygen ionic conductivity of YSZ is influenced by several factors: (1)   Dopant concentration: as the electrolyte of the membrane used in solid oxide fuel cells (SOFCs), the optimum concentration of Y_2O_3 in YSZ is 9.5 mol% which has a higher oxygen ionic conductivity when compared with 8YSZ (8 mol% Y_2O_3) and 10YSZ (10 mol% Y_2O_3)(Hattori et al. 2004). (2) Temperature: the relationship of the temperature and YSZ conductivity follows the Arrhenius equation below (Zhang et al. 2007):

$$\sigma = \frac{\sigma_0}{T} \exp(-\frac{E}{kT})$$

(2.31)

Where σ is the conductivity, σ_0 a material constant, T is the temperature, E is the activation energy for ionic conduction (kcal mol^{-1}), and k is Boltzmann constant ($ohm^{-1}cm^{-1}$). According to the equation, the conductivity of YSZ is reciprocal to temperature. A high operating temperature can result in a high conductivity. The ionic conductivity of YSZ is exhibited over a wide range of temperature between

550°C to 2100°C (Etsell and Flengas 1970). However, the mechanical strength of YSZ will become low at too high a temperature, and the operating cost in industrial applications could be increased at high operating temperatures. A recommended operating temperature for YSZ electrolyte is between 600°C to 1000°C (Nguyen and Takahashi 1995). (3) Grain boundary: the ionic conductivity of YSZ consists of the bulk conductivity and the grain boundary-conductivity. The bulk conductivity is not affected by grain size, while grain boundary conductivity is dependent on this factor. The grain boundary conductivity decreases with grain size from 90 to 800nm (Ivanov et al. 2010). However, it becomes constant when the grain size was varied in the region 4-55μm (Verkerk et al. 1982). The grain size is affected by the addition of impurity to YSZ, concentration of Y_2O_3 and preparation condition of YSZ such as sintering temperature and density. (4) Aging: some studies found the conductivity of YSZ is also influenced by the aging period. After the annealing period of 1000h, the 8YSZ and 8.5YSZ showed significant degradation with time which may be due to the gradual formation of a fine tetragonal phase in the cubic phase (Hattori et al. 2004).

The maximum ionic conductivity of YSZ lies around 8-9 mol% Y_2O_3 doping (Stortelder 2005). At higher doping the attraction between the oxygen vacancies and the yttria will result in the formation of complexes and decreases the mobility of the oxygen vacancies. 8 mol% yttria stabilized zirconia (8YSZ) with cubic structure possesses a high ionic conductivity and a good chemical stability over a wide temperature range and oxygen partial pressure range. It has been used widely in many technology devices such as SOFCs and oxygen sensors.

2.7.2   Platinum

As the membrane separation of SO_2 and O_2 was conducted at high temperature and the electrochemical reaction area is the electrolyte-electrode-gas phase boundary, the requirement of the electrode material needs to meet:

• High melting point;
• Chemical stable at high temperature and in the oxidizing environment;

- Conducting material;

- High thermal conductivity to make sure the temperature of the electrolyte and electrode are the same at any time;

- Small coefficient of thermal expansion;

- Be porous in order to form the triple phase boundary area for allowing oxygen molecules to reach the electrode/electrolyte interface.

Platinum is a metal that should remain metallic in an SO_2/SO_3 atmosphere at temperatures of 850°C, and it also likely prevent to be formed either an oxide or sulphate under these conditions (Mawdsley et al. 2012). Therefore, platinum was used for the cathode and the anode of the membrane in the previous work.

2.7.3 Preparation of Pt/8YSZ/Pt membrane

The membrane pellets consists of yttria (8 mol%) stabilized zirconia (YSZ), provided by Department of Materials and Science Engineering, University of Sheffield. YSZ powder was pressed into disks at 20 MPa using a 30mm steel die, cold isostatically pressing the disks to 200 MPa and then sintering the disks at 1400°C for 6h with a heating and cooling rate of 5°C/min. Finally, a membrane pellet of around 24mm diameter, 2mm thickness, near 100% density was prepared.

Platinum (Pt) ink provided by Gwent Electronic Materials Ltd. was prepared as the anode and the cathode. Firstly, Pt paste was applied on the each side of the YSZ disc using a steel spatula. The Pt film should be as thin and even as possible. Then, the pellet was inserted into a furnace and sintered at 1200°C for around 12 minutes. Afterwards, the furnace was turned off and the pellet cooled with the decrease of furnace temperature. A Pt/8YSZ/Pt membrane pellet was finally made [Figure 2.14] (Atkin 2009).
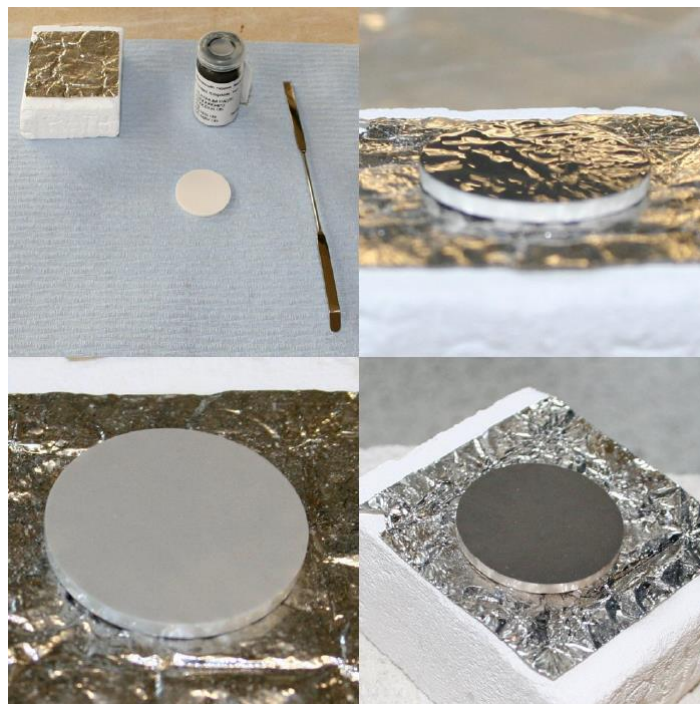
Figure 2.14: *Photo mosaic of platinum electrode application process.*

Clockwise from top left: refractory brick, platinum foil, platinum ink, spatula and bare YSZ pellet; pellet after ink application; pellet after drying of ink at 150°C for 15 minutes; pellet after firing of electrode at 1200°C for 12 minutes, with up ramp rate of 5°C per minute and cooling naturally (Atkin 2009)

2.7.4 The performance of Pt/8YSZ/Pt membrane pellet

In Figure 2.15, the membrane was exposed firstly to the feed stream of He and O_2 at high temperature, connecting with an external dc power supply (the negative polarity of the power supply is connected to the cathode in feed side; while the positive polarity is connected to the anode in permeate side). Oxygen permeated through the membrane to the anode side, and exited with helium to an oxygen analyser. Helium in the feed and permeate side was carrier gas. Current in the electrical circuit was recorded with time by the dc power supply. The concentration of permeated oxygen in helium was measured and recorded by the oxygen analyser. From the beginning of the second hour, the gas composition of the feed stream was changed to 30% SO_2, 10% O_2 in Helium (overall 50 ml/min), and lasting for two hours. Afterwards, the feed changed back to 10% O_2 in Helium (overall 50 ml/min) for 1 hour, in order to replicate the first stage. Finally, the feed revered to 30% SO_2 and 10% Helium for one additional hour, before the experiment was ended (Atkin

2009).
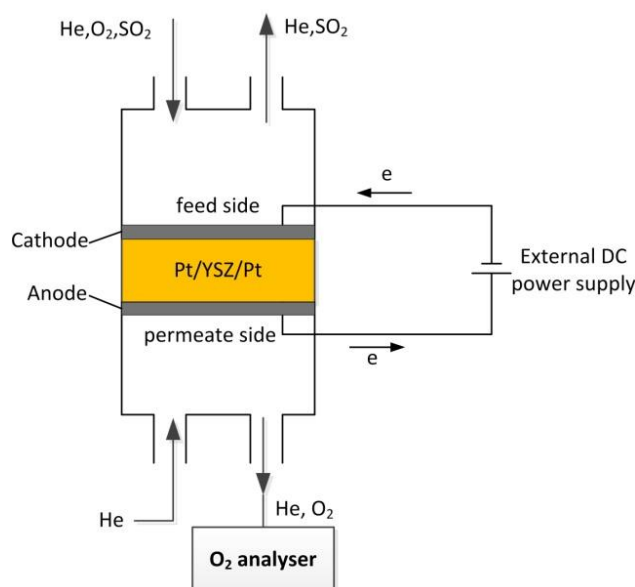
Figure 2.15: *The schematic of the oxygen permeation through Pt/8YSZ membrane*

Experimental results are shown in Figure 2.16. The oxygen concentration in the permeate side demonstrates that oxygen can permeate through the pellet at 850˚C. Once SO_2 was mixed with O_2 in the feed, the current and oxygen concentration corresponding to membrane performance decreased with time. In other words, sulphur dioxide hindered oxygen permeation processes and led to membrane performance degradation. This was confirmed in another test [Figure 2.17].

Interestingly, membrane performance had a partial recovery after a 2-minutes 3V pulse treatment in sulphur dioxide poisoning period [Figure 2.17]. It means that a high but short voltage pulse helped to reduce SO_2 poisoning effect on membrane performance. If this positive effect of voltage pulse on membrane performance recovery is significant, it might provide a promising method to keep membrane at high performance in the presence of high concentration sulphur dioxide. Furthermore, it might be beneficial to figure out the poisoning effect of sulphur-containing impurity gas in fuel on SOFCs, SOECs and sulphur family thermochemical cycles for hydrogen production.
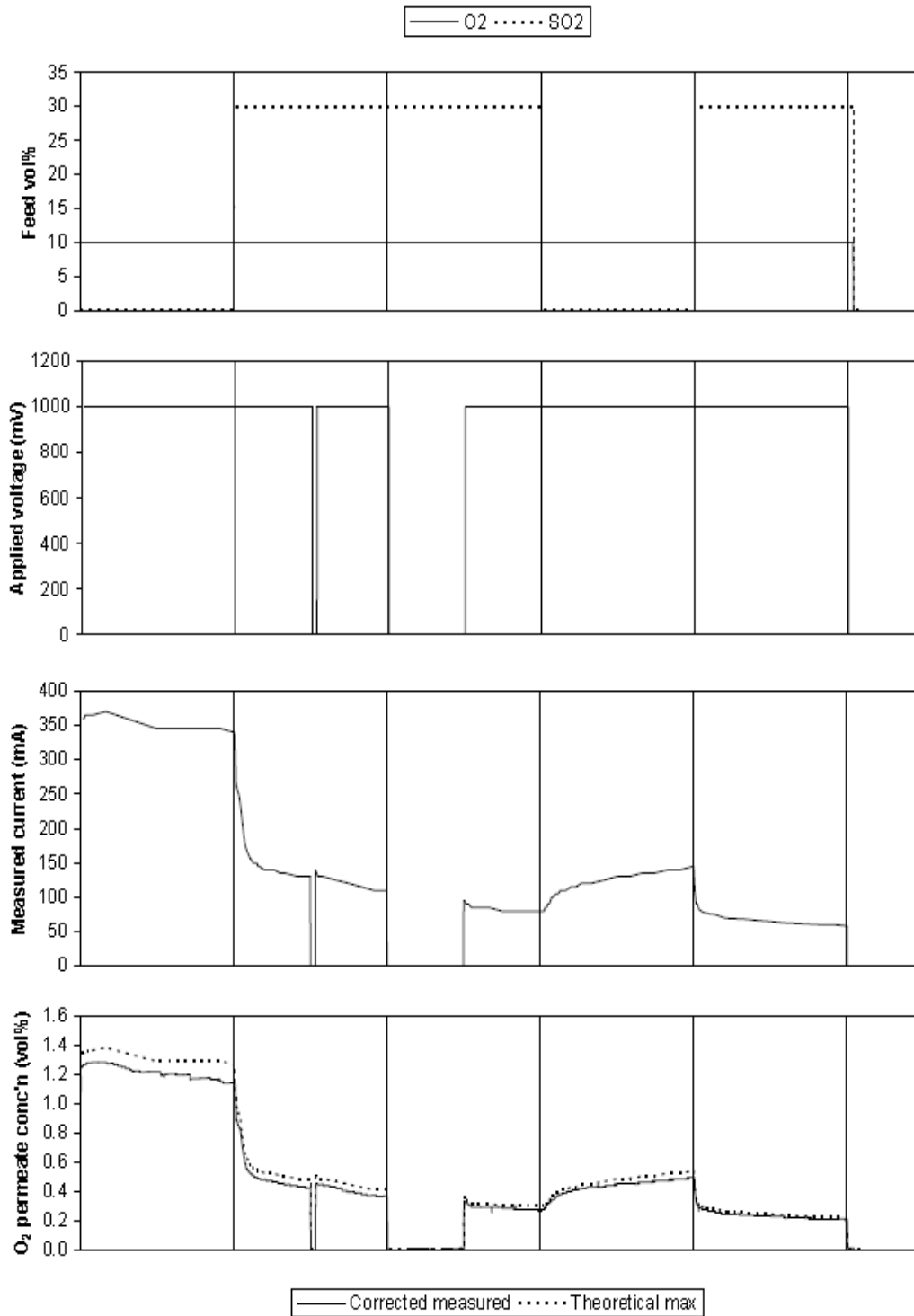
Figure 2.16: *Experimental result of membrane exposure He-O$_2$-SO$_2$ at 800°C with external voltage application—100ml/min pure He in permeate side, 50ml/min 20% O$_2$ in feed.*
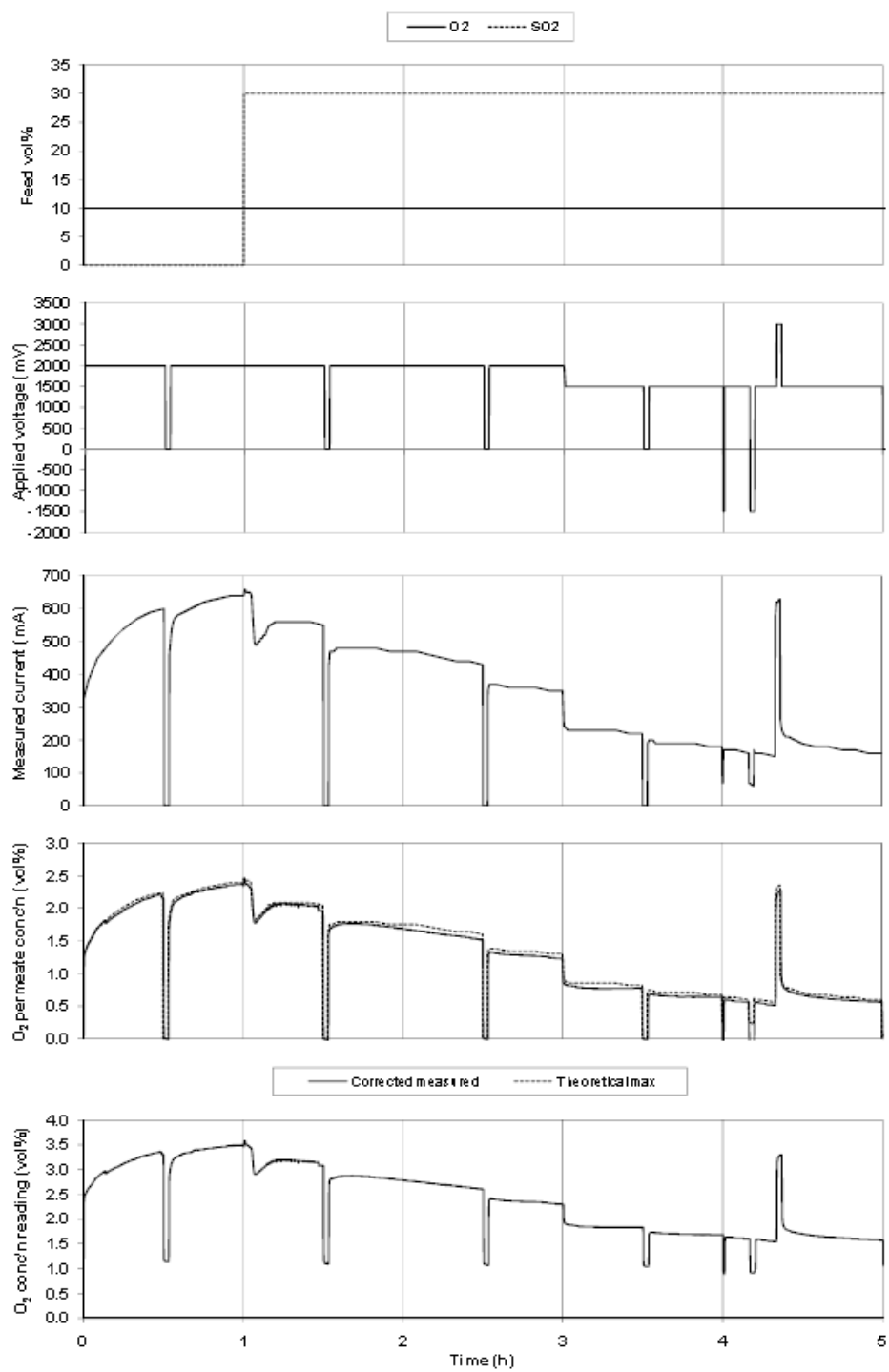
Figure 2.17: *Pt/8YSZ/Pt membrane performance exposed to SO₂ and O₂ at 850°C with negative and positive dc voltage pulses*

Chapter 3

3 Performance degradation of Platinum/8 mol% yttria-stabilized zirconia/Platinum pellets

3.1 Introduction

Removal of oxygen from the products of sulphuric acid thermal decomposition provides a promising method to permit the use of lower temperature sources with the sulphur family of thermochemical cycles. The separation of oxygen (O_2) from sulphur dioxide (SO_2) using Pt/8YSZ/Pt membrane pellet was demonstrated under the similar operating conditions to sulphuric acid thermal decomposition in our previous research. Pt/8YSZ/Pt membrane was proved to be competent to remove oxygen from sulphur dioxide at high temperature, but at the same time membrane performance degraded with time because of the presence of sulphur dioxide.

This performance degradation is very common in solid oxide fuel cells (SOFCs) and solid oxide electrolyser cells (SOECs) when the fuel contains sulphur-containing impurity gases. Sulphur poisoning behaviour of membrane has been characterized by a rapid initial drop in current upon exposure to hydrogen sulphide (H_2S) (type I degradation), followed by a much slower but still significant rate for a long period of time (type II degradation) (Lussier et al. 2008). Possible reasons for membrane performance degradation because of sulphur poisoning effect are summarised in Table 3.1. Type I degradation may be caused by the dissociative adsorption of sulphur species around three-phase boundaries (the active sites for electrochemical reaction) (Zha et al. 2007) (Gould et al. 2009) (Fu et al. 2009) (Nagahara et al. 2008) (Lussier et al. 2008). However, the mechanism of type II degradation in performance

during continuous exposure to sulphur containing gas over a long period of time is still not clear. It would be difficult to explain simply from the sulphur adsorption point of view. There are four different hypothesises. Firstly, a sulphide layer is formed on the electrode surface which increases the size of impedance arcs (Matsuzaki and Yasuda 2000), impedes the transport of the reactant gas onto the Pt surface and the transport of products away from the active Pt sites (He et al. 2002), causes the microstructure change and reduces the triple phase

Cell	Operating conditions	Possible reasons for the type II slow poisoning	References
Electrode: Pt, electrolyte: 8YSZ	H_2S, 750 – 800°C	The formation of sulphide contaminates the electrode surface and increase the interface resistance between electrode and electrolyte	(Matsuzaki and Yasuda 2000)
Electrode: Pt, electrolyte: 8YSZ	H_2S, 700 - 900°C		(He et al. 2002)
Electrode: Pt, electrolyte: 8YSZ	H_2S, 700 – 800°C		(Liu et al. 2001)
Electrode: Ni/YSZ, Ni/GDC Electrolyte: 3YSZ	H_2S, 750°C		(Lussier et al. 2008)
Electrode: Ni/YSZ, electrolyte: 8YSZ	H_2S, 850°C		(Li et al. 2010)
Electrode: Ni/YSZ, electrolyte: 8YSZ	H_2S, 700 - 900°C	Surface reconstruction of nickel leading to new surface on Ni electrode	(Zha et al. 2007)
Electrode: Ni/YSZ, Ni/GDC Electrolyte: 3YSZ	H_2S, 750°C	H_2S may cause migration of nickel in the electrode, thereby degrading the distribution of the precoating Ni phase in the anode	(Lussier et al. 2008)
Electrode: Ni/YSZ or Ni/ScYSZ Electrolyte: YSZ	H2S, 750 and 850°C	H_2S may lead to an irreversible increase of the serial resistance which due to a loss of the Ni particle in the layers closest to the electrolyte	(Hagen et al. 2011)

Table 3.1: *Summary of possible reasons for the slow performance degradation because sulphur poisoning*

boundary (TPB) perimeter for electrochemical reactions (Li et al. 2010), contaminates the anode surface and increases the interface resistances between Pt anode from the

YSZ membrane (Liu et al. 2001). The second possible explanation for type II degradation is surface reconstruction of nickel, which may lead to a new surface on electrode (Zha et al. 2007). Thirdly, type II degradation might be because H_2S may cause migration of nickel in the electrode, thereby degrading the distribution of the precoating Ni phase on the anode (Lussier et al. 2008). Finally, H_2S leads to an irreversible increase of the serial resistance which due to a loss of percolation of the Ni particle in the layers closest to the electrolyte (Hagen et al. 2011). The degradation mechanism of membrane performance because of sulphur poisoning effect, especially for Type II degradation, is important for understanding the electrochemical reactions on electrode surface and reducing performance degradation in the field of SOFCs, SOECs and sulphur family thermochemical cycles. In the case of the first hypothesis: metal sulphide formed on the electrode surface leads to long-term and slowly performance degradation. In previous researches, the concentration magnitudes of sulphur-containing gas were all in ppm in SOFCs or SOECs which means that the formation of sulphide is slow and its amount is small in short time. It makes the surface detection by surface analysis techniques difficult. For a high concentration of SO_2 in the products of acid decomposition, identification of the sulphide formation on the electrode surface becomes possible.

In this chapter, the performance of Pt/8YSZ/Pt pellet was investigated when separating the binary gas mixtures of SO_2 and O_2 at high temperature with a carrier gas, helium (He). The main research scope was the reason for membrane performance degradation during SO_2 exposure period. Surface analytical methods such as X-ray diffusion (XRD), Raman Spectroscopy, Scanning Electron Microscopy (SEM) and Energy Dispersive X-ray Spectroscopy (EDS) were employed to characterize the electrode surface of the membrane pellet. Impedance Spectroscopy (IS) was used to observe the properties of YSZ electrolyte before and after SO_2 exposure tests.

3.2 Theory

3.2.1 Oxygen permeation through YSZ supported membranes

Oxygen permeation through YSZ supported membranes at high temperature is because of the oxygen ionic conductivity of YSZ which results from the mobile oxygen ions hopping from one oxygen occupied vacancy to another. The force of this permeation process is commonly oxygen partial pressure difference between the two sides of the membrane. Applying an electrical potential across the membrane not only provides an external electron conduction path for oxygen ions but also increase oxygen permeation flux (Toghan et al. 2010). This permeation process can be divided briefly into three processes: oxygen reduction on the cathode side, oxygen ion diffusion in the YSZ and oxygen ion oxidation on the anode side [Figure 3.1]. The external DC voltage provides electrons for the reduction and oxidation reactions. When an oxygen-containing feedstock is supplied to the cathode side of the cell, oxygen gas diffuses through the porous cathode and arrives at the gas-cathode-electrolyte interface. There, oxygen molecules are dissociated, ionized, and enter oxygen ion vacancies forming mobile oxygen in the YSZ lattice. The overall reaction is:

$$\frac{1}{2}O_2(g) + V_o + 2e^- = O_o^x \qquad \text{Reduction} \tag{3.1}$$

Once in the YSZ lattice, oxygen ions move under the force of potential gradient. The transport of oxygen ions between vacancies is moderated by the presence of an activation energy barrier. After being conducted through the YSZ electrolyte, mobile oxygen ions are recombined at the electrolyte-anode-gas interface:

$$O_o^x = 2e^- + V_o + \frac{1}{2}O_2(g) \qquad \text{Oxidation} \tag{3.2}$$
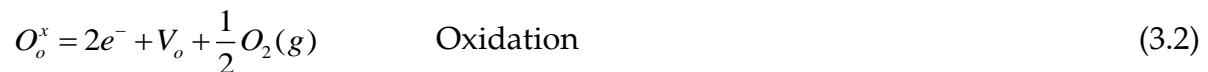
Where,

- V_o is a vacancy at a normal oxygen site in the lattice of the zirconia surface.
- $O_o{}^x$ is a mobile oxygen in a lattice site
- e^- is an electron
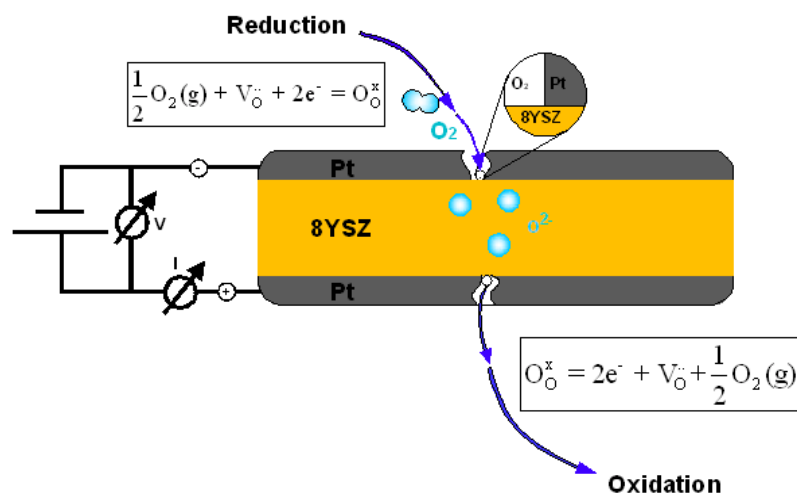
Figure 3.1: *Schematic of oxygen permeation process*

In oxygen permeation process, the key is the triple phase boundary (TPB) which is the contact area of oxygen, platinum and YSZ [Figure 3.2]. The idea of the triple phase boundary is extensively employed in the fuel cell literature, especially with respect to solid oxide fuel cells (SOFCs) and polymer electrolyte membrane fuel cells (PEMFCs). The TPB concept holds that the oxygen reduction reaction (ORR) and the ion oxidation reaction (IOR) can only occur at confined sites, called "the triple phase boundary". In general a high TPB is required for high electrochemical performance. A longer triple phase boundary enhances the electrochemical reactions and increases the cell performance (Ding et al. 2010). Kim et al. (Kim et al. 2010) claimed that the TPB length governed the cell performance especially in the activation polarization regime. Cells with a higher TPB density achieved better fuel cell performance in terms of higher power density and lower electrode impedance. However, measurement of the length of TPB is still a problem so far.

Most of the research on measurement of TPB is modelling rather than experimental. A geometrical model was developed to calculate TPB length for monosized particles in consideration of solid grain size, pore size and porosity of SOFCs electrode (Deng and Petric 2005). TPB length can be optimized by the pore size and porosity with units of m/m^4. But it is difficult to conceptualize a physical quantity with this unit.

Also this model did not account for the coordination number between the ionic and electronic conductors for a composite electrode. After a simulation by discrete element method (DEM) to model the electrode of SOFCs, an analytical model was developed to calculate TPB length (Schneider et al. 2006). The DEM was capable of modelling the composite electrode efficiently and accurately by a macroscopic/microscopic averaged description of the disordered electrode structure. However, this method was just applied to monosized particles. Janardhanan et al. reported another mathematical model to calculate the volume specific TPB length in the porous composite electrode of SOFCs (Janardhanan et al. 2008). This model was based on geometrical considerations accounting for porosity, particle diameter, particle size distribution and solid phase distribution. The results were in reasonable agreement with experimental evaluations of TPB length (Wilson et al. 2006). The model can be used for the calculation of TPB length for uniform and non-uniform particle size distribution. This method may be the most suitable for TPB length evaluation of Pt/YSZ/Pt sample used in the present research whose electrode is not monolayer and has a non-uniform particle size distribution.

Interestingly, Wilson et al. reported a new technique to obtain a complete three-dimensioned reconstruction of a SOFC electrode using dual-beam focused ion beam-scanning electron microscopy (Wilson et al. 2006). They used this data to calculate critical the volume-specific TPB length for their sample to be 4.28×10^{12} m/m^3. This technique may be a promising method in the future to calculate critical microstructural features.
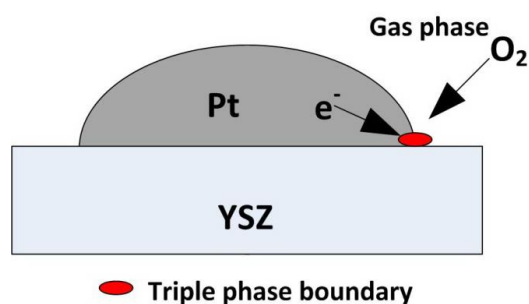
Figure 3.2: *Schematic diagram of the triple-phase boundary*

3.2.2 Oxygen permeation and current

The oxygen reduction and ion oxidation indicates a direct connection between current flow (transport of electrons in the circuit) and the oxygen mass flow rate; transport of four electron results in the conduction of one oxygen molecule. The amount of oxygen permeating n_{O2} (mol/s) can be calculated from the current I (A) and Faraday constant F (96485 c/mol):

$$n_{O_2} = \frac{I}{4F} \tag{3.3}$$

For example, for a water splitting hydrogen production process where all of the oxygen produced passed through a membrane, the production of one mole per second of H_2 (and therefore half a mole per second of O_2) would require a current of 193kA.

Therefore, the current is a linear relationship with the amount of oxygen permeating. The performance of Pt/8YSZ/Pt membrane can be evaluated by the current and the amount of oxygen permeated.

3.2.3 Surface analyses techniques

X-ray Diffraction (XRD)

X-ray diffraction (XRD) is a versatile, non-destructive technique that reveals detailed information about the chemical composition and crystallographic structure of natural and manufactured materials. The basic principle of x ray diffraction is Bragg's law which was first formulated by W. L. Bragg. It states the essential condition which must be met if diffraction is to occur.

$$n\lambda = 2d\sin\theta \tag{3.4}$$

n is an integer, λ is the wavelength of incident wave, d is the spacing between the planes in the atomic lattice, and θ is the angle between the incident ray and the scattering planes. The moving particles include electrons, protons and neutrons.

A crystal lattice is a regular three-dimensional distribution (cubic, rhombic, etc.) of atoms in space. These are arranged so that they form a series of parallel planes separated from one another by a distance d, which varies according to the nature of the material. For any crystal, planes exist in a number of different orientations - each with its own specific d-spacing. When a monochromatic X-ray beam with wavelength (λ) is projected onto a crystalline material at an angle theta (θ), diffraction occurs only when the distance travelled by the rays reflected from successive planes differs by a complete number n of wavelengths. By varying the angle theta (θ), the Bragg's Law conditions are satisfied by different d-spacings in polycrystalline materials. Plotting the angular positions and intensities of the resultant diffracted peaks of radiation produces a pattern, which is characteristic of the sample. Where a mixture of different phases is present, the resultant diffractogram is formed by addition of the individual patterns.

Using the principle of X-ray diffraction, a wealth of structural, physical and chemical information about the material investigated can be obtained. Its applications include direct phase identification, phase quantification, determination of structural data, observation of microstructural information (e.g. crystallite size and strain) and even in situ transformations.

Raman spectroscopy

Raman spectroscopy provides information about molecular vibrations that can be used for sample identification and measurement. The technique involves shining a monochromatic light source (i.e. laser) on a sample and detecting the scattered light. The majority of the scattered light is of the same frequency as the excitation source; this is known as Rayleigh or elastic scattering. A very small amount of the scattered light is shifted in energy from the laser frequency due to interaction between the incident electromagnetic waves and the vibrational energy levels of the molecules in the sample. Plotting the intensity of this shifted light versus frequency results in a Raman spectrum of the sample. Generally, Raman spectra are plotted with respect to the laser frequency such that the Rayleigh band lies at 0 cm^{-1}. On this scale, the band

positions will lie at frequencies that corresponded to the energy levels of different functional group vibrations.

Scanning Electron Microscope (SEM)

Scanning electron microscopy is a powerful technique in the examination of materials. It is used widely in metallurgy, geology, biology and medicine. It is an electron microscope that images a sample by scanning it with an electron beam. The electron beam interacts with the atoms making up the sample producing a signal that contains the sample information. The user can obtain high magnification images, with a good depth of field, and can also analyse individual crystals or other features. A high-resolution SEM image can show detail down to 25 angstroms, or better.

Energy Dispersive X ray Spectroscopy (EDS)

EDS makes use of the X-ray spectrum emitted by a solid sample bombarded with a focused beam of electrons to obtain a localized chemical analysis. All elements from atomic number 4 (Be) to 92 (U) can be detected in principle, though not all instruments are equipped for 'light' elements ($Z < 10$). Qualitative analysis involves the identification of the lines in the spectrum and is fairly straightforward owing to the simplicity of X-ray spectra. Quantitative analysis (determination of the concentrations of the elements present) entails measuring line intensities for each element in the sample and for the same elements in calibration Standards of known composition.

A high energy beam, such as X-ray, is focused into a sample. The inner atom with electron will jump to higher energy shell. At the same time, the electron on the high energy shell will fill the hole created by inner electron jump. The difference in energy between higher energy shell and lower energy shell will be released in the form of X-rays. The number and energy of these X-rays will be measured by EDS detector. The energy of the X-rays is characteristic of the atoms that produced them, forming peaks in the spectrum.

A typical EDS spectrum is portrayed as a plot of X-ray counts vs. energy (in kev).

Energy peaks correspond to the various elements in the sample. Generally they are narrow and readily resolved, but many elements yield multiple peaks. For example, iron commonly shows strong K_α and K_β peaks. Elements in low concentration will generate x-ray peaks that may not be resolvable from the background radiation. Also some peaks from different elements may overlap to a certain degree.

Impedance Spectroscopy (IS)

Impedance spectroscopy is a powerful technology used to characterize a lot of electrical properties of materials and their interface with conducting electrodes. For a sample consisting of electrolyte and electrode, a little AC voltage passes through the sample and the resulting current is measured as the frequency of the voltage varies. Afterwards, the resistance and current at that frequency will be recorded. It can measure the resistances and capacitances of bulk, grain boundary and interface of electrolyte and electrode.

The data can be plotted and interpreted in a number of ways, however a common plot is the Z* plot, where the real and imaginary components of the impedance are plotted respectively against each other. Each data point refers to the impedance at a particular AC voltage frequency. Depending on the sample and the temperature, the Z* plot generally consists of one or more arcs (see the Figure 3.3 for an example). Each of these arcs relates to an electrical component of the sample, i.e. the bulk (high voltage frequency range), grain boundary (low voltage frequency range) and electrode or the interface (lowest voltage frequency range). The width of each arc can be measured and hence the resistance of the component at that temperature concluded.

The main applications of impedance spectroscopy are characterization of materials, characterization of the electrical response of high resistivity ionic and dielectric solid materials by immittance spectroscopy, study of solid state devices, investigation of electrode corrosion problems and electrochemical power sources such as batteries and fuel cell (Barsoukov and Macdonald 2005).
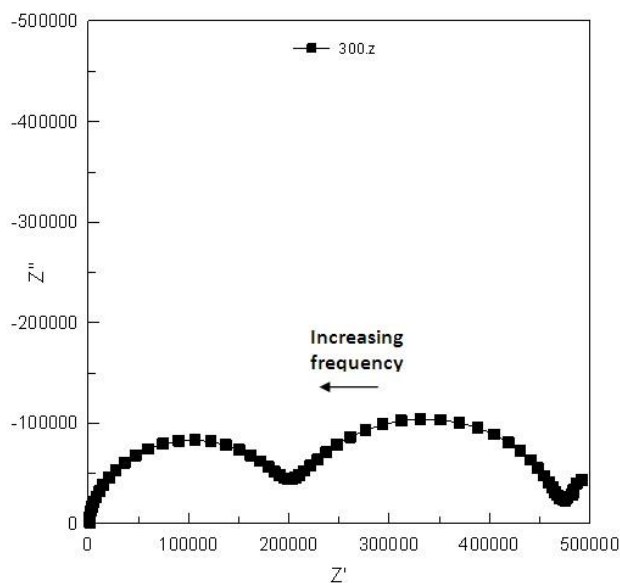
Figure 3.3: *Z* plot for the Pt/8YSZ/Pt pellet at 300˚C, full frequency range of 5Hz - 1.3MHz is shown.*

3.3 Experimental

3.3.1 Preparation of Pt/8YSZ/Pt membrane pellet

8 mol% Yttria-stabilized zirconia (8YSZ) pellets, around 24mm diameter and 2mm thickness, were prepared by The Department of Materials Science and Engineering, University of Sheffield. The disks were produced by compressing 8 mol% yttria YSZ nanopowder (Sigma-Aldrich) in a metal die. The resulting "green" disks were then sintered at 1400°C, producing solid gas-tight ceramic disks of near 100% density.

Platinum ink supplied by Gwent Electronic Materials Ltd. was applied manually on the each face of a YSZ pellet. The pellet was then sintered at 1200˚C for 15 minutes. Afterwards, a membrane with 8YSZ as the electrolyte and platinum as the electrode was made. The preparation procedure of the membrane pellet was introduced in detail in the thesis (Atkin 2009). In this way, the thickness of porous platinum layer was around 10 µm by the SEM image of the membrane pellet [Figure 3.4-3.5].
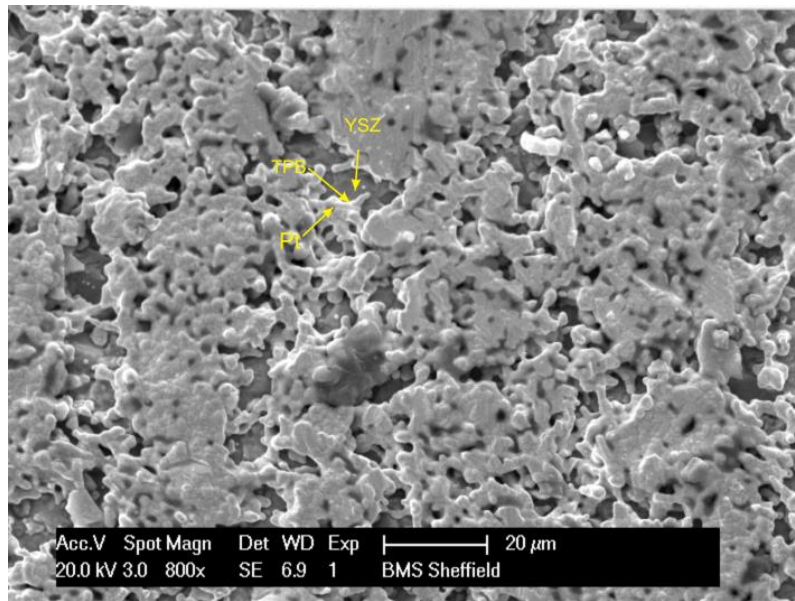
Figure 3.4: *SEM image of a Pt/8YSZ membrane pellet surface, the magnification is 800x*
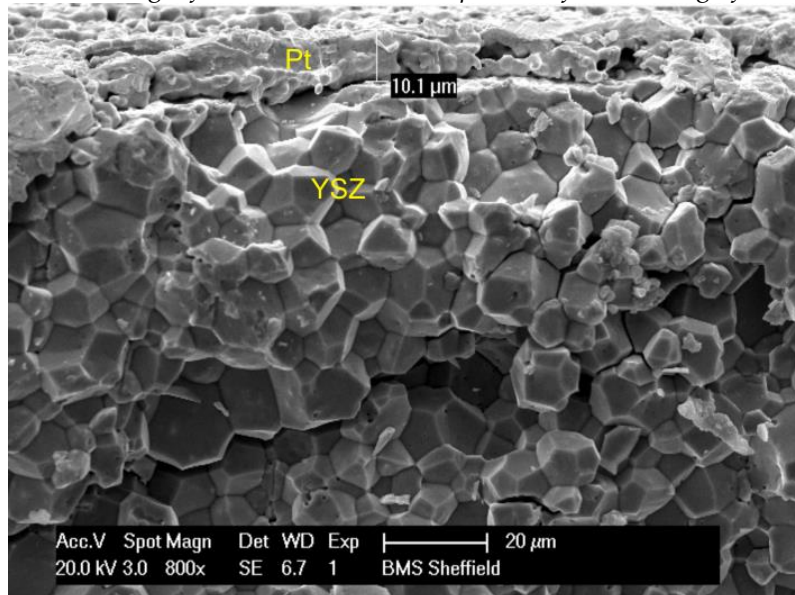
Figure 3.5: *SEM image of a Pt/8YSZ membrane pellet cross section, the magnification is 800x*

3.3.2   Components of oxygen permeation assembly

Tubular furnace

The high temperature is achieved using a Carbolite MTF12/38/250 tubular vertical furnace (Keison Product) which has a worktube of 300mm and 38mm diameter of the inner wall. Its maximum operating temperature is 1200°C and the rate of temperature rise also can be controlled.

The furnace was calibrated in the high temperature range using a K type thermocouple. The relationship between the furnace set point and real temperature was shown in Figure 3.6. The temperature at 700, 800 and 900°C became stable after around 5 minutes. The difference between the three furnace set points and real temperatures was small (686.4/700°C, 788.4/800°C and 887.9/900°C).
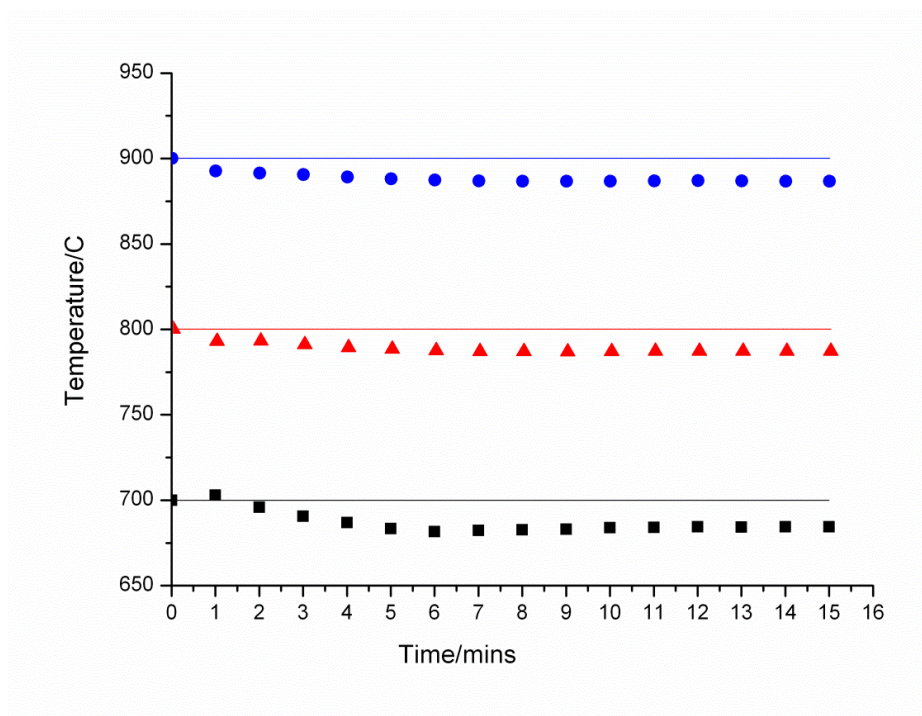
Figure 3.6: *Difference of the furnace setpoint and the real temperature at 700, 800 and 900 ℃*

Oxygen analyser

The 5200 Multi-Purpose Oxygen Analyser is a light weight gas analyser, suitable for the needs of laboratory analysis, and light industrial users who require fast, accurate and reliable gas analysis. The Multi-Purpose uses paramagnetic transducers to determine the oxygen content of gas samples in concentrations up to 100%. Gas sample measurements are shown on the display, and can also be output to a PC connected to the analyzer. The analyser needs to be calibrated before measurement using streams of pure oxygen (100%) and pure helium (0).

Membrane pellet holder

The membrane pellet holder was made from pure quartz which can withstand high

temperature up to 1000˚C in the presence of high concentrations of oxygen and sulphur dioxide. The designed holder consists of two identical halves and was fabricated by the glass-blowing service of the Department of Chemistry in the University of Sheffield [Figure 3.7]. The inlet tubing accepts a Tygon tube passed through the cold gas feed, while the outlet tube connects a length of quartz tube with a female ground glass joint for cooling purpose. The cold gas mixture enters from the inlet, passes through the curved quartz tube for pre-heating and finally meets the membrane pellet in the centre of furnace at high temperature. The design of the membrane holder was derived from heat transfer calculations and a FLUENT simulation (Atkin 2009).
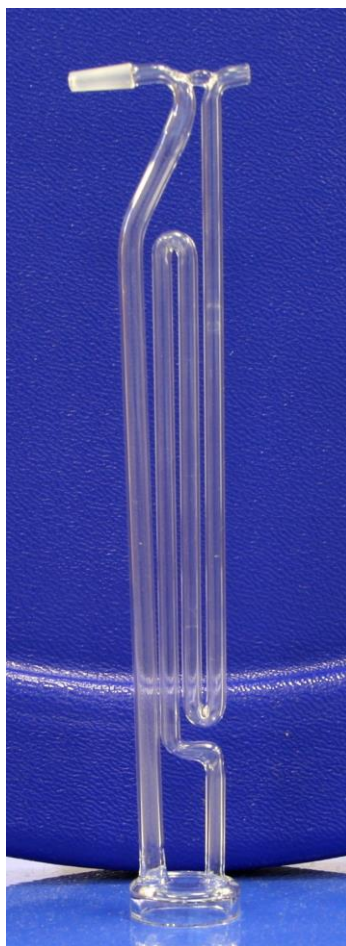
Figure 3.7: *Quartz membrane holder for oxygen permeation experiment*

Other components of the assembly

Other components in the assembly are

- Two supports made from grade 310 stainless steel and two stands made from standard steel. Supports were provided with four legs and stands had four holes, allowing the membrane to be located in the centre of a vertical tubular furnace. A weight (one of the stands) was placed on the top of a support, providing sufficient compressive strength to positively seal the membrane to the quartz holder.

- Two gold ring gaskets located between membrane holder and membrane pellet

- An external dc power supply whose positive port was connected to one of legs of the lower membrane support in permeate side, negative port was connected to the upper support in feed side.

More detail can be found from Atkin's thesis (Atkin 2009).

3.3.3 Schematic diagram of experimental apparatus

In Figure 3.8, gas mixture composed of SO_2, He and O_2 (supplied by BOC) passes through a pre-heating tube (upper membrane holder) to meet the membrane pellet in the centre of the furnace. Oxygen permeated through membrane to the permeate side because of oxygen ionic conductivity of the YSZ electrolyte at high temperatures, while SO_2 and He could not, exiting to fume cupboard through the outlet of the upper membrane holder. The concentration of permeated oxygen in helium was measured by the oxygen analyser and recorded every two seconds by a PC. Helium in the feed side and the permeate side was used as a carrier gas. An external dc power supply was connected to membrane pellet by attaching to membrane supports. Current change with time was recorded every three seconds by the PC.
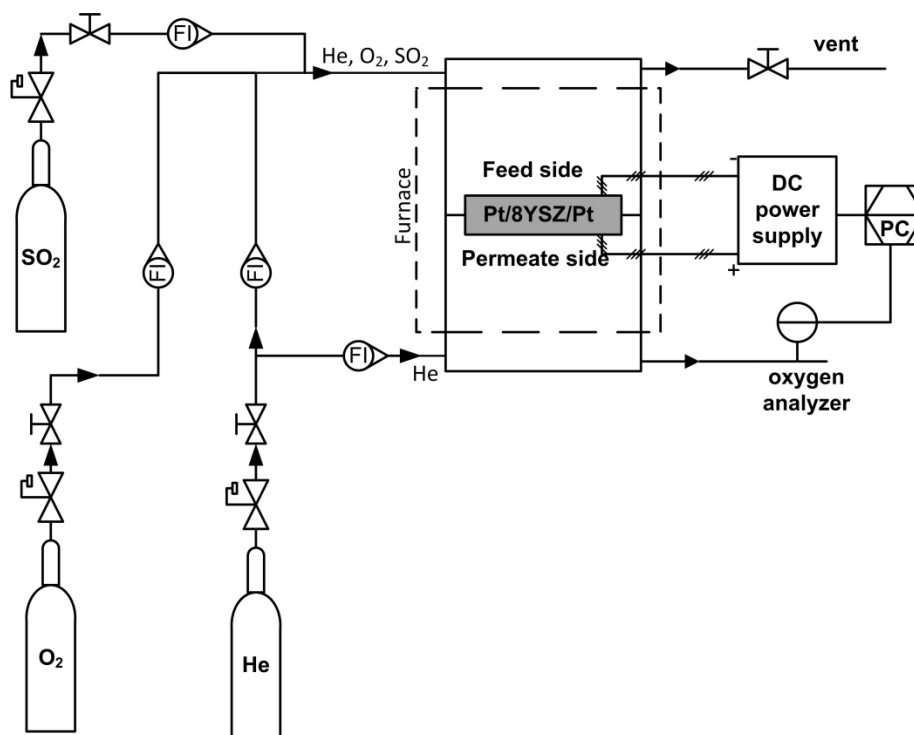
Figure 3.8: *Schematic diagram of experimental apparatus*

3.3.4 Characteristic of membrane performance

A sketch of the experimental setup is shown in Figure 3.8. When the furnace temperature reached 850°C at a ramp rate of 5°C/min, gas mixtures composed of oxygen (5ml/min) and helium (45ml/min) were passed through an upper membrane holder for pre-heating before reacting with the membrane at 850°C. An external voltage of 1.5V was applied. Current flow and oxygen concentration on the permeate side were measured. After around 1-hour of steady state membrane performance, the composition of the feed stream was changed to oxygen (5ml/min), helium (30ml/min) and sulphur dioxide (15ml/min). Oxygen still permeated through the membrane to the anode side while helium and sulphur dioxide did not. The oxygen permeate concentration in carrier gas (pure helium) was measured by the oxygen analyzer and recorded by a computer. The maximum theoretical value of oxygen concentration was calculated based on the current to assess the real result of oxygen concentration measured by the oxygen analyser.

What should be noted is that the current is derived from the electrical conductivity of the whole circuit and ionic conductivity of YSZ electrolyte. The contribution of YSZ

electrolyte electrical conductivity to the measured current also can be calculated.

West (1999) presents that the electrical conductivity σ of YSZ at 850˚C is 0.0211S/cm. Given the membrane face area A (cm²) and thickness L (cm), the conductance G of the membrane can be calculated. For example, the conductance is as follows for the membrane of radius 0.9cm and thickness 0.2cm:

$$G = \frac{\sigma A}{L} = \frac{0.0211 \times (\pi \times 0.9^2)}{0.2} = 0.2683\Omega^{-1}$$

The membrane resistance is the inverse of the conductance, that is 4.72Ω. The whole resistance including membrane resistance and external circuit resistance at 850˚C was around 5.20Ω. Therefore, the contribution of 8YSZ electrical conductivity to the measured current at external voltage of 1.5V is around 250mA.

During the whole run, the overall flow rate of the feed stream was 50ml/min and oxygen accounted for 10%. All the flow rates were controlled by rotameters (standard accuracy: 5% of full scale). The run involved 1 hour SO_2 free period (feed: O_2 and He) and 2 hours SO_2 exposure period (feed: O_2, He and SO_2) with a constant external DC voltage of 1.5V. For an example, the first two graphs in Figure 3.9 shows the operating conditions of the feed gas and external voltage change.

Without external voltage, the oxygen can also permeate through the membrane by the oxygen partial pressure difference between the cathode and the anode sides. In order to counteract the effect of oxygen partial pressure difference, two zero-voltage circuit periods (2 minutes long each) were applied in the experiment. The current and oxygen concentration corresponding to zero voltage were subtracted from the raw data in order to give the corrected values showing only the effect of external voltage on oxygen permeation.

This run was repeated using the same conditions and a different membrane. The results of current and oxygen concentration change with time were shown to be the same as the graphs in the first run.

Before and after the first experiment, impedance of the membrane pellet was

measured by a Solartron 1250 impedance analyser by sweeping the frequencies in the range of 65535Hz to 0.1Hz. The cell used in the second run was analysed before and after SO_2 exposure test by surface analysis techniques including: x-ray diffraction (XRD) with a diffractometer (D500, Siemens, Germany), using Cu Ka1 radiation (λ=1.5406A) with a step of 0.02° (2θ) and a scanning rate of 2° min-1, to detect any possible structural change; Raman spectrometer (R3000, Agiltron Inc) with excitation wavelengths 785nm to study the Raman scattering of monochromatic light from a laser. Scanning electron microscopy (SEM) using a JEOL JEM-2010F microscope equipped with an Oxford Instruments ultrathin window Energy Dispersive x-ray detector to get information about the sample's surface topography and element composition. Another fresh membrane pellet was imaged by SEM as well to compare the surface morphology of the membrane after SO_2 exposure process.

3.4 Result and discussion

3.4.1 Membrane performance in SO_2 exposure period

As shown in Figure 3.9, the current and oxygen concentration permeated through membrane pellet were recorded with time including two periods: SO_2 free period and SO_2 exposure period. What is more, the maximum theoretical oxygen concentration was calculated through current, the fourth graph in Figure 3.9. The oxygen permeated concentration after subtracting the contribution of oxygen partial pressure difference in the zero-voltage circuit period is shown in the bottom graph.

When applied voltage is zero, the positive effect of external voltage on oxygen permeation process was gone. However, there was still small current in the closed circuit. It is resulted from the oxygen ion diffusion process by the oxygen partial pressure difference between feed and permeate sides. This phenomenon is very common in SOFCs and oxygen sensors.

From the current and oxygen concentration, oxygen could permeate through membrane pellet from the feed side during the whole process. In particular, the current and oxygen concentration increased with time and tended to be stable during during the first hour (feed: O_2 and He). It may be attributed to cathode activation, as observed by many researchers during the initial period of cell operation (Jiang et al. 1999) (Zha et al. 2007). Once sulphur dioxide (15ml/min) was introduced to the cathode side from the beginning of the second hour, the cell performance degradation, inferred from a large current and oxygen concentration drop, occurred on a timescale of order seconds, referred to as type I degradation. This was followed by a slow but continuous degradation on the order of minutes, referred to as type II degradation. The degradation process of membrane performances here was similar to previous studies (Li et al. 2010) (Lussier et al. 2008) (Zhai et al. 2010). It is usually thought that the type I degradation is due to the adsorption of sulphur dioxide which occurs within a timescale of seconds (Zha et al. 2007). In this case, the electrode active sites are covered by adsorbed sulphur species. The charge transfer resistance across the cathode layer increases, leading to the rapid and severe cell

performance degradation. Sulphur dioxide adsorption on electrode surface blocks the active sites for oxygen adsorption, oxygen dissociation and the electrochemical reaction.

However, SO_2 adsorption at higher temperatures is not stable. It can be desorbed nearly completely as SO_2 with desorption maxima occurring at 400, 480 and 580K (Astegger and Bechtold 1982). In the case of a membrane pellet exposed in the environment of SO_2-O_2-He, SO_2 adsorption at 1123K on platinum should not be obvious. Another possible reason for type I degradation is the reaction of oxygen and sulphur dioxide in the presence of platinum as a catalyst (Astegger and Bechtold 1982) (Streber et al. 2010). But this reaction should be very slow according to thermodynamic simulation by HSC 5.0 Chemistry (log K= -0.296 at 850°C according to Eq. 3.5). Therefore, a small amount of SO_3 by the reaction of SO_2 and O_2 could not affect significantly the concentration of oxygen in feed decrease, slows the oxygen reduction on the cathode side.

$$SO_2(g) + 0.5O_2(g) \xrightarrow{\text{without catalyst}} SO_3(g)$$

$$(3.5)$$
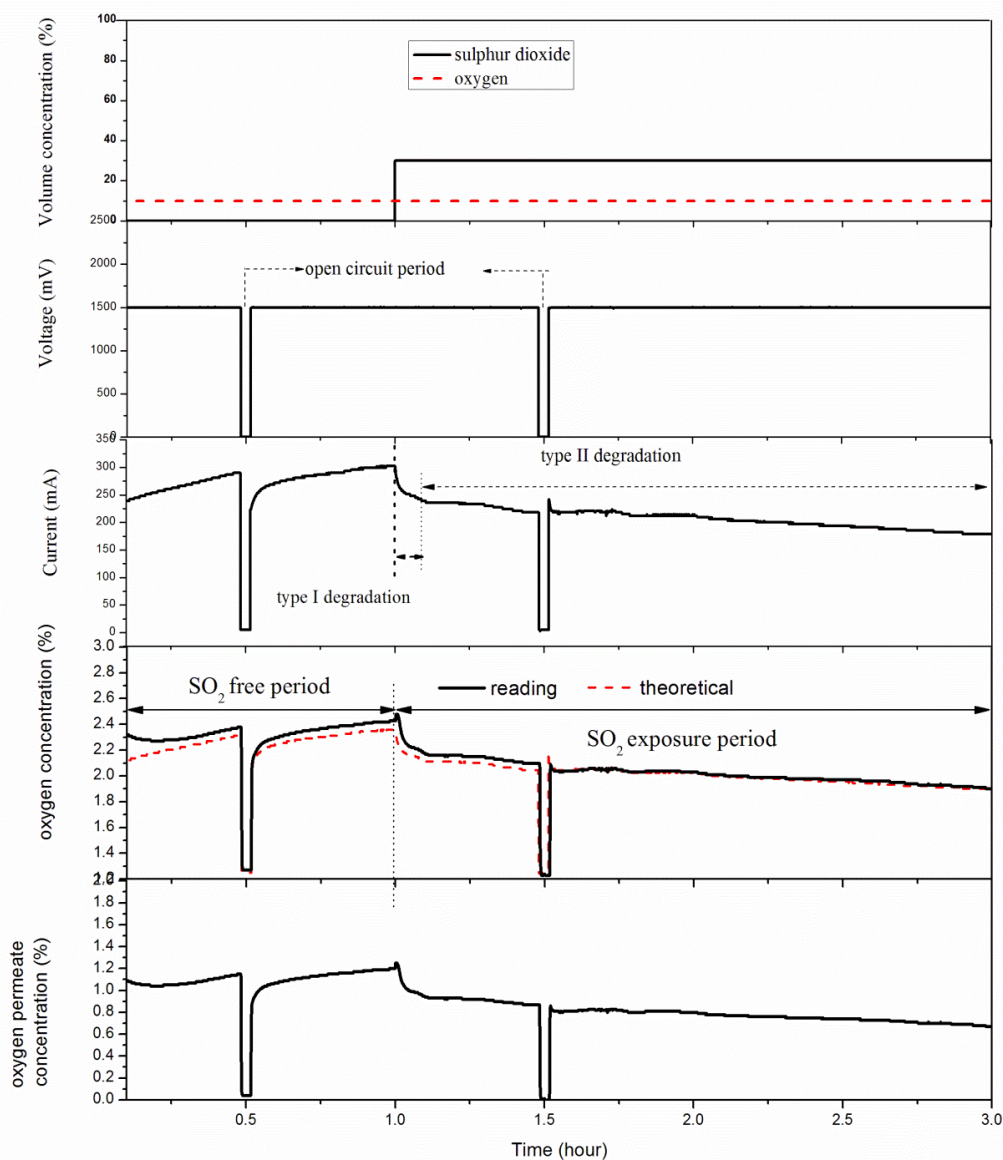
Figure 3.9: *Experimental results of Pt/8YSZ/Pt membrane pellet performance with SO₂ free period and SO₂ exposure period at 850°C*

3.4.2   Impedance spectroscopy for YSZ electrolyte

To assess type II degradation, the impedance and the frequency dependence of capacitance of Pt/8YSZ cell before and after SO₂ exposure were measured at 306°C in air [Figure 3.10-3.11]. Z* plot exhibits two semi-circular arcs, the first small arcs at the high frequency region are commonly attributed to the solid electrolyte, and the large

semicircle at the high Z´ region can be assigned to the response of the Pt/YSZ interface [Figure 3.10]. The measured impedance spectrums were fitted with the equivalent circuit consisting of two RC elements, R_1C_1 and R_2C_2, in series with an element R_0 [Figure 3.12]. R_0 could be a sum of ohmic resistors. R_1C_1 element corresponds to the first small semicircular arc in the high-frequency regime. The second element R_2C_2 corresponds to the second semi-circular arc at medium frequencies, in relation to the electron transfer at the interface of electrolyte and electrode. R_2 represents the interfacial resistance. The impedance (R_1) and capacitance (C_1) in high frequency range show no significant change, before and after SO_2 exposure tests. The second impedance arc (R_2) is bigger after SO_2 exposure test [Figure 3.10], but the capacitance (C_2) did not have any change [Figure 3.11]. This suggests that the membrane performance degradation in SO_2 exposure period may be not due to the electrolyte but to the interface between the cathode and electrolyte. If it was the case, it would tie in with the appearance of the results of surface analysis such as XRD, SEM-EDS and Raman spectroscopy.
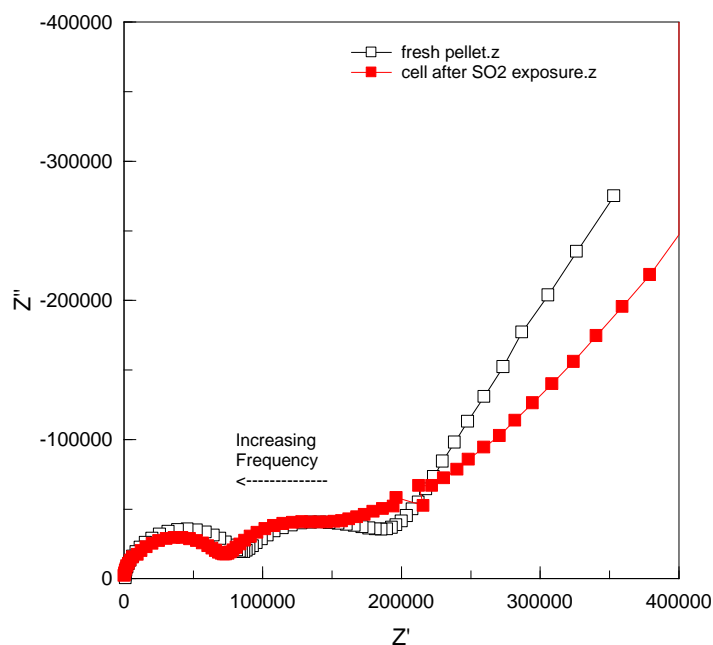
Figure 3.10: *Z* plot for YSZ/Pt at 306°C before and after SO₂ exposure*
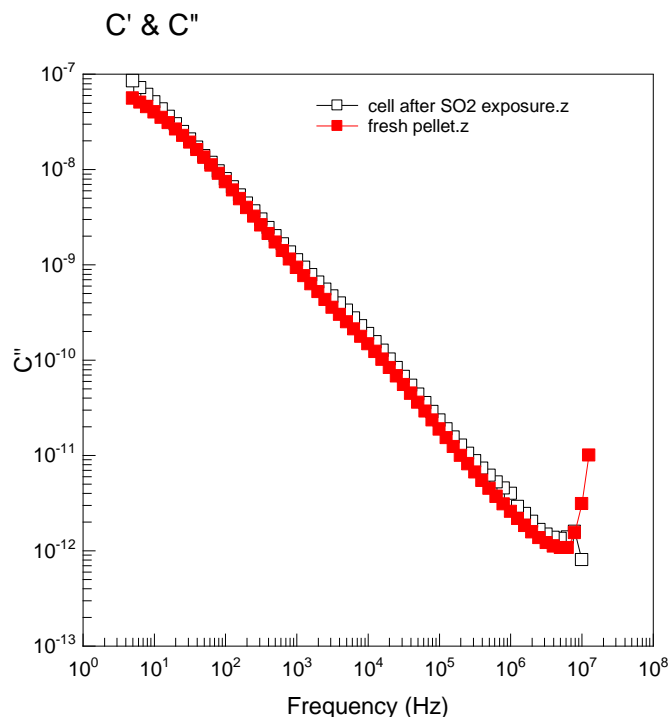
Figure 3.11: *The frequency dependence of the capacitance plot for YSZ/Pt at 306°C before and after SO$_2$ exposure*
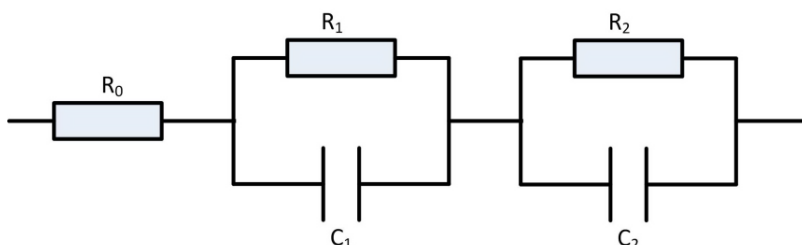
Figure 3.12: *Equivalent circuit for Pt/8YSZ/Pt pellet*

Under the same operating conditions, the first run was repeated using another new YSZ cell. The experimental results including current and permeated oxygen concentration change with time are shown in Figure 3.13 in the same format as in the first run in Figure 3.9. During the SO$_2$ free period (He-O$_2$), the current and permeated oxygen concentration increased slowly with time and approached a constant value at 380mA, which was different from the first run at the same voltage of 1.5V. This may be attributed to the different interface resistances of the membrane. This interface resistance is caused by the interspace between Pt layer and YSZ surface, which affects overall resistance and leads to varying currents at constant voltage. Another

reason is that different YSZ pellets have different resistances. This cannot be avoided using this YSZ pellet preparation method and for the Pt electrode layer coating manually. However, it should be noted that this study examines only the effect of SO_2 poisoning on membrane performance, which can be obtained by comparing the observation of membrane cell before and after SO_2 poisoning. Like the phenomenon found in the first run, current and oxygen concentration had a sudden drop after SO_2 introduced into feed, then decreased slowly and continuously in the rest of SO_2 exposure period.
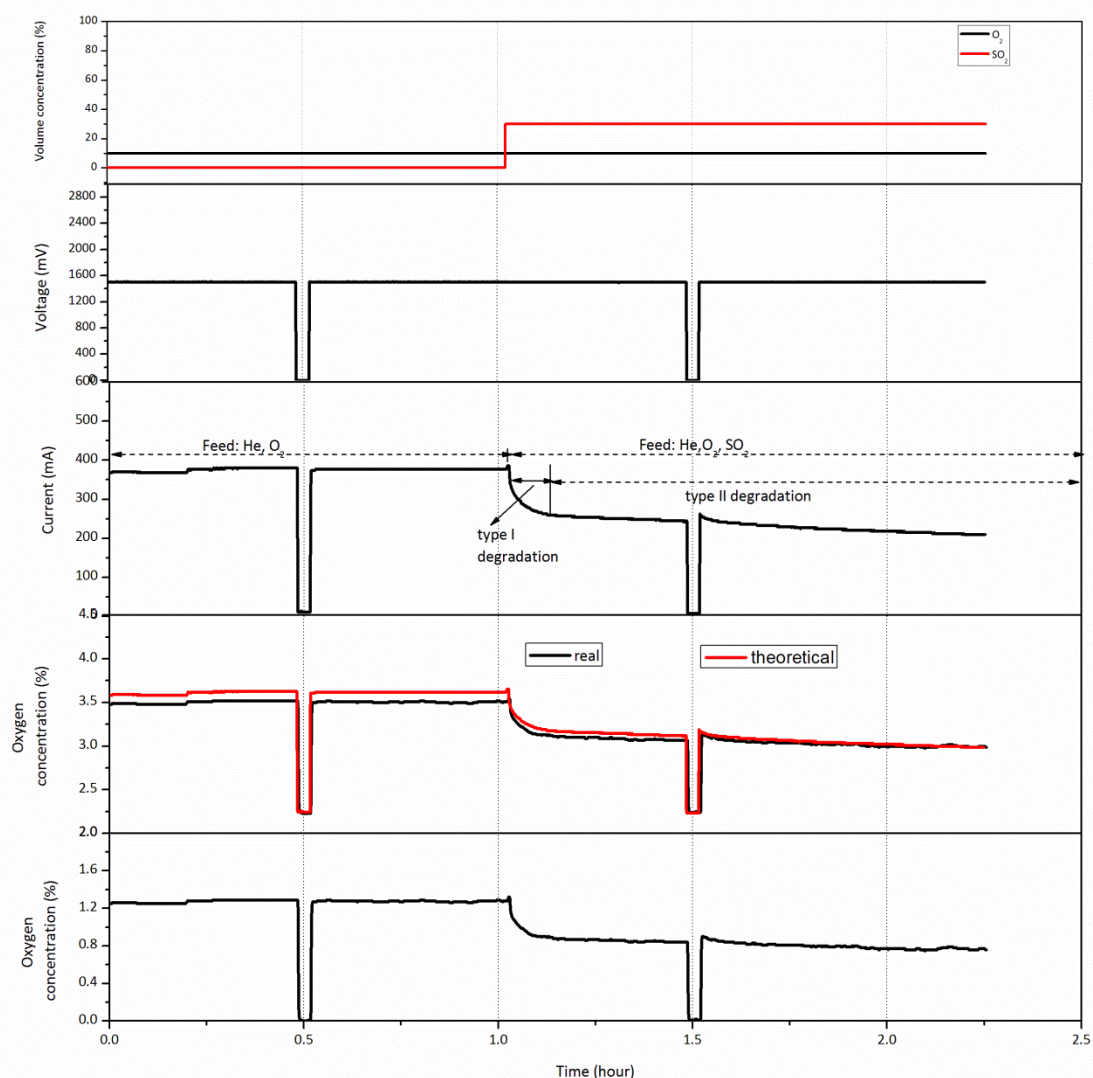
Figure 3.13: *Experimental results of Pt/8YSZ membrane performance exposed to SO_2 at 850℃, the 2nd run.*

3.4.3 Surface analysis for Pt electrode surface

According to the discussion above by impedance spectroscopy, membrane performance degradation in SO_2 exposure period may be due to changes in the electrode. In this case, one hypothesis is that metal sulphide might be formed on the electrode surface, which leads to long-term and slow performance degradation. 15ml/min of SO_2 in feed (overall flowrate was 50ml/min) was much higher than the concentration of sulphur-containing impurity gas (magnitude: ppm) in previous research in SOFCs and SOECs, which makes the sulphidation reaction of platinum with sulphur dioxide more likely.

At the same time, PtOx may be also observed on the platinum surface even if the amount is small (Tsaofang et al. 1991) (Chaston 1964). However, PtOx may not reduce electrode activity sites and decrease the triple-phase boundary (TPB) perimeter and not lead to the electrode poisoning and degradation of membrane performance, according to the electrochemical reactions (Tsaofang et al. 1991).

$$Pt + xO_{ad} \rightarrow PtO_x \tag{3.6}$$

$$PtO_x + 2xe + xV_o \rightarrow Pt + xO \tag{3.7}$$
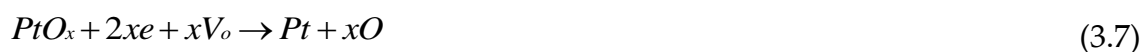
O_{ad} is an oxygen atom adsorbed on the Pt or YSZ surface; V_O is a vacancy at a normal oxygen site in the lattice of the zirconia surface, e is an electron, and O is a mobile oxygen in a lattice site of YSZ.

Raman Spectroscopy

The membrane pellet used in the second run was analysed using a Raman spectrometer equipped with a CCD detector. Raman spectra were obtained in Figure 3.14 and Figure 3.15. For the pellet before the SO_2 exposure process in Figure 3.14, a three-peak Raman feature near 1400cm-1 was found which may be attributed to a type of zirconium bond (Baklanova et al. 2006). Figure 3.15 shows the Raman spectra of the cathode surface after SO_2 exposure. The peak at 1400cm-1 disappeared, and there seem to be a broad peak, not obvious, near 300 cm-1 observed at room temperature, which may be PtS (Merkle et al. 1999). The disappearance of the

three-peaks near 1400cm-1 for the pellet treated by SO_2 exposure indicates that the cathode surface was changed after SO_2 exposure. This change could be due to a new compound layer formed on the cathode surface during the SO_2 exposure period.
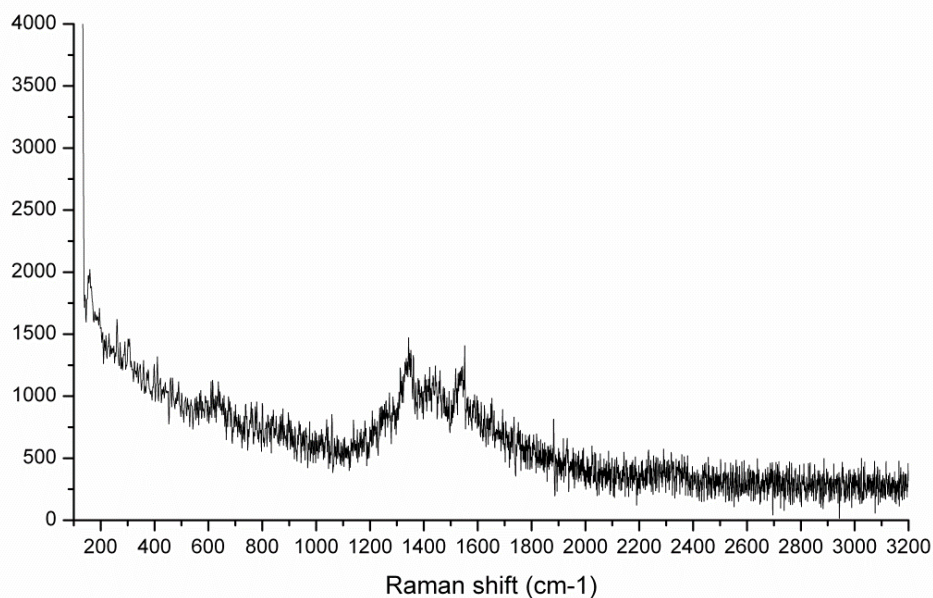
Figure 3.14: *Raman spectrum for 8YSZ/Pt membrane before SO_2 exposure at 850℃, feed side*
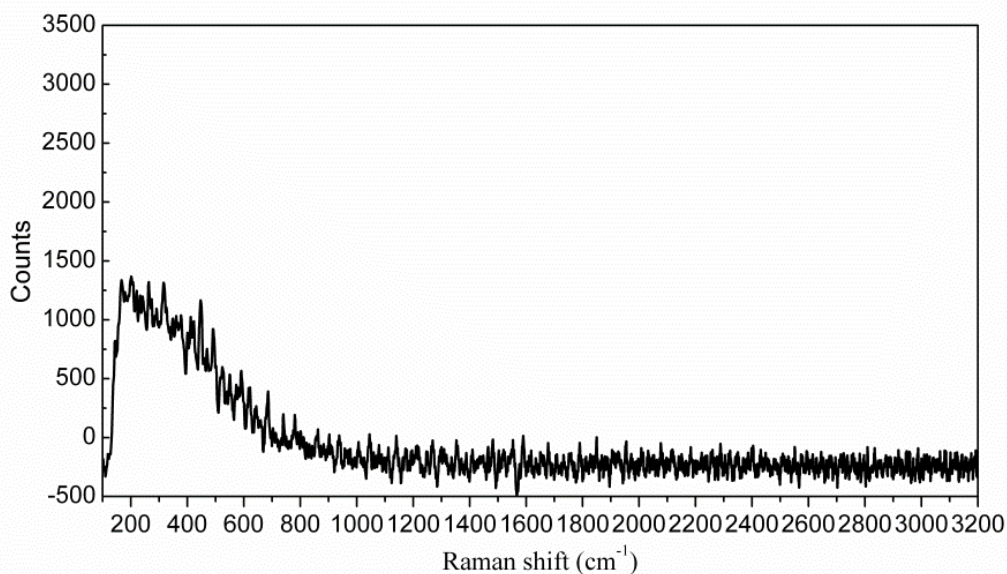
Figure 3.15: *Raman spectrum for YSZ/Pt membrane after SO_2 exposure at 850℃, feed side*

SEM-EDS Analysis

The pellet was also analysed by SEM-EDS. Figure 3.16 shows the porous structure of the cathode surface of the fresh pellet before the SO_2 exposure process, which creates the triple phase boundary of oxygen, platinum and YSZ and enables the oxygen diffusion and reduction. Also the picture shows that the thickness of platinum layer is not even. The elemental analysis at the point 1 was also conducted by EDS plot in Figure 3.17 which shows that there is only platinum on the electrode layer. Moreover, the elemental analysis for the point in the thin area of the electrode layer was done as well. Beside platinum, three new elements of oxygen, zirconium and yttrium were found [Figure 3.18b], which come from the electrolyte made from YSZ.

For the pellet after two hours SO_2 exposure process, the morphology of the cathode surface was similar to that of fresh pellet except that the colour of the electrode became dark [Figure 3.19]. Platinum, silicon and oxygen were detected in the EDS spectrum 1, without elemental sulphur [Figure 3.20]. The silicon and oxygen might be due to the devitrification of the surface of quartz tube made from silicon dioxide at high temperature, then gaseous silicon dioxide adsorbed on the electrode surface. This hypothesis is supported by the observation that the quartz tube was not transparent and its surface appeared white, sparkling and desquamate phenomenon after the experiment [Figure 3.21].

However, sulphur was found in the spectrum 2 when the analysis point changed to the thin area of the electrode layer [Figure 3.22]. The occurrence of sulphur in spectrum 2 indicates that the interaction between sulphur dioxide and platinum on YSZ may be occurring at the inner layer of electrode, even at the TPB boundary. A new membrane pellet sample treated by SO_2 exposure as previously was analysed by SEM-EDS. In the area of thin electrode layer, more sulphur was observed [Figure 3.23].

Overall, after an SO_2 exposure period, a small amount of sulphur was detected at the inner electrode layer or TPB boundary where the reaction of sulphur and platinum or YSZ occurred. This might be able to explain why the membrane performance degraded gradually after SO_2 introduction.
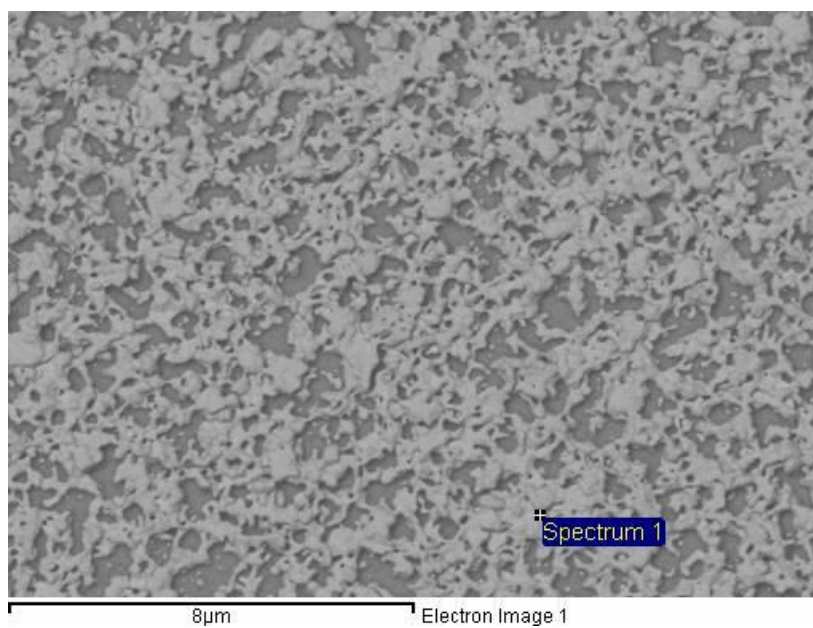
Figure 3.16: *SEM image of a fresh Pt/8YSZ pellet*
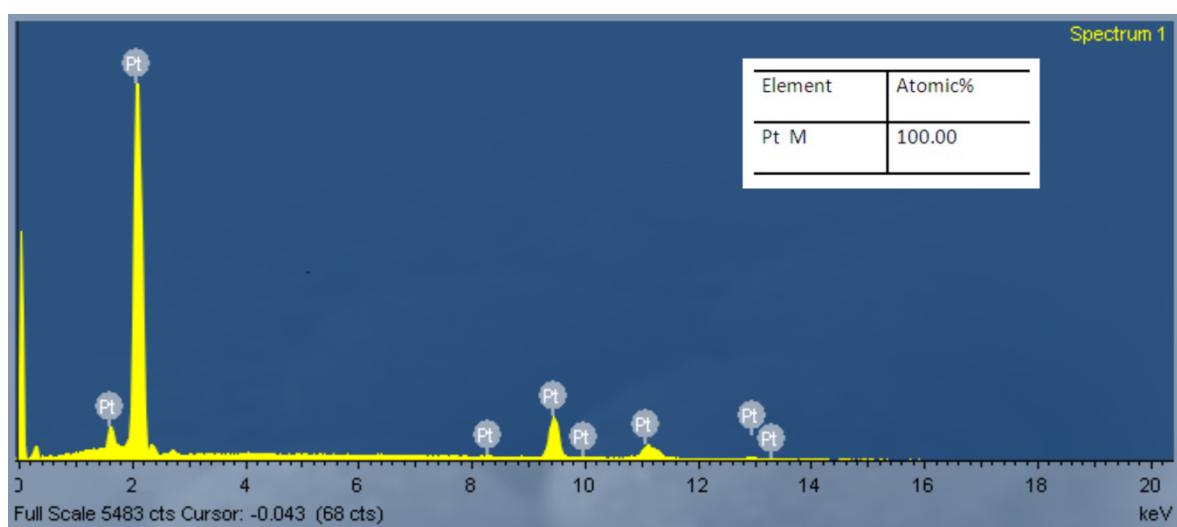
Figure 3.17: *EDS elemental analysis spectrum of a fresh Pt/8YSZ pellet*
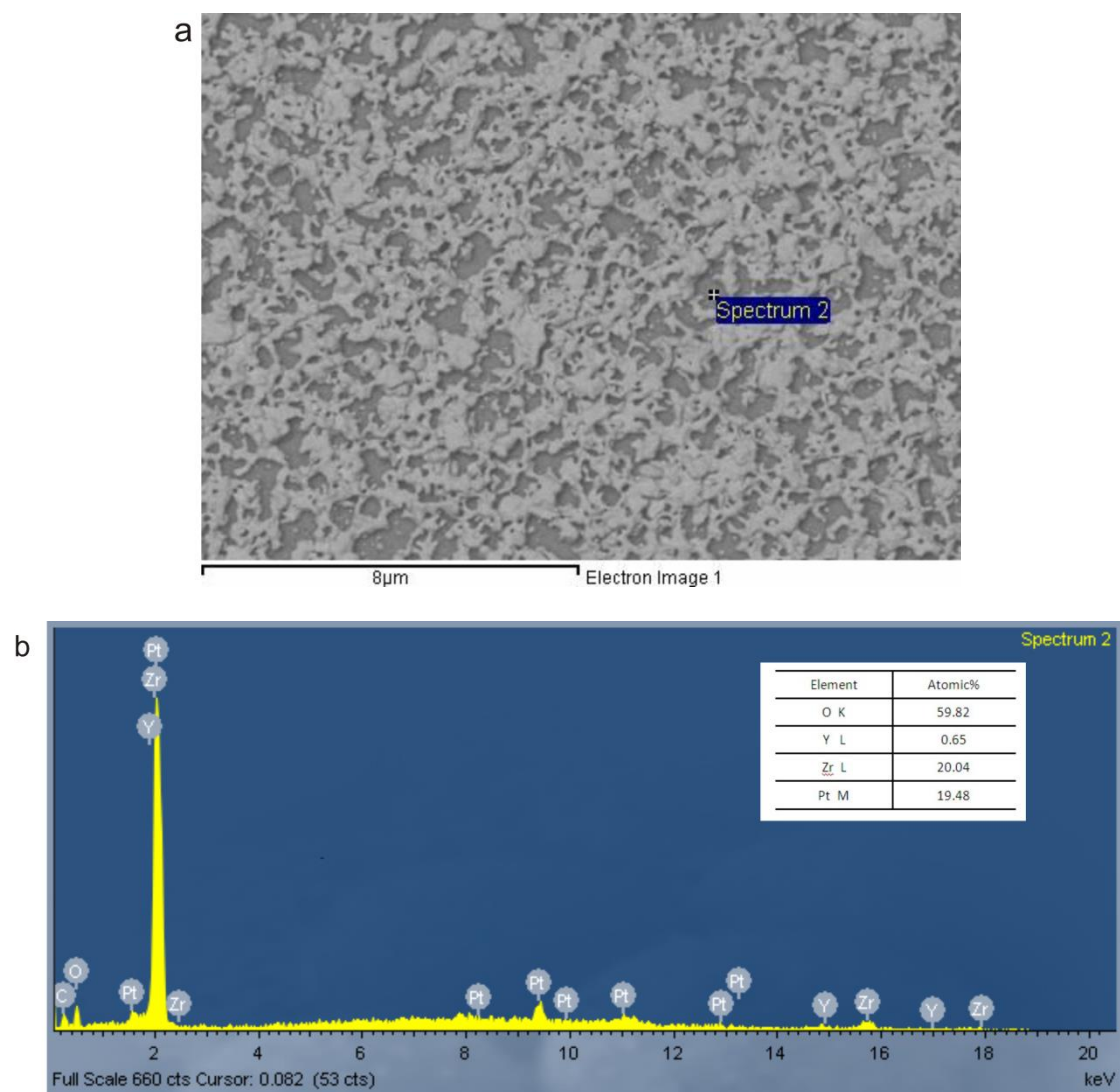
Figure 3.18: *EDS element point analysis for fresh pellet: SEM image (a) and EDS spectrum (b)*
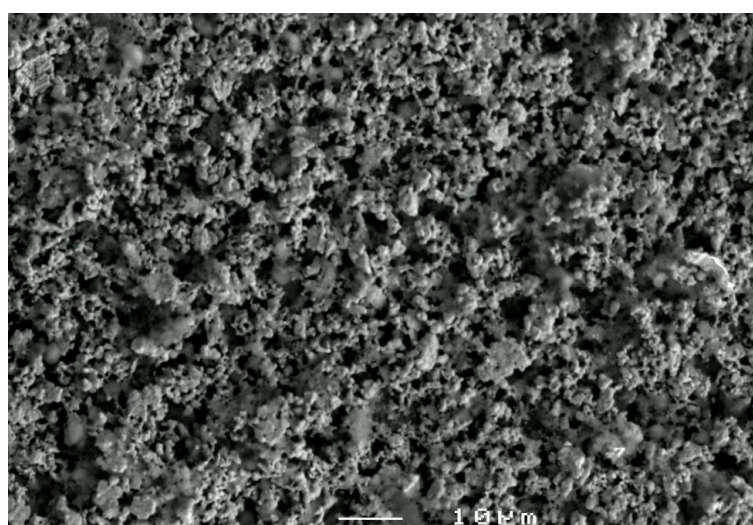
Figure 3.19: *SEM image of the cathode surface of the pellet exposed by SO$_2$*
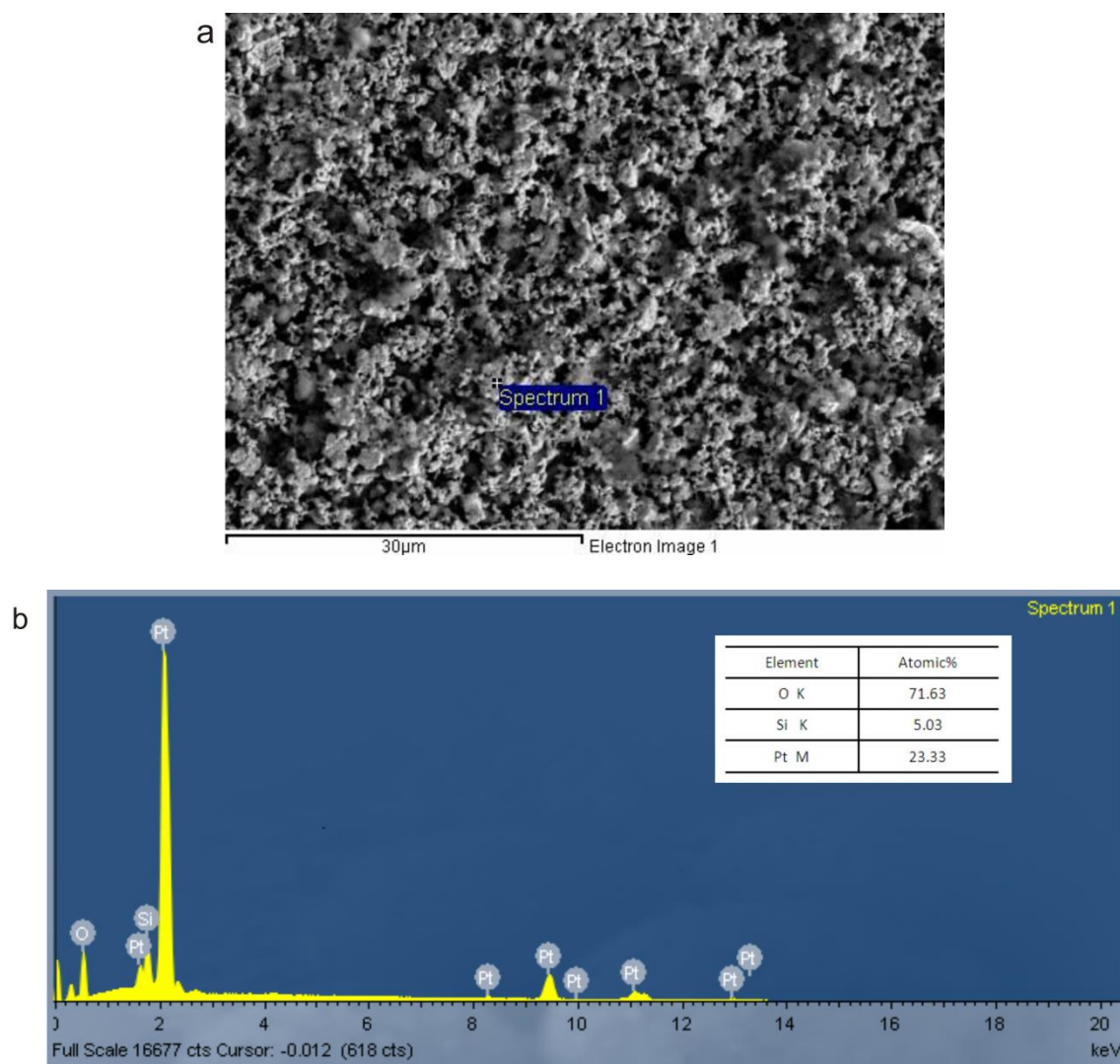
Figure 3.20: *EDS elemental point analysis for the pellet treated by SO₂ exposure: SEM image (a) and EDS spectrum (b)*
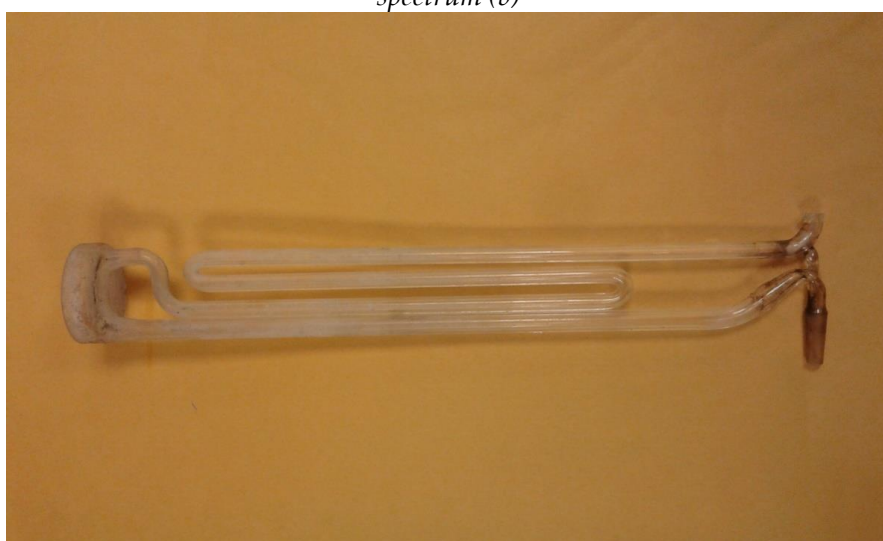
Figure 3.21: *Membrane holder after SO₂ exposure test at 850°C*
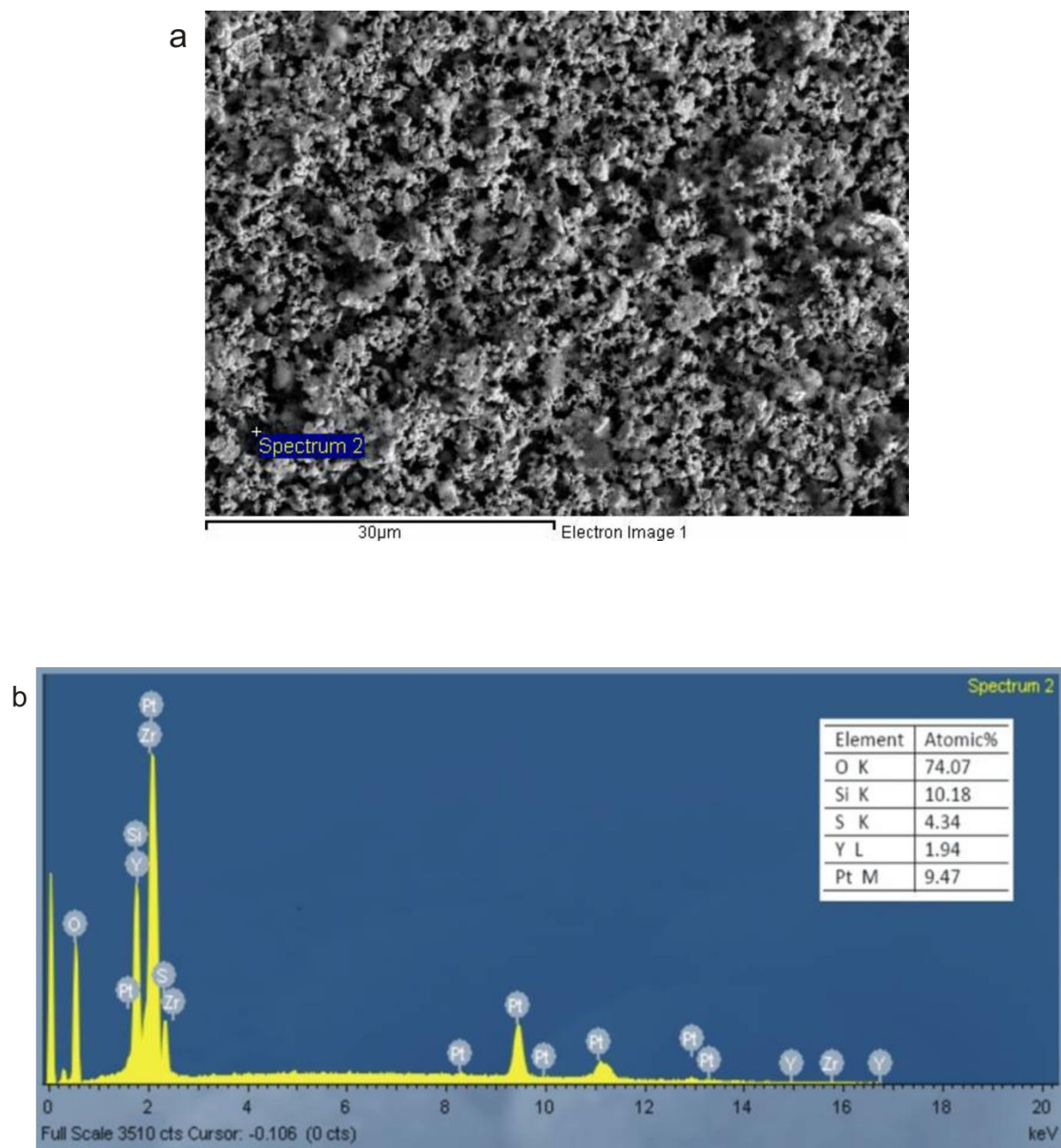
Figure 3.22: *EDS elemental point analysis for the pellet treated by SO$_2$ exposure: SEM image (a) and EDS spectrum (b)*
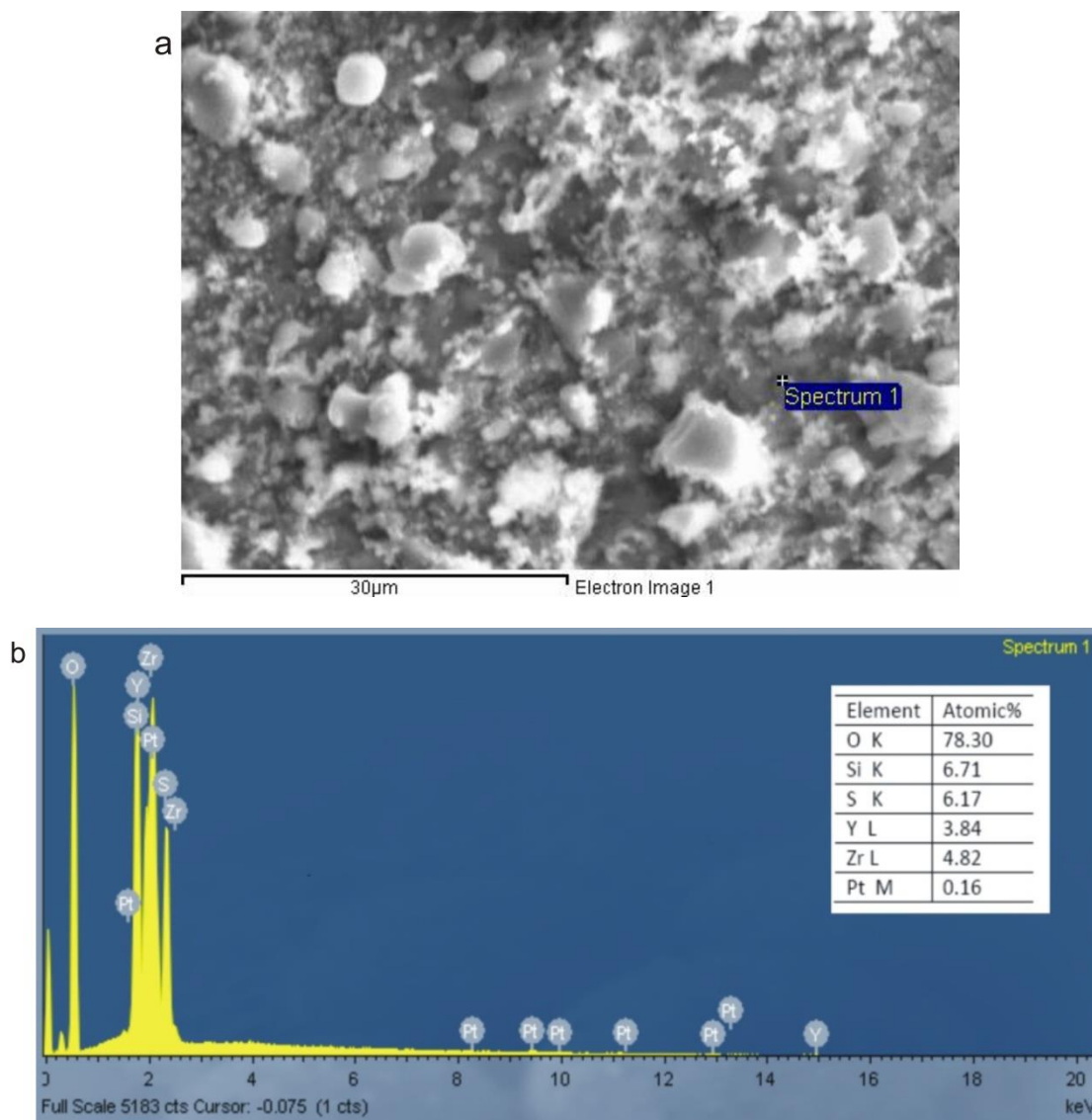
Figure 3.23: *EDS elemental point analysis for a new pellet treated by SO$_2$ exposure: SEM image (a) and EDS spectrum (b)*

XRD Analysis

X-ray diffraction spectra were obtained for the feed side of the pellet after SO$_2$ exposure [Figure 3.24]. The spectra were compared to those recorded for an unused pellet (line A). No crystal structure change for YSZ was observed after the SO$_2$ exposure. With the discolouration of the electrode, a lot of new additional peaks were found in the spectrum after experiment (line B). Searches for suitable IGDD cards found that these additional peaks are most likely caused by the presence of PtS which was also detected by He (He et al. 2002) when a Pt anode was exposed to gas mixtures of H$_2$S-O$_2$. The presence of a PtS layer on the feed surface of pellet suggests

that the Pt active sites on the cathode were decreased and the resistance of oxygen diffusion and permeation was increased. Finally, a PtS layer could contribute to the performance decrease during SO_2 exposure.
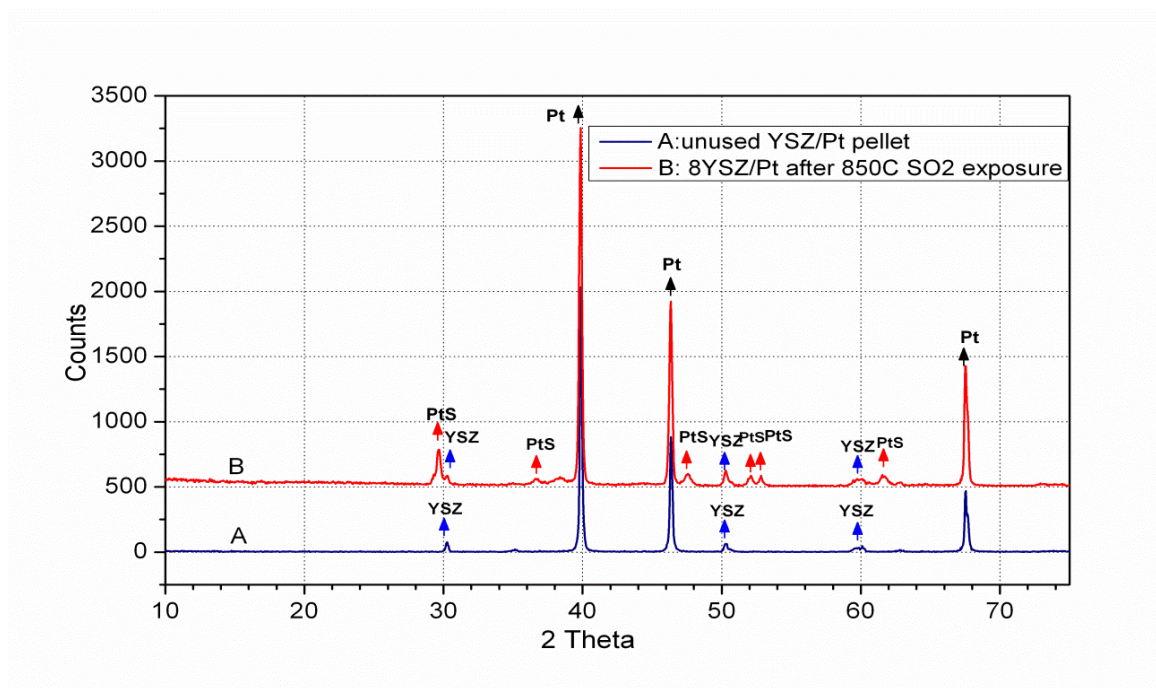
Figure 3.24: *Before and after XRD data for 8YSZ/Pt membrane at 850°C SO_2 exposure, feed side*

Overall, the results of Raman spectroscopy, SEM-EDS and XRD analysis for the cell pellet supports the speculation that platinum sulphide (PtS) was formed on membrane surface in the SO_2 exposure period. However, the mechanism of platinum sulphide formation is so far not clear. It may be formed by electrochemical reactions. Fu et al. employed cyclic voltammetry (CV) to investigate changes in the cathode made of platinum after the introduction of SO_2 (Fu et al. 2009). After a cathode exposure to 1500 ppm SO_2 for 10 min, two evident peaks in CV spectra were found at 0.26 and 0.45V, which may correspond to the following two equations:

$$2\; \underset{\underset{Pt}{}}{\overset{\overset{O}{|}}{S}}\!\!-\!\!\underset{Pt}{O} \quad +2e^- \longrightarrow 2Pt + 2Pt\text{-}S\text{-}O + O_2$$

$$\tag{3.8}$$

$$2Pt-S-O+2e^- \rightarrow 2Pt-S+O_2 \tag{3.9}$$
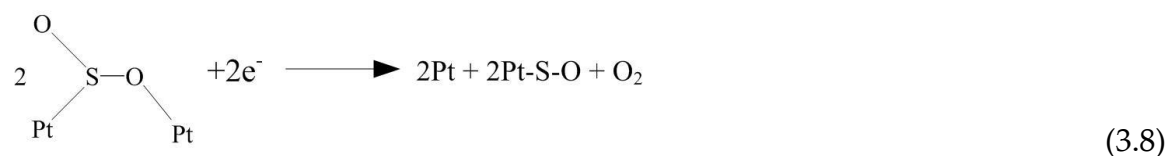
3.5 Conclusion

When separating the binary gas mixtures of SO_2 and O_2 (He is the carrier gas) using 8YSZ/Pt pellet, the performance of the membrane decreases suddenly (type I degradation) and gradually, continuously (type II degradation) after SO_2 introduction. Type I degradation might be attributed to sulphur dioxide adsorption onto platinum surface; resulting in physical blocking of electrode surface and decrease of TPB perimeter (the adsorption is not significant at high temperature). Once the sulphur dioxide adsorption reaches saturation, type II degradation occurred. Type II degradation may be not attributed to YSZ electrolyte according to impedance and capacitance measurement before and after SO_2 exposure test, but is due to the platinum sulphide (PtS) produced in the period of SO_2 exposure. This statement is based on the measurements of specimens before and after SO_2 exposure by a range of surface analysis techniques including Raman spectroscopy, Scanning Electron Microscopy (SEM), Energy Dispersive x-ray Spectroscopy (EDS) and x-ray Diffraction (XRD). PtS changed the morphology of the electrode surface and decreased the length of TPB where the electrochemical reactions occur. The work that follows is focuses upon the development of a method for reducing membrane performance degradation in the SO_2 exposure period to maintain a high level of membrane performance.

Chapter 4

4 Performance recovery of Pt/8YSZ membrane pellet

4.1 Introduction

The main challenge for YSZ membrane application in the separation of the products leaving H_2SO_4 decomposition is the severe membrane performance degradation caused by sulphur which is also one of the major contaminants for SOFC systems. In past work, the sulphur poisoning behaviour of Pt/8YSZ membrane was characterized by a rapid initial drop in current upon exposure to sulphur dioxide (type I degradation), followed by a much slower but still significant rate for a long period of time (type II degradation). Type I degradation is caused by the dissociative adsorption of sulphur species around the three-phase boundaries (the active sites for electrochemical reaction) (Zha et al. 2007) (Gould et al. 2009) (Fu et al. 2009) (Nagahara et al. 2008) (Lussier et al. 2008). Platinum sulphide may be the reason for type II degradation, which could form a sulphide layer on the cathode surface, causing the microstructure to change and reducing the TPB area for electrochemical reactions (Li et al. 2010) (He et al. 2002) (Liu et al. 2001).

The question which results from this observation is how to reduce the sulphur poisoning effect on membrane performance. So far, there are three different options. The first is removing sulphur containing impurities, which may achieve complete recovery (Lussier et al. 2008) (Rasmussen and Hagen 2009) (Feduska and Isenberg 1983) or partial recovery (Li et al. 2010) (Ishikura et al. 2007) (Trembly et al. 2006). The second solution is to employ sulphur-tolerant electrodes which are categorized into three kinds of materials: thiospinels and metal sulphides, metal cermets, and mixed ionic and electronic conductors (Gong et al. 2007). The third method is high

current density which can increase performance regeneration (Li et al. 2010) (Hauch and Mogensen 2010), or applying short but strong dc polarization which alters chemical composition of the electrode surface and leads to an acceleration of the oxygen surface exchange reaction (Baumann et al. 2005).

In the case of separating H_2SO_4 decomposition products using YSZ membrane operation, the first option of removing sulphur dioxide from the feed is impracticable. Sulphur-tolerant electrodes are still being developed mainly for use in SOFCs or SOECs. Even if they are explored, they maybe not work well under the aggressive environment of sulphuric acid thermal decomposition (high temperature, corrosive gas, and even high pressure). The third option was proposed by our research group. By applying a high dc voltage pulse to a Pt/YSZ membrane cell, performance recovery of membrane exposed to gas mixtures of SO_2-O_2-He was observed. Using this finding as the starting point, the following work was undertaken on the effect of voltage pulse upon membrane performance recovery.

- In order to observe the changes of membrane surface and structure, two different Pt/YSZ cells with and without voltage pulse treatment were analysed by x-ray diffraction (XRD), Raman spectroscopy and Scanning electron microscopes (SEM), Energy-dispersive x-ray spectroscopy (EDS).
- The effect of negative voltage pulse on YSZ membrane performance in SO_2 exposure period was studied. This effect was compared with the effect of positive voltage pulse.
- Furthermore, Pt/YSZ membrane performance degradation by SO_2 poisoning and recovery by voltage pulse were studied using *in-situ* impedance measurement.
- Finally, a series experiments were carried out to optimize voltage pulse for achieving a stable membrane performance over a long term SO_2 exposure period.

4.2 Performance recovery by positive voltage pulse

4.2.1 Aim

This work aims to demonstrate the performance of Pt/8YSZ membrane after a positive voltage pulse (the definition of positive voltage is that the direction of electron flowing is from the cathode in feed side to the anode in permeate side), the cell was then analysed by XRD, Raman spectroscopy and SEM-EDS to characterize the membrane surface change before and after voltage pulses.

4.2.2 Experimental

A sketch of the experimental setup is shown in Figure 4.1. When the furnace temperature reached 850°C at a ramp rate of 5°C/min, gas mixtures composed of oxygen (5ml/min) and helium (45ml/min) were passed through an upper quartz tube for pre-heating before contacting the membrane at 850°C. An external voltage of 1.5V was applied. After around 1-hour of SO_2 free period, the composition of the feed stream was changed to oxygen (5ml/min), helium (30ml/min) and sulphur dioxide (15ml/min). Around 75 min later, a 2-minute 4V pulse was applied across the membrane cell. The experiment was stopped after half an hour from the pulse treatment; the cell was cooled naturally in air to room temperature. Current and oxygen permeate concentration in carrier gas (pure helium) were measured and recorded *in-situ* by a computer.

During the whole run, the overall flow rate of the feed stream was 50ml/min and oxygen accounted for 10%. All the flow rates were controlled by rotameters (standard accuracy: 5% of full scale). This run involved 1 hour SO_2 free period (feed: O_2 and He) and 1.5 hours SO_2 exposure period (feed: O_2, He and SO_2) with a constant external DC voltage of 1.5V and a 2-minute 4V pulse.

In order to counteract the effect of oxygen partial pressure difference, two zero-voltage circuit periods (2 minutes each) were applied in this experiment. The current (around 11 milliamp) and oxygen concentration corresponding to zero voltage were

subtracted from the raw data in order to give the corrected values showing only the effect of external voltage on oxygen permeation.
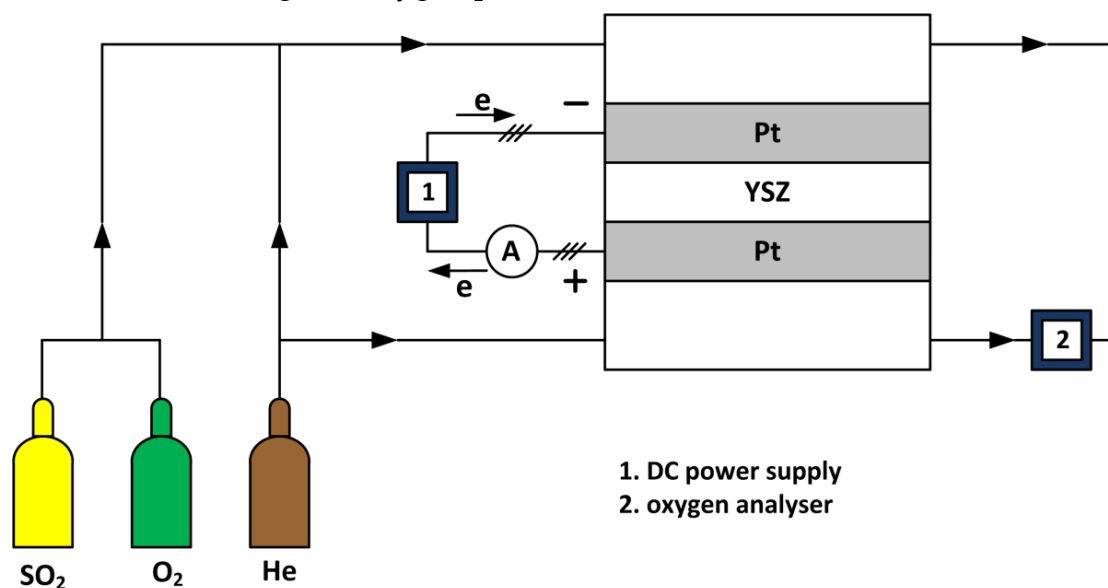
Figure 4.1: *Experimental setup*

After this experiment, the used cell and a fresh cell were analyzed by surface analysis techniques including: X-ray diffraction (XRD) with a diffractmeter (D500, Siemens, Germany), using Cu Ka1 radiation (λ=1.5406A) with a step of 0.02° (2θ) and a scanning rate of 2° min^{-1}, to detect any possible structural change; Raman spectrometer (R3000, Agiltron Inc) with excitation wavelengths 785nm to study the Raman scattering of monochromatic light from a laser; Scanning electron microscopy (SEM) using a JEOL JEM-2010F microscope equipped with an Oxford Instruments ultrathin window Energy Dispersive x-ray detector to get information about the sample's surface topography and element composition.

4.2.3   Results and discussion

For this SO_2 exposure test with a 2-minute 4V pulse application, SO_2 injection to the feed stream caused two stages of degradation to the membrane performance according to the current changes, as expected [Figure 4.2]. After the 4V pulse, current has a jump to 374mA from 272mA and then decreases gradually to 281mA in 10 min later. This jump suggests that membrane performance partly recovers. The decrease in current after pulse was attributed to SO_2 poisoning effect, as previously.
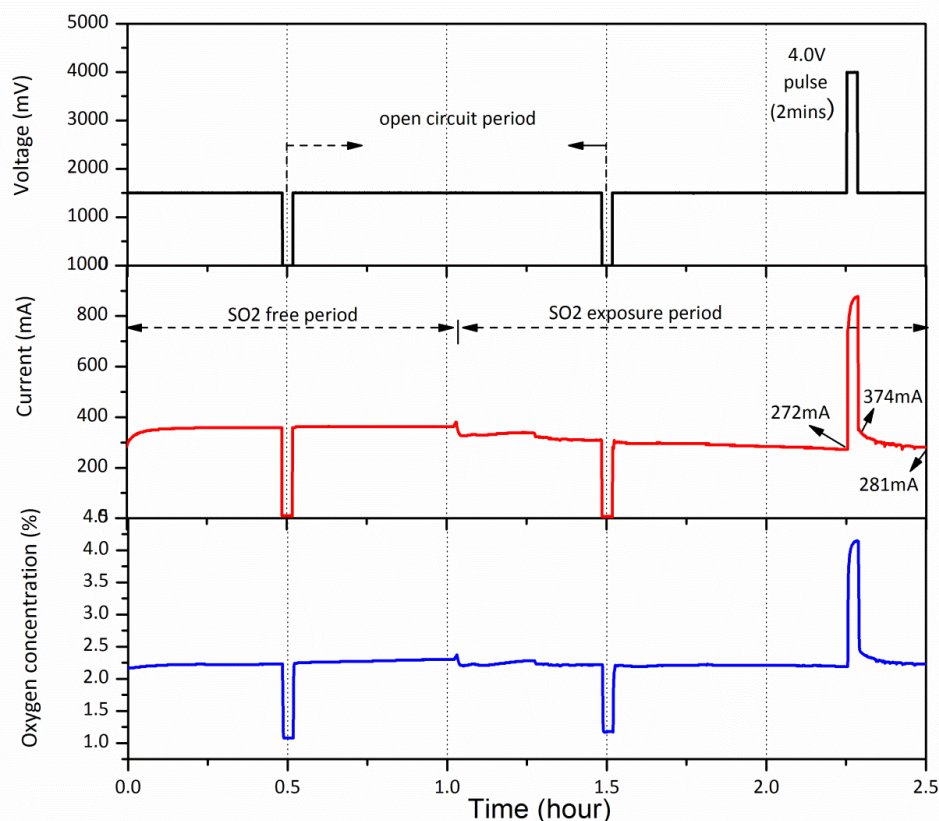
Figure 4.2: *Experimental data for YSZ/Pt pellet exposure to SO_2 and O_2 at 850°C with a 2-minutes 4V positive pulse treatment*

In order to show membrane surface change after voltage pulse, surface analysis results of the cell treated by voltage pulse were compared with that of a fresh cell and a poisoned cell (without voltage pulse treatment).

XRD

From XRD spectra for the cathode surface of the three membrane pellets, there are no differences in the diffraction peak position and shape for the fresh cell (line A) and the cell treated by voltage pulse (line C) [Figure 4.3]. This means that the crystal structure of Pt electrode and YSZ electrolyte was stable after a 2-minute 4V pulse treatment. Compared with the pellet after SO_2 exposure, no platinum sulphide (PtS) peak was found in the XRD data for the cell treated by voltage pulse. The

disappearance of PtS peaks indicates that the voltage pulse could remove PtS from the cathode surface and increase electrochemical activity sites for promoting oxygen permeation process. Alternatively, voltage pulse makes a contribution to the recovery of YSZ/Pt membrane degradation.

Raman spectroscopy

Figure 4.4 shows the membrane cell treated by voltage pulse has a triple-peak near to $1400cm^{-1}$ the same Raman spectra as a fresh cell. However, this peak was not observed from the cell treated by SO_2 exposure. This difference indicates that the cathode surface was changed before and after voltage pulse treatment. This change could be related to the removal of platinum sulphide on the cathode surface, leading the Raman Spectra after voltage pulse reproduced. The noise in spectra may be attributed the coarse cathode surface which affects the scattering of monochromatic light from a laser.

SEM-EDS

EDS spectrum of the cell after voltage pulse treatment also demonstrates that the sulphur element on the cathode surface before voltage pulse treatment was cleaned after 4V pulse treatment [Figure 4.5-4.7]. Figure4.5 shows that only platinum was detected at the cathode surface. For the cathode active area, elements of oxygen, yttrium and zirconium were found, without sulphur [Figure 4.6]. Silicon was attributed to the surface devitrification of the pre-heating quartz tube at high temperature which was confirmed in Figure 3.20. The EDS spectrum for an area scanning in Figure 4.7 was consistent with Figure 4.5 and Figure 4.6.

From these surface analysis results, it is clear that the partial recovery of membrane performance by voltage pulse was related to the change of membrane surface, not related to bulk electrolyte. Platinum and YSZ were both stable for a 2min-4V pulse. The decrease of cell resistance caused by voltage pulse may be due to the removal of sulphur adsorbed on the cathode surface or platinum sulphide dissociation.
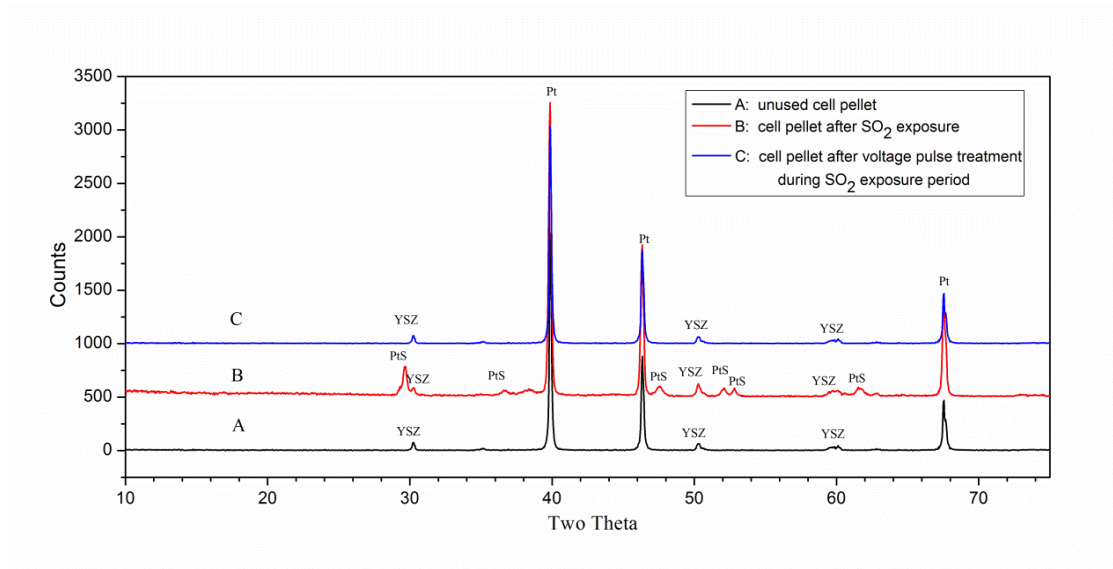
Figure 4.3: *XRD data for the cathode side of YSZ/Pt pellet after 4V pulse treatment*
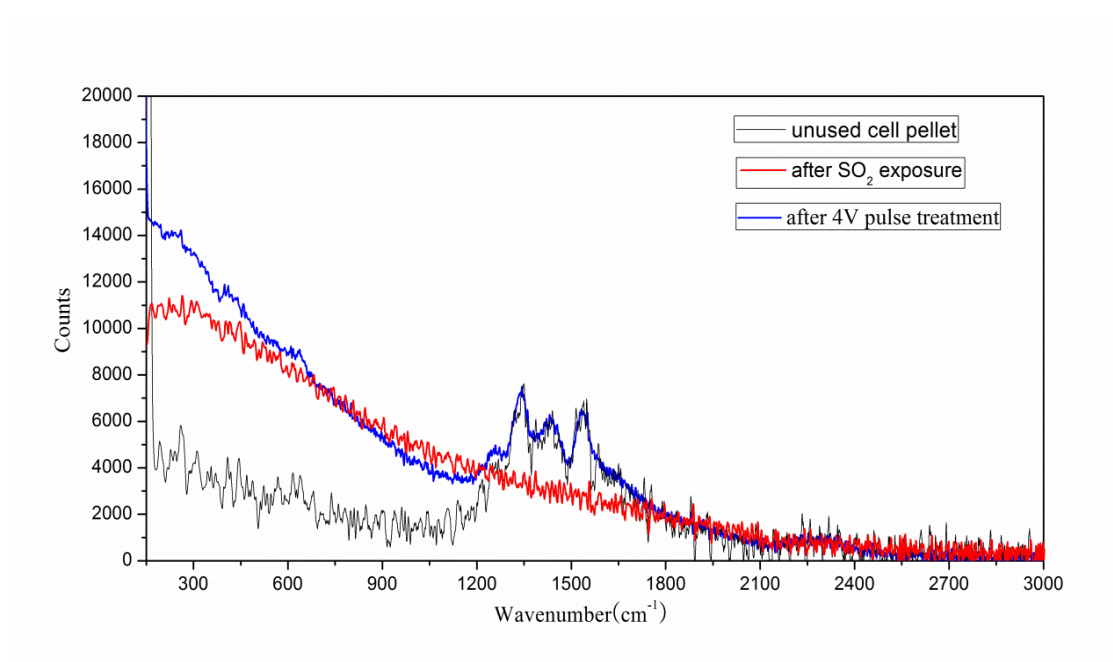
Figure 4.4: *Raman spectra of cathode surface for YSZ/Pt pellet after 4V pulse treatment*
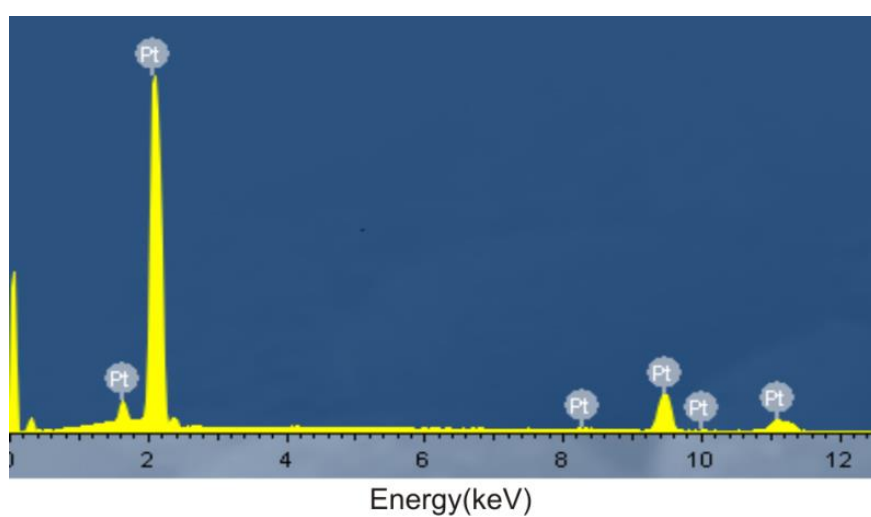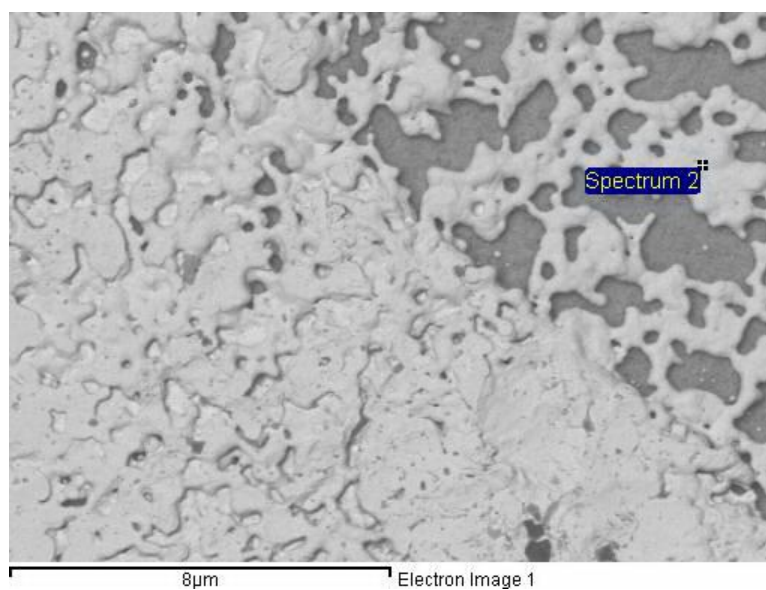
Figure 4.5: *SEM-EDS spectra of the cathode surface for the YSZ/Pt pellet after 4V pulse treatment, Pt surface*
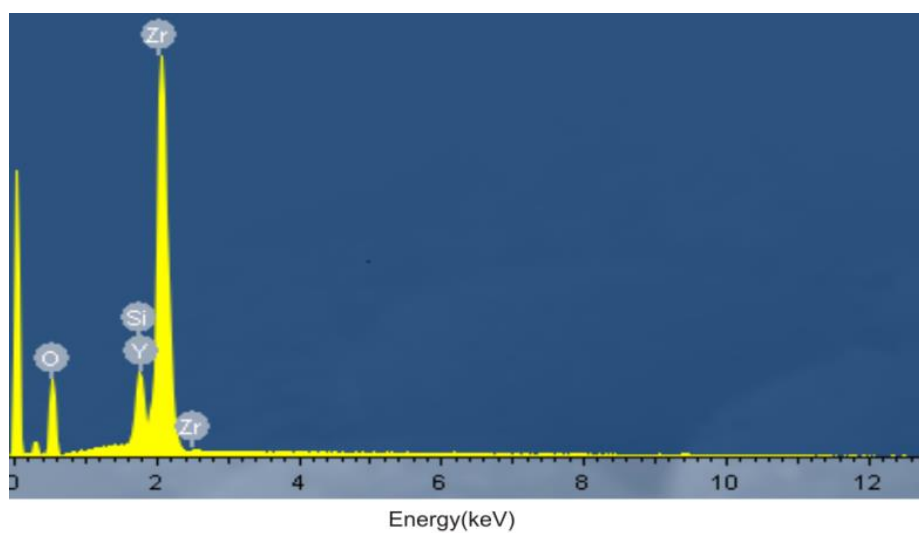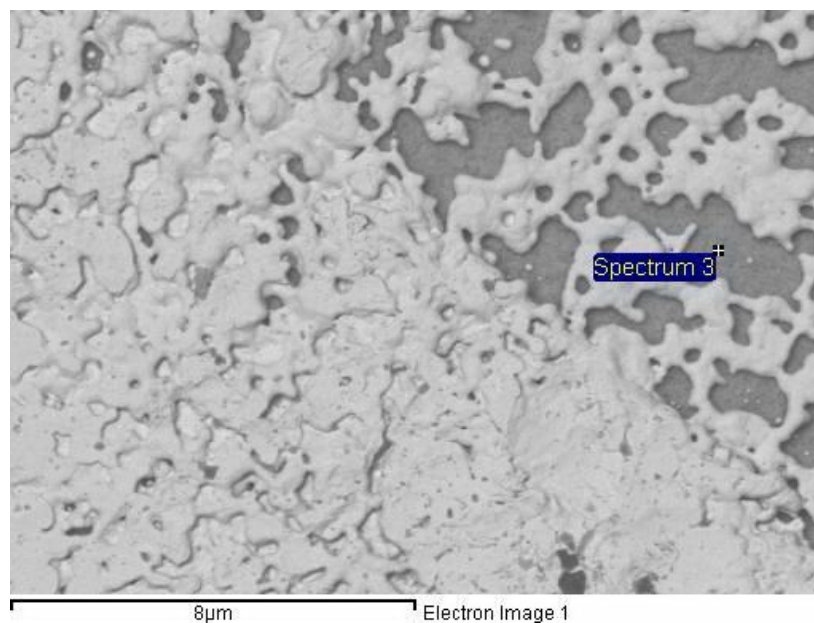
Element	Weight%	Atomic%
O K	34.12	74.61
Si K	3.18	3.96
Y L	3.13	1.23
Zr L	52.67	20.20
Totals	93.10	

Figure 4.6: *SEM-EDS spectra of the cathode surface for the YSZ/Pt pellet after 4V pulse treatment, Pt/YSZ active area*

Element	Weight%	Atomic%
O K	5.07	46.28
Y L	-0.69	-1.13
Zr L	3.17	5.08
Pt M	66.45	49.78
Totals	74.00	
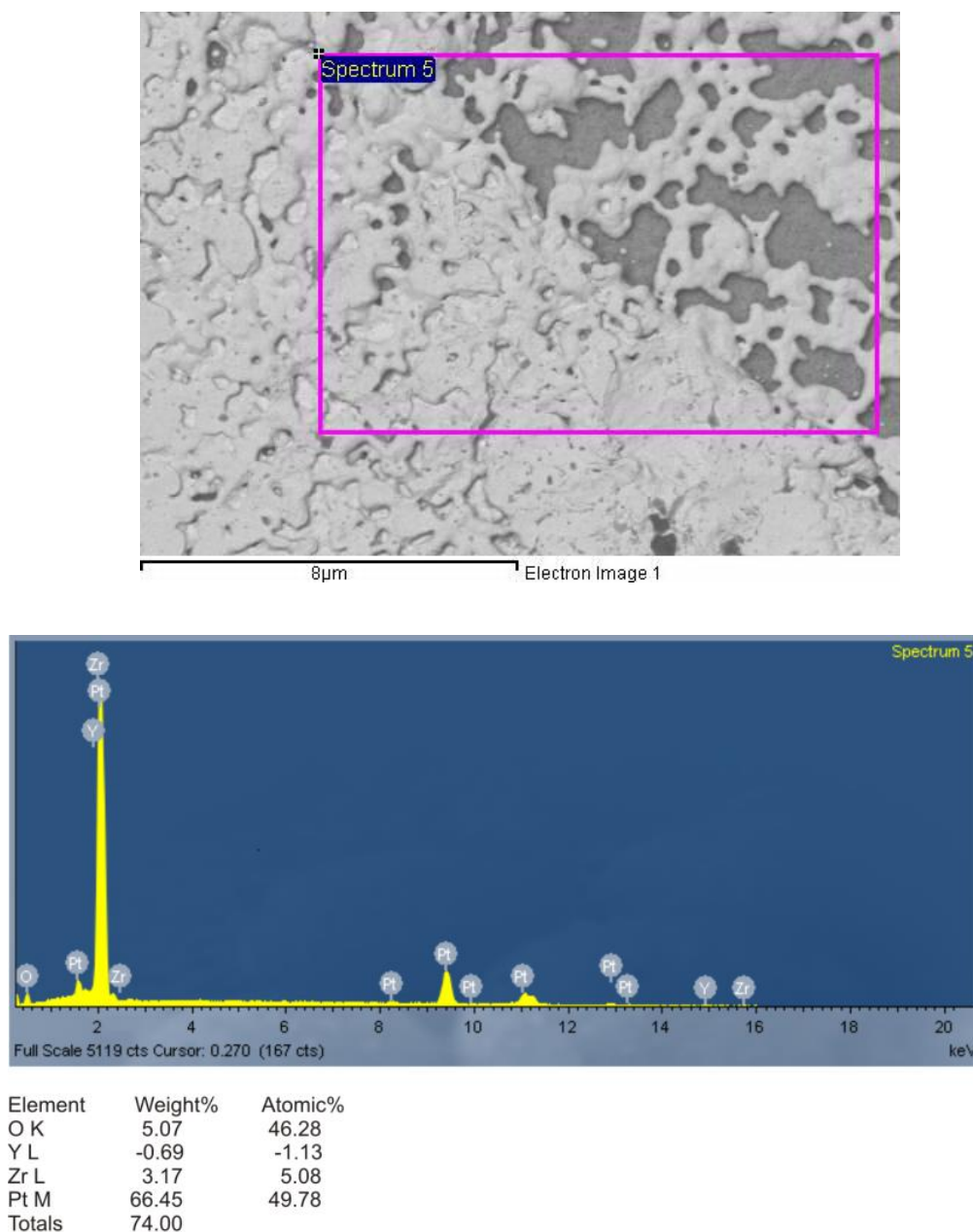
Figure 4.7: *SEM-EDS spectra of the cathode surface for the YSZ/Pt pellet after 4V pulse treatment, Pt/YSZ area*

4.2.4 Conclusion

The effect of high dc voltage pulse on recovery of Pt/YSZ membrane performance was demonstrated experimentally. Cell performance represented by current could recover partly after a 2-minute 4V pulse treatment which might cause removal of sulphur or platinum sulphide dissociation on the cathode surface and lead to the cell resistance decrease. This was supported by surface analysis results such as XRD data,

Raman spectroscopy and SEM-EDS spectra for membrane cells before and after treatment by a voltage pulse. Therefore, an application of high dc voltage pulse across a YSZ membrane might be helpful to reduce performance degradation by sulphur poisoning.

4.3 Membrane performance after voltage pulse in He-O$_2$ period

A question which arose from the conclusion in Section 4.2, how would the YSZ membrane perform with high voltage pulses when the feed does not contain SO$_2$. If there is still an increase in current after pulse, it means that the membrane performance recovery in SO$_2$ exposure period by voltage pulse may be also related to changes in the YSZ electrolyte or Pt electrode.

4.3.1 Aim

To study the behaviour of a Pt/YSZ membrane exposed to a feed stream consisting only of helium and oxygen, before and after high dc voltage pulses.

4.3.2 Experimental

The experimental method was identical to that in the previous run except that throughout the measurement, the composition of feed stream was helium and oxygen, without sulphur dioxide.

Following the same procedure as the positive voltage test, the apparatus was first heated to 850°C and allowed to stabilise at that temperature. With 10% O$_2$ in He (total 50ml/min) and 100ml/min He being applied to feed and product sides of the membrane, current measurement was then taken at applied voltage 1.5V.

Four positive voltage pulses were applied to membrane cell when the experiment was going on for about 1.45 hour (4V, 5s), 2.15 hour (6V, 1s), 3 hour (7V, 0.5s) and 3.5 hour (10V, 0.08s). Half an hour later, the experiment was ended. This four voltage pulses are the result after an optimization process which will be introduced in Section 4.7.

4.3.3   Result and discussion

Figure 4.8 shows membrane current and permeated oxygen concentration behaviour of a Pt/8YSZ membrane subjected to four voltage pulses when the feed stream consists of only He and O_2. Before voltage pulse, the current was stable at around 218mA and permeated oxygen concentration was about 3.02%. After the 4V pulse, current and oxygen permeation concentration changed back quickly, taking a matter of seconds. The same observations were found after 6, 7 and 10V pulse treatments. The small fluctuations of current and oxygen concentration after pulses should be due to reduction of electrode polarization and deceleration of electrochemical reaction on the cathode surface.
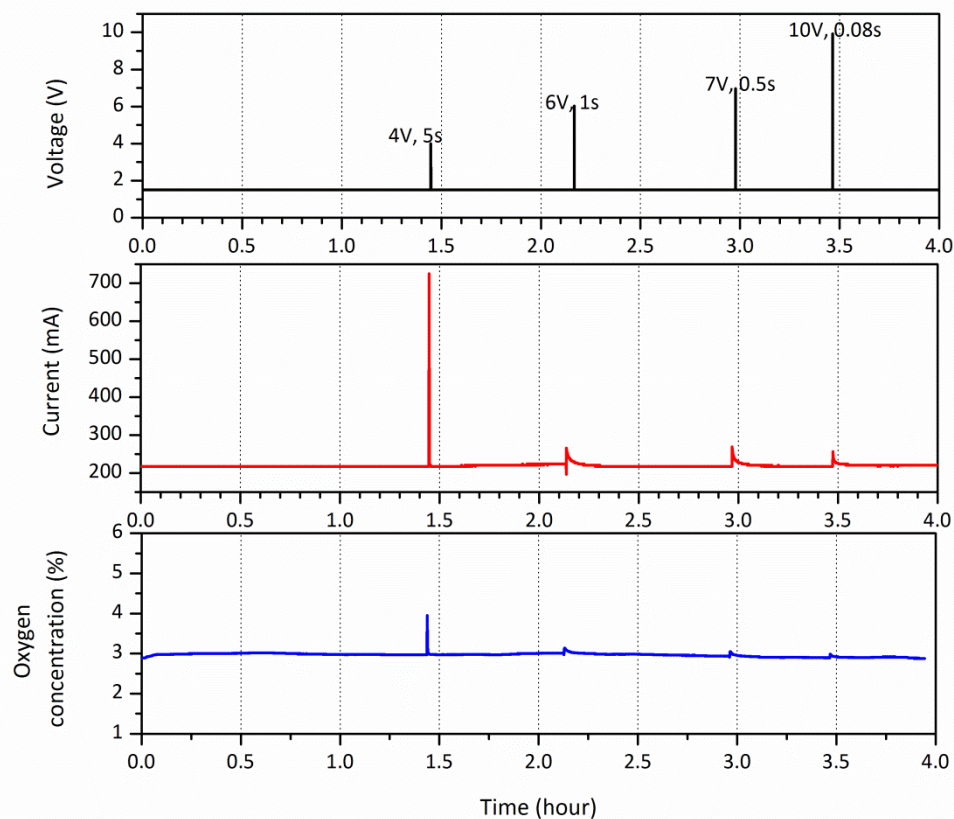
Figure 4.8: *Experimental result of Pt/8YSZ membrane pellet exposed to He-O₂ with four positive voltage pulses, at 850°C*

Therefore, the performance of Pt/YSZ membrane exposed to He-O$_2$ was not affected by high voltage pulses. In other words, YSZ electrolyte and Pt electrode worked well with high voltage pulse at high temperature. Therefore, the remarkable performance recovery of Pt/YSZ cell exposed to He-O$_2$-SO$_2$ was related to sulphur dioxide introduction to feed stream, and this recovery may be due to some interactions of high voltage and SO$_2$ on the cathode surface of membrane.

4.3.4 Conclusion

When a Pt/YSZ membrane was exposed to He-O$_2$ at 850°C, no changes in current and oxygen permeation concentration were found before and after voltage pulses. Membrane performance was stable under feed stream of He and O$_2$, even though high voltage pulses were applied. This indicates that the remarkable membrane performance recovery by a voltage pulse, observed in Section4.2, is related to the sulphur dioxide in the feed, and this recovery may be due to sulphur desorption or platinum sulphide dissociation on the cathode surface by the voltage pulse.

4.4 Membrane performance by negative voltage pulse

The previous studies of oxygen permeation through a Pt/8YSZ membrane with an external dc power supply can be described by Figure 4.9. The cathode side was oxygen reduction, forming oxygen ions for diffusion in the YSZ electrolyte. The anode side was the oxygen ion oxidation reaction, producing oxygen molecules. With oxygen permeation, two electrons with one oxygen ion are transported from the cathode to the anode. Therefore, an external power supply can increase oxygen permeation by providing sufficient electrons for electrochemical reactions and driving the flow of oxygen ions.
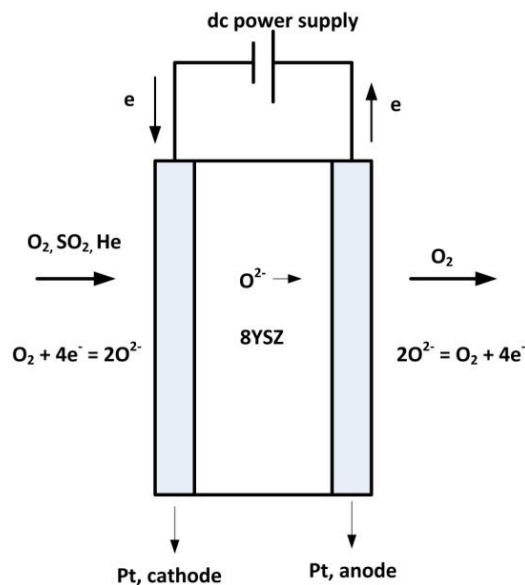
Figure 4.9: *Schematic of a Pt/8YSZ/Pt oxygen separation membrane with an external dc power supply*

However, a high external voltage may create an electron layer on the cathode surface and lead to electrode polarization. Also, this cathodic polarization may be aggravated with sulphur poisoning (Li and Wang 2011) (Hagen et al. 2011). In this time, if a reverse polarity voltage pulse (negative pulse) is applied across the cell, the cathodic polarization might be reduced or removed rapidly. As a result, the cell may start over again and some cell membrane performance recovery may be obtained. Therefore, the next step is to investigate the effect of negative voltage pulse on membrane performance in a SO_2 exposure period.

4.4.1   Aim

The aim of this work is to investigate the membrane performance change before and after a negative voltage pulse treatment during a SO_2 exposure period.

4.4.2   Experimental

The method was identical to that used for the positive voltage run, as described in Section 4.2.2, except that the voltage pulse was negative not positive.

Once at 850°C, with 1.5V being applied across the electrode faces, the feed side was

supplied with 10% O_2 in He (total 50ml/min) for half one hour. The feed was then changed to 30% SO_2 and 10% O_2 in He (total 50ml/min) for 1.5h. From SO_2 introduction in about an hour, a 2-minute of reversed polarity at 3V was applied. The experiment was ended 30minutes after pulse treatment.

The current and permeated oxygen concentration with time were measured and recorded as previously.

4.4.3   Result and discussion

The external voltage change during the run and the resulting measurements are all presented in Figure 4.10. As expected, there was a rapid drop in current and oxygen permeation following the application of SO_2 to the membrane feed side. The period of time over the rapid drop occurs was around 2 minutes, a similar period to that observed in the run with positive voltage pulse. Following this quick drop, current and oxygen concentration decreased continuously and slowly to 209mA and 2.02% respectively for 1h SO_2 exposure time. After a -3V pulse application, the current and oxygen permeation concentration again decreased gradually like before pulse from new starting points of 278mA and 2.32%.

Before SO_2 introduction in feed stream, current and oxygen concentration were constant at around 314mA and 2.41%. It means that oxygen permeation process was stable, which provided a baseline for comparing membrane performance after adding SO_2 in feed. After SO_2 added, the decrease of current and permeated oxygen concentration means that the cell resistance increased and oxygen permeation process was impeded. According to previous study (He et al. 2012) , such decrease may be due to sulphur dioxide adsorption (the rapid current decrease) and platinum sulphide formation (the slow current decrease).

During the negative pulse, the measured current was around negative 600mA and the resistance of whole electrical circuit was 5Ω, calculated by Ohm's Law. It is consistent with the value calculated in section 3.3.4. At the same time, the permeated

oxygen concentration was zero. It suggests that the process of oxygen permeation through YSZ membrane by ionic conductivity was inhibited because of the reversed current. By reserved current, all the electrons accumulated on the cathode surface before pulse might be cleaned up and the cathodic polarization be disrupted.

After the negative voltage pulse, the current and oxygen concentration increased to 278mA and 2.32% from 209mA and 2.02%. A performance recovery of membrane was thus obtained, which is thought to be due to the removal of cathodic polarization by the negative voltage pulse. The current and oxygen concentration before SO_2 poisoning were 314mA and 2.41% respectively so, this recovery was not complete. This means that part of the performance degradation was irreversible. Cathodic polarization increases with sulphur adsorption inhibiting surface diffusion of oxygen atoms to active sites (Brightman et al. 2011). Thus, a simple covering of the cathode surface by SO_2 is not very probable as the exclusive origin of the degradation. Such a cover layer would be removed when cathodic polarization is removed. Therefore, the performance degradation is not just due to sulphur adsorption on the cathode surface or else removing cathodic polarization would have recovered membrane performance completely.

In particular, the sudden increase of permeated oxygen concentration after the pulse may be because the oxygen pressure in the feed side increased during the voltage pulse.

4.4.4   Conclusion

In a way similar to the experiment in Section 4.2, the performance of a Pt/8YSZ membrane pellet before and after a 2-minute 3V negative pulse was investigated during an SO_2 exposure period. According to current and permeated oxygen concentration, membrane performance had a quick degradation and then a slow but continuously degradation after SO_2 introduced into feed stream. A negative voltage pulse could recover membrane performance significantly but not completely. Such incomplete performance recovery indicates that part of performance degradation by

sulphur after a negative voltage pulse was irreversible. Removing cathodic polarization did not recover membrane performance completely.
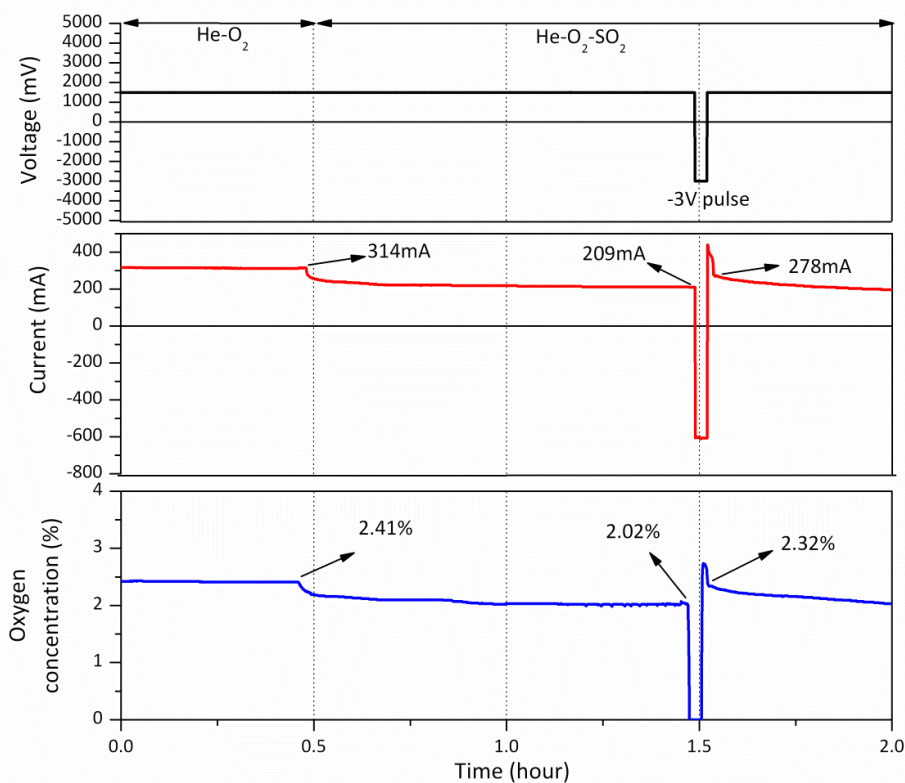
Figure 4.10: *Experimental data for YSZ/Pt pellet exposure to SO$_2$ and O$_2$ at 850°C with a 2-minutes 3V negative pulse treatment*

4.5 Comparison of positive and negative voltage pulse effect

4.5.1 Aim

The aim of this work is to compare the rate of membrane performance recovery by positive and negative voltage pulse.

4.5.2 Experimental

Once the temperature reached to 850°C, 10% of oxygen in helium (total 50ml/min) was supplied to the feed side of the membrane pellet with an external voltage of 1.5V, while the permeate side was swept by helium of 100ml/min. After 1 hour SO$_2$

free period (feed: O_2 and He; permeate: He) and 1.25 hour SO_2 exposure period (feed: O_2, He and SO_2; permeate: He), a 2-minute dc voltage pulse was applied across membrane pellet. The experiment was finished until current decreased to the same value before voltage pulse.

Following this experimental procedure, a total of six experiments were conducted under the same operating conditions with only different magnitude of voltage pulse. These voltage pulses include three positive voltage pulses (3.0, 4.0, and 5.0) and three negative pulses (-3.0, -4.0 and -5.0). The duration of each voltage pulse was 2 minutes.

4.5.3   Result and discussion

The measured current and membrane performance change after current normalization is presented in Figure 4.11 and Figure 4.12 for positive voltage pulse, Figure 4.13 and Figure 4.14 for negative voltage pulse.
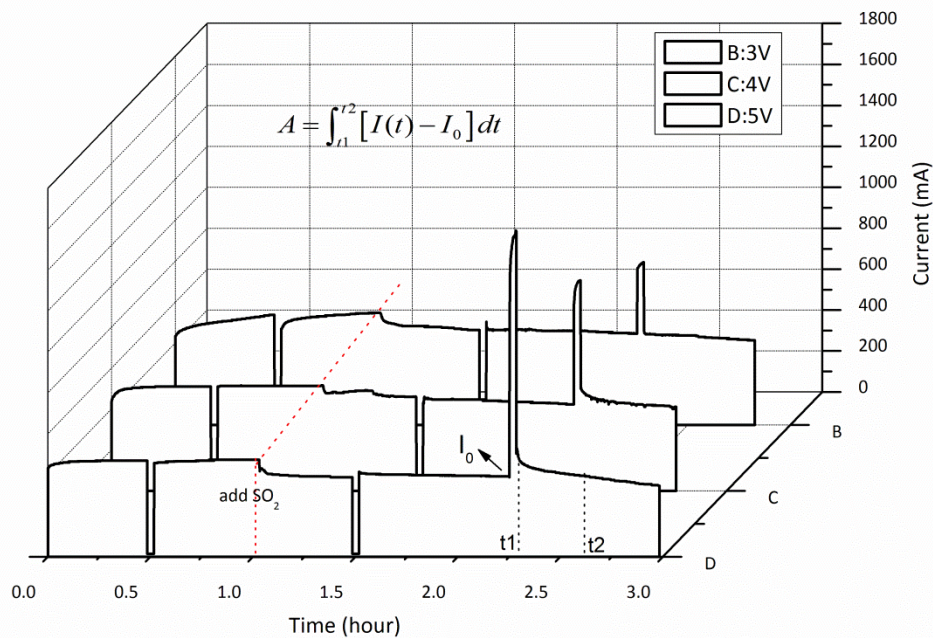
Figure 4.11: *Current change of Pt/8YSZ/Pt membrane pellet exposed to SO_2-O_2 at 850°C, with different positive voltage pulses*
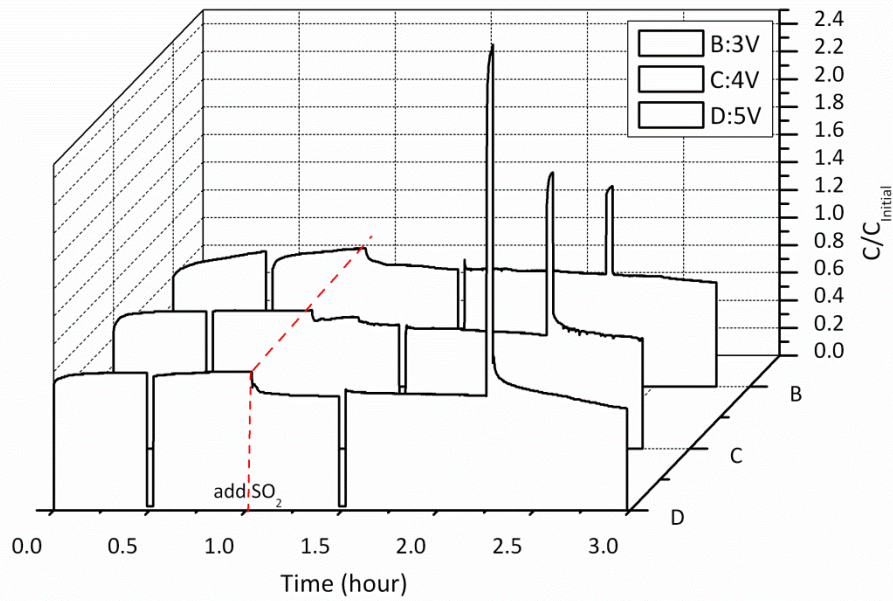
Figure 4.12: *Performance change after current normalization of Pt/8YSZ/Pt membrane pellet exposed to SO$_2$-O$_2$ at 850°C, with different positive voltage pulses*
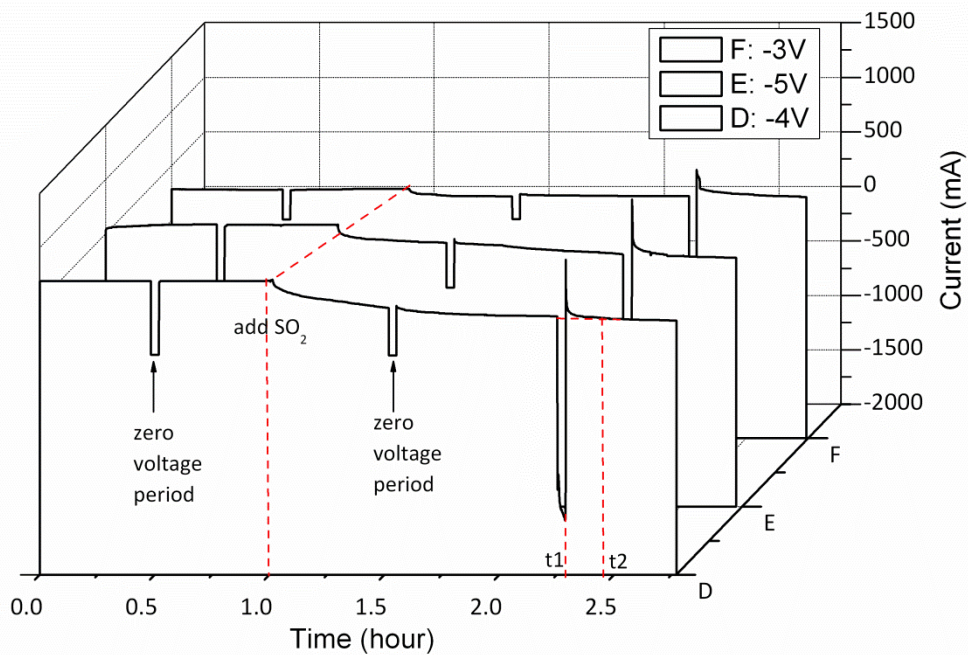
Figure 4.13: *Current change of Pt/8YSZ/Pt membrane pellet exposed to SO$_2$-O$_2$ at 850°C, with different negative voltage pulses*
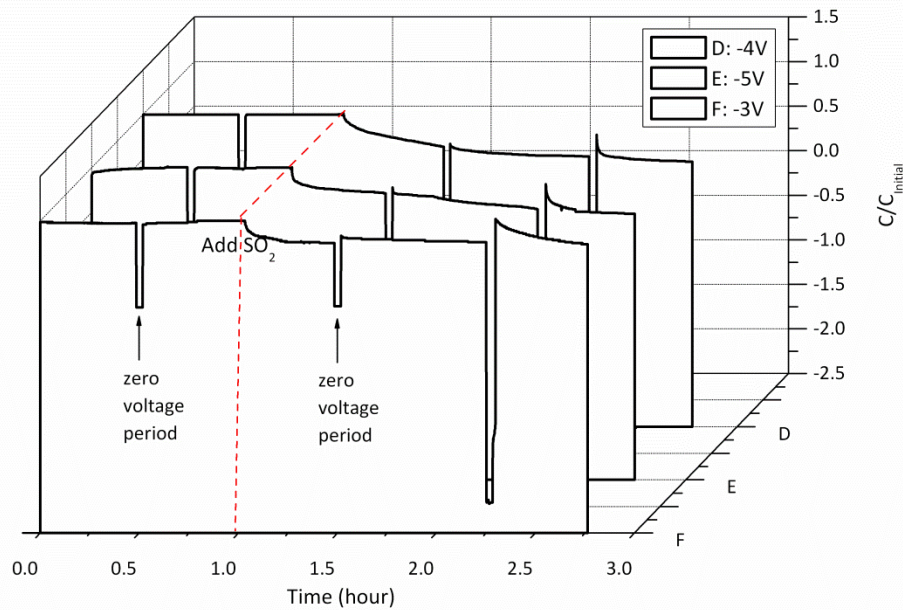
Figure 4.14: *Performance change after current normalization of Pt/8YSZ/Pt membrane pellet exposed to SO$_2$-O$_2$ at 850℃, with different negative voltage pulses*

In these runs, the initial currents are different from each other at the same basic voltage. This may be attributed to the different interface resistances of Pt layer and YSZ surface which affects overall resistance and leads to varying currents at constant voltage. This cannot be avoided for manual coating of the Pt electrode layer. However, it should be noted that this work was to study the effect of voltage pulse on membrane performance recovery, which can be obtained by comparing the current change before and after voltage pulse treatment in each run.

For the runs with different magnitudes of positive and negative voltage pulse, the currents all proceeded steadily for the period without SO$_2$ in feed then showed a rapid decrease after SO$_2$ was added to the feed stream [type I degradation] and a gradual, continued decrease [type II degradation] was observed until the high voltage pulse was applied. This is the same behaviour as seen previously. For each run, it can be seen from Figure 4.12 and Figure 4.14 that current increased after voltage pulse treatment meaning that membrane performance recovers partially.

In general, charge Q is determined by steady current I flowing for a time t as Q=It.

According to eq.3.1-3.3, the charge involved in oxygen permeation through Pt/8YSZ/Pt membrane represents oxygen permeation amount. Therefore, the rate of membrane performance recovery obtained by voltage pulse is defined as recovery area (A) which is the time integral of current [Figure 4.11]. The integral interval is the activation period (t2-t1) in which the current is larger than the value (I_0) before pulse. This integration of current and time was carried out by OriginPro 8.0.

For an example, taking 3.0V pulse run, the recovery duration (t2-t1) is around 19 minutes [Figure 4.15]. The current flow (I_0) before voltage pulse treatment is 326mA. The membrane performance recovery area (A) in this case is 105 mA·min which represents that approximately 25 ml of extra oxygen at RTP (room temperature and pressure) is permeated during the recovery period. Similarly, the recovery areas and extra oxygen permeated for the other five runs were calculated similarly and are shown in Figure 4.16.
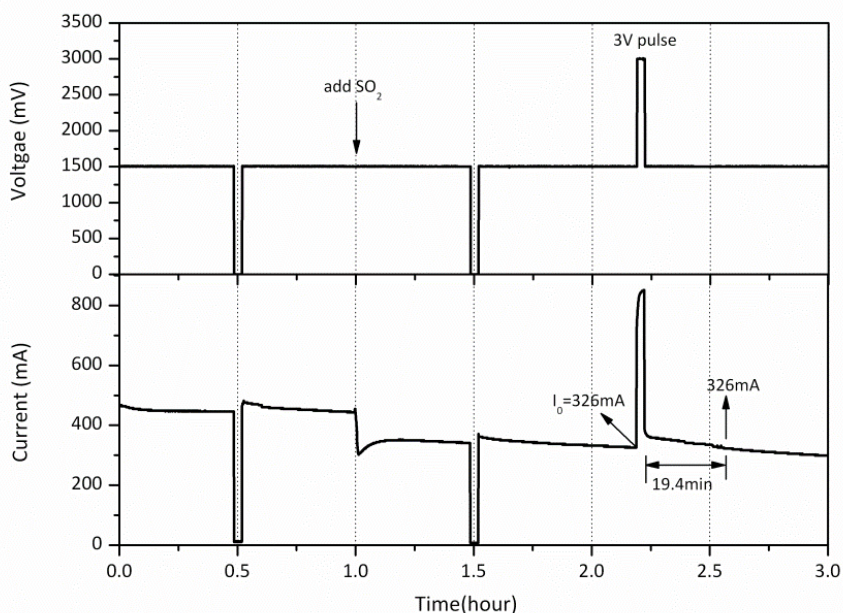
Figure 4.15: *Experimental data for YSZ/Pt pellet exposure to SO$_2$ and O$_2$ at 850°C with a 2-minutes 3V positive pulse treatment*
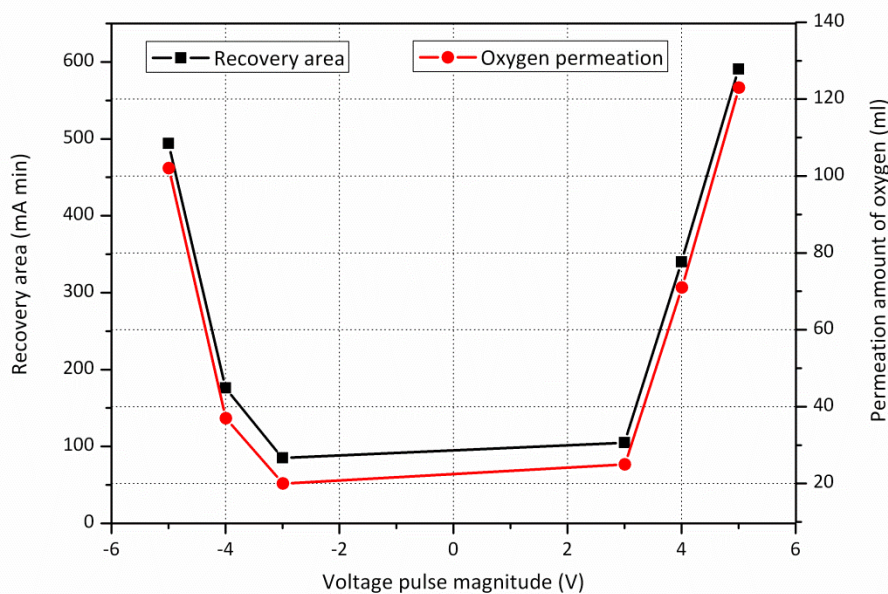
Figure 4.16: *Performance recovery of membrane achieved by different voltage pulse*

In Figure 4.16, it is clear that membrane performance recovery area and the amount of extra permeated oxygen increased with positive voltage pulse range from 3V to 5V. Likewise, high negative voltage pulse, in the range from -3V to -5V, obtained greater performance recovery and more oxygen permeated. This also suggests that negative voltage may have a greater effect on membrane performance, presumably not only removing cathodic polarization. According to previous discussion, high voltage pulses may cause more sulphur removal from the cathode surface by way of sulphur desorption or sulphide dissociation. This will release more active electrode sites for electrochemical reactions and achieve higher membrane performance. Comparing the recovery area and period in Figure 4.16, positive voltage pulses appear to be slightly better, but not by much, than negative voltage pulses.

4.5.4 Conclusion

In the range of 2-minute voltage pulse from -5V pulse to +5V, no significant difference was found in the rates of performance recovery obtained by positive and negative voltage pulses. Also, higher voltage pulse achieved greater performance

recovery. It means that the rate of membrane performance recovery was related to pulse magnitude. Therefore, optimization of voltage pulse is significant and necessary to achieve greatest performance recovery.

4.6 *In-situ* electrical impedance measurement

Electrical impedance measurement is a powerful technique to characterize the electrical properties of materials and their interface with the conducting electrode. Its principles and application have been introduced in Chapter 3. In order to understand the mechanism of Pt/YSZ membrane performance degradation by SO_2 and recovery by high voltage pulses, the impedance of a cell exposed to SO_2 at high temperature was measured *in-situ* using an impedance analyser.

4.6.1   Aim

This work investigates the impedance of Pt/YSZ cell before and after SO_2 added in to feed stream and before and after a high voltage pulse was applied.

4.6.2   Experimental

Electrodes of two YSZ disks, supplied by Department of Materials Science and Engineering, were printed with a microDEK 247 screen-printing machine (DEK, Weymouth, UK) using platinum ink supplied by Gwent Electronic Materials. The diameter of the working surface of the electrode was 1.2 cm resulting in an apparent geometric area of 1.13 cm². Following the ink application, each disk was fired at 1200°C for 15 minutes. One of the cells was used for impedance measurement; the other is used as a reference for comparing surface analysis.

Schematically illustrated in Figure 4.17 is the experimental apparatus for testing the performance of the Pt/YSZ pellet. The pellet was sandwiched into two quartz tubes and sealed with two gold ring gaskets. Stainless steel supports and stands were used to assemble the pellet. The cathode surface was exposed to gas mixtures of pure He, O_2 and SO_2, while the anode surface was exposed to helium. The cell was connected

to an external DC power supply (Micro-controller Based DC Power Supply, Rapid Electronics Ltd) and the current-time (C-t) curve was also automatically recorded by it. Meanwhile, the concentration of permeate oxygen change with time in the anode side was recorded by an oxygen 5200 MultiPurpose analyser.

This experiment included three periods: SO_2 free period (60 min), SO_2 exposure period (195 min), and Post-dc voltage pulse period (15 min). A 0.5-second 7V pulse was applied after a SO_2 exposure period of around 190 min. The flow rates of oxygen and sulphur dioxide in feed were 5 and 15ml/min respectively, of helium 30ml/min (45ml/min in SO_2 free period). The cathode electrode was polarized at 850°C with a constant voltage of 1.5V throughout this experiment, with some zero-voltage circuit periods at 0, 20, 40, 60 min (SO_2 free period), 120, 180, 240min (SO_2 exposure period) and 255, 270 min (post-voltage pulse period) to make electrochemical impedance spectroscopy measurements. All impedance spectroscopy measurements were performed by IVIUMSTAT 111702 analyser by sweeping various frequencies in the range of 1 MHz to 100 mHz using an excitation voltage of 50 mV.

The surfaces of the cell used above (after exposure to SO_2 and voltage pulsing) and of a fresh cell were analyzed by scanning electron microscopy (SEM) (FEI Inspect F).

1. DC voltage pulse generator
2. DC power supply
3. Impedance meter
4. oxygen analyser
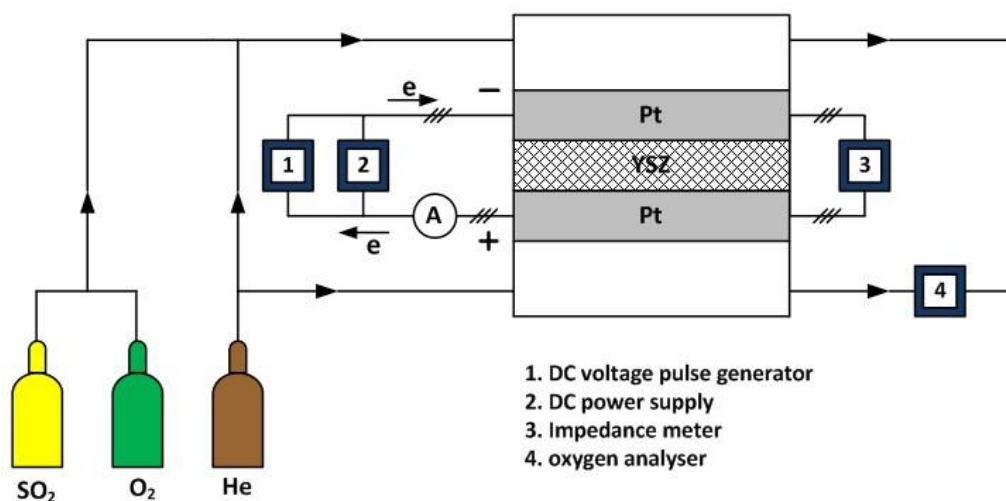
Figure 4.17: *Experimental setup*

4.6.3   Result and Discussion

The current flow through the membrane cell before and after exposure to SO_2 is shown in the bottom graph in Figure 4.18, with gas composition in feed and external voltage with time. The nine impedance measurements are divided to three groups:

- Group A includes the first four measurements which were done in the SO_2 free period [Figure 4.19].

- Group B is the three impedance measurements made in the SO_2 exposure period with the impedance (4) as a base measurement (at He-O_2 60min = SO_2 exposure of 0 minute) [Figure 4.20].

- Impedance measurements (8)-(9) which were performed 2 minutes and 15 minutes after voltage pulse treatment respectively form Group C, along with measurements (4) (SO_2 exposure of 0 minute) and (7) (SO_2 exposure of 180 minutes, just before the voltage pulse) [Figure 4.21].

In these experiments, prior to the SO_2 introduction in feed, the current increased slowly from 131mA to 161mA within one hour [Figure 4.18]. As mentioned in Section 3.4.1, this period was viewed as the electrode activation period (Jiang et al. 1999). The high resistance before applying external voltage was related to the formation of a passive layer during electrode coating preparation. The current passage significantly enhances the electrochemical activity of electrodes for the oxygen reduction reaction. Therefore, the effect of current appears to be related to disappearance of a passive layer which was inhibiting oxygen adsorption/dissociation reaction into YSZ electrolyte surface layer. Meanwhile, impedance spectra were also obtained during this period [Figure 4.19]. Each of them has a similar pattern: an inductive line at the high frequency range, and a depressed capacitive semicircle at the intermediate and low frequency range. According to the four selected time-evolutions of the impedance spectra, the size of impedance arcs after applying external voltage was smaller than before external voltage application. In particular, no change of the serial resistance was observed, but the polarization

part of the impedance decreased on the Pt/YSZ/Pt cell. It may because that external voltage enhanced gradually the electrochemical reaction on the cathode surface with the increase of electrochemical activity site during electrode activation period, and therefore decreased the cathodic polarization. After around 20 min of 1.5V cathodic polarization, the impedance arcs seem to overlap which indicates the cathodic polarization and electrochemical reaction on the cathode surface may reach an equilibrium state.

After start of the SO_2 addition in the feed, the current initially decreased quickly and then slowly with time, to 113mA after a SO_2 exposure period for about 190 min [Figure 4.18]. This confirmed other studies that there were two phases of membrane performance degradation: quick degradation and slow degradation (Lussier et al. 2008) (Li et al. 2010). The quick performance degradation was generally attributed to adsorption of sulphur species on the triple-phase boundary (TPB) area. The slow performance degradation might be due to platinum sulphide formed slowly on the cathode surface, which was proposed by previous study (He et al. 2012). During this 190 min SO_2 exposure period, three impedance measurements were made and the spectra are presented in Figure 4.20. Compared with the impedance arc of the fresh cell before SO_2 exposure (Impedance measurement (4)), the serial and polarization resistances remained constant for impedance measurement (5). It is consistent with slight current change within the 1st hour of the SO_2 exposure period (drop to 155mA from 161mA). With progressing time under SO_2, the serial resistance increased slightly and gradually to higher resistances, and the polarization resistance increased significantly. To obtain more time resolved information about the processes under SO_2 exposure, all the serial (Rs) and polarization (Rp) resistance values derived from the impedance spectra recorded are plotted for the Pt/8YSZ/Pt cell in Figure 4.22. Two distinct regions of different resistance trends, and thus probably also degradation mechanisms, can be identified for Pt/8YSZ/Pt membrane cell. In the SO_2 exposure period of around 190 min, Rs increased slightly by 0.3 ohm. On the other hand, Rp increased significantly from 4.7 to 8.4 ohm. Serial resistance showed

slight increase with SO_2 exposure time, which implied that SO_2 had an influence on the series resistance contributions, including the ionic and electronic conductivity of the cell or the contact between interfaces of the electrode and electrolyte. Given that the YSZ was chemically stable, this increase in Rs may be related to reaction of SO_2 and Pt electrode at the interface area, which was attributed to formation of platinum sulphide (PtS) (Liu et al. 2001). The evident increase in Rp occurred at intermediate frequency and low frequency ranges which have been reported (Kavurucu Schubert et al. 2012) to be related to mass transport properties including the adsorption/desorption of O_2 and the transport to TPB area. When the cathode was poisoned, the Pt active sites for oxygen reduction reaction had decreased with the adsorption of sulphur. However, the driving force for charge transfer was invariable at 1.5V. So, the polarization resistance went up with SO_2 exposure time. Thus, the change of Rs and Rp implies that high concentration of SO_2 has an effect on both the charge transfer resistance and mass transport properties.

After applying a positive 7V pulse across the membrane cell, current has an obvious jump, and then decreases slowly as in previous pulse treatment. This observation confirms the previous studies, where the membrane cell was subject to a 4V pulse after around 75 min SO_2 exposure (He et al. 2012). For the impedance spectra in Figure 4.21, the size of impedance arc, recorded after 2 min of voltage pulse (Impedance (8)), is smaller than that before the voltage pulse (impedance (7)), with sulphur exposure. This observation was consistent with the study on the effect of applied current on H_2S poisoning behaviour of Ni/8YSZ anode at 850°C (Fu et al. 2009).The increase of current after pulse treatment means that the overall resistance of the membrane cell decreased. Such a decrease shown in the impedance spectrum included a slight decrease of Rs and a greater decrease of Rp [Figure 4.23]. This implies again that the high voltage pulse has an effect on charge transfer and mass transfer resistances, this effect may be helpful the removal of sulphur on cathode surface by electrochemical reaction to reduce membrane performance degradation.

The cathode surfaces of the cell from the SO_2 test and of a fresh cell were studied by

electron microscopy [Figure 4.24]. Before the SO_2 exposure test, the as-prepared electrode shows a typical microstructure for a thick-film metal electrode. Some surface faceting is visible, as expected [Figure 4.24a and b]. However, after SO_2 exposure test, small fibres can be seen on the top surface of the platinum electrode and the Pt-YSZ interface [Figure 4.24c]. Some surface restructuring is also visible, shown in Figure 4.24d. This could be attributed to formation of a 2-D surface sulphide (Bartholomew et al. 1982). Before sulphur adsorption on Pt reaches saturation, 2-D surface sulphide of $p(1x1)$ could be observed at 850°C [Figure 4.25]. However, more direct evidence is necessary to confirm this difference in electrode surface before and after SO_2 exposure test.
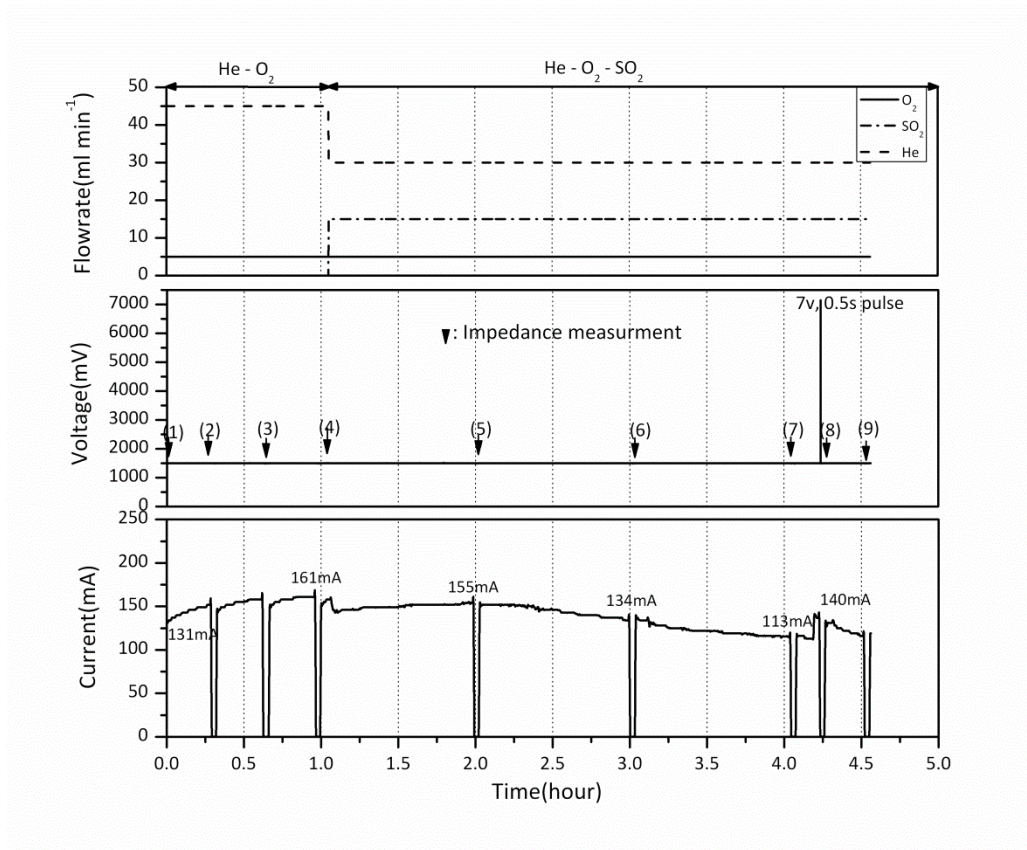
Figure 4.18: *Performance degradation and recovery of Pt/8YSZ/YSZ exposed to He-O2-SO2 at 850°C*
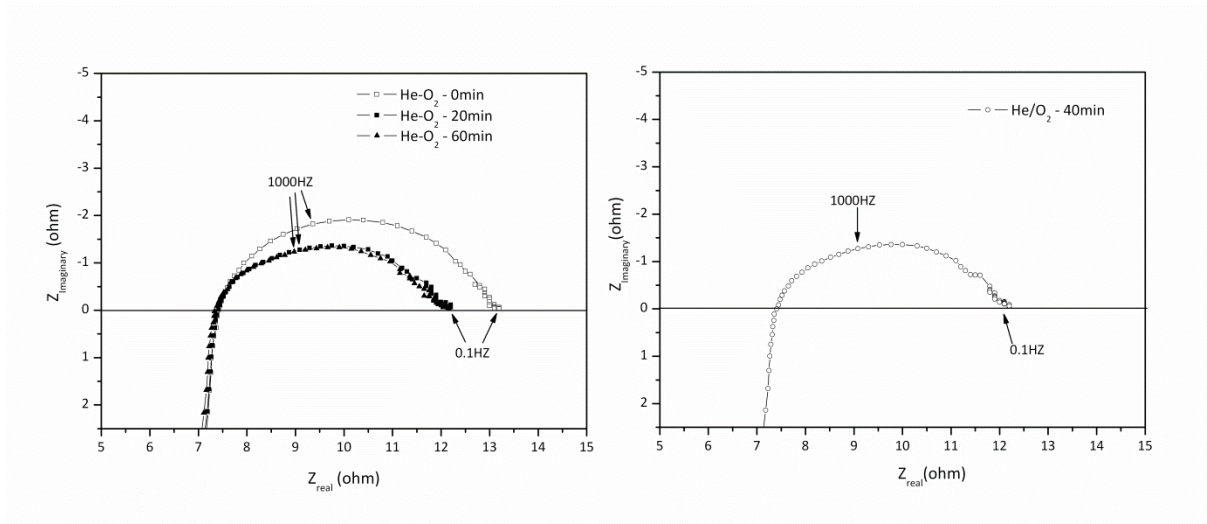
Figure 4.19: *Impedance spectra of Pt/8YSZ/Pt cell recorded in SO$_2$ free period (Group A), at 850°C*
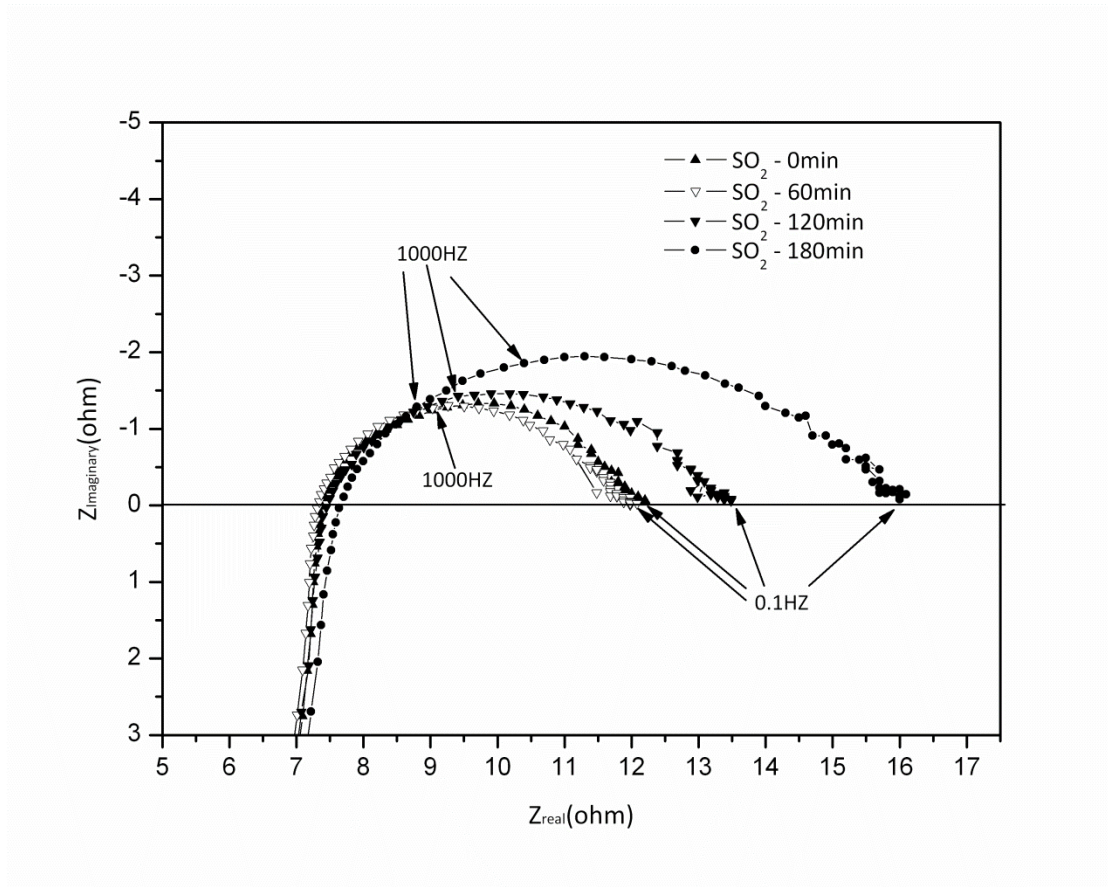
Figure 4.20: *Impedance spectra of Pt/8YSZ/Pt cell recorded before and after SO$_2$ addition to feed (Group B), at 850˚C*
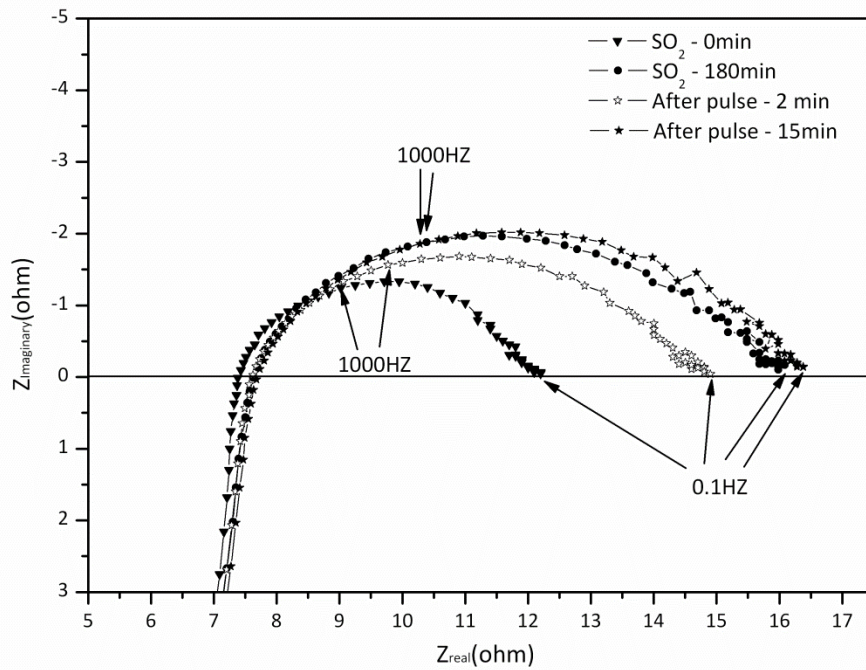
Figure 4.21: *Impedance spectra of Pt/8YSZ/Pt cell recorded before SO$_2$ addition, before and after voltage pulse treatment (Group C), at 850˚C*
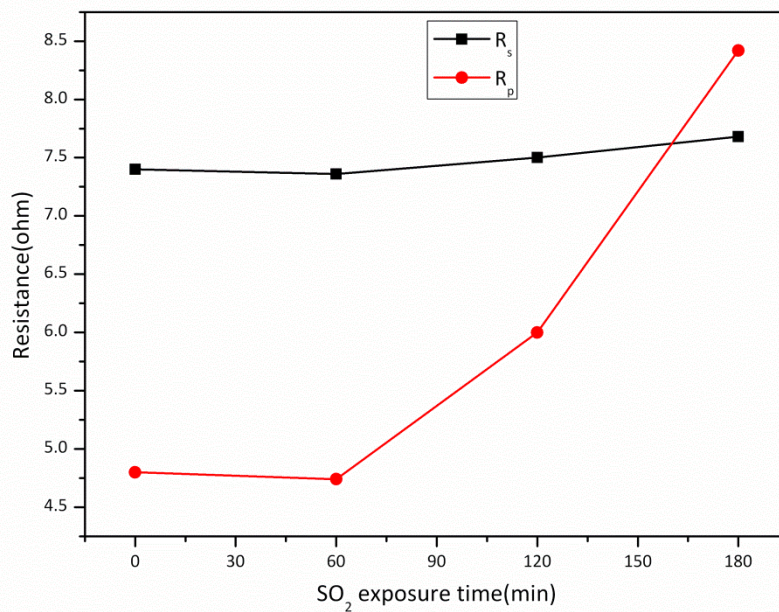
Figure 4.22: *Pt/8YSZ/Pt cell, serial resistance (Rs) and polarization resistance (Rp) derived from impedance spectra (Group B) recorded in SO$_2$ exposure period, at 850°C.*
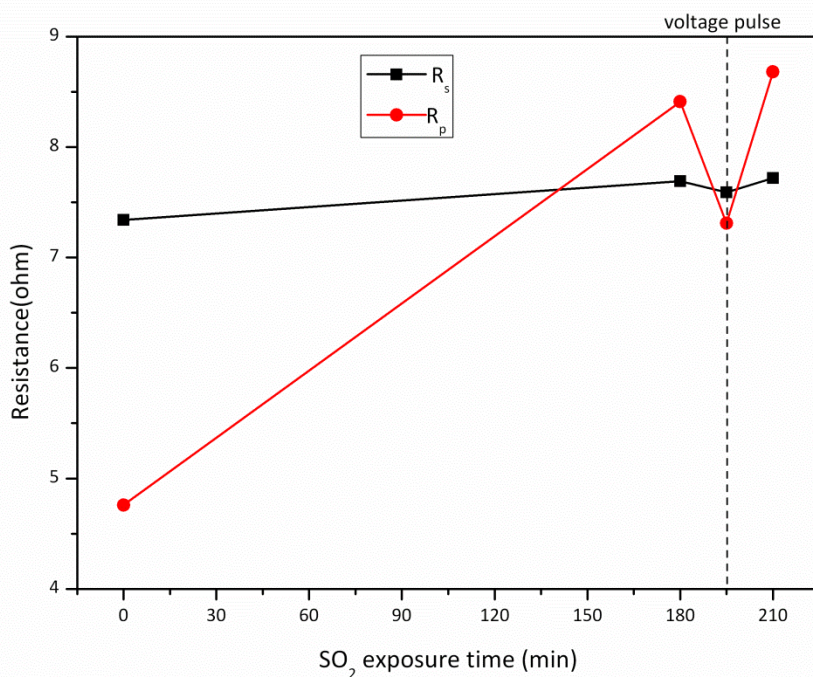
Figure 4.23: *Pt/8YSZ/Pt cell, serial resistance (Rs) and polarization resistance (Rp) derived from impedance spectra (Group C), at 850°C*
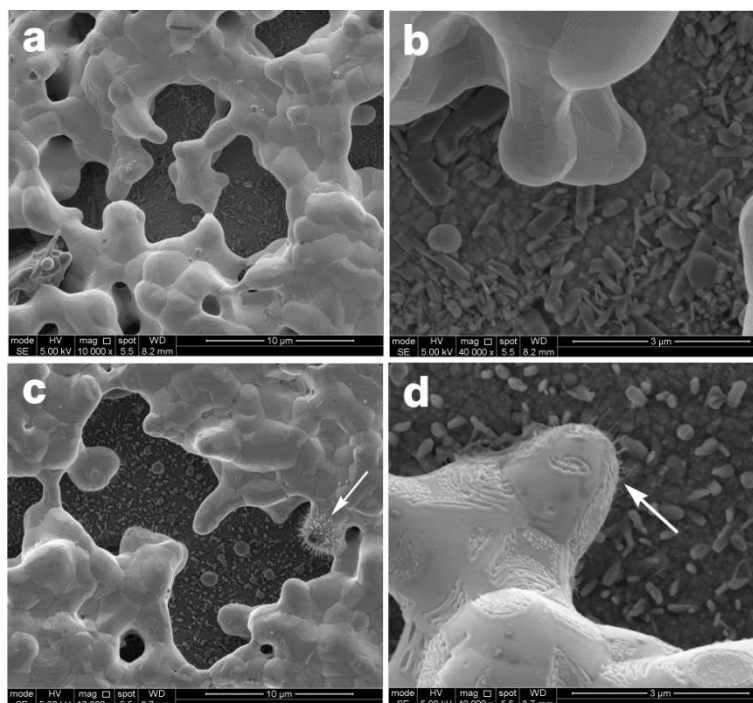
Figure 4.24: *Electron microscopy images of the surface of freshly prepared cell before the test (a) and (b), the cathode surface of the cell used in the SO₂ exposure test (c) (d).*
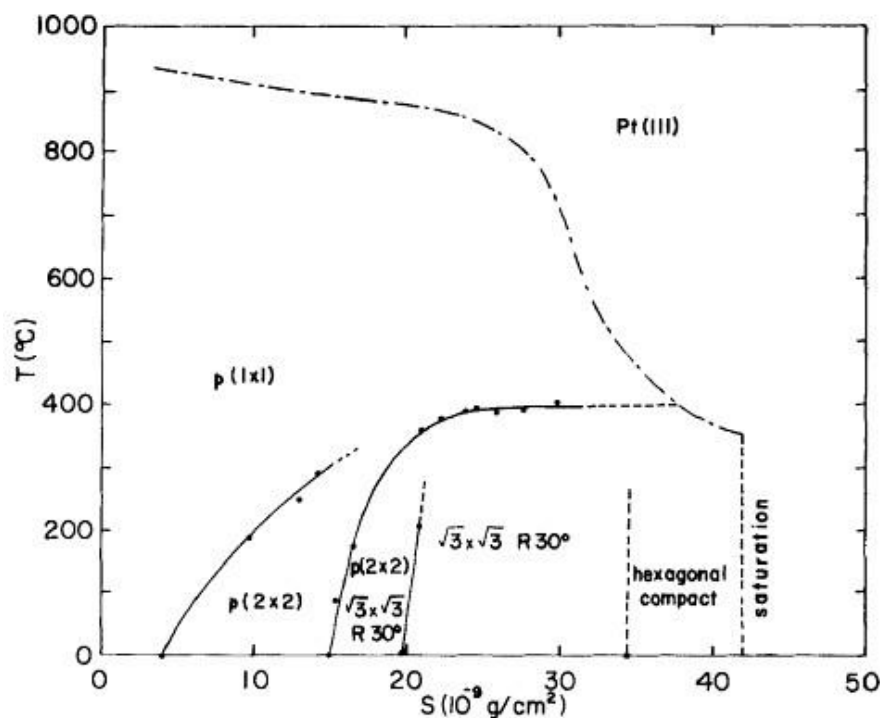
Figure 4.25: *Surface structures of sulphur on Pt (111) as a function of coverage and temperature (Bartholomew et al. 1982)*

4.6.4　Conclusion

The performance degradation and recovery by voltage pulse of Pt/8YSZ/Pt pellet exposed to 30% sulphur dioxide with 10% oxygen in helium (total: 50ml/min) at 850°C was investigated by *in-situ* impedance measurements. Before SO_2 addition in the feed, the current of the Pt/YSZ cell increased slowly and became stable. It was consistent with the impedance in this period decreasing slowly and saturating in half an hour, which was thought to be mainly due to disappearance of a passive layer on electrode surface and the increase of the electrochemical activity for the oxygen reduction reaction. When SO_2 was added in the feed, the current degraded significantly initially and then decreased slowly. Corresponding to the current decrease, the serial and polarization resistance from impedance spectra both increased with time. The increase in polarization resistance was more significant, mainly due to sulphur adsorption. The slight increase in serial resistance may be attributed to formation of sulphide in the interface area of Pt and YSZ. Application

of a 7V pulse on the membrane cell in the SO_2 exposure period obtained a significant increase in current which included a visible decrease in polarization resistance and a slight decrease in serial resistance. It implies that high voltage pulse has an effect on charge transfer and mass transfer properties, and this effect might help the removal of sulphur on cathode surface by electrochemical reactions.

4.7 Optimization of voltage pulse magnitude and duration

By application of high dc voltage pulse, performance recovery of a Pt/YSZ membrane exposed to a high concentration SO_2 at high temperature has been confirmed. In order to achieve the greatest performance recovery, an optimization of the voltage pulse is necessary.

4.7.1 Aim

The aim of this work is to optimize voltage pulse (magnitude and duration) for achieving the greatest performance recovery of Pt/YSZ membrane.

4.7.2 Experimental

A series of experiments were carried out with different pulse magnitudes and widths [Table 4.1]. The operating conditions and experimental procedure are the same as the method described in Section 4.2.2. When the temperature was 850°C, an external dc voltage of 1.5V was applied across a Pt/YSZ membrane whose cathode was exposed to oxygen (5ml/min) in helium (45ml/min) and anode was exposed to helium (100ml/min). After around 1h electrode activation period, 15ml/min of helium in feed stream was replaced by sulphur dioxide. From this moment on, the experiment entered a SO_2 exposure period. One hour later, a high voltage pulse was applied. Once the pulse was over, membrane performance recovery period starts. Experiment was stopped by the moment of current decreased to the value before voltage pulse treatment. The result of current and oxygen permeate concentration change with time was recorded as well.

Pulse magnitude/ V	Pulse width/second							
4.0	0.5	1	3	5	10			
6.0	0.1	0.5	1	3	10			
7.0	0.1	0.2	0.5	1	3	10		
10.0	0.03	0.05	0.08	0.1	0.2	0.5	1	3

Table 4.1: *Optimization of the voltage pulses (magnitude and duration)*

4.7.3 Result and discussion

A series of experiments based on Table 4.1 were carried out to optimise the value and duration of voltage pulse. As expected, current begun to decrease since SO_2 added to feed until a high voltage pulse applied which obtained an increase of current. The rate of performance recovery was assessed by the integration of current (permeated oxygen concentration) and recovery time. For an example in Figure 4.26, after 1 hour SO_2 exposure current decreased from 431mA to 281mA accounting for about 65% of membrane performance remaining. Once applying an external 4V for 1 second pulse across membrane (consuming around 3 joule based on the cell resistance before pulse), current had a step increase to 419mA from 281mA (around 32% of membrane performance was recovered) and decreased gradually with time as previously. Recovery period was 17min, which is the period of current deceased again to the value I_0 (C_0) before pulse treatment. In this way, the recovery period and the recovery area after each pulse are shown in Figure 4.27. Optimum pulse duration can be obtained by comparing recovery area or recovery period. The greatest performance recovery was obtained after 4V pulse for 5 seconds, 6V pulse for 1 second, 7V pulse for 0.5 second and 10V pulse for 0.08 seconds. Too short or too long pulse was against obtaining greater recovery. In the four optimum voltage pulses, 10V pulse for 0.08 second was the best for achieving the greatest rate of membrane performance recovery and consuming the least energy if the overall resistance (R) of each cell was the same [Figure 4.28].

According to the impedance spectra of membrane cell exposed to SO_2, different SO_2 exposure period means different extent of cathodic polarization and serial resistance

increase. Thus, SO$_2$ exposure period may be irrelevant to the optimum voltage pulse. However, this conjecture needs further research in the future.
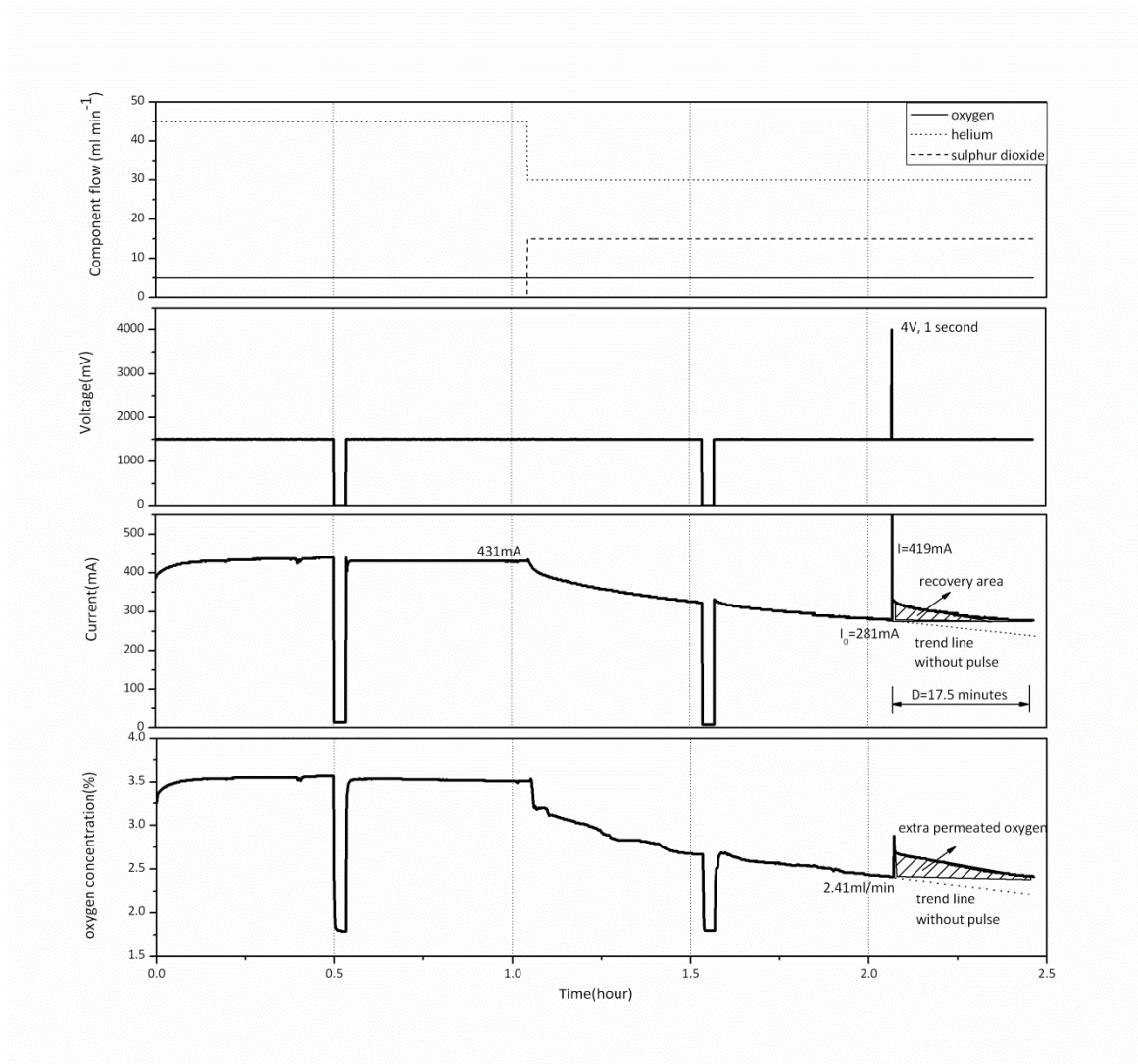
Figure 4.26: *Pt/8YSZ/Pt performance degradation and recovery at 850°C, the cathode exposed to He-O$_2$-SO$_2$ and the anode exposed to He.*
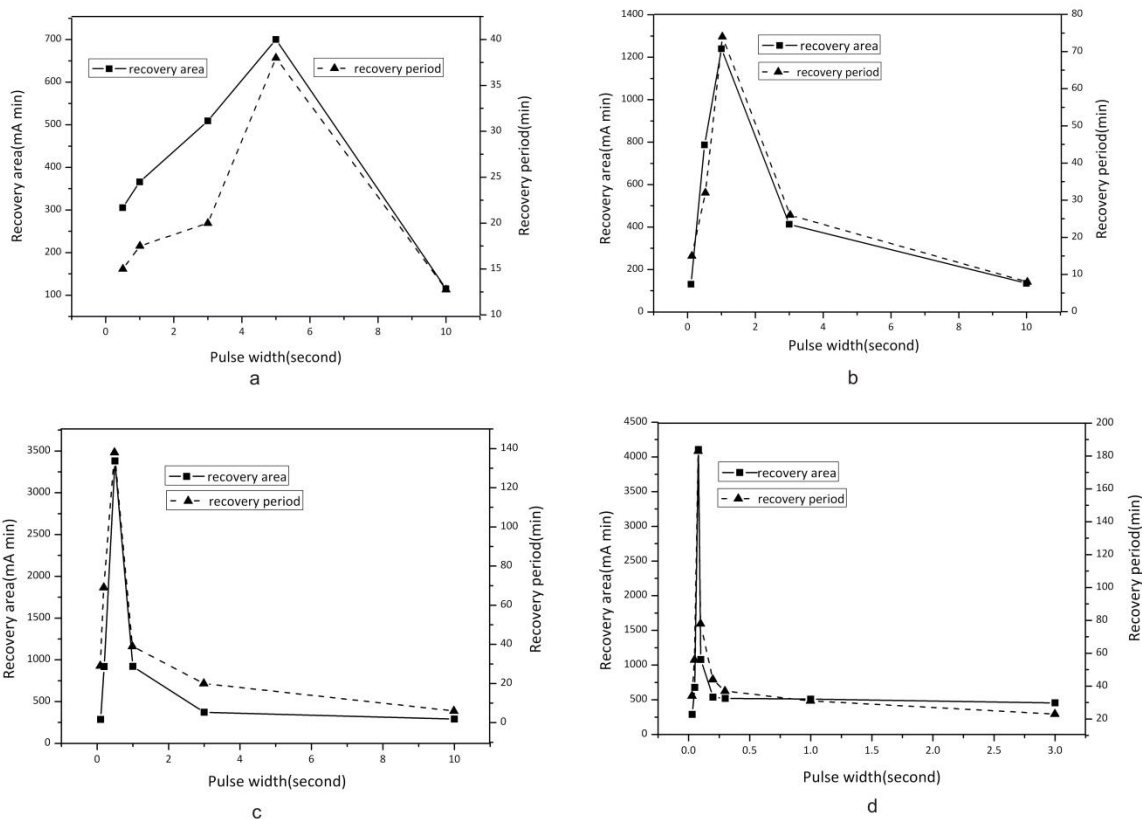
Figure 4.27: *Cell performance recovery period and recovery area after pulse treatment, a): 4V pulse with 0.5, 1, 3, 5 and 10 seconds; b): 6V pulse with 0.1, 0.5, 1, 3 and 10 seconds; c): 7V pulse with 0.1, 0.2, 0.5, 1, 3 and 10 seconds; d) 10V pulse with 0.03, 0.05, 0.08, 0.1, 0.2, 0.5, 1 and 3 seconds*
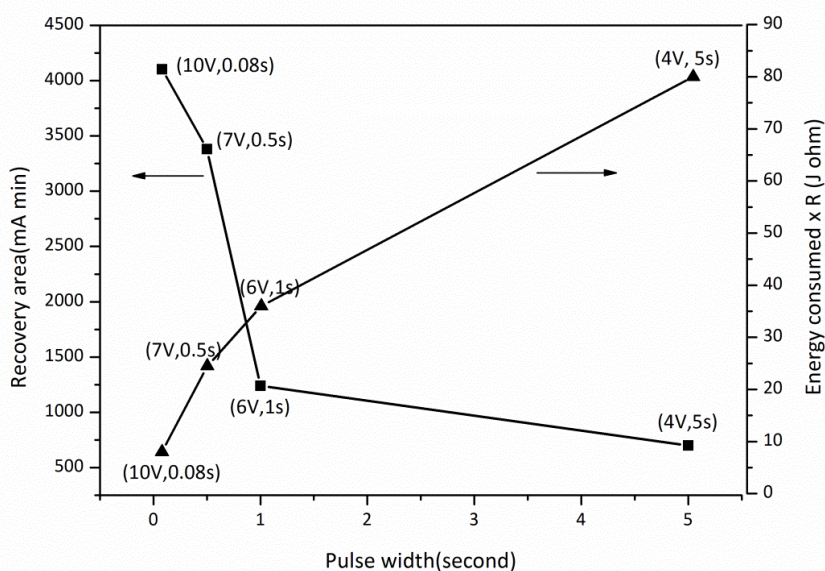
Figure 4.28: *Membrane performance recovery and energy consumed of optimum voltage pulses*

In order to explain the effect of different voltage pulses on rate of performance recovery, oxygen permeation through YSZ was introduced. On the cathode surface, the electrochemical reaction between oxygen and YSZ can be described with the following overall reaction:

$$O_2(g) + 2V_o^{\cdot\cdot} + 4e^- \rightarrow 2O_o^x$$
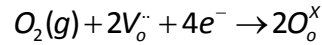
$V_o^{\cdot\cdot}$ is an oxygen vacancy and O_o^x is a normal oxygen ion in the YSZ lattice. A possible oxygen reduction on the interface of Pt and 8YSZ is shown in Figure 4.29 (Chen et al. 2003).
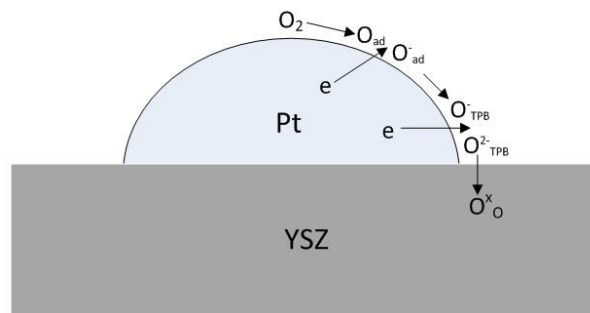
Figure 4.29: *Schematic of oxygen reduction path on Pt electrode*

This overall reaction can be divided into six elementary steps, as follows:

Step1: $O_2\ (bulk) \rightarrow O_2(interface)$

Step2: $O_2\ (interface) \rightarrow 2O_{ad}$

Step3: $O_{ad} + e^- \rightarrow O_{ad}^-$

Step4: $O_{ad}^- \rightarrow O_{TPB}^-$

Step5: $O_{TPB}^- + e^- \rightarrow O_{TPB}^{2-}$

Step6: $O_{TPB,Pt}^{2-} + V_{O,YSZ}^{\cdot\cdot} \rightarrow O_{O,YSZ}^x$
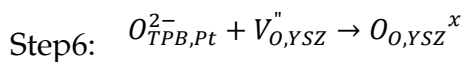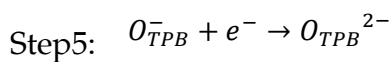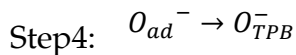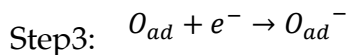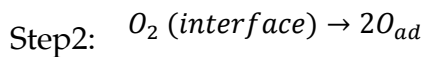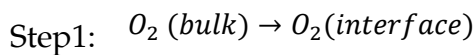
Step 1 and 2 is actually oxygen adsorption and dissociation process. The rate of oxygen adsorption onto platinum surface per unit area is given by $r = k(c_0 - c)$, where c is the local surface concentration of oxygen, c_0 is the surface concentration at equilibrium with oxygen, and k is a surface exchange coefficient which depends on

temperature, oxygen pressure and electrode (Mutoro et al. 2011) (Mosleh et al. 2009) (Sasaki and Maier 2003). Once adsorbed, oxygen can also diffuse along the platinum surface, with 1-dimensional flux per unit width of $N = -D(\partial c / \partial x)$, where D is the surface diffusion coefficient. This is the surface diffusion process with oxygen ionization (step3, 4 and step 5). Step 6 is the charge transfer reaction by forming a mobile oxygen ion in the YSZ lattice. According to these six steps, the rate of oxygen reduction on the cathode surface can possibly be affected by oxygen pressure, electrode surface and microstructure, current density through the cathode, oxygen ion conductivity of YSZ. In the case of 8 mol% yttria-stabilized zirconia at 850°C, oxygen ion conductivity of YSZ will remain the same for constant oxygen pressure (approximately 10^{-4} atm). Therefore, the rate controlling steps for the oxygen reduction reaction could be oxygen supply in feed, oxygen adsorption, surface diffusion of the oxygen intermediate species on the Pt surface, and incorporation of the oxygen ions into the YSZ electrolyte lattice.

The rate controlling step in this case can be indicated by current and permeate oxygen concentration change under different voltages and oxygen flow rates in the feed [Figure 4.30]. When the oxygen in feed is 5ml/min, the current and oxygen permeation concentration increased at the same rate after increasing external voltage from 0 to 4V. Continuing increase to 6V, however, the current jumped, against Ohm's law, to around 4A from 1.7A for 4V. On the contrary, oxygen permeation concentration had a slight increase first and then decreased slowly. At this time, an increase in oxygen flow rate in feed to 7ml/min made the current reduce to around 3A but the permeate oxygen concentration rise gradually. This suggests that 5ml/min of oxygen in the feed was insufficient for oxygen reduction at 6V. In other words, the rate controlling step for oxygen permeation process at 6V was changed to oxygen pressure in feed from surface exchange or surface diffusion on the interface between Pt surface and YSZ at below 4V. As expected, when oxygen flow rate and voltage came down, current and oxygen concentration had the same changes as previously. Therefore, the rate controlling step for oxygen reduction on the cathode

exposed to He-O_2-SO_2 (5ml/min O_2 in feed) with constant 1.5V polarization might be surface exchange and diffusion. High or long voltage could increase the oxygen permeation process and even cause the rate controlling step to shift to oxygen pressure in feed from surface exchange and diffusion.

It is worth noting that the membrane cell was broken into many small pieces after this experiment. This was attributed that high voltage for a long time produced a lot of heat which could cause the working temperature of membrane cell to increase and affect its mechanical strength.
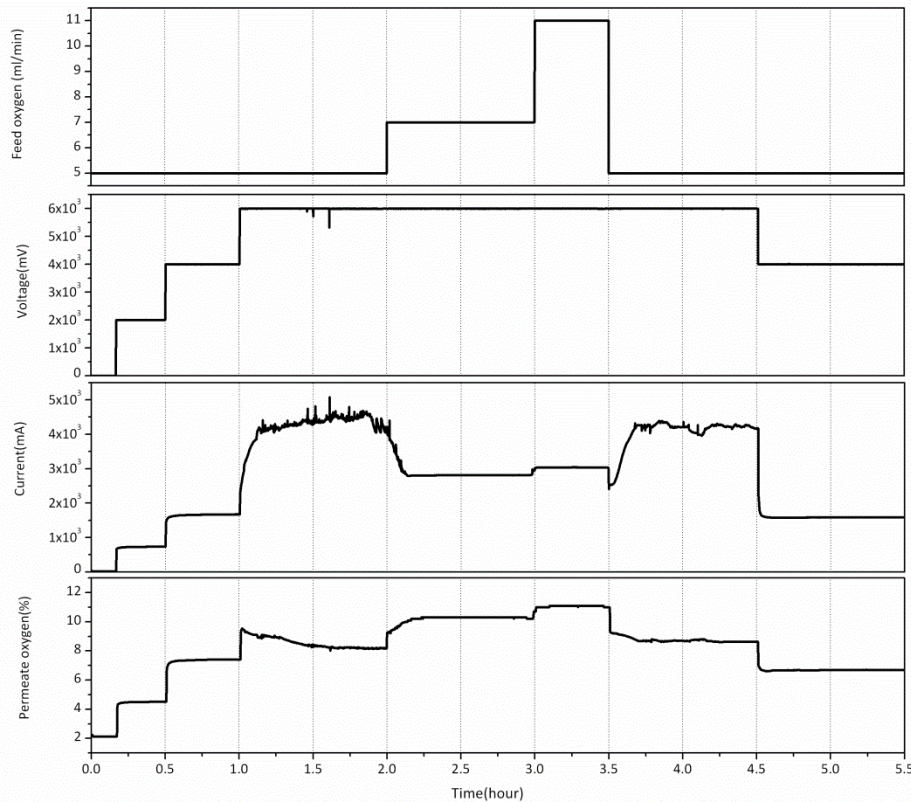
Figure 4.30: *Current and permeate oxygen concentration with external DC voltage and oxygen in feed, Pt/8YSZ/Pt at 850°C*

Therefore, too high or too long voltage pulses were not beneficial to membrane performance recovery. They may promote oxygen reduction dramatically, leading to the oxygen in the feed being insufficient and the rate controlling step for oxygen permeation process changed to oxygen pressure in feed. Even worse, the high

current density could produce a lot heat and a broken membrane cell.

4.7.4 Conclusion

According to the rate of performance recovery, the voltage pulse was optimised in terms of pulse magnitude and duration. The optimum voltage pulse in this study was 10V, 0.08 second for achieving the greatest rate of membrane performance recovery. The results showed that high or long voltage pulse obtained great rate of performance recovery, because they could reduce significantly cathodic polarization and serial resistance which was regarded to be related to sulphur desorption and sulphide dissociation respectively from the cathode surface. However, large voltage pulse in terms of magnitude and duration may lead to the rate controlling step for oxygen permeation process being changed to oxygen pressure in feed for a given oxygen flow rate and could result in a broken membrane cell.

4.8 Optimization of voltage pulse frequency

4.8.1 Aim

The aim of this work is to optimize voltage pulse frequency for maintaining a relative high and stable membrane performance in SO_2 exposure period.

4.8.2 Experimental

A series of experiments were carried out with the similar experimental method to previous run in Section 4.7. The electrode activation period was also 1 hour, but the SO_2 exposure period in each run was 2 hours. After 1 hours SO_2 exposure, the first pulse was applied and repeated by four different frequencies [Table 4.2].

Frequency (pulse/hour)	Voltage pulse (10V, 0.08 second)			
	Test 1	Test 2	Test 3	Test 4
	1 pulse/hr	2 pulses/hr	3 pulses/hr	4 pulses/hr

Table 4.2: *Optimization of the voltage pulses frequency*

4.8.3   Results and discussion

Before studying voltage pulse frequency, membrane performance in SO_2 exposure period was observed without any voltage pulse treatment. The current change with time is presented in Figure 4.31, with the current after normalisation shown in the bottom graph. SO_2 was introduced into feed from the 2nd hour, after which the current decreased slowly following the initial quick poisoning stage. After 2 hours, the SO_2 addition was cut off when the current was 296mA accounting for 65.0% of membrane performance remaining.
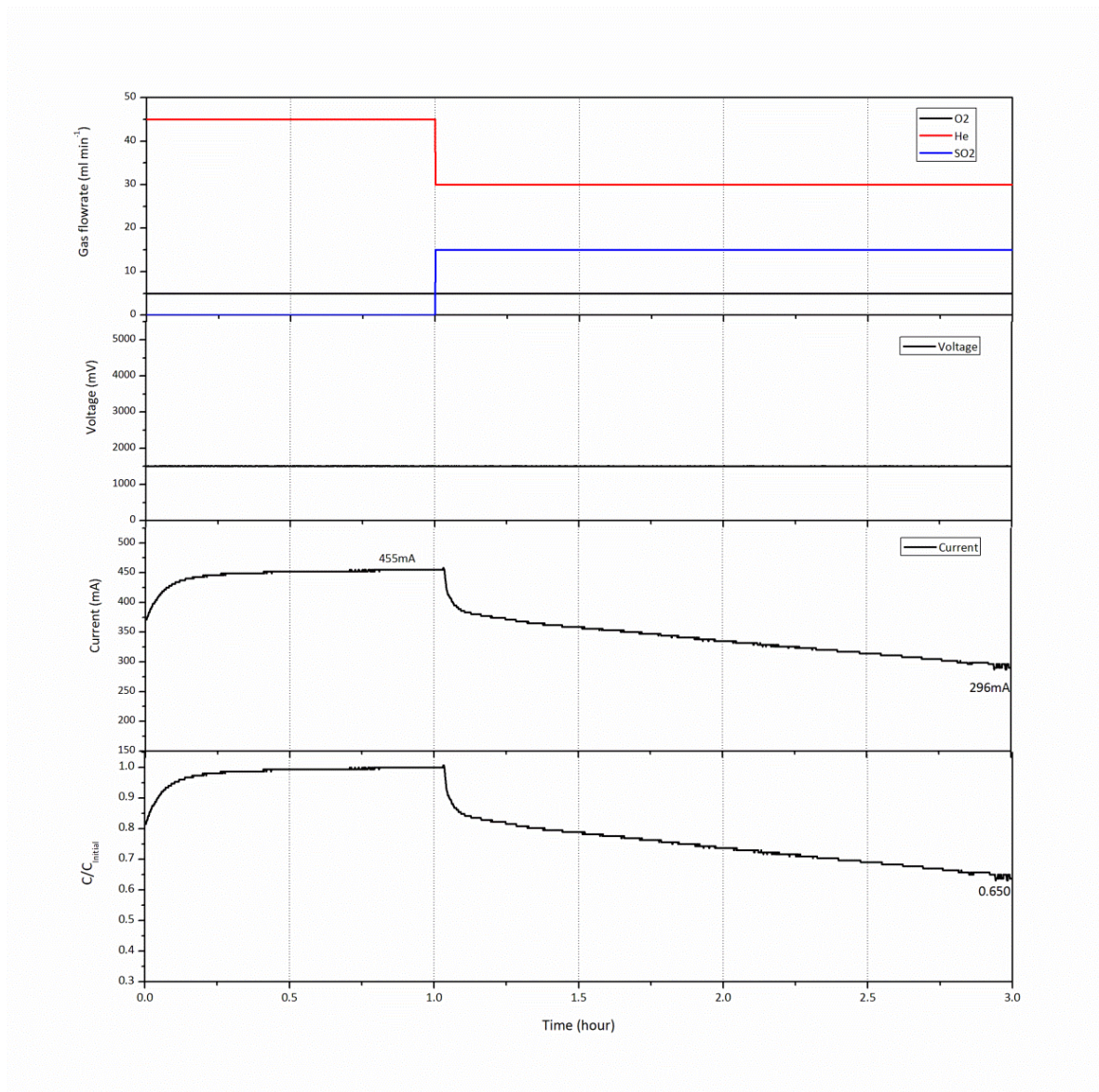
Figure 4.31: *Performance change of Pt/YSZ membrane exposed to SO_2, at 850°C*

In the same manner in Figure 4.31, current change under SO_2 of Pt/YSZ membrane treated by 10V (0.08s) pulse with different frequencies is shown in Figure 4.32-4.35. With periodical voltage pulses, the current improvements of Pt/YSZ membrane can be repeated in each test. Even though the samples were different, the current still responded in exactly the same way to voltage pulses.

By looking at the normalised graphs, it can be seen that the degrees of degradation over SO_2 exposure period before starting to pulse are different. It may be related that the samples had different porous electrode surface, since all the other factors including the temperature, the pressure, feed streams and the electrolyte in these cases are the same. But based on the present results, it is difficult to explain well the relationship of electrode structure and degree of cell performance degradation by SO_2.

After 2 hours SO_2 exposure time, the final currents are 401, 493, 438 and 588mA for the four tests with voltage pulse frequencies are 1, 2, 3 and 4 pulses/hour respectively. At the same time, the rates of remaining membrane performance assessed by current are 89.3%, 88.0%, 86.6% and 92.6%. The extent of membrane performance recovery before and after voltage pulses in each test is plotted in Figure 4.36 in terms of performance improvement and recovery area (shaped area in current graph). It is indicated that performance recovery is the greatest after 4 pulses. In other words, the membrane cell used in test 4 achieved the most stable performance in a 2-hour SO_2 exposure period. Therefore, high frequency of voltage pulse is helpful to improve membrane performance in SO_2 exposure period. However, higher frequency of voltage pulse means more energy consumed. From the current change with time in Figure 4.32-4.35, the energy consumed by voltage pulses and the moles of extra oxygen derived from the recovery area are shown in Figure 4.37. The energy use of four voltage pulses in the test 4 is 12.39 J which is more than the other three tests with fewer pulses. Meanwhile, the extra oxygen permeated of 3.68×10^{-4} mol in this test is the greatest.
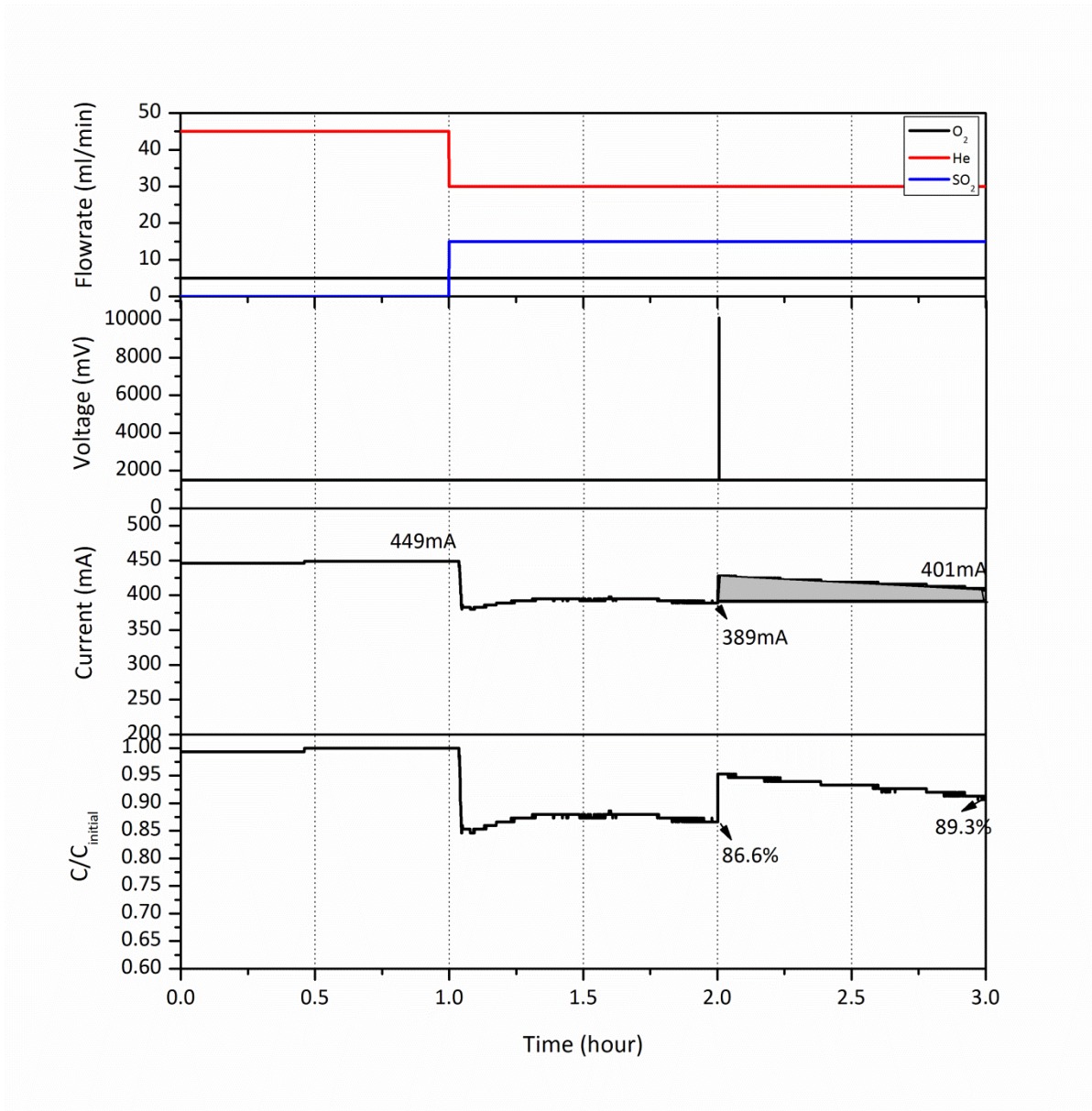
Figure 4.32: *Performance change under SO₂ of Pt/YSZ membrane treated by voltage pulse frequency of 1 pulse per hour, at 850°C*
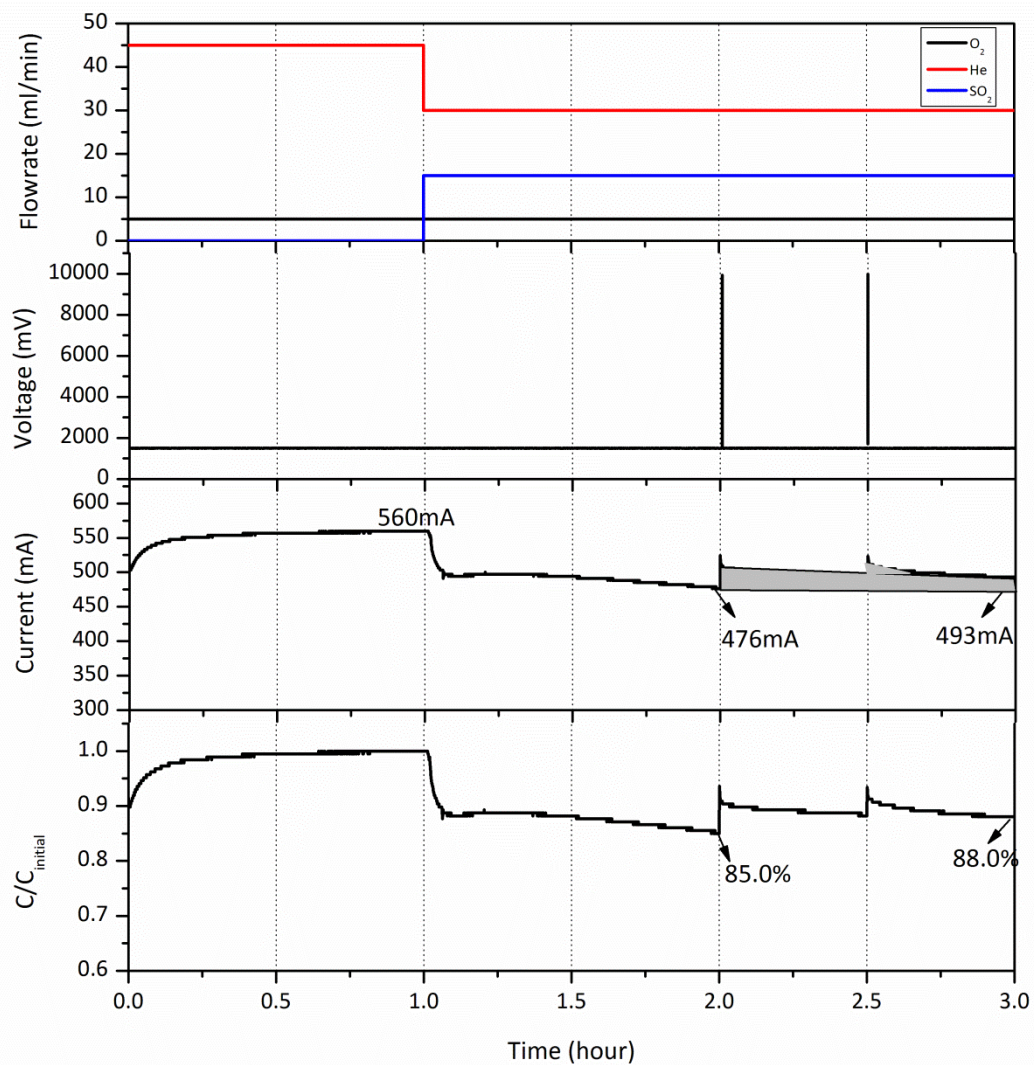
Figure 4.33: *Performance change under SO₂ of Pt/YSZ membrane treated by voltage pulse frequency of 2 pulses per hour, at 850°C*
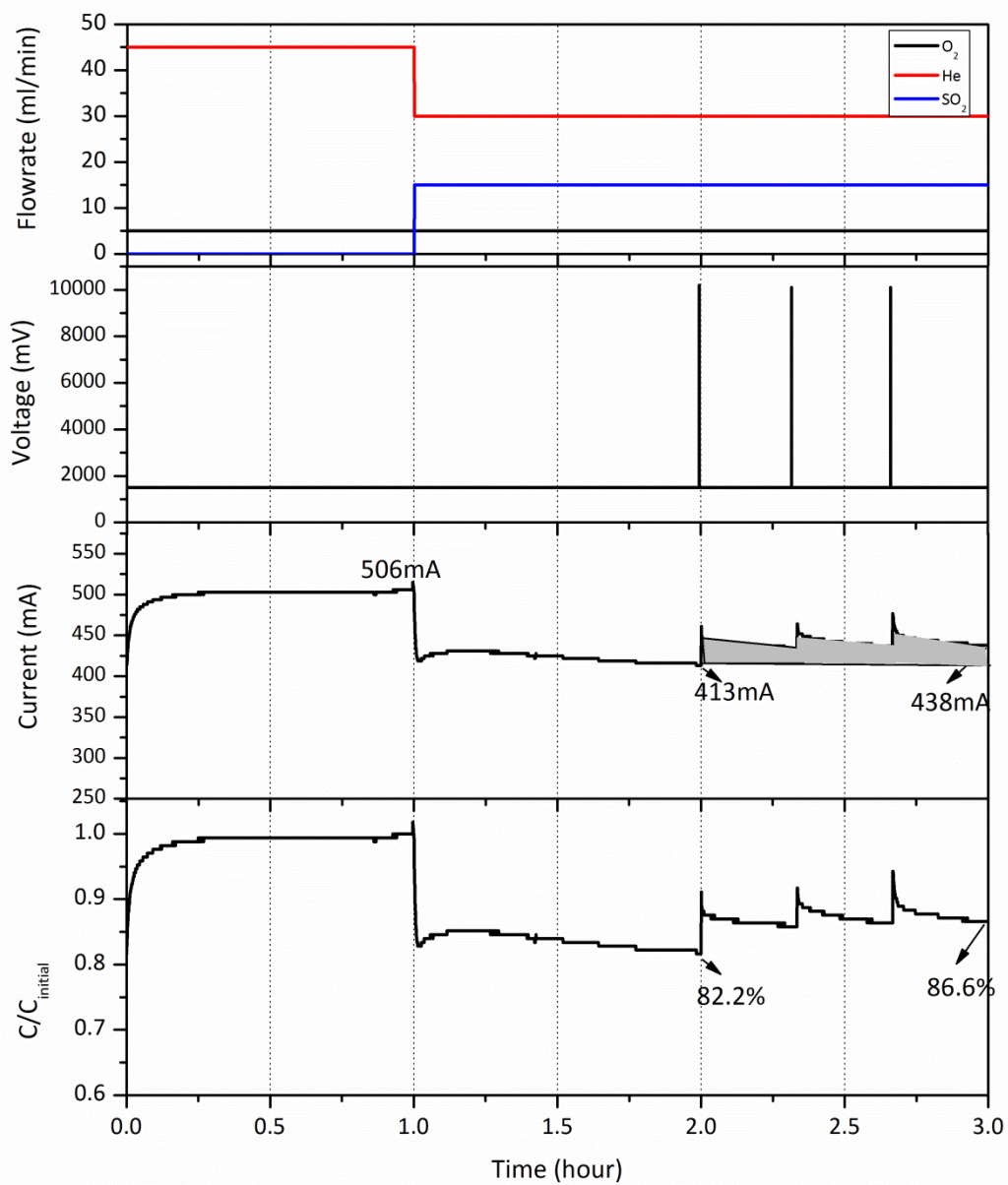
Figure 4.34: *Performance change under SO_2 of Pt/YSZ membrane treated by voltage pulse frequency of 3 pulses per hour, at 850°C*
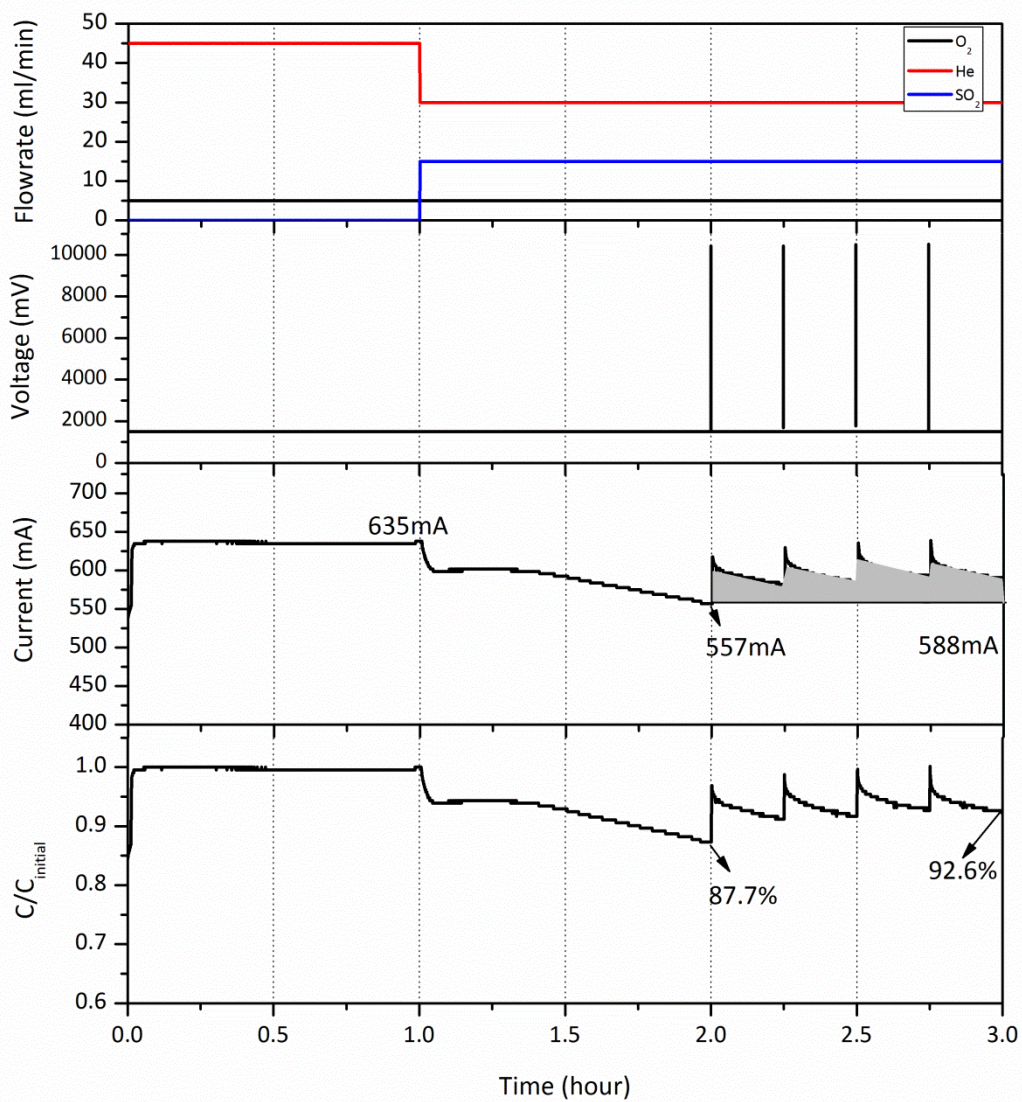
Figure 4.35: *Performance change under SO₂ of Pt/YSZ membrane treated by voltage pulse frequency of 4 pulses per hour, at 850°C*
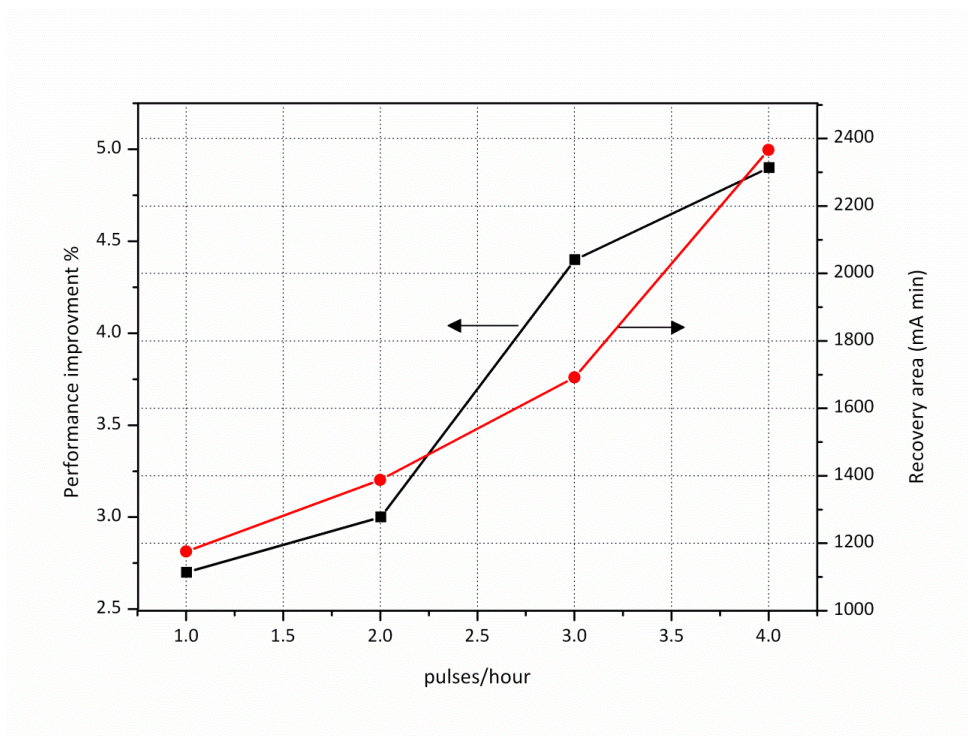
Figure 4.36: *The extent of membrane performance recovery by voltage pulses*
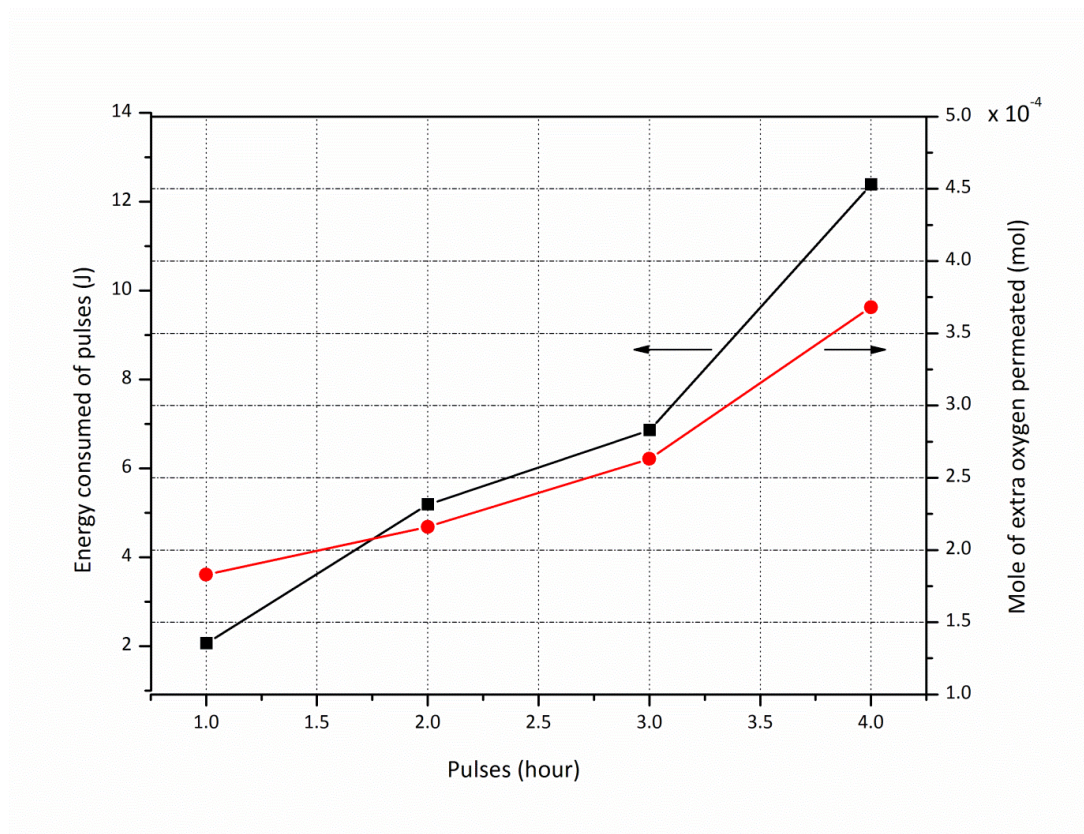
Figure 4.37: *Energy consumed of voltage pulses and mole of extra oxygen permeated*

As mentioned before, a high voltage pulse can obtain partial performance recovery of Pt/YSZ membrane exposed to high concentration SO_2 by removing sulphur from cathode surface or Pt/YSZ active area. Such improvement in membrane performance could be repeated by applying periodical voltage pulses. If the voltage pulse frequency is too low, its contribution to maintain membrane performance is small. Thus membrane performance recovery is insignificant. When the pulse interval is shorter, the positive effect of voltage pulse on membrane performance becomes attractive and membrane performance gets stable.

According to the economic comparison of membrane performance with and without pulsing in Figure 4.38, the energy consumed because of current improvement by voltage pulses is very low (213J in test 4 accounts for 2.2% of the energy consumption without pulses).
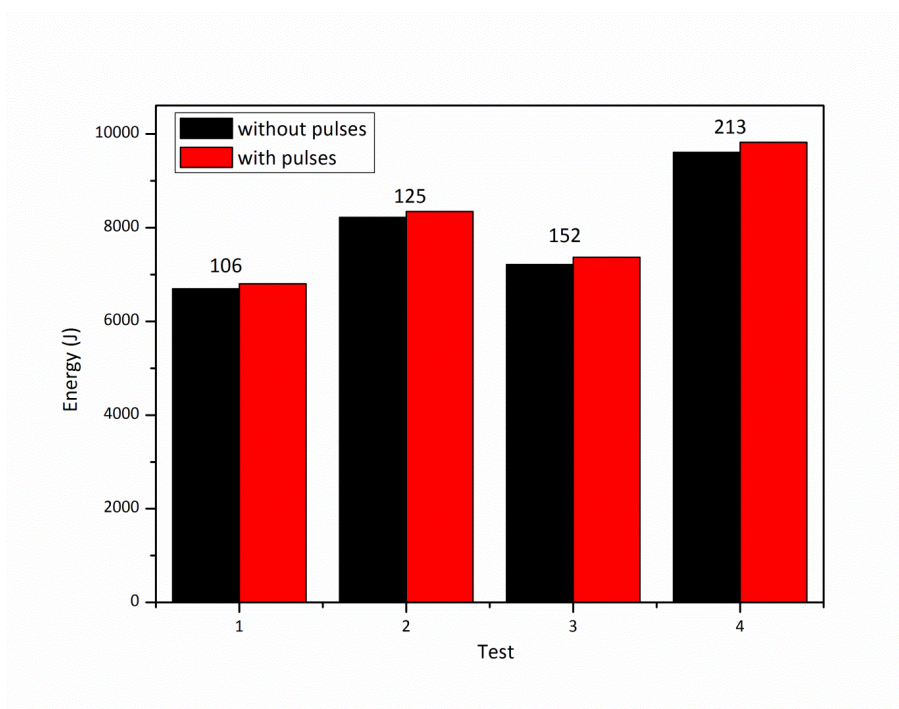
Figure 4.38: *The comparison of energy consumed in the four tests without and with pulses*

Therefore, high pulse frequency was recommended in consideration of membrane performance improvement and energy consumption of voltage pulses. However, this recommendation may be amended after a long SO_2 test with many more high

voltage pulses. Because along with the removal of sulphur from the cathode surface or Pt/YSZ interface by a high voltage pulse, the platinum electrode may also undergo changes in surface structure (Bay and Jacobsen 1997) (Emery et al. 1998) (Adler 2004) (Poppe et al. 1998) although this change was not detected by surface analysis techniques such as XRD, XPS and TEM (Xin 1997). Therefore, too frequent voltage pulses may cause surface structure changes of the Pt cathode, which could affect membrane performance. This is also inferred by the observation that the membrane cell was broken under high voltage for a long time [Figure 4.30].

In order to determine the optimum pulse frequency, it is required in the future to observe membrane performance and analyse its structure change after a long SO_2 exposure period with high frequency of voltage pulses. What need reminds is that the SO_2 exposure period before applying voltage pulse in my research is 1 hour. Therefore, the effect of SO_2 exposure period before pulses on cell performance recovery should be determined firstly in the future work.

4.8.4 Conclusion

Four 2-hour SO_2 exposure tests with different pulse frequencies of 10V for 0.08 second were carried out at 850°C and with constant external voltage of 1.5V. It was confirmed that membrane performance degradation could be reduced significantly by high voltage pulses in an extended SO_2 exposure period. The performance recovery could be repeated by periodic voltage pulses. Also the currents of different membrane cells in each run responded the same way to voltage pulses. By comparing the current after normalization and recovery area, the membrane cell used in the test 4 with a frequency of 4 pulses per hour had the most stable performance. At the same time, energy used by these pulses and per mole of oxygen produced are 12.39J and 33.7kJ/mol.

In terms of cell performance improvement and the extra oxygen permeated by voltage pulse treatment, it is indicated that shorter pulse interval was more helpful to keep membrane performance at high level and high pulse frequency was

recommended for maintaining a stable membrane performance in a short SO_2 exposure test. However, high frequency voltage pulse raises the energy consumed and may affect the electrode surface. Therefore, more work on membrane performance in a long SO_2 exposure period are required in the future to determine the optimum pulse frequency in consideration of the extra oxygen permeated, energy consumption by voltage pulses and the influence of voltage pulse on electrode surface.

4.9 Conclusion

After the study on the mechanism of performance degradation of Pt/YSZ exposed to SO_2 and O_2 at high temperature, membrane performance recovery by high voltage pulses was researched. Comparing the surface analysis results of XRD, SEM-EDS and Raman spectroscopy for two Pt/YSZ pellets before and after voltage pulse treatment, the performance recovery may be attributed to removal of platinum sulphide on the cathode surface by a voltage pulse applied in SO_2 exposure period. Positive and negative voltage pulses could both obtain partial membrane performance recovery, and their effects were similar when measured by comparing recovery area and recovery period. Using *in-situ* electrical impedance measurement, the impedance of Pt/YSZ shown that polarization resistance and serial resistance both increased with SO_2 exposure time. This might be attributed to sulphur adsorption on the cathode surface and platinum sulphide on the interface of Pt and YSZ, respectively. Application of a 7V pulse on membrane cell in SO_2 exposure period obtained a significant increase in current which included a visible decrease in polarization resistance and a slight decrease in serial resistance. It implies that high voltage pulse has an effect on charge transfer and mass transfer properties, and this effect might help the removal of sulphur on cathode surface by electrochemical reactions.

According to the rate of performance recovery, the voltage pulse was optimised in

terms of pulse magnitude and duration. The results showed that high or long voltage pulses could obtain a substantial rate of performance recovery because they appear to cause sulphur desorption from the cathode surface and sulphide decomposition in the interface area of electrode and electrolyte. However, too long or too high voltage pulses may lead to the rate controlling step for oxygen permeation process changing to oxygen pressure in the feed for a constant oxygen flowrate. The optimum voltage pulse in this study was 10V for 0.08 second in terms of performance recovery area and energy usage. This pulse was then used in the experiments to optimise pulse frequency. In four 2-hour SO_2 exposure tests, membranes had the most stable performance when voltage pulse frequency was 4 pulses per hour. The energy consumption rose with the pulse frequency to 12.39J of 4 pulses in test 4. At the same time, the energy used per mole of oxygen produced was 33.7kJ/mol. Too low pulse frequency obtains a small amount of performance recovery. High frequency pulse could achieve high stable membrane performance and was recommended in a short SO_2 exposure test in consideration of cell performance improvement and economic comparison of membrane performance with and without pulsing. For a long SO_2 exposure run, more work is needed to optimise the pulse frequency in consideration of extra oxygen permeated, energy consumption of voltage pulse and influence of high frequency high voltage pulses on electrode surface.

Overall, the performance degradation of Pt/YSZ exposed to high concentration SO_2 at high temperature could be reduced by high voltage pulses and these have been seen to affect both charge transfer and mass transfer properties of the membrane cell. This effect may cause sulphur removal from the cathode of the membrane by desorption or dissociation processes. This provides a promising method to improve the overall efficiency of the sulphur family of thermochemical cycles or reduce the effect of sulphur containing impurities on SOECs performance. In this case, the optimum voltage pulse magnitude and duration for achieving the most stable membrane performance in SO_2 exposure time was 10V for 0.08 second. High

frequency was helpful for achieve a high and stable membrane performance in short SO_2 exposure tests. In order to determine the optimum pulse frequency, more work on observing membrane performance in long SO_2 exposure periods with high frequency voltage pulses are required.

Chapter 5

5 Performance of YSZ tubular membrane for oxygen separation from sulphur dioxide and comparison with Performance of Pellet system

5.1 Introduction

In the field of solid oxide fuel cells (SOFCs), there are two appropriate configurations, planar and tubular. The planar design offers higher oxygen production/removal capacity per unit volume but requires interconnect materials and cumbersome seals, which have to be stable during thermal cycling (Ciacchi et al. 2002). On the other hand, from the point of view of long term stability and demonstration of plant technology, the tubular concept is far more advanced and plays a leading role in the SOFCs field (Blum et al. 2005). Although one of the important obstacles in the development of SOFCs is high temperature sealing, much smaller sealing perimeter is needed for tubular cells than for planar cells, and the sealing part of tubular SOFCs can be located at a zone where the temperature is much lower than the main part of the fuel cell. In addition, the tubular design has been reported to be easily scaled-up, have better thermal cycling capability and higher mechanical stability (Shi et al. 2012). In the last few years, significant progress has been achieved in tubular SOFC development by Siemens Westinghouse Power Corporation (SWPC), a Japanese company TOTO and a U.S. company Acumentrics (Westwood, MA) (Blum et al. 2005). Some large-scale tubular SOFC demonstration units have been operated for increasing durations and demonstrated good cell performance (Lim et al. 2010).

Like the development of YSZ membranes in SOFCs systems, research and development of YSZ tubular membranes applied to sulphuric acid thermal decomposition for the S-I thermal cycle has the potential to be very significant. A tubular membrane consisted of a 8 mol% yttria-stablized zirconia cylinder was

therefore tested. Oxygen permeation characteristics of this tubular membrane exposed to O_2 and SO_2 at high temperatures was demonstrated. The main content in this chapter includes:

- Design and fabrication of tubular YSZ membranes and other components;

- Construction of membrane separation assembly including sealing test and electrical connection for external dc voltage application;

- Examination of tubular membrane performance under He-O_2 in feed;

- Examination of tubular membrane performance under He-O_2-SO_2 in feed;

- Tubular membrane performance before and after a strong but short dc voltage pulse;

- Comparison of oxygen permeation fluxes of tubular and planar membranes from the point of view of electrode, electrolyte and fluid flow dynamics.

As previously, all experiments were carried out at a constant temperature (850°C) and pressure (1.0 atm). The pressure was limited to atmospheric to simplify the apparatus. Recording the oxygen permeation performance with a He-O_2 feed, along with the pre-exposure characterization, provides a baseline against which the performance in the presence of SO_2 can be compared.

Only the inner face of the YSZ tubular membrane was exposed to the test mixture. The other 'permeate' face was maintained at zero oxygen partial pressure by sweeping the face with helium.

YSZ is a poor electronic conductor and requires an external electron conduction path to operate electrochemically. The external potential applied across the membrane was set at 1.5V. The positive polarity output terminal of the dc power supply was connected to the inner face of the membrane (cathode surface), while the negative polarity output terminal was connected to the outer face of the membrane (anode surface). The partial pressure of oxygen in the feed before and after SO_2 introduction was assumed to remain constant.

5.2 YSZ tubular membrane specification and fabrication

The 8Y-FSZ (8 mol% yttria full stabilized zirconia) tube was provided by Dynamic Ceramic Ltd and has the highest oxygen ionic conductivity and good chemical stability over wide temperature and oxygen partial pressure range. Figure 5.1 shows a photograph of the tube. The material properties provided by the company are given in Table 5.1.

Figure 5.1: *The photograph of 8Y-FSZ tube (OD 21mm x ID 16mm x Length 220mm)*

Density	Rexural strength (800°C)	Compressive strength	Modulus of elasticity	Poissons Ratio	Hardness	
g/cm^3	MPa	MPa	GPa		Hv$_{0.3}$	
5.7	270	1500	160	0.30	700	
Fracture toughness	Max. use Temp.	Thermal expansion coeff.	Thermal conductivity	Thermal shock resistance	Resistivity 25°C	Resistivity 1000°C
MPam$^{1/2}$	°C	x 10^{-6}/°C	W/mK	ΔT°C	Ohm.cm	Ohm.cm
3.5	1800	11	2.5	200	10^8	<10^3

Table 5.1: *Material properties of 8Y-FSZ tube*

Metalor 6082 platinum (Pt) ink supplied by the Department of Material and Science

Engineering (The University of Sheffield) was coated on the inner and outer wall of the YSZ tube. Initially, Pt paste was painted on the inner wall of YSZ tube sporadically using a long steel spatula. A plug made from PTFE mounted on a long stand steel stick was pushed slowly and evenly through the tube. After three times, the tube was placed into a furnace and sintered at 900°C in air for two hours with a heating and cooling speed of 5°C per minute to burn out the organics and create an adhered porous platinum layer on the YSZ tube surface. Following the inner wall painting, platinum ink was coated to the outer face using a small brush. This Pt layer was also deposited on the outer surface of the tube by the same sintering program (sinter in air at 900°C for 2 h with heating/cooling rate of 5°C min^{-1}). The steps involved in the Pt/8YSZ/Pt membrane preparation are shown in Figure 5.2.
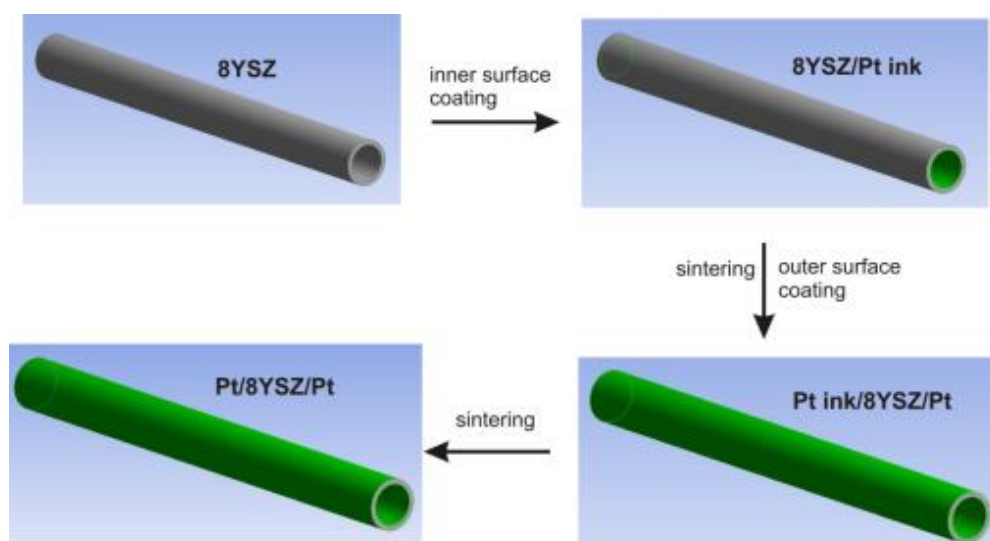
Figure 5.2: *Preparation of Pt/8YSZ/Pt tubular membrane*

Due to the manual coating of the platinum ink, the thickness of platinum layer was not uniform, expecially for the inner electrode layer [Figure 5.3]. But the aim of this work was to observe the oxygen permeation process across a tubular YSZ membrane exposed to high concentration SO$_2$, as well as the performance change after dc voltage pulse treatment. The effect of electrode on membrane performance is not within the scope of this work.
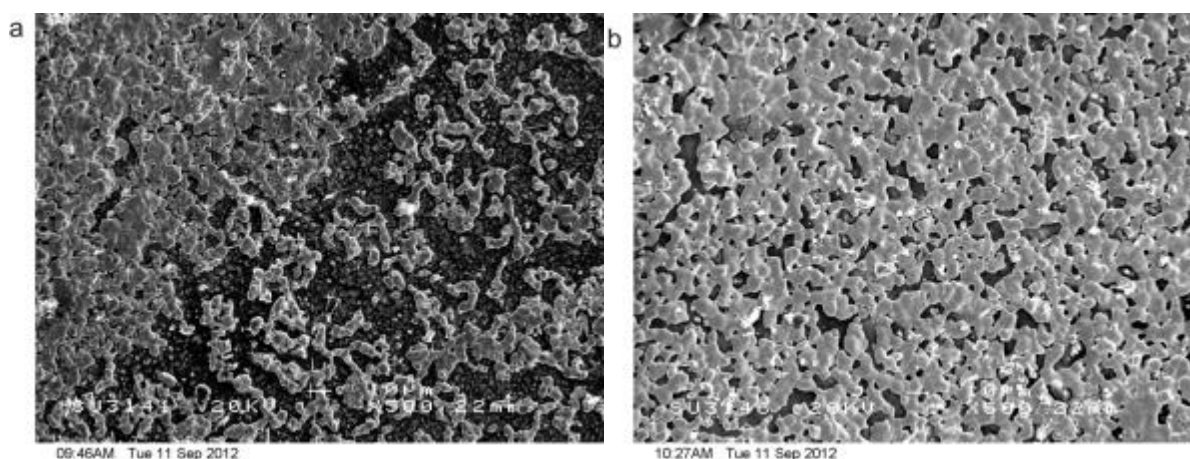
Figure 5.3: *The SEM image of the inner Pt electrode layer (a) and outer Pt electrode layer(b)*

5.3 Membrane exposure/permeance apparatus

5.3.1 Description and schematic

The experimental rig process schematic is shown as Figure 5.4. The rig was designed to allow a measured mix of GC grade helium, high purity oxygen, and/or sulphur dioxide to be fed from high pressure cylinders to the feed side of the membrane tube. As previously, a measured supply of helium was fed to the permeate side to act as the sweep gas, maintaining zero oxygen partial pressure on the permeate side. The gases, supplied by BOC Company, were regulated to be around 1 bar. The membrane tube was located in the centre of a furnace whose temperature can be varied as required. An external dc power supply was connected to the inner and outer electrode surfaces of the tube, in order to apply dc voltage through the membrane. It was also linked to a computer using USB port for recording electrical current. A gas analyser was located outside of the furnace to measure oxygen concentration with helium on the permeate side.
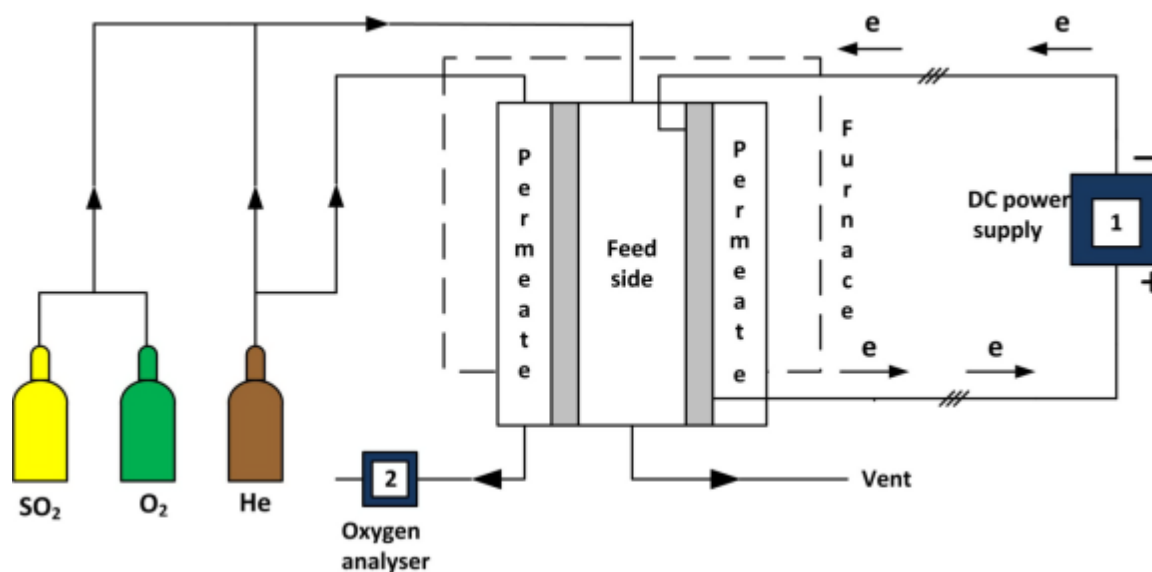
Figure 5.4: *Schematic of membrane tubular separation process*

5.3.2 Apparatus for oxygen permeation process

The core of the whole apparatus is a Carbolite MTF tube furnace (MTF 12/38/250), whose inside diameter is 38mm and heating length is 250mm. The dimension of YSZ tube mentioned above also is determined from this furnace. Each component in the oxygen permeation process assembly is introduced as following.

Pre-heating quartz tube

The design of pre-heating quartz tube was derived from the membrane holder used in YSZ pellet system (Section 3.3.2). It was designed after a heating calculation, the detail of this calculation can be found in Appendix A.

The quartz tube, consisted of a S-shape tube and a head and is fabricated by Robson Scientific. Its design and fabrication are presented as Figure 5.5. The bottom end is the inlet of feed gases, while the other end is docked with the membrane tube.
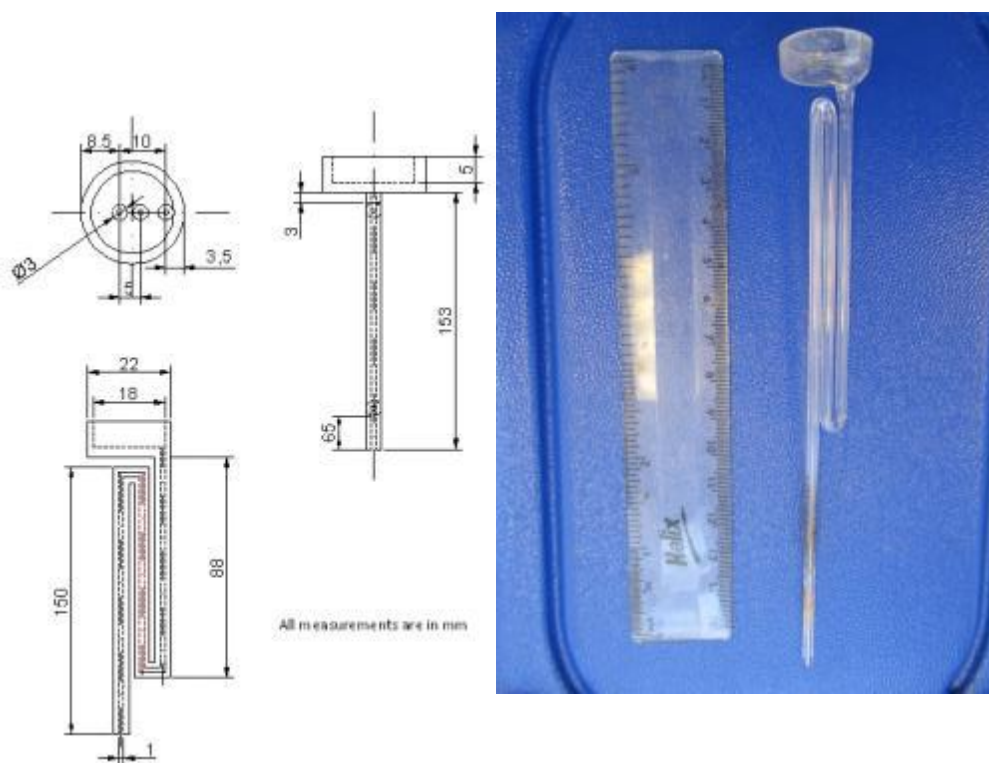
Figure 5.5: *Schematic design and fabrication of pre-heating quartz tube*

Support and top weight

Similar to the membrane holder support in the YSZ pellet system (Atkin 2009) , a support and a weight are designed to provide sufficient force for sealing. The support is made from stainless steel 310 which has a good acid corrosion resistant and mechanical strength at high temperature [Figure 5.6]. It has four legs for the top weight [Figure 5.7] having four holes, and it allows the membrane tube to stand along the central axis of tubular furnace. The weight is fabricated by standard carbon steel since it operates at relative low temperature, being located outside of the furnace.
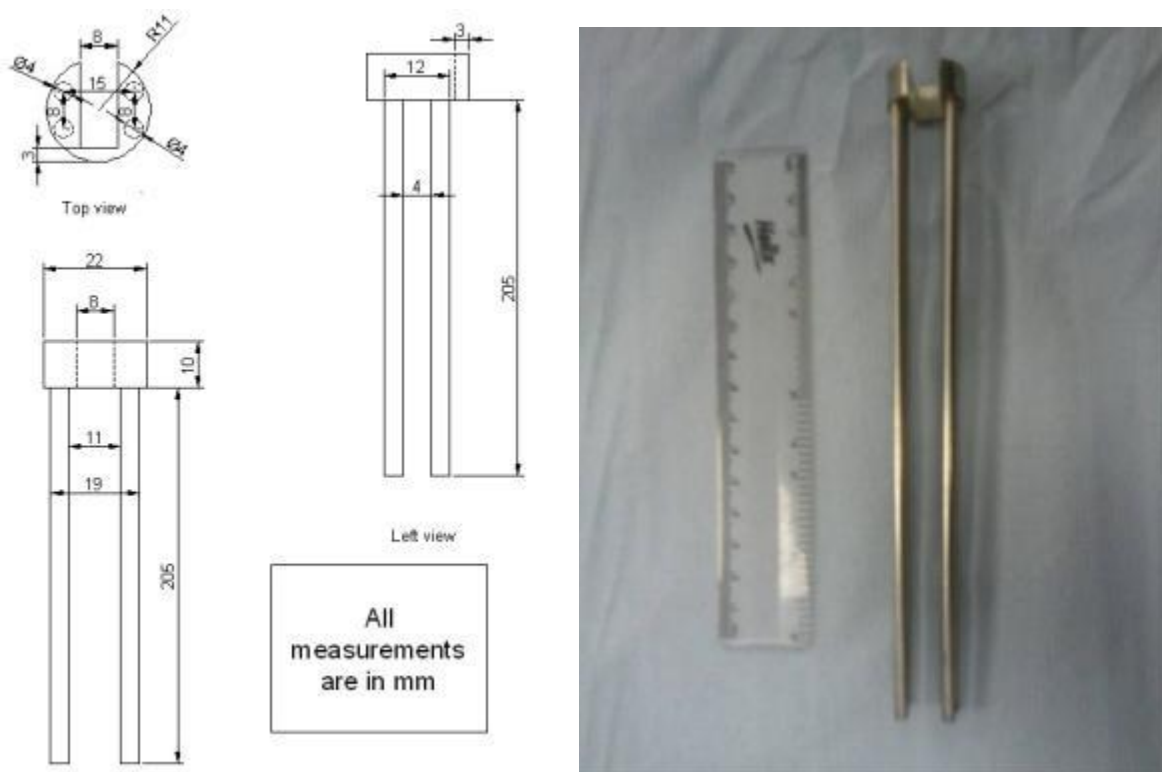
Figure 5.6: *Schematic design and fabrication of the support*
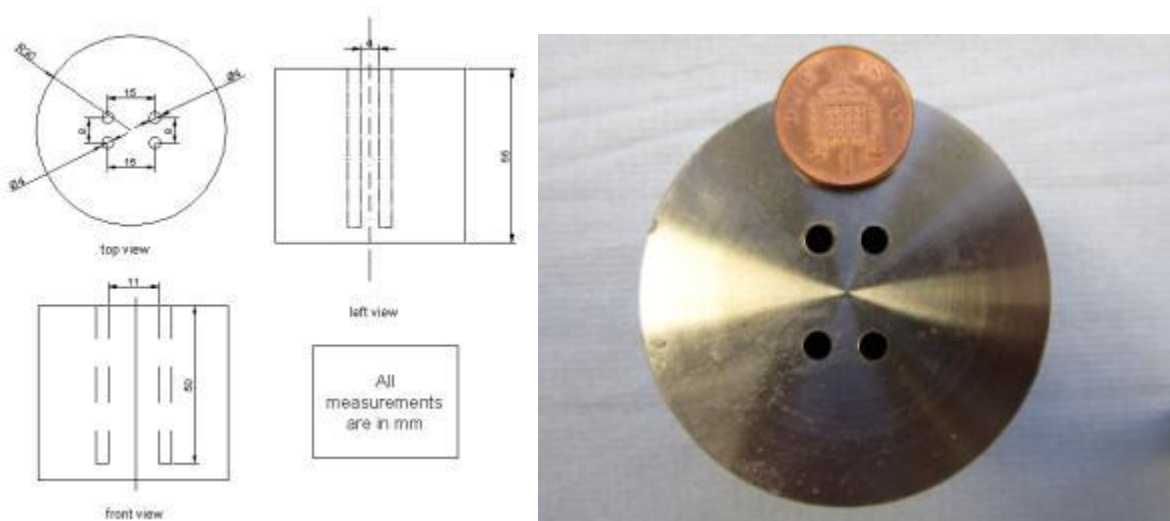
Figure 5.7: *Schematic design and fabrication of the top weight*

Long quartz tube

This hollow quartz tube [Figure 5.8] was made by Robson Scientific as well. One of its ends is open, while the other closed end is provided with five holes. One of these holes is 3mm in diameter to make the inlet of the pre-heating tube pass through exactly; the remaining four holes are 4mm in diameter to place the weight on the top

of the support. The open end will be attached to a stand.

After covering the pre-heating tube, the support and the membrane tube, an annular space is formed between the membrane tube and this quartz tube.

Top view

Front view

Let view

360

28.8

32

360

15

All measurements are in mm
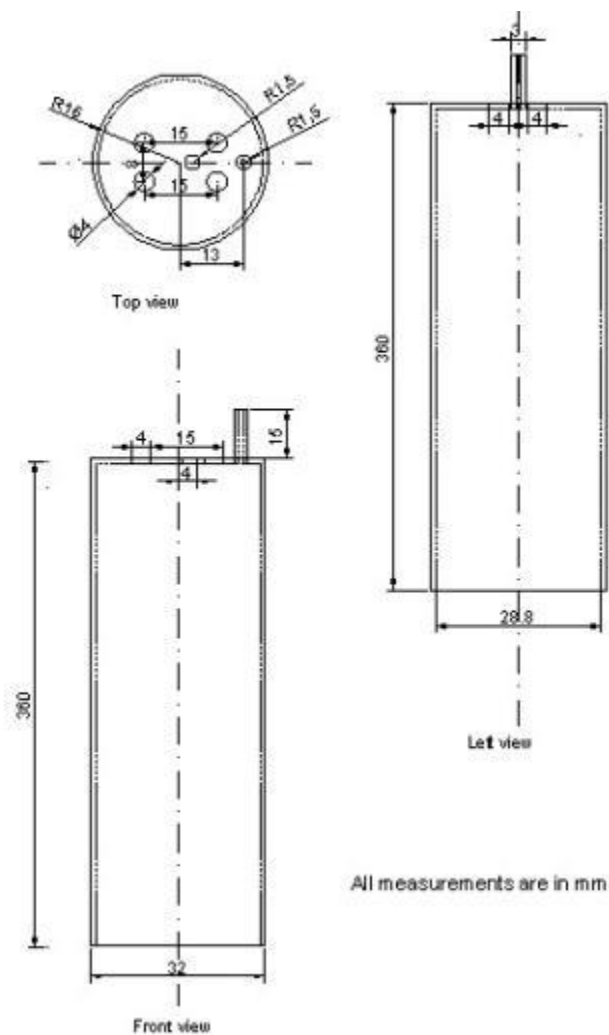
Figure 5.8: *Schematic design and fabrication of the long quartz tube*

Bottom stand

This stand made from standard steel is the most complicated part in the assembly. It has two holders for sustaining the membrane tube and the long quartz tube, respectively [Figure 5.9]. Inside the membrane tube holder, there is a channel for the exhaust of a retentate stream after the oxygen permeation process. Outside the membrane tube holder, there is a small hole leading to an outlet for permeated oxygen. In the quartz tube holder, a PTFE roll is used to make sure the quartz tube is

upright and to avoid contact between the stand and the quartz tube.

The outlets of oxygen and retentate, are threaded and connected with PFTE tubing to an oxygen analyser and vent respectively.
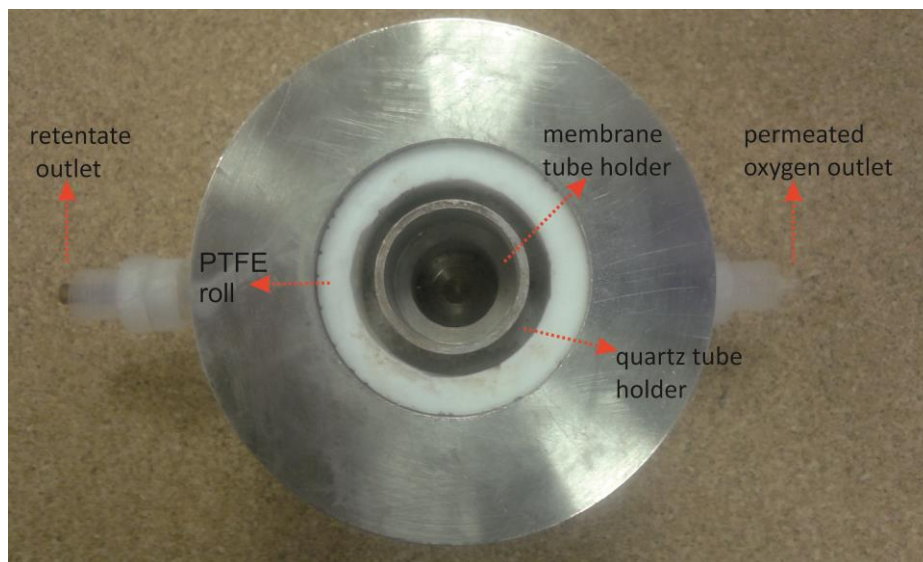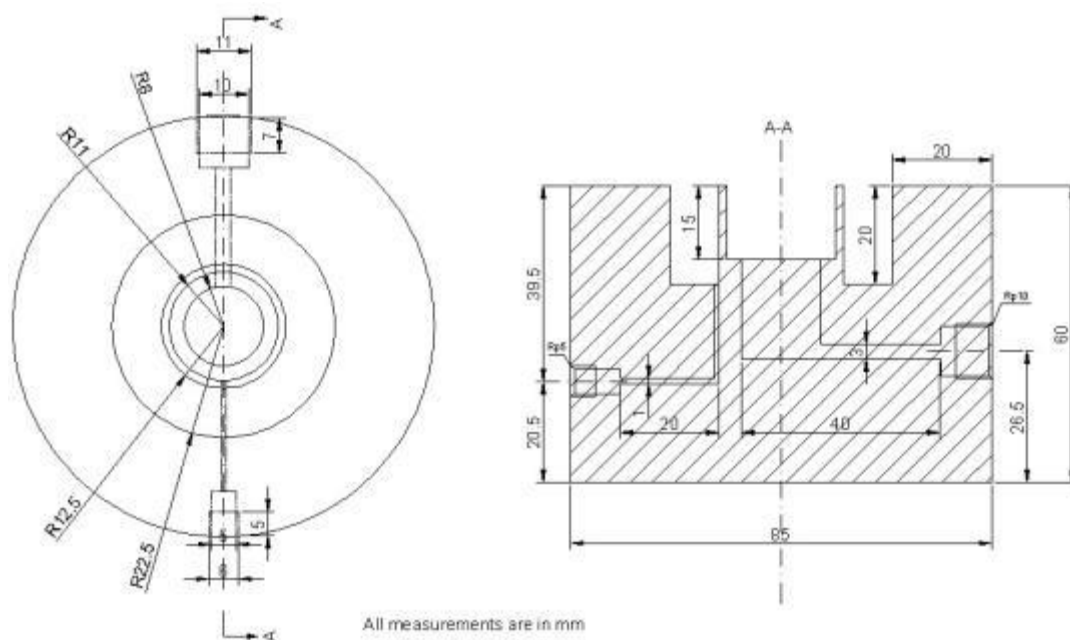
Figure 5.9: *Schematic design and fabrication of the bottom stand*

5.3.3   The assembly

Figure 5.10 shows the assembly containing all components mentioned above, including a top weight, a support, a quartz tube, a pre-heating tube, a YSZ tube and

a bottom stand. Gas mixtures containing helium, oxygen and sulphur dioxide enter the rig from the inlet, pass through the pre-heating tube and the YSZ tube. Oxygen permeates to the permeate side and then exits with helium. While helium and sulphur dioxide flow out through the bottom stand to the vent.

The assembly connection is sealed with the top weight, support and bottom stand. Although the support is exposed to oxygen and helium at high temperature, a continuous insulating oxide layer is developed on the surface of the support after several initial tests. This layer prevents the further oxidation reaction on the support surface.

As shown in Figure 5.4, an external dc power supply is required to apply a dc voltage cross membrane tube. The membrane electrical connection is described in detail in Section 5.4. Two ring gaskets are placed at the ends of membrane tube. Also a kind of sealant tap is used to seal the ends of quartz tube. More detail on sealing test is introduced in Section 5.5.
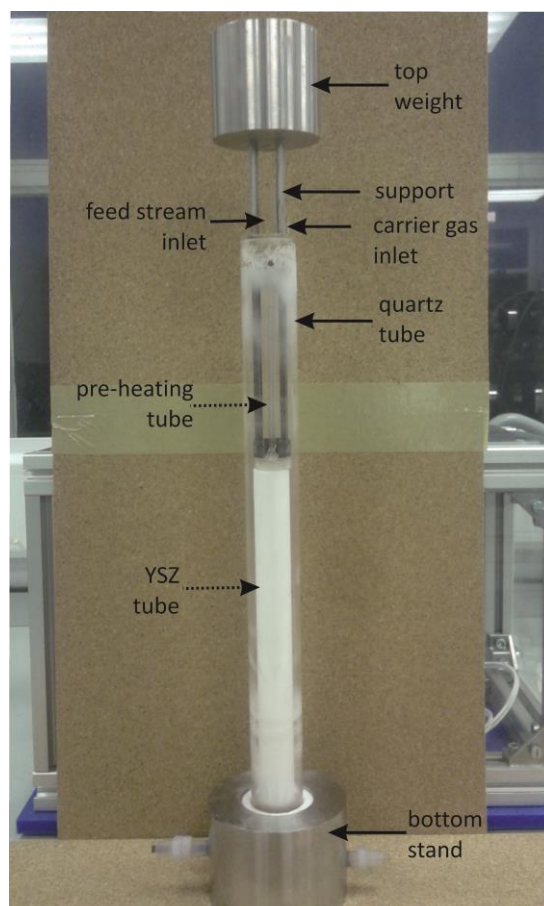
Figure 5.10: *Assembly of the rig*

5.4 Membrane electrical connection

The connection of outer membrane surface to power supply is through a piece of gold sheet attaching on the membrane tube holder. Once membrane tube is held, its outer surface, coated by the platinum layer connects to the gold sheet very well [Figure 5.11]. In this method, the outer surface of Pt/YSZ/Pt tube could be connected indirectly to external power supply via the bottom stand and the gold sheet.

For the inner membrane surface, a platinum wire (0.25mm thickness, 5cm length) is set inside of membrane tube [Figure 5.12]; the other end of platinum wire is connected to the support. Indirectly, the inner surface of membrane is connected to external power supply by the support and the platinum wire.

Figure 5.11: *Electrical connection of tube outer electrode surface to power supply*

Figure 5.12: *Electrical connection of tube inner electrode surface to power supply*

5.5 Sealing test

The membrane tube and the pre-heating quartz tube could not be permanently bonded together because of differential thermal expansions and the need to remove the membrane for inspection. Therefore, gaskets are required to seal the ends of the membrane tube and the quartz tube.

5.5.1   Sealing at the ends of membrane tube

The separation process was conducted at 850°C and in acidic conditions. The inner and outer electrodes of the membrane tube would be connected to an external power supply. Therefore any gasket needs to meet the following requirements: 1) it can withstand high temperature up to 850°C minimum; 2) it is electrically insulated; 3) it has good acid corrosion resistance.

Thermoculite 866 supplied by Flexitalli. Ltd. is thought to be a promising candidate for the gasket. It has been used specially for sealing solid oxide fuel cell (SOFCs) and has proved to be very successful in this role. Thermoculite 866 is a very special sealing material in that it is entirely free of any organic binder material but it is available in sheet form, is very soft, easily cut into gaskets and has excellent sealing characteristics. Thermoculite 866 consists of just chemically exfoliated vermiculite (CEV) and steatite, nothing else is added. Thermoculite 866 has been adopted by a number of fuel cell development teams in Europe and the US. One Thermoculite 866 ring gasket is shown in Figure 5.13.

Figure 5.13: *A Thermoculite 866 ring gasket*

Sealing tests of Thermiculite 866 gasket were carried out at experimental operating conditions. All components were assembled as Figure 5.10 with two thermoculite 866 ring gaskets seated on the ends of membrane tube. The assembly was put into the furnace and sealed the two ends by Kao Wool from Thermal Ceramics. Afterwards, the furnace controller was turned on and the membrane tube heated up at 1°C/min to 850°C. At 850°C, helium as the testing gas entered the rig from the pre-heating tube; then passed through the membrane tube and the bottom stand; finally to exit to a flowrate bubble meter for measuring the flowrate of the output stream. The sealing effect of gaskets was determined by a comparison of the flowrates of the feed stream (controlled by a rotameter) and the output stream (obtained from the bubble meter).

Four different flowrates of helium (25, 50, 75 and 100ml/min) were tested. Each test was repeated at least three times. The flowrates of helium before and after passing through the rig are shown in Table 5.2. It can be seem from this table that there was almost no apparent gas leakage.   Figure 5.14 shows the gasket after sealing test. It shows that the gasket was largely intact, albeit with a small reduction in thickness.

Feed stream (set by rotameter)	25 ml/min	50 ml/min	75 ml/min	100 ml/min
Output stream (calculated by bubble meter)	25 ml/min	50 ml/min	74.8 ml/min	99.6 ml/min

Table 5.2: *The flowrate of helium before and after flowing through the rig at 850°C*

Figure 5.14: *Thermoculite 866 gasket after sealing test at 850°C*

5.5.2 Sealing at the ends of the quartz tube

Vacuum bag sealant tape is provided by TYGAVAC Advanced Materials Ltd [Figure 5.15]. It has the capability of forming a strong bond to a wide range of film types and surfaces. Its maximum service temperature is 400°C and it can be removed easily after experiments.

As previously in section 5.5.1, the assembly was built up and the testing gas was helium. After coating some sealant tap at the ends of the quartz tube, the furnace was turned on and the rig heated up to 850°C. Then helium flowed into the rig from the carrier gas inlet and exited finally from the permeate gas outlet. The operating condition was also at 850°C and one atmosphere. The flowrate bubble meter was also used to assess the sealing effect. The flowrate of helium was set successively at 25, 50, 75 and 100 ml/min. Repeat the procedure three times for each test and calculate the average time the bubble takes. If the bubble is burst during any of the tests, the timing test must be redone. According to Table 5.3, the velocities of helium before and after flowing through the rig were the same roughly. Thus, the sealing effect of sealant tap in this case was satisfied.

Figure 5.15: *Vacuum bag sealant tape*

Feed stream (set by rota meter)	25 ml/min	50 ml/min	75 ml/min	100 ml/min
Output stream (calculated by bubble meter)	24.5 ml/min	48 ml/min	75 ml/min	100 ml/min

Table 5.3: *The flow rate of helium before and after flowing through the rig at 850°C*

5.6 Measurement of permeate oxygen and electrical current

A gas analyser (5200 Multi Purpose) was used to measure the concentration of permeated oxygen. Before using it, calibration was carried out by helium (0%) and oxygen (100%). The oxygen concentration in the permeate stream was shown on the Multi Purpose display, and recorded every two seconds by a PC connected to the analyzer.

Electrical current is also a representation of membrane performance. For a given membrane cell and operating conditions, the greater current means increased oxygen transport and so better membrane performance. The current and output voltage were both logged every three seconds during an experimental run on a PC via a USB cable connection from a remote programmable linear regulated power supply.

5.7 Oxygen permeation performance

5.7.1 Aim

The aim of this work was to investigate the oxygen permeation process using a Pt/8YSZ/Pt membrane cylinder at 850°C, when the feed stream is gas mixtures of He-O_2 or He-O_2-SO_2.

5.7.2 Method

The method is similar to the YSZ pellet tests mentioned in Section 3.3.4. After the furnace was stable at 850°C and the air tightness of the rig was confirmed, gas mixtures consisted of oxygen and helium were introduced into the rig. The flow rate of oxygen was increased from 2.5ml/min to 5 and 10ml/min. With constant application of 1.5V, oxygen in the feed permeated from the inside of the membrane tube to the outside, then exited to the oxygen analyser with helium (100ml/min). Electrical current across the membrane tube and permeated oxygen concentration in helium were recorded.

Afterwards, another run of around 1.5 hours was carried out whereby the furnace

was heated up to 850°C and the O_2 permeation measured at 1.5V in a similar fashion to that used for YSZ pellet tests. Once the O_2 flux stabilised, 15ml/min of the helium in the feed steam was replaced with SO_2, such that the oxygen feed concentration remained constant. As previously, the current measured by a DC power supply and O_2 flux monitored by an oxygen analyser were logged to a PC.

5.7.3 Result and discussion

The progress of oxygen flow rate change in feed is shown in the top graph in Figure 5.16. During the whole experiment, three 2-minute zero-voltage circuit periods were applied to deduct the contribution of permeated oxygen because of oxygen partial pressure difference in feed and permeate sides. The current and permeate oxygen concentration in product side are also present in Figure 5.16. The result is assessed by a comparison between ideal and real permeated oxygen concentration in the bottom graph of Figure 5.16, which shows that the ideal oxygen concentration has almost the same profile as the real oxygen concentration. At the same time, it confirms again the rig seal was good.

Transport of oxygen through YSZ without applied voltage can be described with the Wagner theory (Stortelder 2005):

$$J(O_2) = \frac{RT}{16F^2L} \frac{\sigma_{ion}\sigma_{el}}{\sigma_{ion}+\sigma_{el}} \ln(\frac{P_{O_2,1}}{P_{O_2,2}}) \tag{5.1}$$

Where J_{O2} is the oxygen permeated flux, R the gas constant, T the temperature, L is the membrane thickness, F the Faraday constant, σ_{el} the electronic conductivity, σ_{ion} the ionic conductivity, $P_{O2,1}$ and $P_{O2,2}$ are the oxygen partial pressure at both sides of the electrolyte. The Wagner equation (eq.5.1) explains that current and permeated oxygen concentration during the zero-voltage periods increased with the oxygen flow rate in feed increases from 2.5ml/min to 5ml/min and then to 10ml/min.

Membrane performance before and after introducing SO_2 into feed is shown in Figure 5.17. As expected, the current change with time is corresponded to oxygen permeated concentration in the whole experiment. During SO_2 free period, current and O_2 concentration remains steady at around 600mA and 3.2%, respectively. Once

sulphur dioxide is added, the current and permeated oxygen concentration decrease suddenly and then reduce gradually. This phenomenon is the same as the performance change of Pt/YSZ pellets exposed to SO_2. Likewise, this performance degradation also might be due to SO_2 adsorption or platinum sulphide on the membrane surface, which may change the surface morphology of membrane and lead to the decrease of electrode activity site and triple-phase boundary (TPB) area.
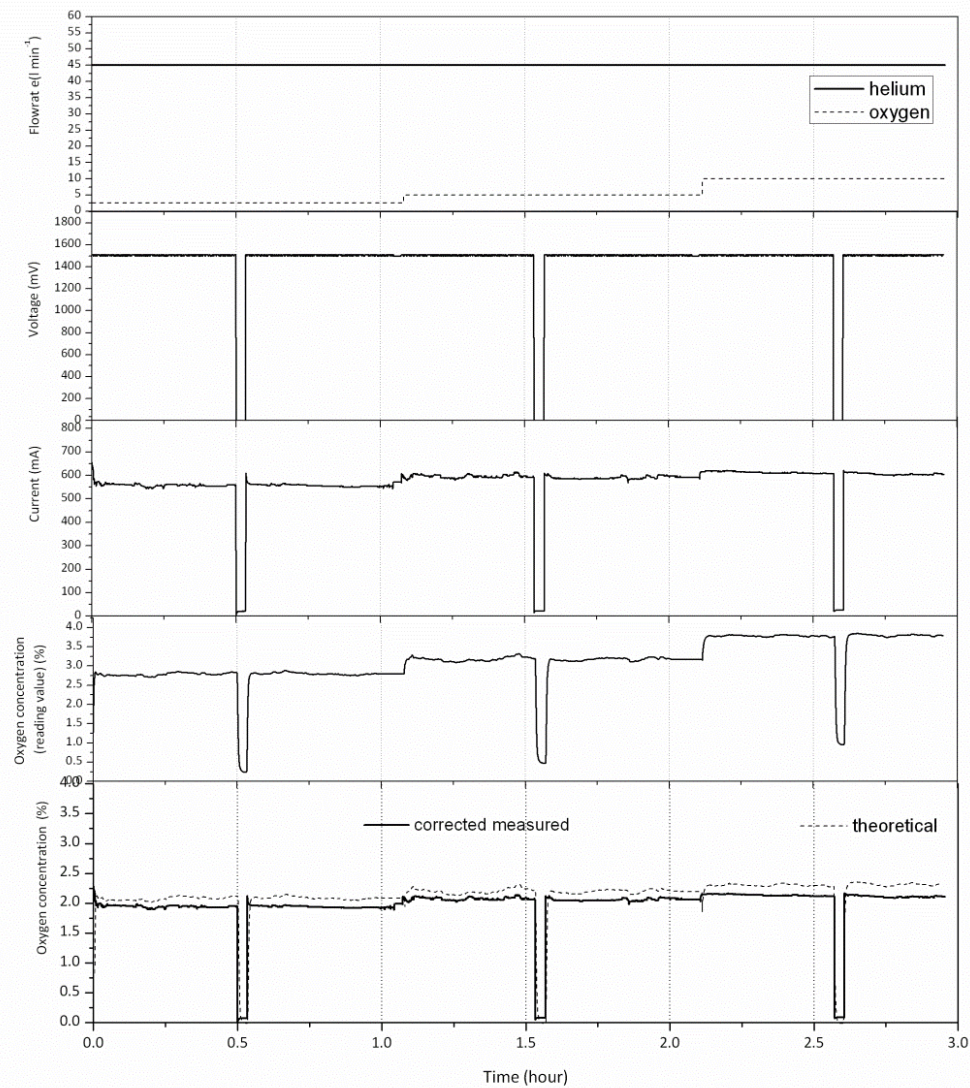
Figure 5.16: *Experimental results of oxygen permeation when the feed is He-O$_2$, at 850˚C.*
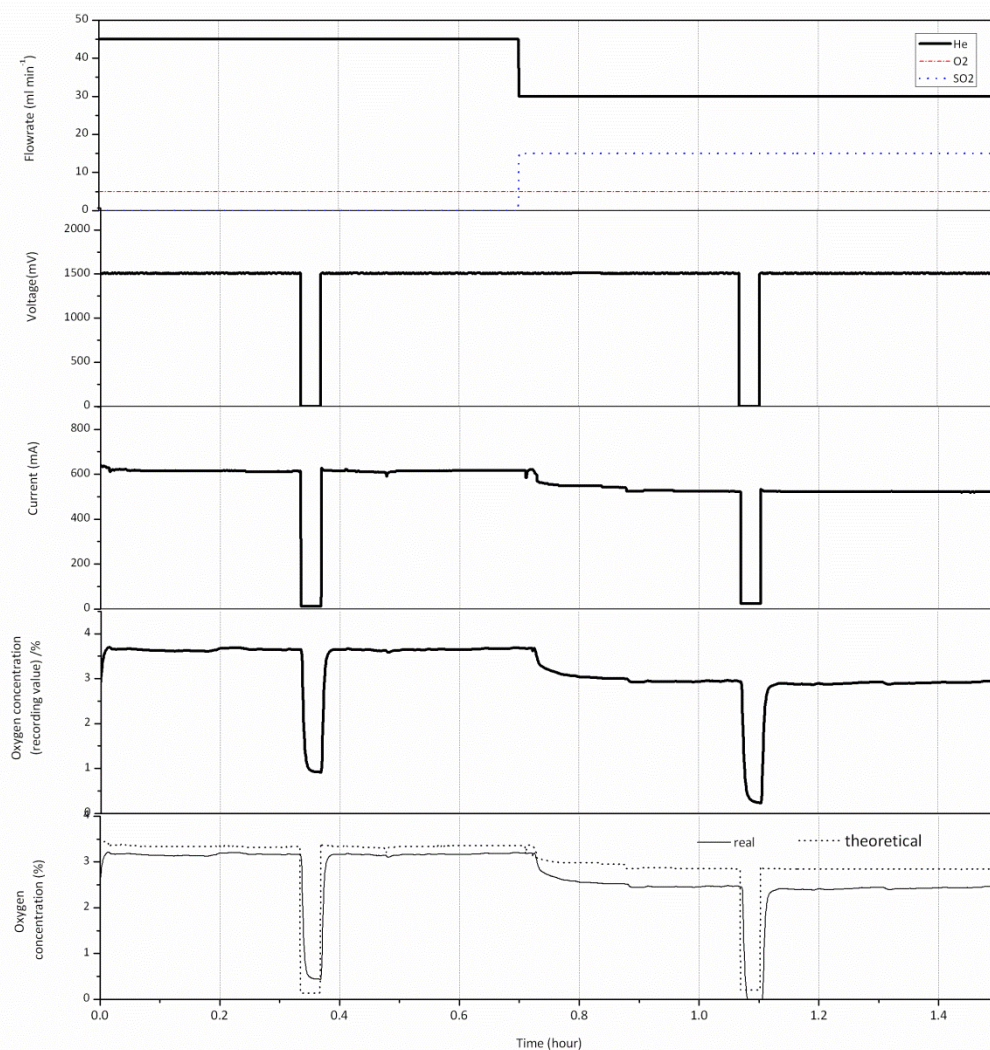
Figure 5.17: *Experimental results of oxygen permeation when the feed is He-O$_2$-SO$_2$, at 850˚C.*

5.8 Membrane performance after high dc voltage pulse

5.8.1 Aim

The aim of this work was to observe membrane performance change after a strong but short dc voltage pulse in SO$_2$ exposure period.

5.8.2 Method

The rig was set up as the previous experiment. The furnace was heated to 850˚C and the feed contain 10% O$_2$ in He (total 50ml/min) and the permeate side fed with

100ml/min of pure He as the carrier gas. A constant voltage of 1.5V was applied for one hour, after which the feed composition was changed to 10% O_2 and 30% SO_2 in He (total 50ml/min). In the later stage of the experiment, the basic voltage was still 1.5V. A positive voltage pulse of 3.0V was applied for 10 seconds. Afterwards, the voltage was back to 1.5V. As previous experiments, the external voltage was dropped to zero for 2 minutes per hour in order to establish the oxygen analyser reading corresponding to zero induced flow. This enabled the calculation of the corrected permeate oxygen concentration to which the current flowing is compared.

After this experiment, the membrane tube was broken into small pieces for analysis including XRD and SEM-EDS.

5.8.3   Result and discussion

The experimental data is presented in the familiar format in Figure 5.18. The current flowing equalises after the first hour He-O_2 feed period. The current recorded at the end of He-O_2 period at 1.5V is 692mA. The change in current and permeate oxygen concentration upon addition of SO_2 to feed follows the same profile to that observed previously [Figure 5.17]. After current has a sudden and gradual drop from 692mA to 581mA, a 3V pulse is applied across the membrane tube. The current after the pulse is 611mA, greater than 581mA. This raise in membrane tube performance after pulse treatment, the same phenomenon as found in membrane pellet experiment, may be attributed to sulphur desorption or platinum sulphide dissociation on the cathode surface. After pulse treatment, current and oxygen concentration decrease gradually with time as before.
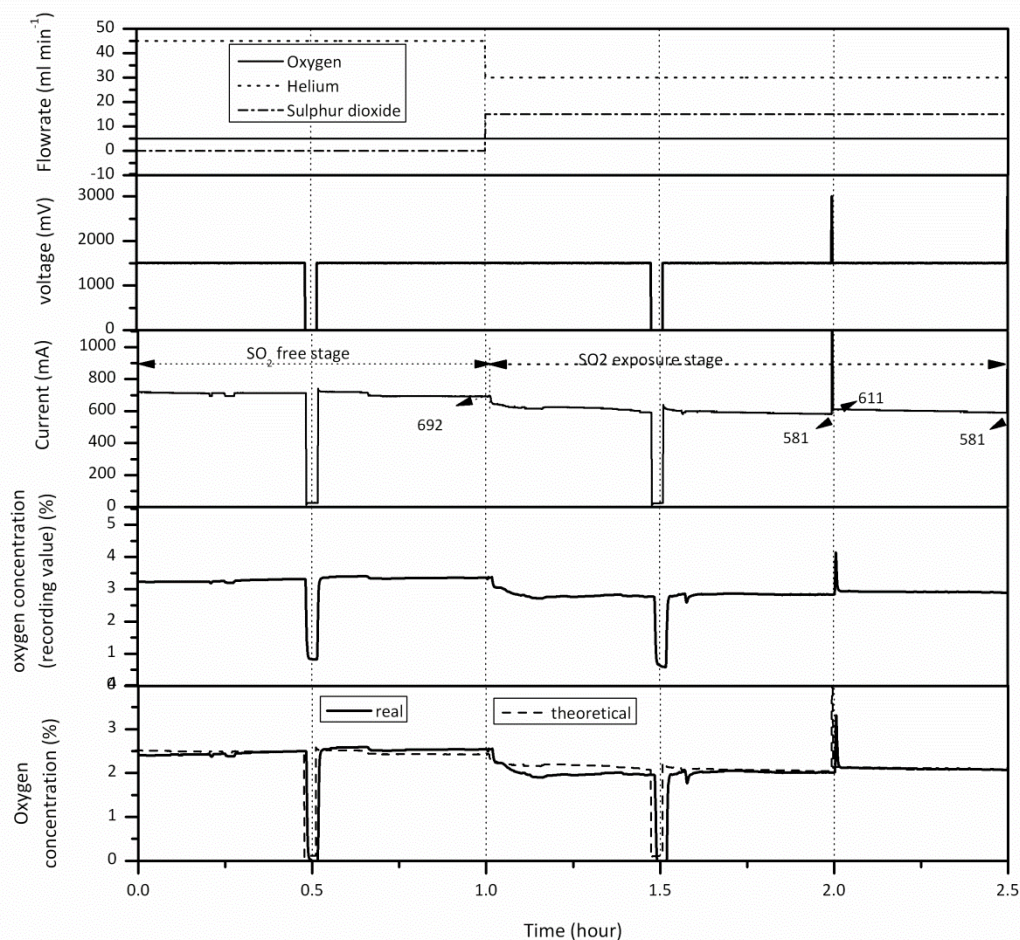
Figure 5.18: *Results of oxygen permeation when the feed is He-O₂-SO₂, with a 3V, 10 seconds voltage pulse treatment.*

XRD

The XRD spectrum of the fresh membrane cell is the same as that of the used membrane cell [Figure 5.19]. There is not platinum oxide (PtO at $2\theta=60°$; PtO_2 at $2\theta=40.5°$) and platinum sulphide (PtS at $47.5°$; PtS_2 at $17.6°$) observed from the cathode and anode surface. Therefore, no change in the crystal structures of Pt electrode and YSZ electrolyte is detected, which means that this Pt/8YSZ tube could be performed very well in SO_2-O_2 environment at high temperature.
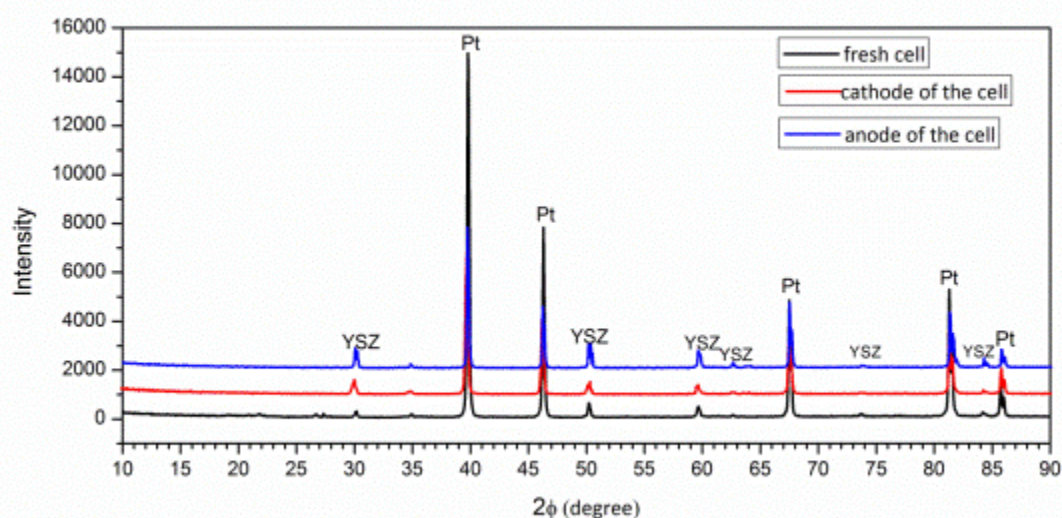
Figure 5.19: *XRD data of membrane tube feed side, permeate side after experiments*

SEM-EDS

Only platinum is detected on the cathode surface, but zirconium is also found at the electrode-electrolyte active area [Figure 5.20]. Apparently, zirconium is detected from the substrate of the membrane. On the right of the Pt peak at 2.048keV in the EDS spectrum, there is a small peak marked sulphur. According to XRD data in Figure 5.19, this peak should not be sulphur but bismuth whose Mα energy is 2.419keV and falls at a similar position in the EDS spectrum to sulphur whose Kα energy is 2.307keV. The platinum paste used to date, supplied by Metalor, contain a small amount of "bismuth-based flux" to facilitate bonding to the surface. The presence of bismuth was proved by XPS analysis in previous work (Atkin 2009). As expected, there was only platinum found on the anode surface [Figure 5.21].

The carbon shown in Figure 5.20 and Figure 5.21 came from the carbon coating process in the sample pre-treatment. EDS spectrum yields oxygen peaks because oxygen is a relatively light atom. In this case, the oxygen peaks may be obtained by fitting the amount of platinum detected from the x-rays emitted from the specimen, even if no platinum oxide was detected by XRD [Figure 5.19]. Therefore, oxygen peaks in this case could be ignored.
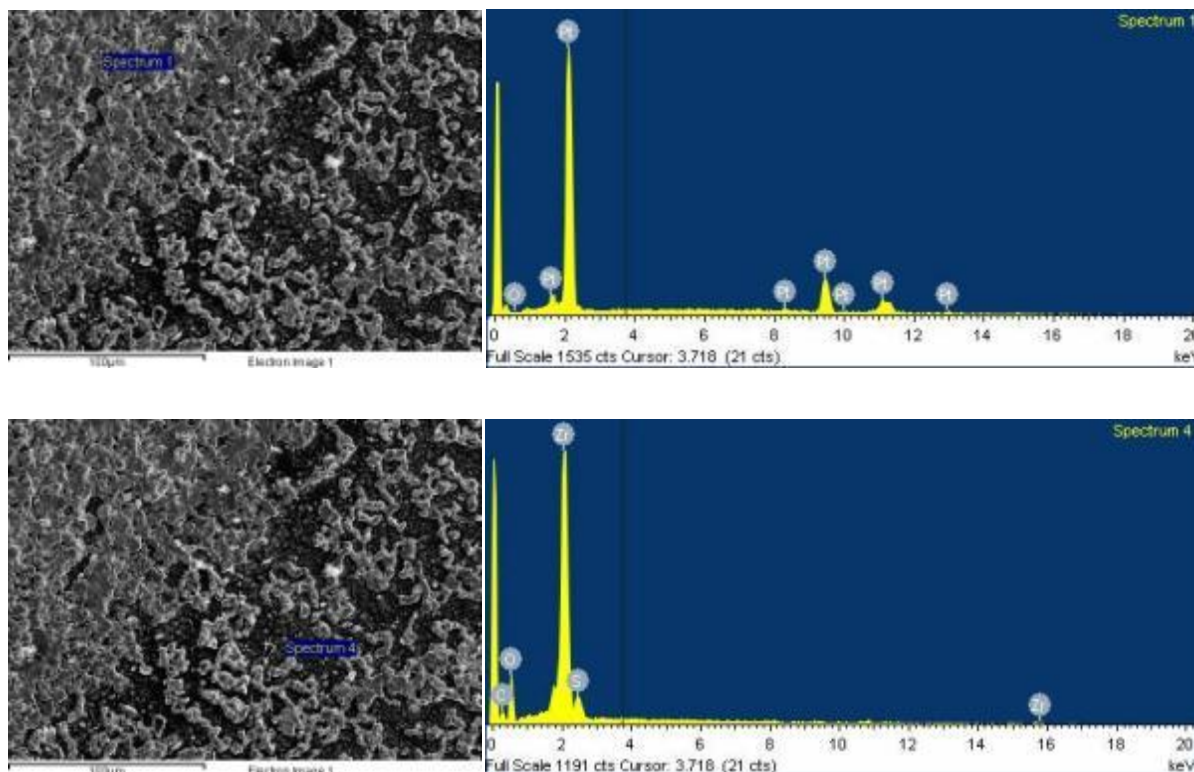
Figure 5.20: *The SEM-EDS spectrum of the inner membrane surface*
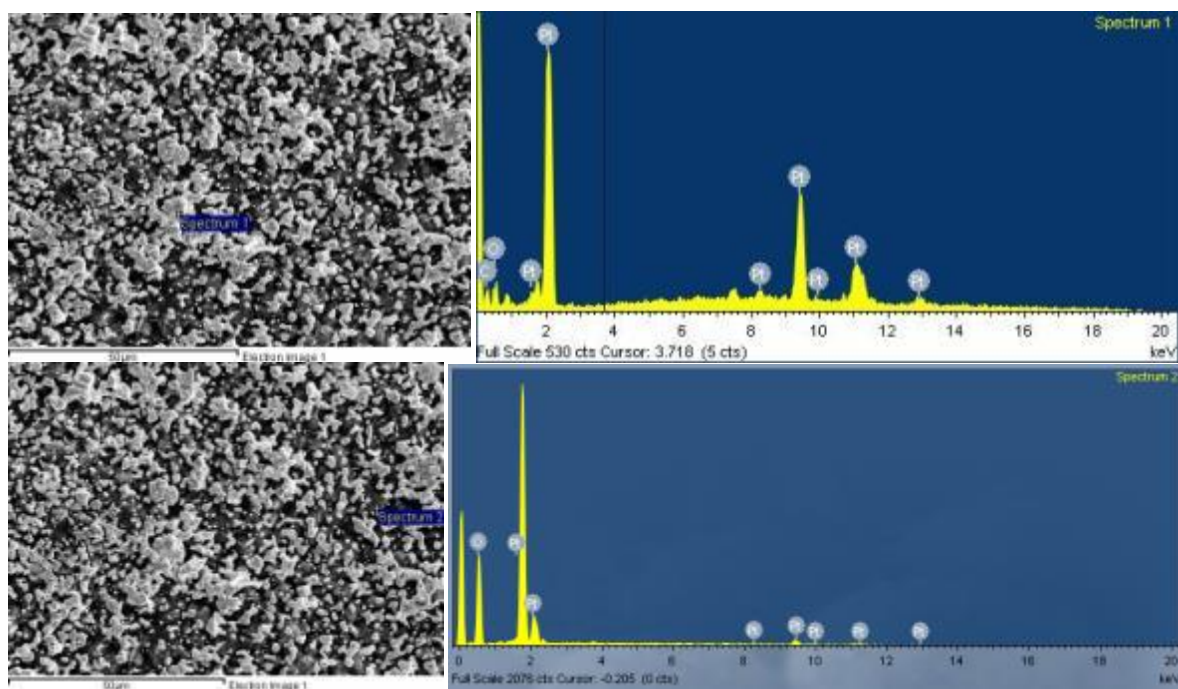
Figure 5.21: *The SEM-EDX spectrum of the outer membrane surface*

5.9 Conclusion

Oxygen permeation process of a Pt/8YSZ tube exposed to He-O_2 or He-O_2-SO_2 was demonstrated at 850°C with a constant 1.5V polarization. Oxygen could permeate through the membrane tube and the permeate flux increased with oxygen partial pressure in feed. As expected, current and permeated oxygen concentration decreased with SO_2 exposure time, which may be due to SO_2 adsorption or sulphide formation on the cathode surface. Also a partial recovery in membrane performance after applying a DC voltage pulse in SO_2 exposure period was observed. The cathode and anode of the membrane tube after a voltage pulse test had the same XRD diffraction patterns as a fresh membrane cell. From SEM-EDS spectrums, no visible change in the electrode surface morphology was observed after all experiments.

5.10 Oxygen permeation flux of planar and tubular membrane

Two typical experiments (Section 3.3 and section 5.8.3) were sampled and the permeate oxygen concentrations with time are presented in [Figure 5.22]. The electrode surface areas of the membrane pellet and the membrane tube were 2.54 and 9.04 cm², respectively. The membrane tube had a smaller oxygen permeation flux than the membrane pellet. Based on the features of membrane pellet and tubular systems [Table 5.4], the effect of Pt paste, YSZ thickness and gas flow dynamic on oxygen permeate flux is discussed briefly.

Properties	Pt/8YSZ pellet	Pt/8YSZ tube
Pt paste	GEM C2000904P3	Metalor 6082
YSZ thickness	2.0mm	2.5mm
Direction of the gas flow	Perpendicular to the cathode surface	Parallel to the cathode surface

Table 5.4: *Main differences of planar and tubular membrane system*
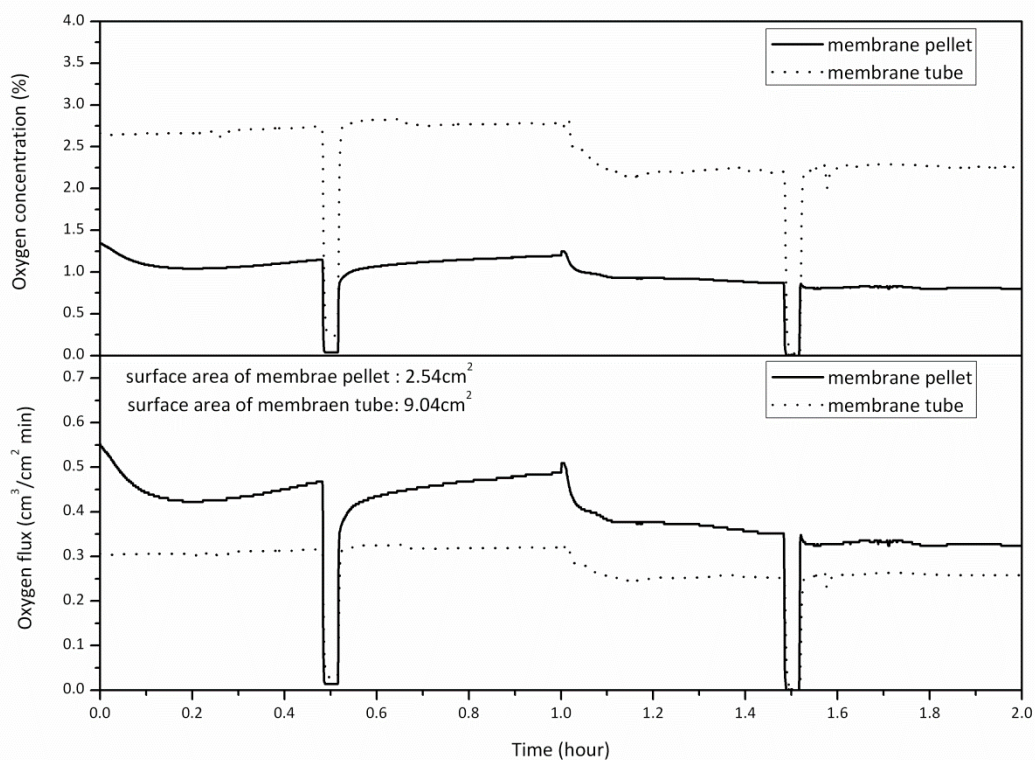
Figure 5.22: *Oxygen permeation flux of membrane pellet and membrane tube*

5.10.1 Platinum paste

Platinum pastes used for electrode preparation were a fuel cell grade platinum ink supplied by Gwent Electronic Materals (GEM) (product code: C2000904P3) for YSZ pellet and Metalor 6082 for YSZ tube. Metalor 6082 contains a bismuth-based frit to aid surface adhesion, while GEM paste does not. Considering the crystal structure and thermal properties of bismuth and the inhomogeneity of the platinum electrode surface, it is difficult to determine the influence of the bismuth impurity on oxygen permeation flux.

5.10.2 YSZ thickness

When oxygen permeates through a YSZ supported membrane, the whole oxygen diffusion process can be divided into gas phase diffusion, oxygen adsorption and dissociation, surface diffusion of oxygen species, migration of oxygen species to the electrolyte through the three-phase boundaries, oxygen ion diffusion in the

electrolyte and migration of oxygen species to the electrode, surface diffusion of oxygen species and oxygen desorption (Yoon et al. 2003). In order to investigate how the electrolyte thickness's influence on oxygen diffusion, the processes of oxygen adsorption and surface diffusion are assumed very fast. In other words, the rate-limiting stage of oxygen diffusion is oxygen ion diffusion in the YSZ. Assuming the bulk diffusion is steady, the oxygen ion diffusion through YSZ can be described by Fick's law.

$$J = -D\frac{\partial \phi}{\partial x}$$

(5.2)

Where

- J is the diffusion flux (per unit area per unit time)
- D is the diffusion coefficient or diffusivity in dimensions of (length^2 time^{-1})
- φ (for ideal mixtures) is the concentration in dimensions of [(amount of substance)length^{-3}]
- x is the position (length)

In generally, the diffusion coefficient in gas-solid diffusion process depends on several factors 1) temperature and pressure; 2) shape of solid; 3) gas species and chemical composition; 4) defects of the lattice in the solid; 5) Anisotropy of the lattice. Temperature and pressure are the external factors, while the rest are internal factors which influence the diffusion efficiency by the diffusion activation energy (E_A) and the maximum diffusion coefficient (D_0) (Yongning 2006).

The operating conditions of the oxygen permeation processes in the planar and tubular membrane systems were the same. The gas composition in the feed stream and their flowrates were the same as well. The electrolytes were both made from the same materials: 8mol% Y_2O_3-ZrO_2. The lattice of Pt electrodes were all isotropic not anisotropic. Therefore, YSZ thickness becomes the only influencing factor of the diffusion coefficient.

The diffusion coefficient in solids at different temperatures is often found to be well predicted by (Helmut 2007):

$$D = D_0 e^{-E_A / k_B T} \qquad (5.3)$$

Where,

- D is the diffusion coefficient
- D_0 is the maximum diffusion coefficient
- E_A is the activation energy for diffusion in dimensions of [energy (amount of substance)$^{-1}$]
- T is the temperature in units of [absolute temperature]
- K_B is the Boltzmann constant in dimensions of [energy temperature^{-1}]

The oxygen diffusion in YSZ was examined used molecular dynamic simulations and energy minimization calculations (Devanathan et al. 2006). Figure 5.23 presents the results on the oxygen diffusion coefficient (D) as a function of reciprocal temperature (1/T) for 6, 8, and 10 mol% YSZ.
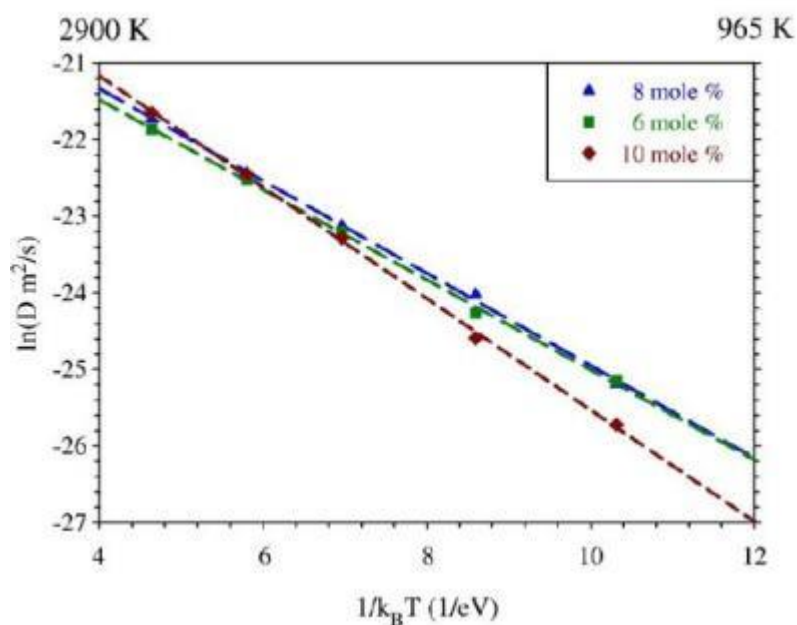
Figure 5.23: *Arrhenius plot of the diffusion coefficient as a function of reciprocal temperature (1/T) for 6, 8, and 10 mol% YSZ (Devanathan et al. 2006).*

At 1123K, the oxygen diffusion coefficient was figured out as 1.257 x 10^{-11} m^2/s. After taking membrane thickness, oxygen diffusion coefficient and oxygen concentration gradient together, the oxygen diffusion fluxes of membrane pellet and tube were calculated [Table 5.5]. The oxygen diffusion flux of membrane pellet (2mm

thickness) is 6.819×10^{-12} mol/cm^2 s, a little greater than 5.455×10^{-12} mol/cm^{2}s of membrane tube (2.5mm thickness). Reviewing the calculation of oxygen diffusion flux, its main influence factors are temperature (related to the diffusion coefficient D) and oxygen concentration difference through the membrane (the force of oxygen diffusion). The thickness of membrane can be viewed as diffusion resistance. Thicker membrane will increase diffusion resistance and decrease oxygen diffusion flux.

Properties	Membrane pellet	Membrane tube
Membrane thickness	2.0mm	2.5mm
Oxygen diffusion coefficient	1.257×10^{-11} m^2/s	1.257×10^{-11} m^2/s
Oxygen concentration gradient	-5425 mol/m^4	-4340 mol/m^4
Oxygen diffusion flux	6.819×10^{-12} mol/cm^2 s	5.455×10^{-12} mol/cm^{2}s

Table 5.5: *Oxygen diffusion fluxes of the membrane pellet and tube*

At 1000°C, the oxygen permeation flux through ceramic membrane consisting of porous alumina support and 5μm 8 mol% yttria stabilized zirconia (YSZ) was 4.8×10^{-8} mol/cm^2 s, which was measured, *in situ*, on an electrochemical vapour deposition (EVD) apparatus by the oxygen pressure in the feed side of 0.03 atm and permeate side of 10^{-5} atm (Lin et al. 1992). Using different electrodes and the same electrolyte, oxygen-permeation flux through YSZ/Pd composite membranes (2-3μm thickness) in the 900-1050°C temperature range were in the 2×10^{-9} to 5×10^{-8} mol/cm^{2}s range (Kim and Lin 2000). In the present case of YSZ thickness being thicker in magnitude by 1000 times, the oxygen permeation fluxes of Pt/8YSZ pellet (6.819×10^{-12} mol/cm^2 s) and Pt/8YSZ tube (5.455×10^{-12} mol/cm^2 s) at 850°C were reasonable and credible.

5.10.3 Flow dynamic (CFD simulation)

The direction of the flowing feed gas was perpendicular to the cathode surface of the pellet while parallel to the inner surface of the tube. This may cause different gas flows near the membrane surfaces. This is potentially interesting when considering that oxygen diffusion from the gas bulk to the membrane surface is the first stage in the whole oxygen permeation process. For example, back flow mixing will alter the pressure gradient in the region near the membrane surface, affecting oxygen

adsorption onto the membrane surface. A simulation was carried out using Fluent, Ansys Workbench to model the gas flowing in the region of membrane surface and evaluate the oxygen permeation process in two different systems from a flow dynamic perspective.

5.10.3.1 Membrane pellet system

Geometry

The flow domain was modelled as a cylinder of height 5mm and diameter 19mm with circular entry and exit holes. The entry and exit holes were 1mm diameter and 3mm diameter respectively, to imitate the real membrane holder dimensions. The outline of the flow domain in 3D, as displayed in Design Modeler, is depicted in Figure 5.24.
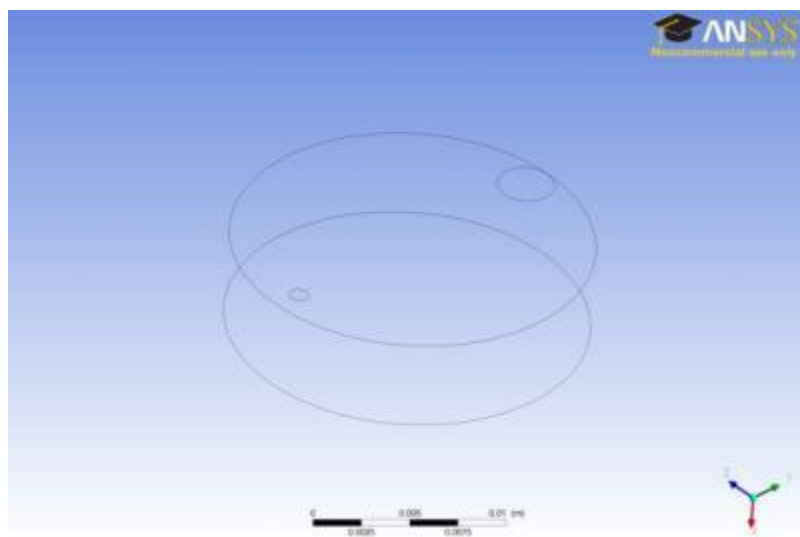
Figure 5.24: *Outline of flow domain for FLUENT simulations. The smaller hole is the flow inlet and the larger hole is the flow outlet.*

The simulations did not introduce any complexity which is unnecessary at this stage. The flow domain does not account for oxygen permeation through the membrane or any leakage that may be occurring.

Mesh and Compute

Before the mesh creation stage, the gas flowing through the domain was simplified appropriately. The operating conditions were at a temperature of 850°C and a pressure of one atmosphere. The gas mixture can be viewed as ideal gas. This meant that the gas, flowing at 850°C, could be scaled to room temperature using the ideal

gas equation. Pure helium replaced gas mixtures. The calculated entry mass flowrates are shown in Table 5.6:

Volumetric flowrate (ml/min)		Mass flow rate (m/s) (1mm Diameter)	Reynolds number (Re)
25˚C, 1atm	850˚C, 1atm		
50.00	188.42	4.00	32.7

Table 5.6: *Mass flowrate of helium used in FLUENT simulations, calculated based on room temperature and pressure flowrates of 50ml/min, with explanation based on the ideal gas law and the properties of helium at room temperature.*

The system was assumed to be isothermal and the laminar flow model was employed. A number of meshes were tested and the largest mesh which did not alter the results was used. This mesh had a minimum cell size of 0.001mm. The boundary conditions and computation model of the simulation process by Fluent was set [Table 5.7].

Boundary conditions	Velocity inlet	Pressure outlet		
	4.00 ml/min	0		
Solution methods	Pressure-Velocity Coupling	Spatial Discretization		
	SIMPLE	Gradient	Pressure	Momentum
		Green-Gauss Node Based	Second Order	Second Order Upwind

Table 5.7: *The boundary conditions and the selection of computational model by Fluent*

Data collection

Emanating from the inlet, the velocity streamlines and vectors in all domains were recorded. Graphical output of the contours of velocity and pressure magnitude were recorded for a plane (plane 1) which crosses the inlet and outlet holes, is perpendicular to the lower face which represents the membrane surface. Perpendicular to plane 1, another plane (plane 2) was defined [Figure 5.25]. The velocity and pressure data were also recorded for some lines on the two planes. These lines are between 0 and 5mm from the inlet face, in 1.25mm steps [Figure 5.25].
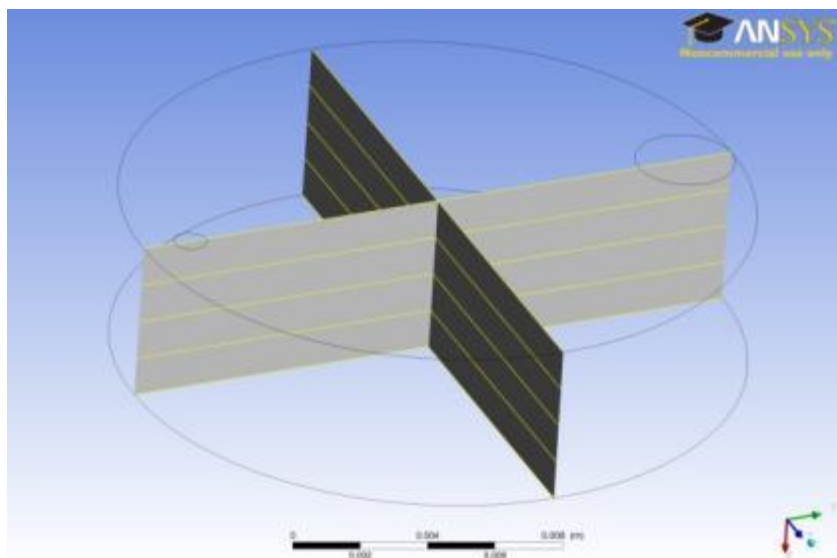
Figure 5.25: *Outline of flow domain for FLUENT simulations showing lines and planes along which velocity magnitude data is collected. These lines run parallel and perpendicular to an imaginary line joining the entry and exit holes. The lines are 0, 1.25, 2.5, 3.75, 5mm from the inlet face.*

Result
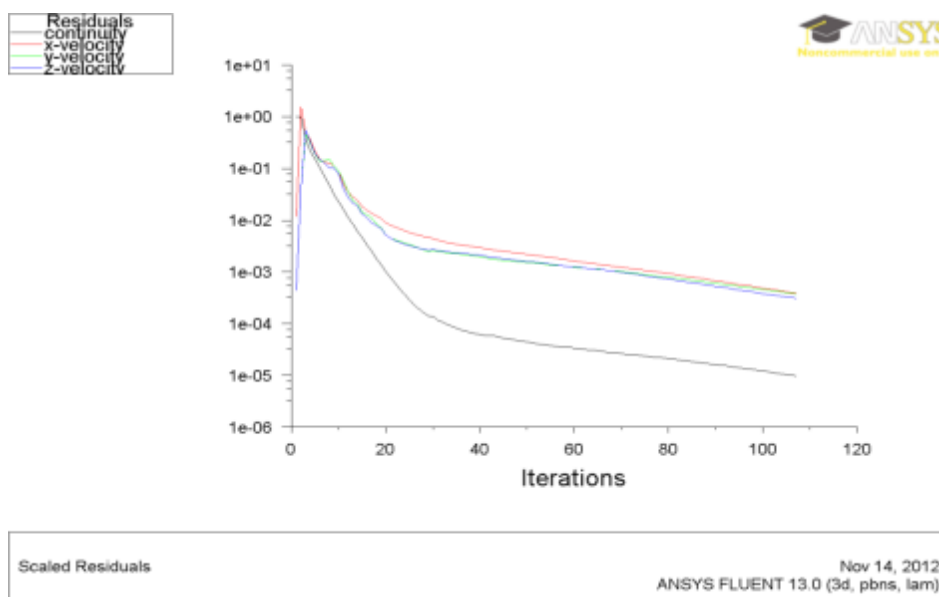
Figure 5.26: *The iteration process*

When monitoring x-y-z velocity of 10^{-3}m/s and continuity velocity of 10^{-5}m/s, convergence was achieved at the 108th iteration step [Figure 5.26]. The gas velocities in the simulations were recorded in several different ways. Firstly, Figure 5.27 (front view) and Figure 5.28 (top view) show the gas velocity distribution by streamline in all domains. The following pictures show velocity and pressure contour on plane 1 (crossing the inlet and outlet), plane 2 (perpendicular to plane 1),

and velocity and pressure along the lines on the planes. Velocity and pressure contours are displayed in Figure 5.29 and Figure 5.30 respectively. Similarly, Figure 5.33 - 5.34 show the velocity and pressure contour on the plane 2. The velocity and pressure change along the ten lines are also shown in Figure 5.31 - 5.32, Figure 5.35 - 5.36.
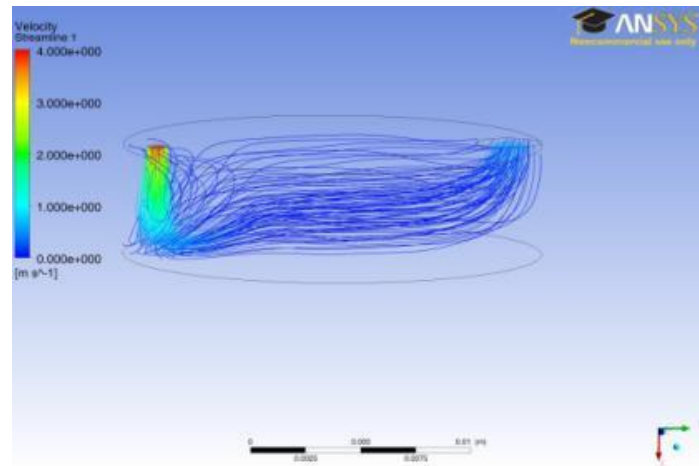
Figure 5.27: *Velocity streamline of gas flowing through all domains (front view)*
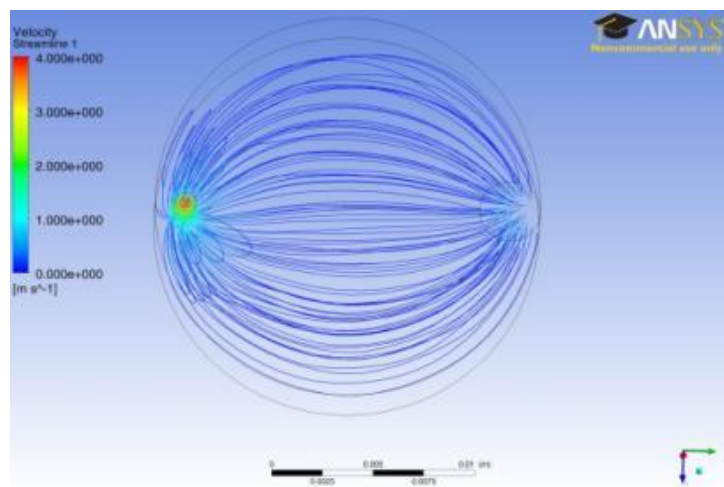
Figure 5.28: *Velocity streamline of gas flowing through all domains (top view)*
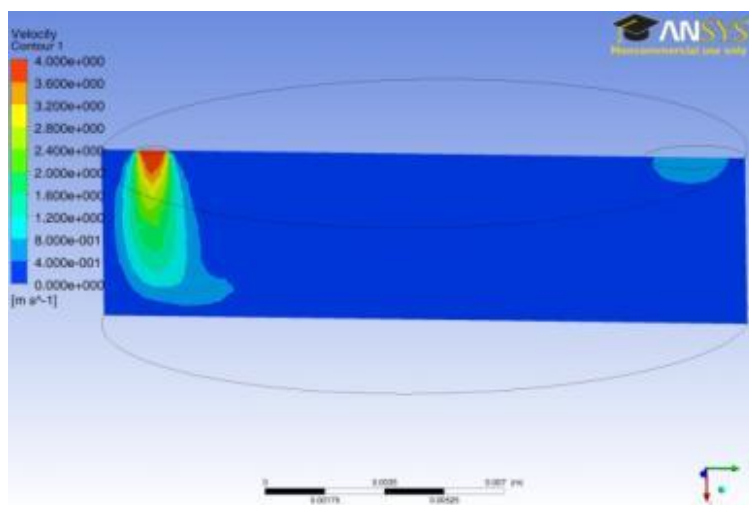
Figure 5.29: *Velocity contour on the plane 1*
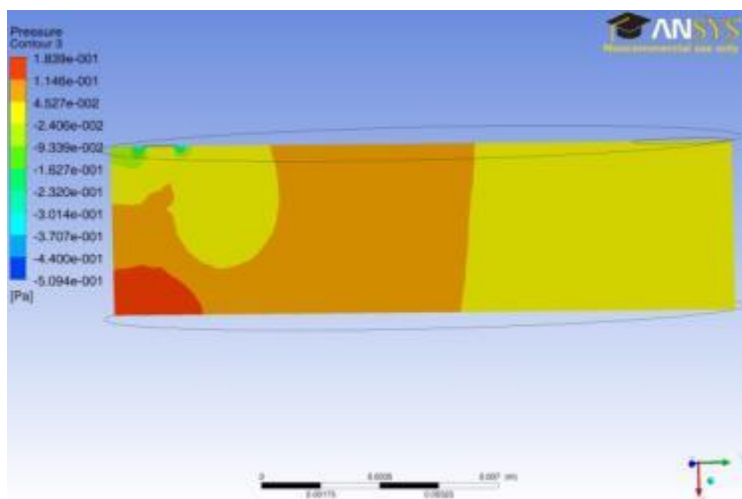
Figure 5.30: *Pressure contour on the plane 1*
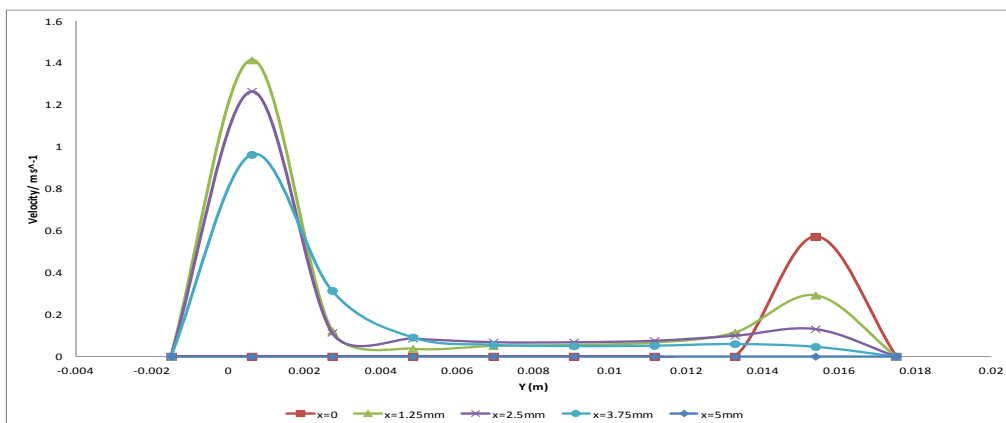
Figure 5.31: *Velocity along the lines on the plane 1*
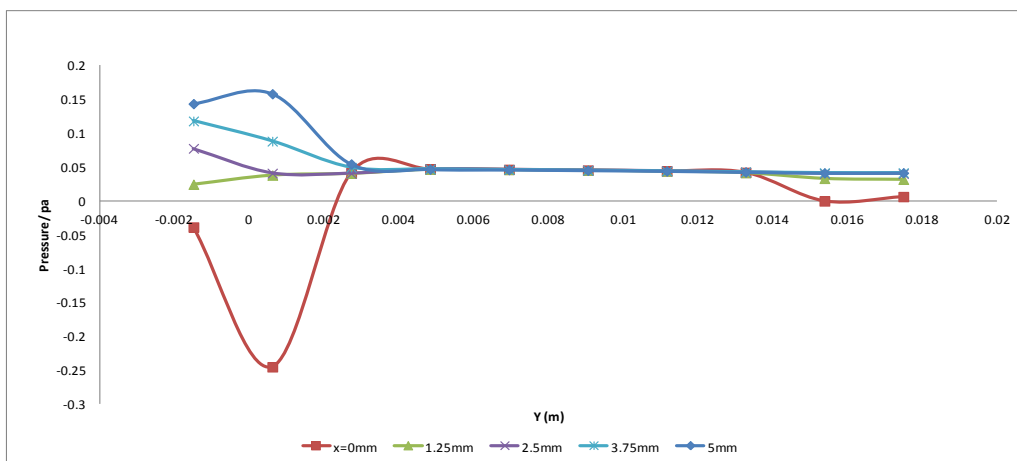
Figure 5.32: *Pressure along the lines on the plane 1*
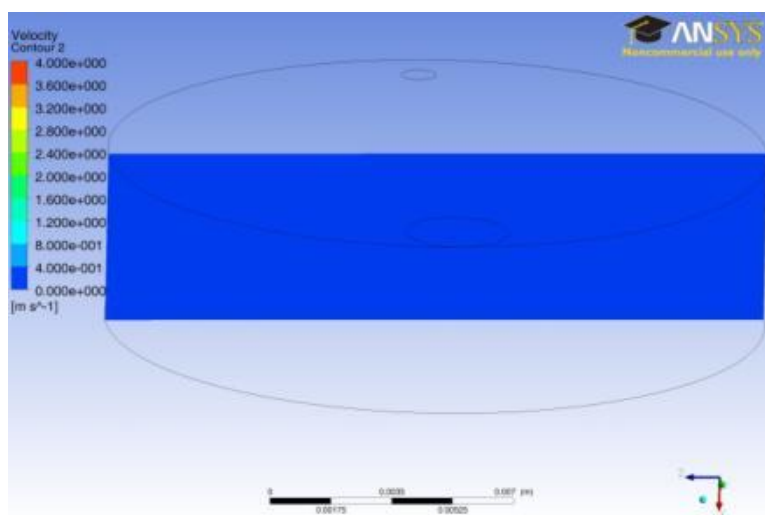
Figure 5.33: *Velocity contour on the plane 2*
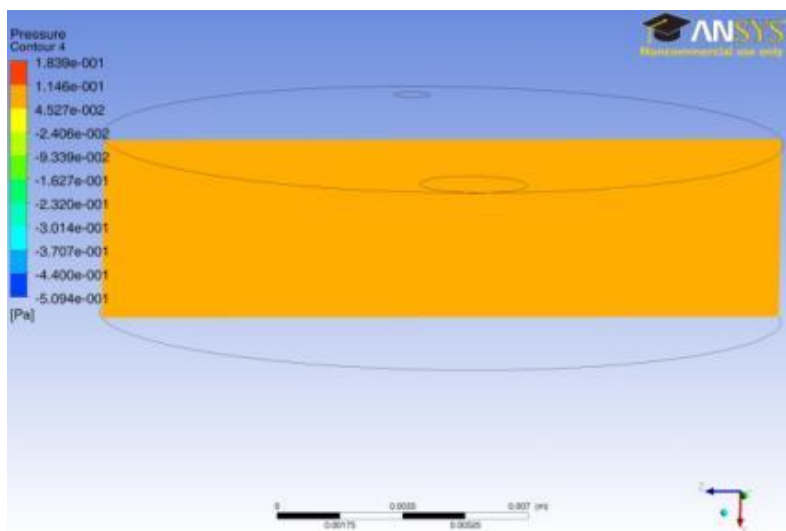
Figure 5.34: *Pressure contour on the plane 2*
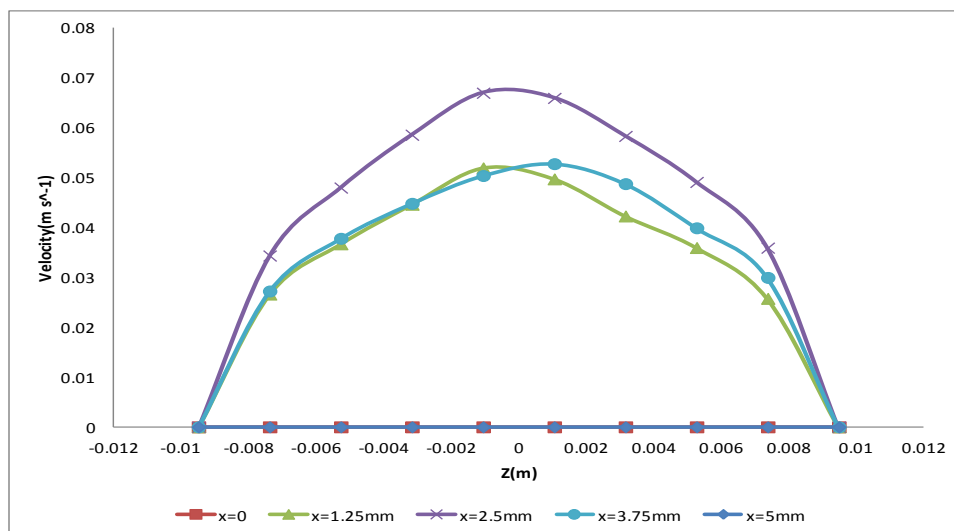
Figure 5.35: *Velocity along the lines on the plane 2*
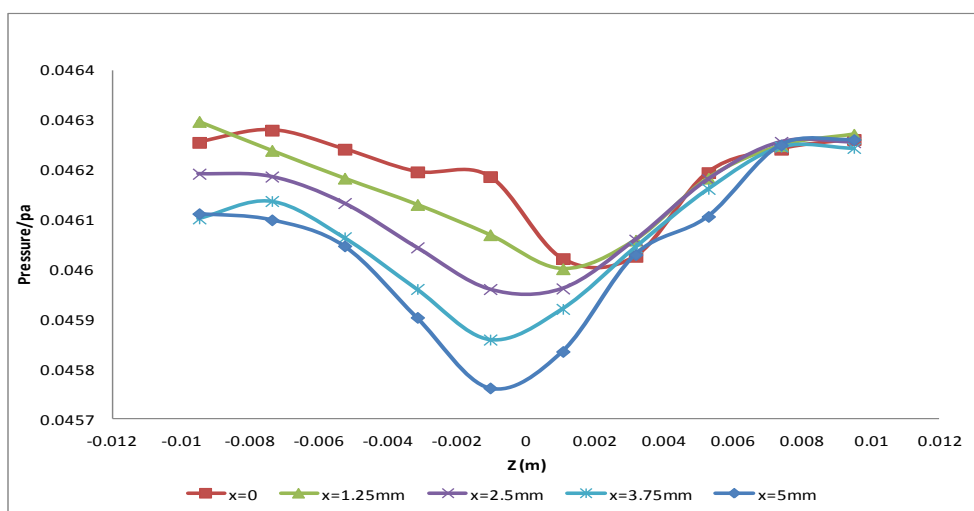
Figure 5.36: *Pressure along the lines on the plane 2*

5.10.3.2 Membrane cylinder

Geometry

The geometry of membrane cylinder separation system is similar to membrane pellet system. The flow domain was modelled as a cylinder of length 185mm (the working length of membrane tube is 180mm, the length of pre-heating quartz tube is 5mm) and diameter 16mm with an inlet (diameter 1.0mm) and an outlet (diameter 16mm). Gas flows into the cylinder from the inlet after pre-heating period, then passes through the membrane cylinder and exits from the outlet. The outline of the flow domain, as displayed in FLUENT, is depicted in Figure 5.37.

Mesh and Compute

As previously, pure helium was viewed as an ideal gas. The mass flow rate was also 4.00 m/s, the Reynolds number was 32.7 based on the diameter of the inlet tube. The boundary conditions were velocity inlet (4.00 m/s) and pressure outlet (0). The system was assumed to be isothermal and the laminar flow model was employed. Solution methods were the same as shown in Table 5.7. The geometry was meshed by the minimum cell size of 0.01mm; other options of mesh size did not alter the results.
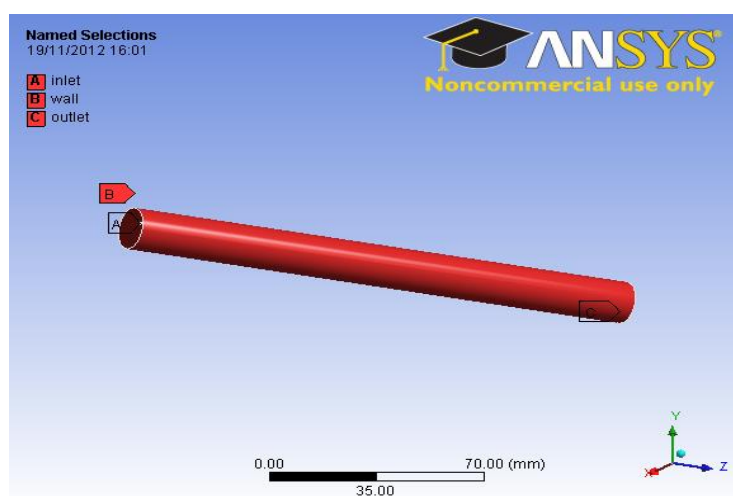
Figure 5.37: *The geometry of membrane tube separation system*
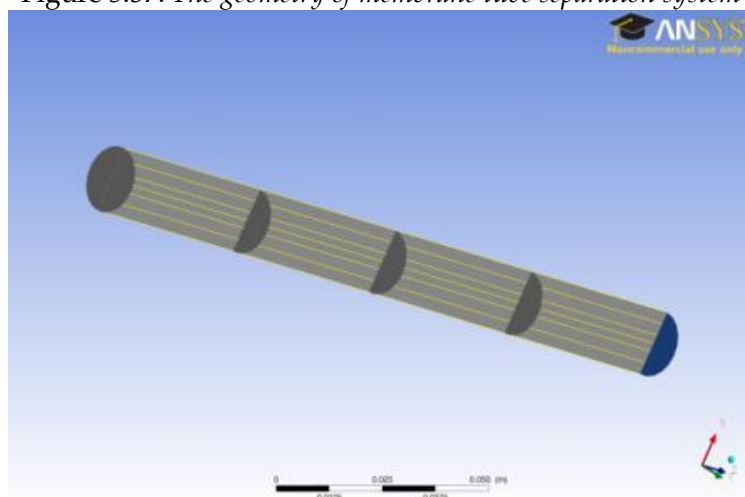
Figure 5.38: *Outline of flow domain for FLUENT simulations showing lines and planes along which velocity magnitude data is collected. One plane crosses the inlet and outlet. The other five planes is parallel to outlet face [from inlet face, z=0, 46.25, 92.5, 138.75 and 185mm (outlet)]. These lines run parallel to Z axis. X coordinates of these lines are -1.5, 1.5, 4.5, 6.5, 8.5, 11.5 and 14.5mm.*

Data collection

The velocity streamline in all domains was recorded, which shows the gas velocity distribution through the tube from the inlet to the outlet. The gas velocity and pressure contour were recorded for six planes and lines between the inlet and outlet. One plane is in the middle of the tube across the inlet and outlet holes, on which seven lines were defined as their x coordinates: -1.5, 1.5, 4.5, 6.5, 8.5, 11.5 and 14.5 from the inlet side. Other planes are perpendicular to the Z axis (being parallel to x-y plane), of which z coordinates are 0 (inlet), 46.25, 92.5, 138.75 and 185mm (outlet) [Figure 5.38]. In addition, the velocity and pressure change along the lines were recorded as well.

Result

From the inlet, the velocity streamline in all domains is shown in Figure 5.40. Figure 5.41 and Figure 5.42 present the velocity and pressure contour in the middle planes. Velocity and pressure change along the lines located in this plane were displayed in Figure 5.43 - 5.44.   The graphs of pressure contour on the planes parallel to x-y plane are displayed in Figure 5.45.
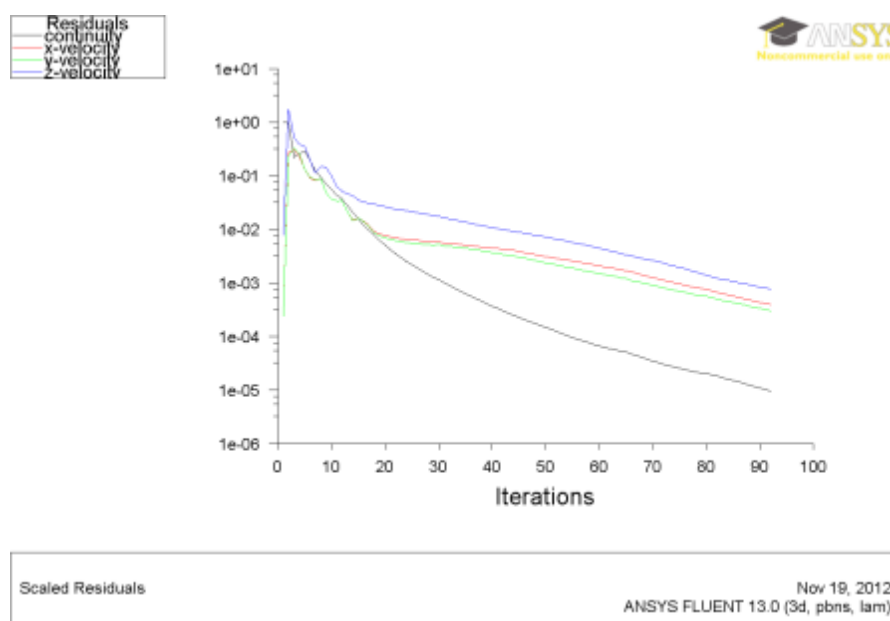
Figure 5.39: *The iteration process*
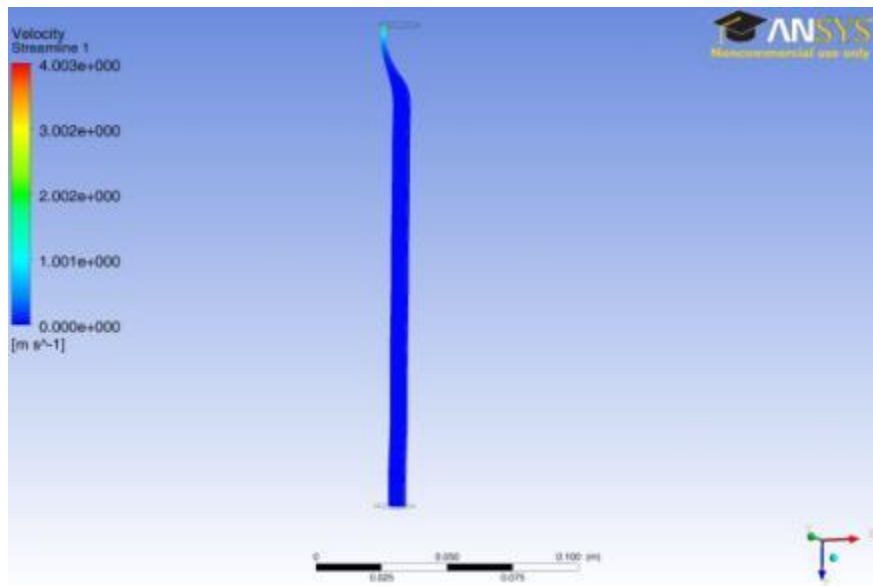
Figure 5.40: *Velocity streamline for all the domains*
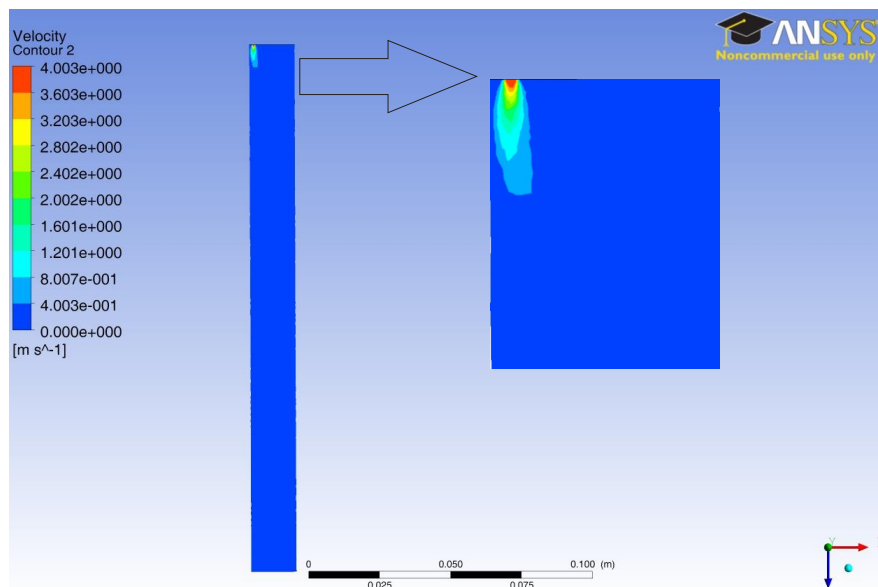
Figure 5.41: *Velocity contour in the middle plane which across the inlet and outlet*
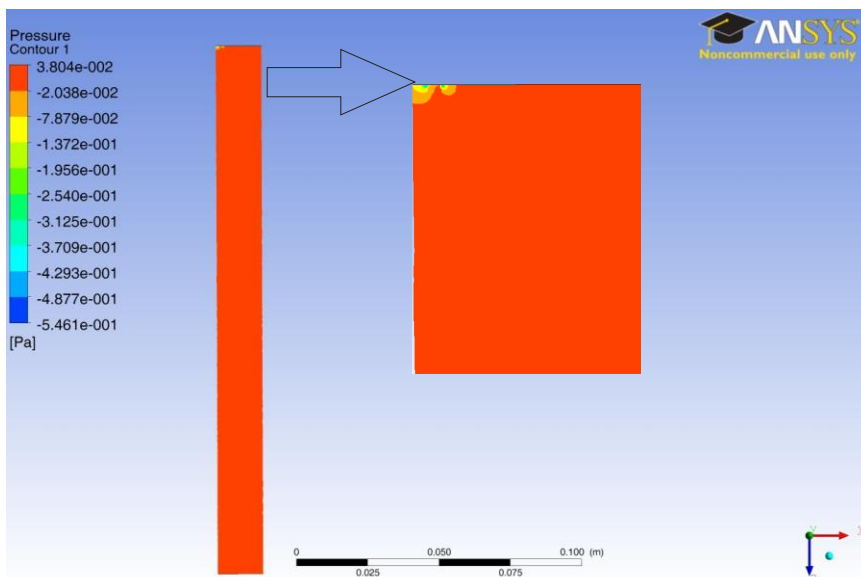
Figure 5.42: *Pressure contour in the middle plane which across the inlet and outlet*
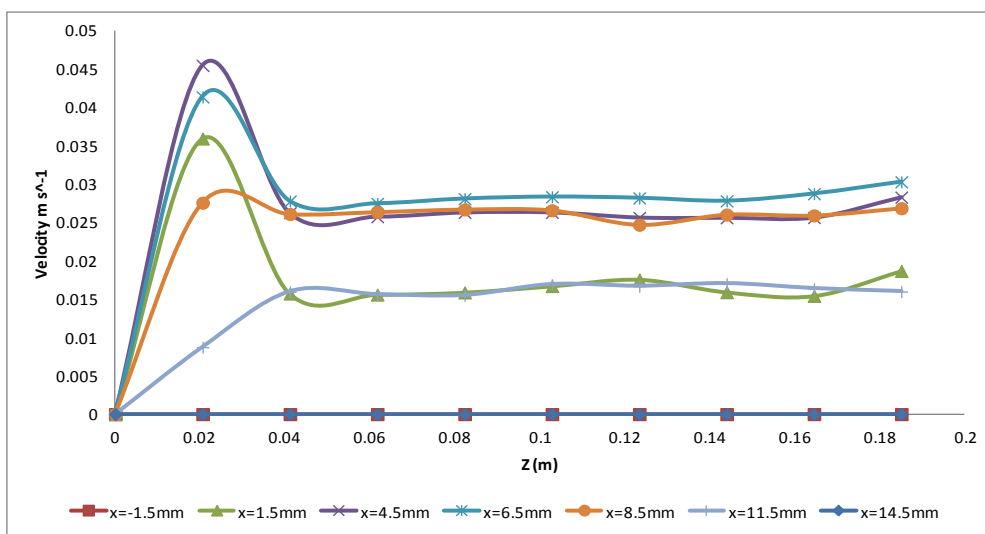
Figure 5.43: *Velocity change along the lines on the middle plane*
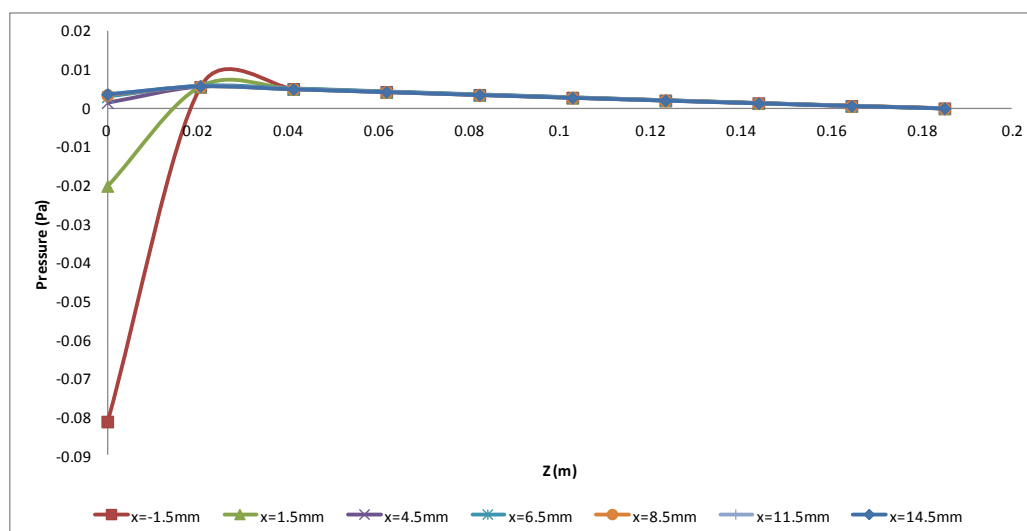
Figure 5.44: *Pressure change along the lines on the middle plane*
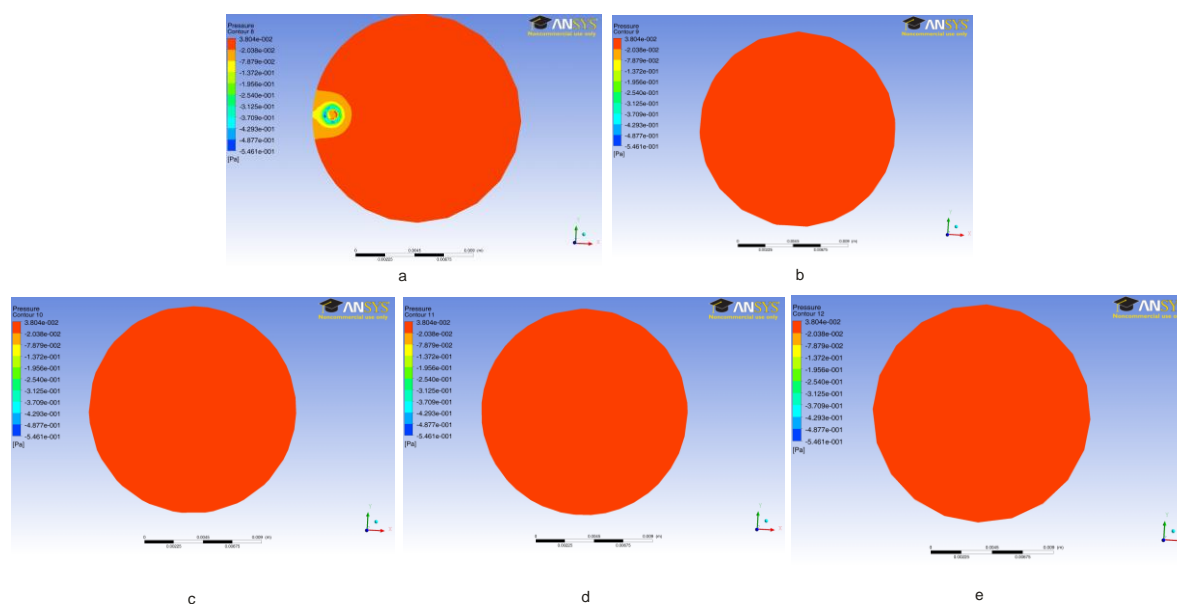
Figure 5.45: *Pressure contour in the planes which are parallel to the outlet face: a) z=0 (inlet); b) z=46.25; c) z=92.5; d) z=138.75; e) z=185 (outlet)*

5.10.3.3 Discussion

According to the simulations for membrane pellet and membrane tube systems, the gas velocity both had a sudden decrease and then became stable after the gas entered the computational domains [Figure 5.27] [Figure 5.40], which was illustrated again by the velocity contours on the planes [Figure 5.29] [Figure 5.41]. In particular, the gas

velocities along the membrane surface were the smallest, approaching zero [Figure 5.31] [Figure 5.34] [Figure 5.43].

In the oxygen bulk phase, the velocity was approximately constant at 0.05m/s in the pellet system [Figure 5.31] [Figure 5.34], while it was calculated to be a maximum of 0.03m/s in the centre of the tube system [Figure 5.43]. From the graphs of pressure contour on the middle planes [Figure 5.30] and pressure change along the lines [Figure 5.32] [Figure 5.36], there was some backflow produced because of non-uniform gas pressure in the gas bulk for the membrane pellet system. On the contrary, there was no obvious pressure fluctuation in membrane tube for decreasing along the fluid flow direction [Figure 5.42] [Figure 5.44] [Figure 5.45]. The gas pressure was around 0.04Pa near membrane pellet surface [Figure 5.32] and 0.005Pa near membrane tube surface [Figure 5.44]. Therefore, the higher oxygen permeation flux of the membrane pellet may be due to a backflow and a greater gas pressure near membrane surface, than that of the membrane tube.

5.11 Conclusion

A tubular membrane configuration was designed, procured and assembled in order to investigate the oxygen permeation of YSZ tube membrane under the same operating conditions as in the study of YSZ pellet membrane.

As expected, oxygen can permeate through membrane tube at 850°C. With an external voltage application, the oxygen permeation process was promoted significantly and stable at a relatively high performance. The presence of sulphur dioxide in feed caused membrane performance degradation which increased slowly with exposure time. During the SO_2 exposure period, a partial performance recovery was obtained after a strong but short dc voltage application across membrane tube.

After all experiments, the membrane tube underwent XRD and SEM-EDS analysis. XRD spectrums of used and fresh membrane tubes indicated that the degradation and recovery in performance is unlikely to be related to the inherent behaviour of YSZ or Pt, but will be associated with other complications. From SEM-EDS spectrum,

no visible change in electrode surface morphology was observed and no sulphur was detected from the cathode surface of the membrane tube.

Under the same operating conditions, the oxygen permeate flux of YSZ membrane tube was smaller than that of YSZ membrane pellet. It may be due to

- YSZ thickness: thicker YSZ tube has a bigger oxygen diffusion resistance than the YSZ disk,

- Gas flow near membrane surface: a lot of backflow increase gas pressure gradient near the surface of YSZ membrane pellet.

Chapter 6

6 Sulphuric acid thermal decomposition

6.1 Introduction

In sulphur-Iodine (S-I) thermal cycle, sulphuric acid decomposition is the most energy consuming and technical demanding stage. It takes place in two steps, a non-catalytic thermal decomposition of the acid to form gaseous sulphur trioxide (SO_3) and water (H_2O) at temperatures above 350°C, followed by a catalytic decomposition of the SO_3 to produce the sulphur dioxide (SO_2) and oxygen (O_2) products (eq.6.1-6.2).

$$H_2SO_4 \rightarrow SO_3 + H_2O \tag{6.1}$$

$$SO_3 \rightarrow SO_2 + 0.5O_2 \tag{6.2}$$

After studying the performance of a YSZ membrane exposed to O_2-SO_2 at high temperature, a further step is to integrate YSZ membrane separation process with sulphuric acid thermal decomposition to study the effect of membrane operation on SO_2 yield under more realistic conditions. Before this, acid decomposition needs to be achieved at a scale which is commensurate with the membrane studies. This chapter reports some initial work which has been undertaken with this objective.

Decomposition of sulphuric acid has been studied and demonstrated previously (Zhang et al. 2011) (Nagaraja et al. 2009) (Brutti et al. 2007) (Barbarossa et al. 2006) (Brittain and Hildenbrand 1983). In general, the technical process is that liquid sulphuric acid is injected into vaporization system for obtaining gaseous acid which afterwards is dissociated into water steam and sulphur trioxide, and decomposed catalytically into sulphur dioxide and oxygen in a decomposition reactor. Gaseous

products are finally cooled down by a condenser system for acid collection or product analysis.

The primary objective of this work is to demonstrate acid decomposition at a laboratory scale. The second objective is to study acid conversion under a specific operating condition. Finally, stability of the catalyst after a long operating time is studied. This chapter describes the initial experimental approach taken in pursuit of these objectives. First of all, the apparatus and details of the equipment, including design, system assembly and approach were described. Secondly, the method used to process the data to obtain the acid conversion fraction was introduced. Thirdly, experimental results for each test are presented. Finally, an assessment of the current results and plans for future work was provided.

6.2 Description of apparatus

6.2.1 Overview

The apparatus for acid injecting, decomposing, condensing and collecting liquid effluent is arranged for straight-through downward processing of acid as shown schematically in Figure 6.1. The units for these four processes are shown as an acid injector, a decomposer, a condenser and a collection flask, respectively. This arrangement eliminates bends or curves where acid could collect, corrode, and accumulate corrosion products. Produced gases, which are primarily sulphur dioxide and oxygen, are separated by gravity from the cooled liquid in the collection flask. The remaining gases are bubbled to distilled water and then hydrogen peroxide (H_2O_2) solution. The final gas is mainly oxygen which was monitored by a gas analyser before venting to fume hood. The basic components of the apparatus are shown in Figure 6.2 prior to installing the acid injector. A picture of the complete apparatus with this equipment installed is shown in Figure 6.3.
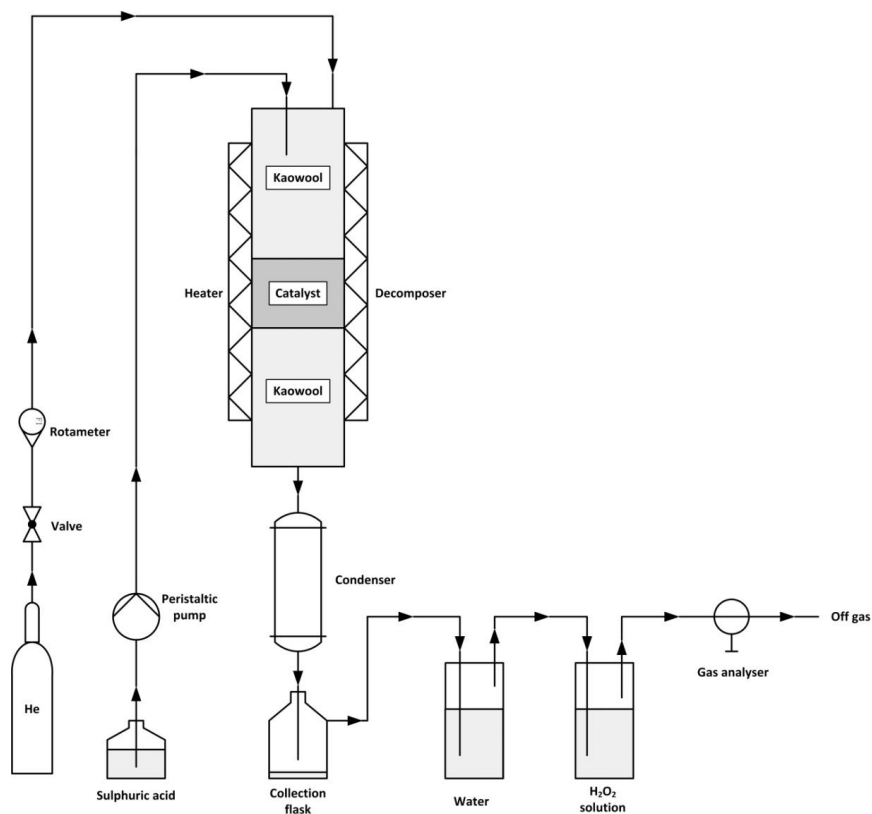
Figure 6.1: *Schematic of straight-through sulphuric acid injector, catalytic decomposer, condenser, products collection flask and separation process*
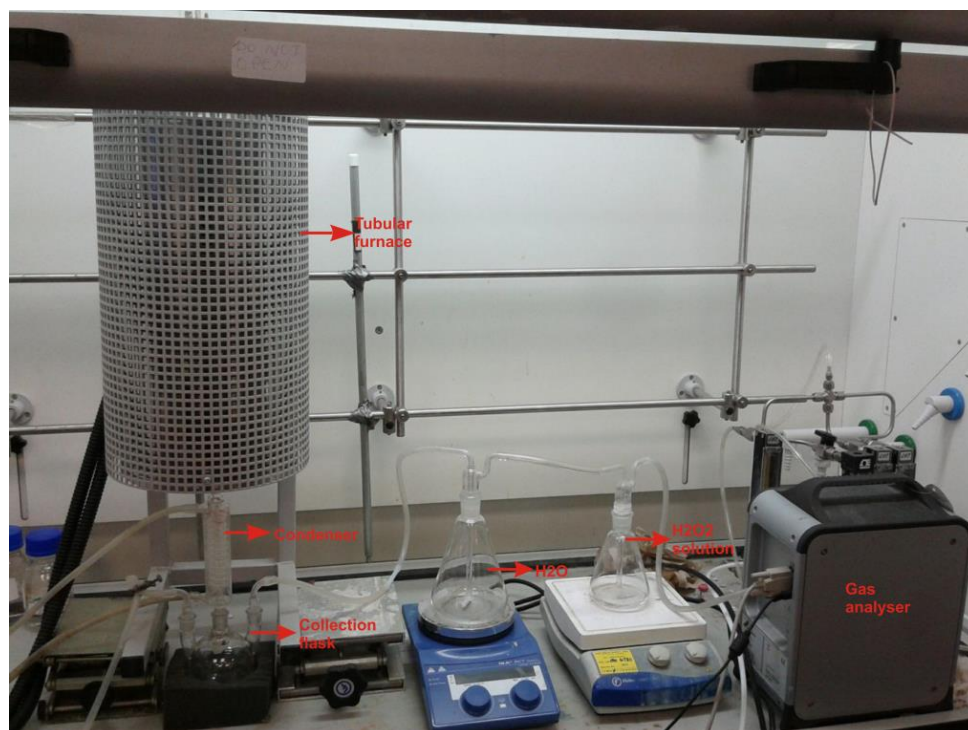
Figure 6.2: *Straight-through sulphuric acid tubular, catalytic decomposer, condenser, collection flask and products separation system, prior to installing peristaltic pump*
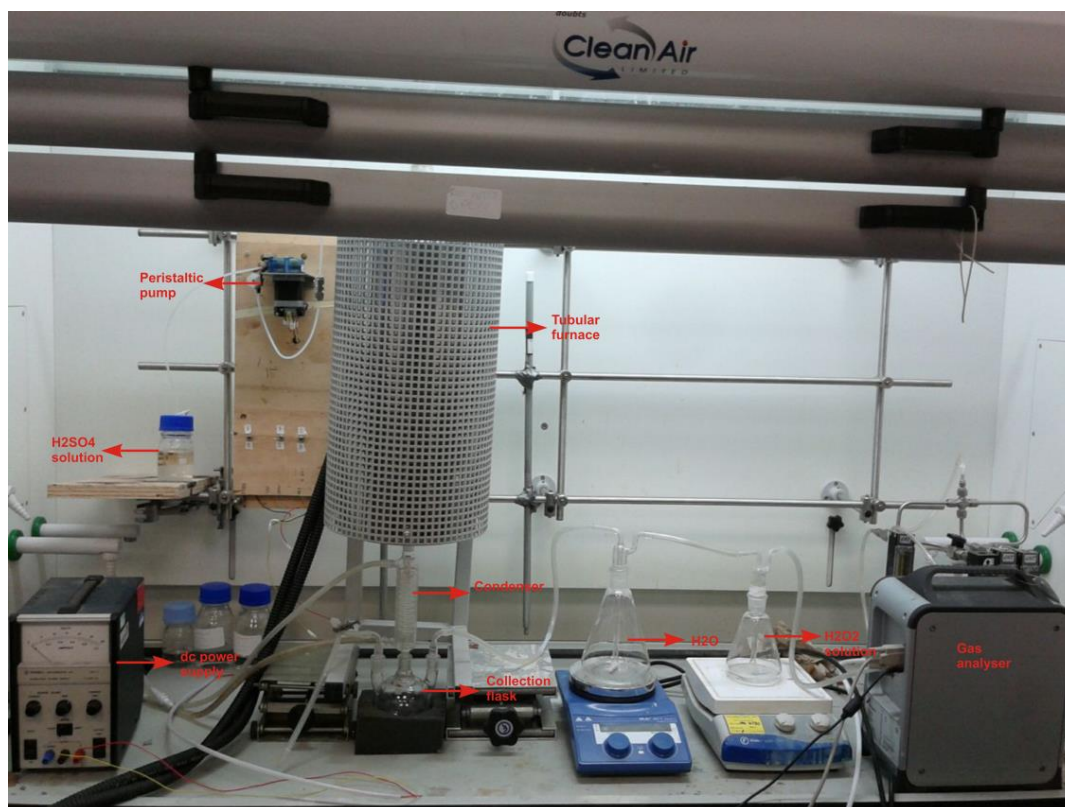
Figure 6.3: *Fully instrumental straight-through peristaltic pump, catalytic decomposer, condenser, products collection and separation system.*

6.2.2 Details of apparatus operation

All apparatus is located in a fume hood. The acid pump for feeding liquid sulphuric acid to the decomposer was connected to a dc power supply. Part of the decomposer was exposed to the outside of the furnace in order to seal the connection between decomposer and acid injecting tubing at low temperature. Gas-tightness of the connections between the condenser, the decomposer and the collection flask was achieved by ground glass joints. High temperature was provided by the tubular furnace. Helium as carrier gas entered from the top of the decomposer. Its flow rate was controlled by a rotameter.

Peristaltic pump

A 200 series stepper motor driven peristaltic pump (model number: 202-SMA-150-016), supplied by Williamson Manufacturing Company Limited, was used to provide a compact, accurate and reliable means of dosing a wide range of liquids [Figure 6.4]. The approximate flow rate range is from 0.02 to 21 ml/min.

Figure 6.4: *A 200 series stepper motor powered pump*

The tube (I.D 1.6mm) through the pump was made from viton which can work excellently with high concentration sulphuric acid (75-100%), according to the chart of chemicals and their compatibility with viton (http://www.fbs-online.com/Centre/Prod/Viton-chem-com-res.htm).

Tubular furnace

The decomposer described above was inserted into a Carbolite MTF12/38/400 tubular furnace. This furnace has a work tube of 450mm length and 38mm inside diameter and a maximum operating temperature of 1200°C. The furnace has been specified with an "L stand" which allows it to be assembled vertically. Figure 6.5 shows the furnace situated in the fume hood.
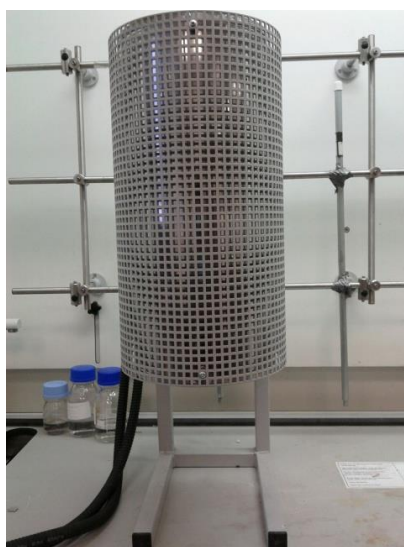
Figure 6.5: *Tubular furnace in a fume hood*

Decomposer

The decomposer (490mm length, 28.8mm internal diameter) was designed according to the dimensions of the tubular furnace, and was fabricated by Robson Scientific [Figure 6.6]. It was made from quartz which has excellent chemical stability under acid environment and can withstand over 1500°C. The bottom ground joint (14/20) was connected to the condenser.
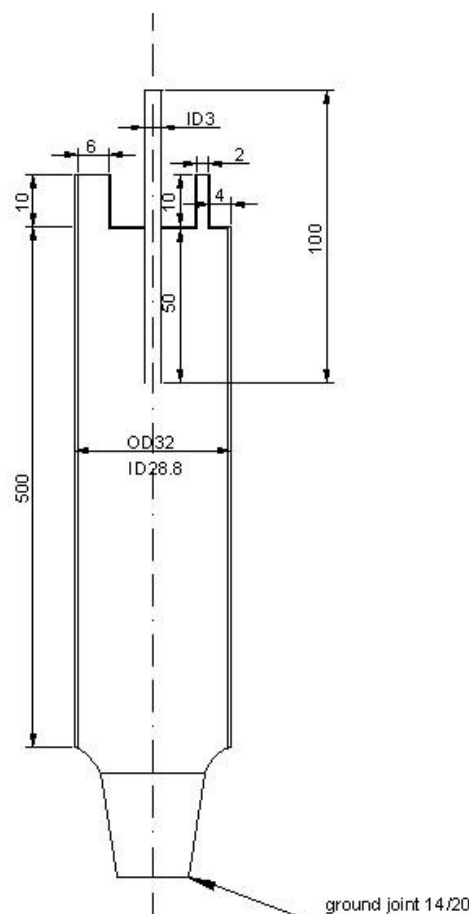
Figure 6.6: *Schematic diagram of quartz decomposer for sulphuric acid decomposition. All measurements are in mm*

At feasible operating temperatures, between 1023K and 1173K, the reduction of SO_3 does not take place without a catalyst. On the contrary, because of the presence of catalyst, the temperature of H_2SO_4 decomposition can be decreased by around 300K to 1150K (Barbarossa et al. 2006); Following a literature review of catalysts used in H_2SO_4 thermal decomposition, platinum 0.5%/alumina pellets , supplied by Alfa Aesar, were employed in this work [Figure 6.7]. Some catalyst was filled in the middle of the decomposer (around 5mm length), sandwiched between ceramic Wool

layers [Figure 6.8].

Figure 6.7: *Pt/Al$_2$O$_3$ catalyst (Pt, 0.5% on 1/8in alumina pellets, reduced)*

Figure 6.8: *Decomposer filled with catalyst and ceramic wool layers*

6.2.3 Analysis method

A popular method for collecting products is that the gaseous products are trapped in Bunsen reactors contained an I$_2$/I$^-$ aqueous solution to quickly form sulphuric acid

and hydrogen iodide at low temperature. SO_2 yield can be derived from the increase of I^- concentration measured by Ionic Chromatograph (IC) (Barbarossa et al. 2006) (Brutti et al. 2007) (Kondamudi and Upadhyayula 2010). In this study, however, a different method was proposed.

The catalytically decomposed products (SO_2, O_2, H_2O, and un-decomposed SO_3) are cooled in the condenser. Unreacted SO_3 recombines with H_2O to form sulphuric acid and is collected by a flask. The remaining gases consisted of SO_2, O_2 and a small amount of SO_3 are bubbled to deionized water in order to adsorb SO_3, then to excess H_2O_2 solution in order to remove SO_2 by eq. 6.3. In future work, the peroxide scrub can be removed, allowing the membrane to be exposed to the full decomposition oviducts.

$$SO_2 + H_2O_2 \rightarrow H_2SO_4 \qquad (6.3)$$

The final gas is oxygen yield is measured by a gas analyser. Yield of SO_2 can also, in principle, be derived from the amount of oxygen produced in acid decomposition. In the present work, on-line oxygen concentration in helium with time was measured every two seconds by the gas analyser. The total amount of oxygen was calculated by the integration of oxygen concentration with time. Therefore, the total amount of SO_2 produced from acid decomposition was got by eq. 6.1 - 6.2 and eq. 6.4.

$$V_{so_2} = 2V_{O_2} = 2\int_{t1}^{t0} C_{O_2} F dt \qquad (6.4)$$

Where V_{SO2} is total volume of sulphur dioxide, V_{O2} is volume of oxygen, t0 is the beginning time of experiment, t1 is the ending time of experiment, C_{O2} is the volume concentration which measured by gas analyser every two seconds, F is the total flowrate of final gas.

At the same time, the SO_2 yield calculated from oxygen can be assessed by the amount of H_2SO_4 in H_2O_2 solution after titration using NaOH solution.

$$m_{H2SO_4} = m_{H2SO_4} \%M \qquad (6.5)$$

Where m_{H2SO4} is the total mass of sulphuric acid in H_2O_2 solution, $m_{H2SO4}\%$ is the density of H_2SO_4 in H_2O_2 solution, M was the total mass of H_2SO_4-H_2O_2 solution. Nevertheless, it is noticed that the data obtained by the titration process was not accurate because of the losses in the SO_3 adsorption process caused by SO_2 solubility in H_2O at room temperature [Figure 6.9].
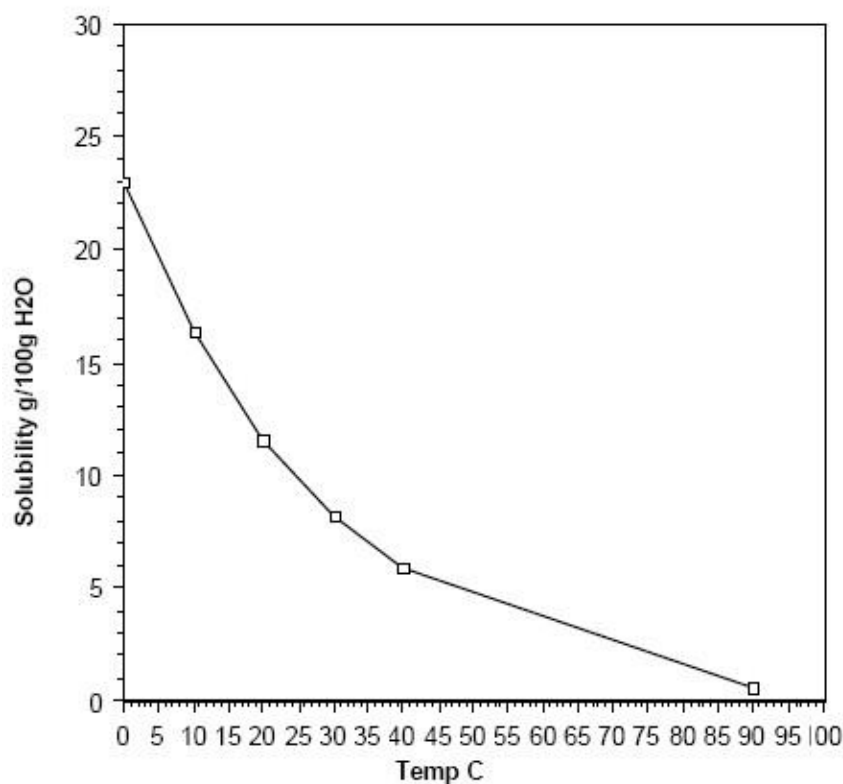
Figure 6.9: *SO$_2$ solubility in H$_2$O at different temperature (Source: Kirk Othmer Ency of Chemical Technology)*

6.3 Experimental section

The experimental apparatus used in this work is shown in Figure 6.1. The main components are: as follows a H_2SO_4 feed system, a decomposition reactor, product cooling and separation system.

Sulphuric acid feeding system: approximate 98% of sulphuric acid (around 1.84g/cm^3) prepared by mixing 65% SO_3 fuming sulphuric acid (Alfa Aesar) with deionized water was fed to the decomposer by the peristaltic pump.

Decomposition reactor: The high-temperature reactor was contained within the tubular furnace equipped with a temperature controller. 100ml/min of Helium was supplied into the decomposer and passing through all rig. Also helium was used to check the air tightness of the rig before starting every experiment. The residence time of H_2SO_4/He flux in the reactor was about 5 seconds, 0.5 seconds of which was taken up in passing through the catalyst bed.

Product cooling and separation system: The gaseous flux effusing from the reactor was composed of He, H_2SO_4, SO_3, SO_2, O_2, H_2O. Unreacted H_2SO_4, SO_3 and H_2O were condensed and collected by the bottom collection flask. Afterwards, the remaining gases were bubbled to water and hydrogen peroxide solution (35% H_2O_2 solution supplied by Alfa Aesar diluted by deionized water) successively in order to adsorb SO_3 and separate SO_2 from O_2. Oxygen concentration in helium was measured by a gas analyser and recorded every 2 seconds by a PC. After the experiment was completed, H_2O_2-H_2SO_4 solution was titrated by 0.1N NaOH solution using a titration kit (T50/T70/T90 Titrator, METTLER TOLEDO).

All experiments were grouped into three sections: Section I was a commissioning test to demonstrate sulphuric acid decomposition. Section II was to determine sulphur dioxide conversation yield under a specific operating condition. Section III was to investigate the stability of Pt/Al_2O_3 catalyst after a series of experiments. The operating conditions in the three sections were shown in Table 6.1. Fresh catalyst was used for each section.

	Section I	Section II	Section III
Operating pressure	1.0 bar	1.0 bar	1.0 bar
Operating temperature	850°C	850°C	850°C
Acid injection rate	0.08ml/min = 0.0015mol/min	0.11ml/min =0.0021mol/min	0.11 ml/min =0.0021mol/min
Duration for acid pumping	30 min	30 min	8.5 h
Flowrate of helium	100ml/min	100 ml/min	100ml/min

Table 6.1: *The operating conditions of sulphuric acid thermal decomposition*

XRD measurements of catalyst, before and after Section III, were carried out by Phillips PW 1830 using Cu Ka1 radiation (λ=1.5406A) with a step of 0.02° (2θ) and a scanning rate of 2° min^{-1}. The spectra will be presented in the subsequent section.

6.4 Result and discussion

6.4.1 Commissioning test

Once temperature was reached, gas tightness of the rig was tested. Afterwards, liquid acid was injected into decomposer by the peristaltic pump. The temperature of the quartz tube exposed to air was around 200°C. Therefore, the sulphuric acid could be gasified and dissociated to sulphur trioxide and steam before meeting the catalyst.

A few minutes after acid injection, the reading of oxygen concentration in gas analyser rose with time, reaching a maximum value of 23.6% at the 38th minute, then decreased quickly to 4.7% within half an hour and then more slowly to 2.43% at the end of experiment [Figure 6.10]. Oxygen concentration change not only proved the occurrence of H_2SO_4 decomposition reaction, but indicated the beginning and ending times of acid decomposition. The flow of acid before entering decomposer and oxygen before passing through gas analyser made that the duration of acid pumping was shorter than oxygen detection time.

After this experiment, a little liquid was found from the bottom collection flask,

which was acidic tested by pH paper. The mass of H_2O_2 solution was increased, evidencing the combination reaction of SO_2 and H_2O_2.
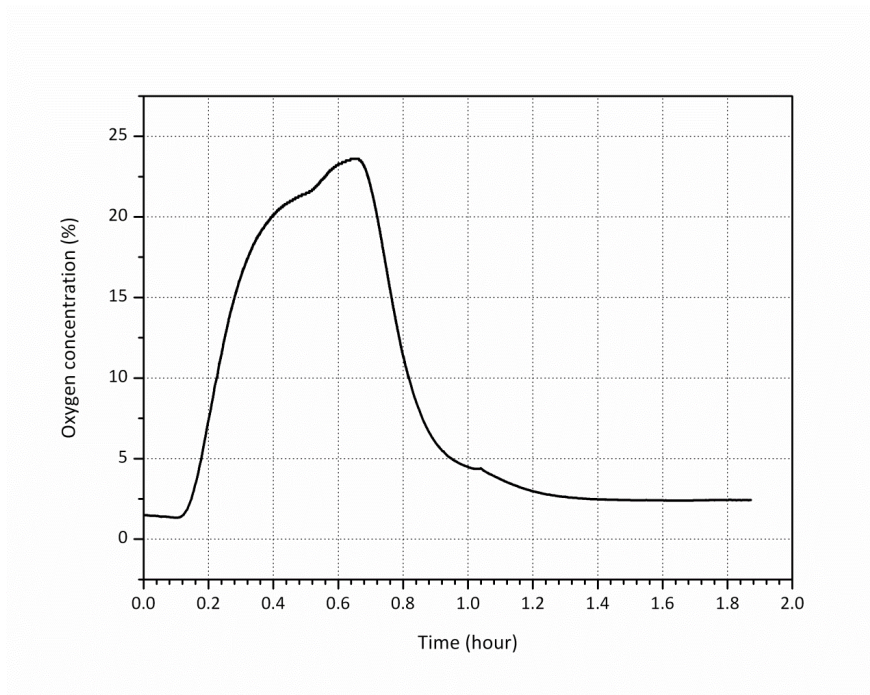
Figure 6.10: *Oxygen concentration change with time in H_2SO_4 thermal decomposition (Section I)*

6.4.2 SO_2 yield

Sulphuric acid thermal decomposition was repeated at the same operating conditions as Section I, but with a different acid injection rate and fresh catalyst.

Oxygen concentration with time is shown in Figure 6.11. According to equation 6.1, 6.2 and 6.4, sulphur dioxide yield at 850°C was calculated to be around 25.4% molar. This agrees well with the result got from chemical titration. However, literature reports suggest that at 850°C the yields can be as high as 85% with Pd catalyst (Barbarossa et al. 2006), and 75% in the presence of Al-Fe_2O_3 catalyst (Kondamudi and Upadhyayula 2010). These values are much higher than obtained in the present experiment, but it must be noticed that the residence times used by Barbarossa and Kondamudi were higher than the one used in this study. The conversion of SO_3 to SO_2 is a slow process, and Berezkina has shown the influence of the residence time of the sulphur oxides at high temperature on SO_2 yield (Berezkina et al. 1988). Therefore, short residence time will lead to low SO_2 conversion yield. This is

consistent with the value obtained by Barbarossa at 850°C in absence of catalyst (Barbarossa et al. 2006).

As described previously there are two main reactions in sulphuric acid decomposition. Sulphuric acid dissociation to SO_3 is instantaneous and does not affect the kinetics of the process. SO_3 decomposition to SO_2 and O_2 is kinetically controlled reaction (Schwartz et al. 2000), which has been considered to be an irreversible first-order reaction (Kim et al. 2013) (Karasawa and Hoshino 2005). The decomposition rate constant of SO_3 decomposition, k, can express in an Arrhenius formula,

$$k = A\exp(-\frac{E}{RT})$$
(6.6)

Where A is pre-exponential factor (S^{-1}), E is activation energy (J/mol), R is gas constant (J/(mol K)), and T is temperature (K). A and E are accepted as 1.0×10^4 s^{-1} and 90900 J/mol respectively. These values are taken from Brutti et. al who reported these values for a SO_3 decomposition in an electrical furnace by using a Fe_2O_3 on SiO_2 catalyst (Brutti et al. 2007).

When the decomposition of SO_3 is assumed to be homogeneous reaction of first order, the thermal decomposition rate (X_{SO3}) with reaction time (t) is expressed as follows,

$$\ln\frac{1}{1-X_{SO3}} = kt$$
(6.7)

When the residence time of gaseous acid passing through Pt/Al_2O_3 catalyst bed is 0.5s, the conversion of SO_3 at 850°C, according to eq.6.6 and 6.7, is around 0.256 which is consistent with the experimental value in present study.

The stability of Pt/Al_2O_3 catalyst was tested at 850°C and the results are shown in Figure 6.12. Results show that Pt/Al_2O_3 catalyst presented good stability, and its activity does not decrease within 8.5h during SO_2 yield are around 25%. This also could be inferred by the XRD spectrums of catalyst before and after experiment

[Figure 6.13].
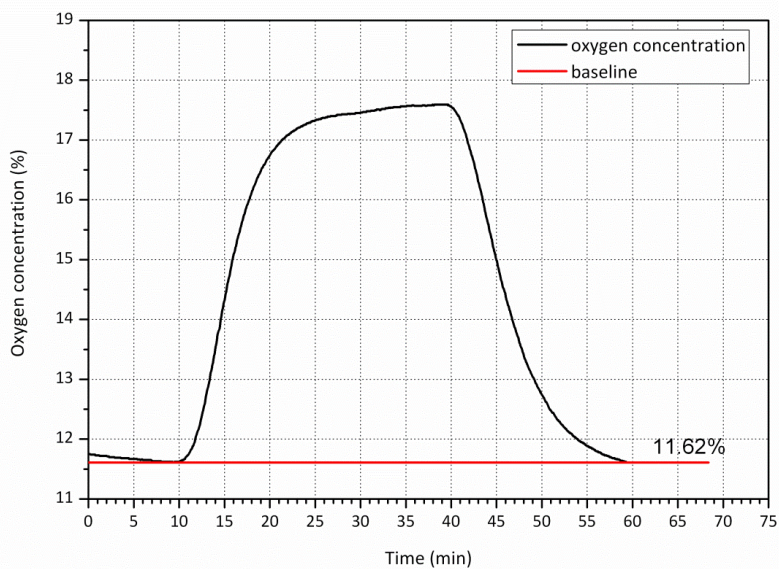
Figure 6.11: *Oxygen concentration change with time in H₂SO₄ thermal decomposition (Section II)*
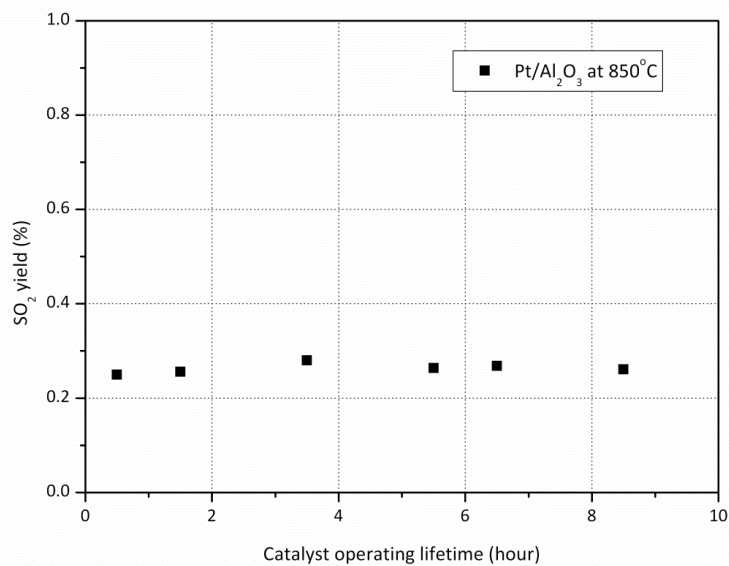
Figure 6.12: *Pt/Al₂O₃ catalyst activity based on SO₂ yield as a function of the catalyst operating lifetime (Section III)*
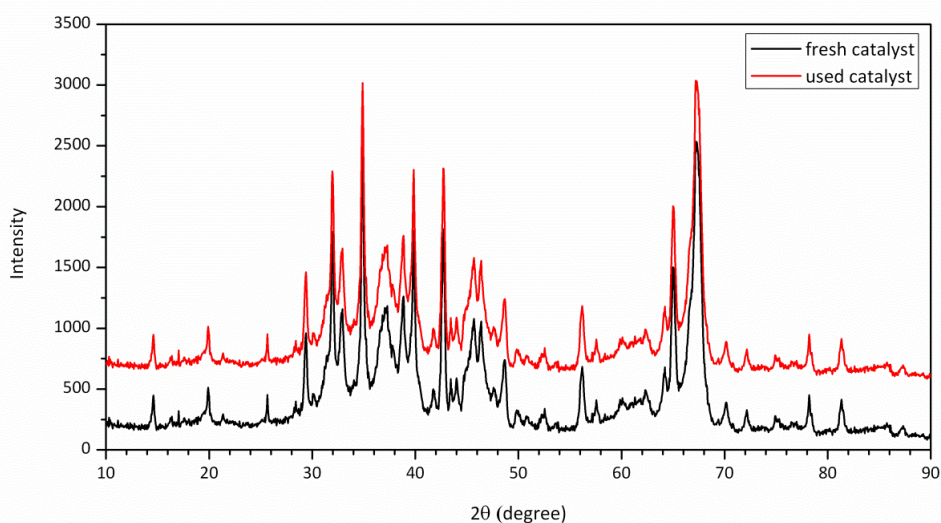
Figure 6.13: *XRD data of Pt/Al₂O₃ catalyst before and after acid decomposition*

6.5 Conclusion

As a stage of the integration process of membrane operation with sulphuric acid thermal decomposition, some initial acid thermal decomposition was carried out in laboratory.   Time did not permit this work programme to be completed but interesting initial results were obtained and a potential apparatus, suitable for use with the existing membrane systems was developed. In particular an experimental apparatus including an acid feeding system, a decomposition reactor, an outcoming gas collector system and gases separation system was designed and assembled.

Different from the previous popular product collection method for SO_2 yield by I_2/I^- solution and Ionic Chromatograph, an on-line process was proposed for the first time to monitor oxygen concentration with time to determine acid conversion of H_2SO_4 thermal decomposition. By comparing to other results in similar operating conditions, this method was shown to be feasible and promises easy derivation of the yield of H_2SO_4 decomposition.

SO_2 yield in these initial experiments was only around 25% in the presence of Pt/Al₂O₃ catalyst at 850°C. It may be due to the much shorter residence time (0.5 second) of gaseous acid in the catalyst-containing part of the reactor which may

make inefficient use of the catalyst during acid decomposition. So in order to obtain high SO$_2$ yield, extension of the residence time of the gaseous acid passing through catalyst in the decomposer is necessary for future work.

Chapter 7

7 Overall conclusion and future work

7.1 Overall conclusion

The demand for clean, secure, and sustainable energy sources has stimulated great interest in the sulphur-iodine thermal cycle (S-I cycle), a promising approach that produces hydrogen at large scale and high efficiency. In the S-I cycle, sulphuric acid decomposition requires the greatest heat input, typically at temperatures in the range of 800–900°C. Higher temperatures tend to favour greater efficiency. If the high temperature can be decreased to some extent, yet keeping efficiency in the same level, or even higher, then a great deal of resources can be saved. An electrolyte of a ceramic membrane, yttria-stabilized zirconia (YSZ) with high oxygen ion conductivity has been proposed to separate oxygen from the products of sulphuric acid (H_2SO_4) decomposition. In this way, the yield of SO_2 that is recycled to Bunsen reaction in the S-I cycle could be increased and the overall efficiency of S-I cycle could be improved. In other words, the temperature of H_2SO_4 decomposition could be reduced for a given SO_2 yield.

Among the challenges of utilizing YSZ membranes in the separation process after H_2SO_4 decomposition is severe degradation of membrane performance due to sulphur poisoning, also a common problem in solid oxide fuel cells (SOFCs). In this work, such performance degradation of a Pt/8YSZ/Pt pellet exposed to $SO_2/O_2/He$ (30% SO_2) at 850°C has two phases: a sudden decrease, followed by a gradual and continuous decrease. The initial quick degradation was attributed to sulphur dioxide

adsorption onto the platinum surface; resulting in physical blocking of electrode surface and decrease of TPB length. Once the sulphur dioxide adsorption reaches saturation, further gradual degradation occurred. Based on analysis of the membrane cell before and after the SO_2 exposure test, the slow degradation was not related to the YSZ electrolyte but rather to an interaction between Pt electrode and sulphur dioxide which causes polarization resistance and serial resistance increase. It is postulated that this is caused by the formation of platinum sulphide.

This performance degradation can be reduced significantly by a short but strong dc positive or negative voltage pulse which has an effect on both charge transfer and mass transfer properties, and it is suggested that this effect might help the removal of sulphur on the cathode by electrochemical reactions. The recovery rates of cell performance obtained by positive and negative voltage pulses were similar. In this work, the optimum voltage pulse magnitude and duration for achieving the most stable membrane performance in SO_2 exposure time was 10V, 0.08s length. For the short SO_2 exposure periods studied, high pulse frequency was recommended to maintain a high and stable membrane performance although it raises energy consumed to 12.39J of 4 pulses. More works are needed in the future to optimize voltage pulse frequency in consideration of cell performance improvement and energy consumption. To ensure understanding of the long-term influence of high voltage on electrode surface, membrane performance should be observed in the future for longer SO_2 exposure periods with high pulse frequency.

Under the same operating conditions, oxygen permeation process of a Pt/8YSZ tubular membrane was demonstrated. However, the oxygen permeation flux of the YSZ tubular membrane was smaller than that of the YSZ planar membrane. It was due that YSZ tube was thicker and a lot of backflow existed near the surface of YSZ planar membrane. There should be future work to improve tubular membrane construction and configurations.

Initial experiments on the thermal decomposition of H_2SO_4 to produce SO_2 was

carried out at 850°C in a quartz tube reactor with 98% sulphuric acid feed over alumina supported Pt catalyst, using helium as an inert carrier gas. SO_2 yield was only around 25%, such low yield may be due to short residence time (0.5 second) of gaseous acid in the catalyst bed. Distinct from the normal product collection method for SO_2 yield by I_2/I^- solution and Ion Chromatograph, on-line monitoring of oxygen concentration with time was proposed for the first time to determine acid conversion of H_2SO_4 during thermal decomposition. By comparing to other results in similar operating conditions, this method was shown to be feasible and enables easy derivation of the yield of H_2SO_4 decomposition.

7.2 Future work

7.2.1   Electrode morphology

In this study, performance degradation of a Pt/YSZ membrane by SO_2 poisoning and its recovery by a dc voltage pulse was successfully investigated by comparing the current change and permeated oxygen concentration in each experiment. Nevertheless, the Pt electrode coated manually was inhomogeneous, which may interfere with oxygen permeation processes through the YSZ. For example, uneven platinum layers may have an influence on oxygen permeation process by increasing the interface resistance between electrode and electrolyte, and affect the surface-exchange kinetics which controls oxygen permeation flux. Therefore, a thin and uniform electrode layer of YSZ membrane may be helpful for further studies on the sulphur poisoning behavior and the mechanism of sulphur removal by dc voltage pulses.

7.2.2   YSZ tubular configuration

Initial experiments were conducted on tubular membranes with partial success. Although in my work the oxygen permeation flux of YSZ tubular membrane was not

as good as YSZ planar membrane, tubular cells can be easily scaled-up, need much smaller sealing area, have better thermal cycling capability and high mechanical stability. Therefore, more efforts are needed to improve tubular membrane configuration in the future.

7.2.3   Integration of membrane operation and acid decomposition

In this work, H_2SO_4 thermal decomposition was demonstrated successfully. A promising and feasible method based on oxygen yield to determine sulphuric acid conversion was proposed for the first time. Further work was beyond the scope of this project. The following recommendations are made to optimize operating conditions for acid decomposition. Afterwards, membrane operation could be integrated with acid decomposition. The schematic of a proposed experimental rig is shown in Figure 7.1.
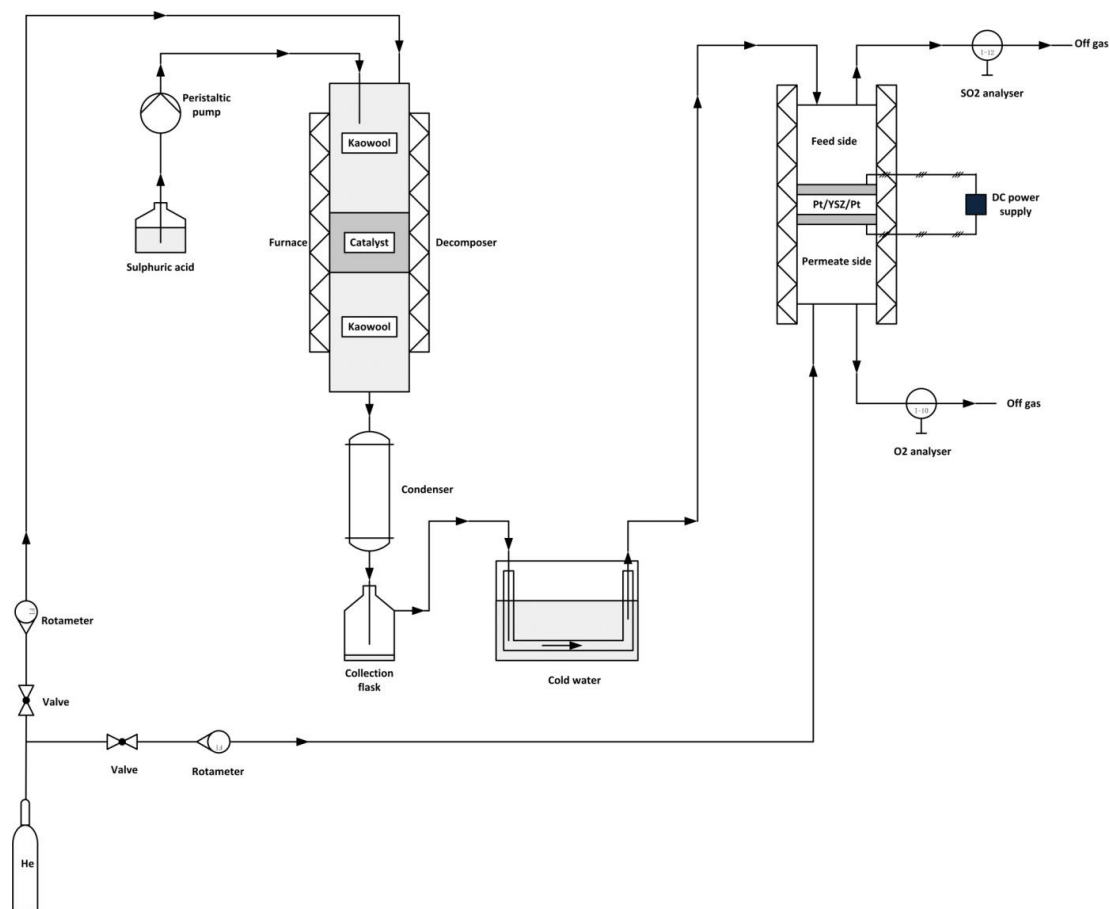
Figure 7.1: *Schematic of experimental rig*

The experimental method could be: Concentrated sulphuric acid is injected into a decomposer by a peristaltic pump (or syringe pump). The acid is gasified at the top of the decomposer and then flows through the catalyst bed. The gaseous products are cooled down by a condenser. Unreacted sulphuric acid and water are collected by a collection flask. Afterwards, the residual gases consisting of SO_3, SO_2, O_2 and He flow through a U-bend tube which is submerged in cold water. Subsequently, gas mixtures of SO_2, O_2 and He would be introduced to the feed side of a YSZ membrane. The concentrations of sulphur dioxide in feed side and oxygen in permeate side are measured by gas analyzers. The effect of removing oxygen from product gases by YSZ membrane on acid conversion would be examined by comparing the amount of SO_2 in off gas.

References

Adler SB (2004), 'Factors Governing Oxygen Reduction in Solid Oxide Fuel Cell Cathodes', *Chemical Reviews* **104** (10), 4791-4844.

Adris AM, Pruden BB, Lim CJ, Grace JR (1996), 'On the reported attempts to radically improve the performance of the steam methane reforming reactor', *The Canadian Journal of Chemical Engineering* **74** (2), 177-186.

Aochi A, Tadokoro T, Yoshida K, Kameyama H, Nobue M, Yamaguchi T (1989), 'Economical and technical evaluation of UT-3 thermochemical hydrogen production process for an industrial scale plant', *International Journal of Hydrogen Energy* **14** (7), 421-429.

AShcroft AT, Cheetham AK, Foord JS, Green MLH, Grey CP, Murrell AJ, Vernon PDF (1990), 'Selective oxidation of methane to synthesis gas using transition metal catalysts', *nature* **344** (6264), 3.

Astegger S, Bechtold E (1982), 'Adsorption of sulfur dioxide and the interaction of coadsorbed oxygen and sulfur on Pt(111)', *Surface Science* **122** (3), 491-504.

Atkin I (2009). Improvement of sulphur dioxide yield from the sulphuric acid thermal decomposition process by membrane separation. <u>Department of Chemical and Process Engineering</u>. Sheffield, University of Sheffield. **PhD:** 236.

Badwal SPS, Foger K (1996), 'Solid oxide electrolyte fuel cell review', *Ceramics International* **22** (3), 257-265.

Baklanova NI, Titov AT, Boronin AI, Kosheev SV (2006), 'The yttria-stabilized zirconia and interfacial coating on Nicalon™ fiber', *Journal of the European Ceramic Society* **26** (9), 1725-1736.

Balat H, Kirtay E (2010), 'Hydrogen from biomass - Present scenario and future prospects', *International Journal of Hydrogen Energy* **35** (14), 7416-7426.

Barbarossa V, Brutti S, Diamanti M, Sau S, De Maria G (2006), 'Catalytic thermal decomposition of sulphuric acid in sulphur-iodine cycle for hydrogen production', *International Journal of Hydrogen Energy* **31** (7), 883-890.

Barelli L, Bidini G, Gallorini F, Servili S (2008), 'Hydrogen production through sorption-enhanced steam methane reforming and membrane technology: A

review', *Energy* **33** (4), 554-570.

Barsoukov E, Macdonald JR (2005), *Impedance Spectrosocopy Theory, Experiment, and Applications*, John Wiley & Sons, Inc., Hoboken.

Bartholomew CH, Agrawal PK, Katzer JR, D.D. Eley HP, Paul BW (1982). Sulfur Poisoning of Metals. Advances in Catalysis, Academic Press. **Volume 31:** 135-242.

Baumann FS, Fleig J, Konuma M, Starke U, Habermeier HU, Maier J (2005), 'Strong Performance Improvement of La0.6Sr0.4Co0.8Fe0.2O3 – SOFC Cathodes by Electrochemical Activation', *Journal of the Electrochemical Society* **152** (10), A2074 - A2079.

Baumann FS, Fleig Jr, Konuma M, Starke U, Habermeier H-U, Maier J (2005), 'Strong Performance Improvement of La0.6Sr0.4Co0.8Fe0.2O3?-? SOFC Cathodes by Electrochemical Activation', *Journal of the Electrochemical Society* **152** (10), A2074-A2079.

Baur E, Preis H (1937), 'Über Brennstoff-Ketten mit Festleitern', *Zeitschrift für Elektrochemie und angewandte physikalische Chemie* **43** (9), 727-732.

Bay L, Jacobsen T (1997), 'Dynamics of the YSZ-Pt interface', *Solid State Ionics* **93** (3-4), 201-206.

Belaissaoui B, Thery R, Meyer XM, Meyer M, Gerbaud V, Joulia X (2008), 'Vapour reactive distillation process for hydrogen production by HI decomposition from HI-I2-H2O solutions', *Chemical Engineering and Processing: Process Intensification* **47** (3), 396-407.

Berezkina LG, Borisova SI, Saenko ND, Sushchev VS (1988), 'Chromatographic study of the thermal decomposition of spent sulfuric acid', *Journal Name: J. Appl. Chem. USSR (Engl. Transl.); (United States); Journal Volume: 60:9; Other Information: Translated from Zh. Prikl. Khim.; 60: No. 9, 2088-2090(Sep 1987)* Medium: X; Size: Pages: 1929-1931.

BESENBRUCH GE, BROWN LC, Funk JF, SHOWALTER SK (2000). HIGH EFFICIENCY GENERATION OF HYDROGEN fuels using nuclear power. Kentucky, Sandia National Laboratory.

Blum L, Meulenberg WA, Nabielek H, Steinberger-Wilckens R (2005), 'Worldwide SOFC Technology Overview and Benchmark', *International Journal of Applied Ceramic Technology* **2** (6), 482-492.

Brightman E, Ivey DG, Brett DJL, Brandon NP (2011), 'The effect of current density on H2S-poisoning of nickel-based solid oxide fuel cell anodes', *Journal of Power Sources* **196** (17), 7182-7187.

Brittain RD, Hildenbrand DL (1983), 'Catalytic decomposition of gaseous sulfur trioxide', *The Journal of Physical Chemistry* **87** (19), 3713-3717.

Brown LC, Besenbruch GE, Lentsch RD, Schultz KR, Funk JF, Pickard PS, Marshall AC, SHOWALTER SK (2003). High efficiency generation of hydrogen fuels using nuclear power.

Brutti S, Bencivenni L, Barbarossa V, Sau S, Maria GD (2006), 'Gas phase dissociation of H2SO4: A computational study', *The Journal of Chemical Thermodynamics* **38** (11), 1292-1300.

Brutti S, De Maria G, Cerri G, Giovannelli A, Brunetti B, Cafarelli P, Barbarossa V, Ceroli A (2007), 'Decomposition of H2SO4 by Direct Solar Radiation', *Industrial & Engineering Chemistry Research* **46** (20), 6393-6400.

Caputo G, Felici C, Tarquini P, Giaconia A, Sau S (2007), 'Membrane distillation of HI/H2O and H2SO4/H2O mixtures for the sulfur-iodine thermochemical process', *International Journal of Hydrogen Energy* **32** (18), 4736-4743.

Chaston JC (1964), 'Reaction of oxygen with the platinum metals', *Platinum Metals Review* **8** (2), 50-54.

Chauveau F, Mougin J, Bassat JM, Mauvy F, Grenier JC (2010), 'A new anode material for solid oxide electrolyser: The neodymium nickelate Nd2NiO4+Î´', *Journal of Power Sources* **195** (3), 744-749.

Chen XJ, Khor KA, Chan SH (2003), 'Identification of O2 reduction processes at yttria stabilized zirconia|doped lanthanum manganite interface', *Journal of Power Sources* **123** (1), 17-25.

Ciacchi FT, Badwal SPS, Zelizko V (2002), 'Tubular zirconia-yttria electrolyte membrane technology for oxygen separation', *Solid State Ionics* **152-153** 763-768.

Cohen JE (2002). World population in 2050: assessing the projections, Rockefeller Univerisity and Columbia University.

Connolly SM, Zabolotny E, McLaughlin DF, Lahoda EJ (2009), 'Design of a composite sulfuric acid decomposition reactor, concentrator, and preheater for hydrogen generation processes', *International Journal of Hydrogen Energy* **34** (9), 4074-4087.

de Souza RF, Padilha JC, Goncalves RS, de Souza MO, Rault-Berthelot J (2007), 'Electrochemical hydrogen production from water electrolysis using ionic liquid as electrolytes: Towards the best device', *Journal of Power Sources* **164** (2), 792-798.

Demirbas A (2008), 'Biohydrogen Generation from Organic Waste', *Energy Sources, Part A: Recovery, Utilization, and Environmental Effects* **30** (5), 475-482.

Deng X, Petric A (2005), 'Geometrical modeling of the triple-phase-boundary in solid oxide fuel cells', *Journal of Power Sources* **140** (2), 297-303.

Devanathan R, Weber WJ, Singhal SC, Gale JD (2006), 'Computer simulation of defects and oxygen transport in yttria-stabilized zirconia', *Solid State Ionics* **177** (15-16), 1251-1258.

Dincer I (2002), 'Technical, environmental and exergetic aspects of hydrogen energy systems', *International Journal of Hydrogen Energy* **27** (3), 265-285.

Ding C, Lin H, Sato K, Kawada T, Mizusaki J, Hashida T (2010), 'Improvement of electrochemical performance of anode-supported SOFCs by NiO-Ce0.9Gd0.1O1.95 nanocomposite powders', *Solid State Ionics* **181** (25-26), 1238-1243.

Dunn S (2002), 'Hydrogen futures: toward a sustainable energy system', *International Journal of Hydrogen Energy* **27** (3), 235-264.

Dunn S (2001). Hydrogen Futures: Toward a Sustainable Energy System. J. A. Peterson. Washington DC, Worldwatch institute.

Edwards PP, Kuznetsov VL, David WIF, Brandon NP (2008), 'Hydrogen and fuel cells: Towards a sustainable energy future', *Energy Policy* **36** (12), 4356-4362.

Eguchi K, Hatagishi T, Arai H (1996), 'Power generation and steam electrolysis characteristics of an electrochemical cell with a zirconia- or ceria-based electrolyte', *Solid State Ionics* **86-88, Part 2** (0), 1245-1249.

Elder RH, Priestman GH, Allen RWK (2009), 'Dewatering of HIx solutions by pervaporation through Nafion® membranes', *International Journal of Hydrogen Energy* **34** (15), 6129-6136.

Emery DA, Middleton PH, Metcalfe IS (1998), 'The effect of electrochemical current pumping on the work function of solid electrolyte supported catalysts', *Surface Science* **405** (2-3), 308-315.

Etsell TH, Flengas SN (1970), 'Electrical properties of solid oxide electrolytes', *Chemical Reviews* **70** (3), 339-376.

Feduska W, Isenberg AO (1983), 'High-temperature solid oxide fuel cell - technical status', *Journal of Power Sources* **10** (1), 89-102.

Figueiredo FML, Marques FMB (2013), 'Electrolytes for solid oxide fuel cells', *Wiley Interdisciplinary Reviews: Energy and Environment* **2** (1), 52-72.

Freni S, Calogero G, Cavallaro S (2000), 'Hydrogen production from methane through catalytic partial oxidation reactions', *Journal of Power Sources* **87** (1-2), 28-38.

Fu J, Hou M, Du C, Shao Z, Yi B (2009), 'Potential dependence of sulfur dioxide poisoning and oxidation at the cathode of proton exchange membrane fuel cells', *Journal of Power Sources* **187** (1), 32-38.

Ginosar DM, Petkovic LM, Glenn AW, Burch KC (2007), 'Stability of supported platinum sulfuric acid decomposition catalysts for use in thermochemical water splitting cycles', *International Journal of Hydrogen Energy* **32** (4), 482-488.

Ginosar DM, Rollins HW, Petkovic LM, Burch KC, Rush MJ (2009), 'High-temperature sulfuric acid decomposition over complex metal oxide catalysts', *International Journal of Hydrogen Energy* **34** (9), 4065-4073.

Goldstein S, Borgard J-M, Vitart X (2005), 'Upper bound and best estimate of the efficiency of the iodine sulphur cycle', *International Journal of Hydrogen Energy* **30** (6), 619-626.

Gong M, Liu X, Trembly J, Johnson C (2007), 'Sulfur-tolerant anode materials for solid oxide fuel cell application', *Journal of Power Sources* **168** (2), 289-298.

Gould BD, Baturina OA, Swider-Lyons KE (2009), 'Deactivation of Pt/VC proton exchange membrane fuel cell cathodes by SO2, H2S and COS', *Journal of Power Sources* **188** (1), 89-95.

Grunwaldt J-D, Basini L, Clausen BS (2001), 'In Situ EXAFS Study of Rh/Al2O3 Catalysts for Catalytic Partial Oxidation of Methane', *journal of catalysis* **200** (2), 321-329.

Hadj-Kali MK, Gerbaud V, Lovera P, Baudouin O, Floquet P, Joulia X, Borgard J-M, Carles P (2009), 'Bunsen section thermodynamic model for hydrogen production by the sulfur-iodine cycle', *International Journal of Hydrogen Energy* **34** (16), 6625-6635.

Hagen A, Rasmussen JFB, Thyden K (2011), 'Durability of solid oxide fuel cells using sulfur containing fuels', *Journal of Power Sources* **196** (17), 7271-7276.

Hattori M, Takeda Y, Lee JH, Ohara S, Mukai K, Fukui T, Takahashi S, Sakaki Y, Nakanishi A (2004), 'Effect of annealing on the electrical conductivity of the Y2O3–ZrO2 system', *Journal of Power Sources* **131** (1–2), 247-250.

Hattori M, Takeda Y, Sakaki Y, Nakanishi A, Ohara S, Mukai K, Lee J-H, Fukui T (2004), 'Effect of aging on conductivity of yttria stabilized zirconia', *Journal of Power Sources* **126** (1-2), 23-27.

Hauch A, Ebbesen SD, Jensen SH, Mogensen M (2008), 'Highly efficient high temperature electrolysis', *Journal of Materials Chemistry* **18** (20), 2331-2340.

Hauch A, Jensen SH, Ebbesen SD, Mogensen M Durability of solid oxide electrolysis cells for hydrogen production, Technical University of Denmark.

Hauch A, Mogensen M (2010), 'Ni/YSZ electrode degradation studied by impedance spectroscopy: Effects of gas cleaning and current density', *Solid State Ionics* **181** (15-16), 745-753.

He G, Elder RH, Sinclair DC, Allen RWK (2012), 'High temperature oxygen separation for the sulphur family of thermochemical cycles - Part II: Sulphur poisoning and membrane performance recovery', *International Journal of Hydrogen Energy* **38** (2), 785-794.

He P, Liu M, Luo JL, Sanger AR, Chuang KT (2002), 'Stabilization of platinum anode catalyst in a H2S-O2 solid oxide fuel cell with an intermediate TiO2 layer', *Journal of the Electrochemical Society* **149** (7), A808-A814.

Helmut M (2007), *Diffusion in solids*, Springer, Munster.

Holladay JD, Hu J, King DL, Wang Y (2009), 'An overview of hydrogen production technologies', *Catalysis Today* **139** (4), 244-260.

Huang C, T-Raissi A (2005), 'Analysis of sulfur-iodine thermochemical cycle for solar hydrogen production. Part I: decomposition of sulfuric acid', *Solar Energy* **78** (5), 632-646.

Hwang G-J, Onuki K, Nomura M, Kasahara S, Kim J-W (2003), 'Improvement of the thermochemical water-splitting IS (iodine-sulfur) process by electro-electrodialysis', *Journal of Membrane Science* **220** (1-2), 129-136.

Hwang S-T (2001), 'Inorganic membranes and membrane reactors', *Korean Journal of Chemical Engineering* **18** (6), 775-787.

Ishihara T, Jirathiwathanakul N, Zhong H (2010), 'Intermediate temperature solid oxide electrolysis cell using LaGaO3 based perovskite electrolyte', *Energy & Environmental Science* **3** (5), 665-672.

Ishihara T, Kannou T (2011), 'Intermediate temperature steam electrolysis using LaGaO3-based electrolyte', *Solid State Ionics* **192** (1), 642-644.

Ishikura A, Sakuno S, Komiyama N, Sasatsu H, Masuyama N, Itoh H, Yasumoto K (2007), 'Influence of H2S Poisoning on Anode Layer of SOFC', *ECS Transactions* **7** (1), 845-850.

Ivanov V, Shkerin S, Rempel A, Khrustov V, Lipilin A, A N (2010), 'The grain size effect on the yttria stabilized zirconia grain boundary conductivity', *Journal of Nanoscience and nanotechnology* **10** (11), 5.

Jain IP (2009), 'Hydrogen the fuel for 21st century', *International Journal of Hydrogen Energy* **34** (17), 7368-7378.

Janardhanan VM, Heuveline V, Deutschmann O (2008), 'Three-phase boundary length in solid-oxide fuel cells: A mathematical model', *Journal of Power Sources* **178** (1), 368-372.

Ji P, Feng W, Chen B (2009), 'Comprehensive Simulation of an Intensified Process for H2 Production from Steam Gasification of Biomass', *Industrial & Engineering Chemistry Research* **48** (8), 3909-3920.

Jiang SP, Love JG, Zhang JP, Hoang M, Ramprakash Y, Hughes AE, Badwal SPS (1999), 'The electrochemical performance of LSM/zirconia-yttria interface as a function of a-site non-stoichiometry and cathodic current treatment', *Solid State Ionics* **121** (1-4), 1-10.

Jiang X, Ferrigno R, Mrksich M, Whitesides GM (2003), 'Electrochemical Desorption of Self-Assembled Monolayers Noninvasively Releases Patterned Cells from Geometrical Confinements', *Journal of the American Chemical Society* **125** (9), 2366-2367.

Jing F, Hou M, Shi W, Fu J, Yu H, Ming P, Yi B (2007), 'The effect of ambient contamination on PEMFC performance', *Journal of Power Sources* **166** (1), 172-176.

Johnston B, Mayo MC, Khare A (2005), 'Hydrogen: the energy source for the 21st century', *Technovation* **25** (6), 569-585.

Kane C, Revankar ST (2008), 'Sulfur-iodine thermochemical cycle: HI decomposition flow sheet analysis', *International Journal of Hydrogen Energy* **33** (21), 5996-6005.

Karasawa HAS, Hoshino K (2005). Thermal Decomposition of SO3. <u>Nuclear Production of Hydrogen-Third information Exchange Meeting</u>. Oarai, Japan, OECD Publishing.

Kavurucu Schubert S, Kusnezoff M, Michaelis A, Bredikhin SI (2012), 'Comparison of the performances of single cell solid oxide fuel cell stacks with Ni/8YSZ and Ni/10CGO anodes with H2S containing fuel', *Journal of Power Sources* **217** (0), 364-372.

Kim J, Lin YS (2000), 'Synthesis and oxygen-permeation properties of thin YSZ/Pd composite membranes', *AIChE Journal* **46** (8), 1521-1529.

Kim YB, Hsu C-M, Connor ST, Gur TM, Cui Y, Prinz FB (2010), 'Nanopore Patterned Pt Array Electrodes for Triple Phase Boundary Study in Low Temperature SOFC', *Journal of the Electrochemical Society* **157** (9), B1269-B1274.

Kim YS, No HC, Choi JY, Yoon HJ (2013), 'Stability and kinetics of powder-type and pellet-type iron (III) oxide catalysts for sulfuric acid decomposition in practical Iodine-Sulfur cycle', *International Journal of Hydrogen Energy* **38** (9), 3537-3544.

Kondamudi K, Upadhyayula S (2010), 'Kinetic studies of sulfuric acid decomposition over Al-Fe2O3 catalyst in the sulfur-iodine cycle for hydrogen production', *International Journal of Hydrogen Energy* **In Press, Corrected Proof**

Kubo S, Nakajima H, Kasahara S, Higashi S, Masaki T, Abe H, Onuki K (2004), 'A demonstration study on a closed-cycle hydrogen production by the thermochemical water-splitting iodine-sulfur process', *Nuclear Engineering and Design* **233** (1-3), 347-354.

Laguna-Bercero MA, Skinner SJ, Kilner JA (2009), 'Performance of solid oxide electrolysis cells based on scandia stabilised zirconia', *Journal of Power Sources* **192** (1), 126-131.

Lanchi M, Ceroli A, Liberatore R, Marrelli L, Maschietti M, Spadoni A, Tarquini P (2009), 'S-I thermochemical cycle: A thermodynamic analysis of the HI-H2O-I2 system and design of the HIx decomposition section', *International Journal of Hydrogen Energy* **34** (5), 2121-2132.

Lessing P (2007), 'A review of sealing technologies applicable to solid oxide electrolysis cells', *Journal of Materials Science* **42** (10), 3465-3476.

Leybros J, Carles P, Borgard J-M (2009), 'Countercurrent reactor design and flowsheet for iodine-sulfur thermochemical water splitting process', *International Journal of Hydrogen Energy* **34** (22), 9060-9075.

Li TS, Wang WG (2011), 'The mechanism of H2S poisoning Ni/YSZ electrode studied by impedance spectroscopy', *Electrochemical and Solid-State Letters* **14** (3), B35-B37.

Li TS, Wang WG, Chen T, Miao H, Xu C (2010), 'Hydrogen sulfide poisoning in solid oxide fuel cells under accelerated testing conditions', *Journal of Power Sources* **195** (20), 7025-7032.

Lim T-H, Park J-L, Lee S-B, Park S-J, Song R-H, Shin D-R (2010), 'Fabrication and operation of a 1 kW class anode-supported flat tubular SOFC stack', *International Journal of Hydrogen Energy* **35** (18), 9687-9692.

Lin X, Hass KC, Schneider WF, Trout BL (2002), 'Chemistry of Sulfur Oxides on Transition Metals I: Configurations, Energetics, Orbital Analyses, and Surface Coverage Effects of SO2 on Pt(111)', *The Journal of Physical Chemistry B* **106** (48), 12575-12583.

Lin YS, de Vries KJ, Brinkman HW, Burggraaf AJ (1992), 'Oxygen semipermeable solid oxide membrane composites prepared by electrochemical vapor deposition', *Journal of Membrane Science* **66** (2-3), 211-226.

Liu M, He P, Luo JL, Sanger AR, Chuang KT (2001), 'Performance of a solid oxide fuel cell utilizing hydrogen sulfide as fuel', *Journal of Power Sources* **94** (1), 20-25.

Liu Q, Yang C, Dong X, Chen F (2010), 'Perovskite Sr2Fe1.5Mo0.5O6 as electrode materials for symmetrical solid oxide electrolysis cells', *International Journal of Hydrogen Energy* **35** (19), 10039-10044.

Lussier A, Sofie S, Dvorak J, Idzerda YU (2008), 'Mechanism for SOFC anode degradation from hydrogen sulfide exposure', *International Journal of Hydrogen Energy* **33** (14), 3945-3951.

Marina OA, Pederson LR, Williams MC, Coffey GW, Meinhardt KD, Nguyen CD, Thomsen EC (2007), 'Electrode performance in reversible solid oxide fuel cells', *Journal of the Electrochemical Society* **154** (5), B452-B459.

Matsuzaki Y, Yasuda I (2000), 'The poisoning effect of sulfur-containing impurity gas on a SOFC anode: Part I. Dependence on temperature, time, and impurity concentration', *Solid State Ionics* **132** (3-4), 261-269.

Mawdsley JR, Carter JD, Myers DJ, Lewis MA, Krause TR (2012), 'Sulfur trioxide electrolysis studies: Implications for the sulfur-iodine thermochemical cycle for hydrogen production', *International Journal of Hydrogen Energy* **37** (15), 11004-11011.

Merkle RKW, Pikl R, Verryn SMC, D. DW (1999), 'Raman spectra of synthetic braggite (Pd,Pt,Ni)S', *Mineralogical Magazine* **63** (3), 363-367.

Momirlan M, Veziroglu TN (2002), 'Current status of hydrogen energy', *Renewable and Sustainable Energy Reviews* **6** (1-2), 141-179.

Mosleh M, SÃ¸gaard M, Hendriksen PV (2009), 'Kinetics and mechanisms of oxygen surface exchange on La 0.6Sr0.4FeO3-δ thin films', *Journal of the Electrochemical Society* **156** (4), B441-B457.

Mutoro E, Crumlin E, Biegalski M, Christen H, Leonard D, Borisevich A, Rohnke M, Janek J, Yang SH (2011), Enhancing electrode kinetics of SOFC cathode materials by structural or compositional surface modification, *in* 'ACS National Meeting Book of Abstracts',

Nagahara Y, Sugawara S, Shinohara K (2008), 'The impact of air contaminants on PEMFC performance and durability', *Journal of Power Sources* **182** (2), 422-428.

Nagaraja BM, Jung KD, Ahn BS, Abimanyu H, Yoo KS (2009), 'Catalytic Decomposition of SO3 over Pt/BaSO4 Materials in Sulfur-Iodine Cycle for Hydrogen Production', *Industrial & Engineering Chemistry Research* **48** (3), 1451-1457.

Nguyen QM, Takahashi T (1995), *Scicence and Technology of Ceramic Fuel Cells*, Amsterdam.

O'Brien JE, Stoots CM, Herring JS, Hartvigsen J (2006), 'Hydrogen production performance of a 10-cell planar solid-oxide electrolysis stack', *journal of fuel cell science and technology* **3** (2), 213-219.

Ohya H, Nakajima H, Togami N, Aihara M, Negishi Y (1994), 'Separation of hydrogen from thermochemical processes using zirconia-silica composite membrane', *Journal of Membrane Science* **97** (0), 91-98.

Onuki K, Hwang G-J, Shimizu S (2000), 'Electrodialysis of hydriodic acid in the presence of iodine', *Journal of Membrane Science* **175** (2), 171-179.

Orme CJ, Jones MG, Stewart FF (2005), 'Pervaporation of water from aqueous HI using Nafion-117 membranes for the sulfur-iodine thermochemical water splitting process', *Journal of Membrane Science* **252** (1-2), 245-252.

Orme CJ, Klaehn JR, Stewart FF (2009), 'Membrane separation processes for the benefit of the sulfur-iodine and hybrid sulfur thermochemical cycles', *International Journal of Hydrogen Energy* **34** (9), 4088-4096.

Padro CEG, Putsche V (1999). Survey of the Economics of Hydrogen Technologies. Colorado, National Renewable Energy Laboratory.

Park H, Vecitis CD, Hoffmann MR (2008), 'Electrochemical Anodic Oxidation of Organic Compounds Coupled with the Cathodic Production of Molecular Hydrogen', *Journal of Physical Chemistry* **112** (33), 7616 - 7626.

Ponyavin V, Chen Y, Mohamed T, Trabia M, Hechanova AE, Wilson M (2008), 'Parametric study of sulfuric acid decomposer for hydrogen production', *Progress in Nuclear Energy* **50** (2-6), 427-433.

Poppe J, Schaak A, Janek J, Imblihl R (1998), 'Electrochemically Induced Surface Changes on Microstructured Pt Films on a Solid YSZ Electrolyte', *Berichte der Bunsengesellschaft/Physical Chemistry Chemical Physics* **102** (8), 1019-1022.

Rashkeev SN, Ginosar DM, Petkovic LM, Farrell HH (2009), 'Catalytic activity of supported metal particles for sulfuric acid decomposition reaction', *Catalysis Today* **139** (4), 291-298.

Rasmussen JFB, Hagen A (2009), 'The effect of H2S on the performance of Ni-YSZ anodes in solid oxide fuel cells', *Journal of Power Sources* **191** (2), 534-541.

Ratafia-Brown J, Manfredo L, Hoffmann J, Ramezan M (2002). Major Environmental Aspects of Gasification-Based Power GenGeneration Technologies.

Sakurai M, Nakajima H, Amir R, Onuki K, Shimizu S (2000), 'Experimental study on side-reaction occurrence condition in the iodine - sulfur thermochemical hydrogen production process', *International Journal of Hydrogen Energy* **25** (7), 613-619.

Sasaki K, Maier J (2003), 'Chemical surface exchange of oxygen on Y2O3-stabilized ZrO2', *Solid State Ionics* **161** (1-2), 145-154.

Schneider LCR, Martin CL, Bultel Y, Bouvard D, Siebert E (2006), 'Discrete modelling of the electrochemical performance of SOFC electrodes', *Electrochimica Acta* **52** (1), 314-324.

Schwartz D, Gadiou R, Brilhac J-F, Prado G, Martinez G (2000), 'A Kinetic Study of the Decomposition of Spent Sulfuric Acids at High Temperature', *Industrial & Engineering Chemistry Research* **39** (7), 2183-2189.

Shi H, Yang G, Liu Z, Zhang G, Ran R, Shao Z, Zhou W, Jin W (2012), 'High performance tubular solid oxide fuel cells with BSCF cathode', *International Journal of Hydrogen Energy* **37** (17), 13022-13029.

Sims REH, Schock RN (2007). Energy supply. Cambridge.

Stambouli AB, Traversa E (2002), 'Solid oxide fuel cells (SOFCs): a review of an environmentally clean and efficient source of energy', *Renewable and Sustainable Energy Reviews* **6** (5), 433-455.

Stewart FF, Orme CJ, Jones MG (2007), 'Membrane processes for the sulfur-iodine thermochemical cycle', *International Journal of Hydrogen Energy* **32** (4), 457-462.

Stiegel GJ, Ramezan M (2006), 'Hydrogen from coal gasification: An economical pathway to a sustainable energy future', *International Journal of Coal Geology* **65** (3-4), 173-190.

Stojic DL, Marceta MP, Sovilj SP, Miljanic SS (2003), 'Hydrogen generation from water electrolysis--possibilities of energy saving', *Journal of Power Sources* **118** (1-2), 315-319.

Stortelder JK (2005), 'Ionic Conductivity in Yttria-Stabilized Zirconia Thin Films grown by Pulsed Laser Deposition',

Streber R, Papp C, Lorenz MPA, Hoìˆfert O, Zhao W, Wickert S, Darlatt E, Bayer A, Denecke R, Steinruìˆck HP (2010), 'Influence of Steps on the Adsorption and Thermal Evolution of SO2 on Clean and Oxygen Precovered Pt Surfaces', *The Journal of Physical Chemistry C* **114** (46), 19734-19743.

Suárez-González MA, Blanco-Marigorta AM, Peña-Quintana JA (2011). Review on hydrogen production technologies from solar energy. International

Conference on Renewable Energies and Power Quality. Las Palmas de Gran Canaria.

Sun C, Hui R, Roller J (2010), 'Cathode materials for solid oxide fuel cells: a review', *Journal of Solid State Electrochemistry* **14** (7), 1125-1144.

Tanaka N, Yamaki T, Asano M, Maekawa Y, Onuki K (2010), 'Electro-electrodialysis of HI-I2-H2O mixture using radiation-grafted polymer electrolyte membranes', *Journal of Membrane Science* **346** (1), 136-142.

Tanksale A, Beltramini JN, Lu GM (2010), 'A review of catalytic hydrogen production processes from biomass', *Renewable and Sustainable Energy Reviews* **14** (1), 166-182.

Toghan A, Rösken LM, Imbihl R (2010), 'The electrochemical promotion of ethylene oxidation at a pt/YSZ catalyst', *ChemPhysChem* **11** (7), 1452-1459.

Tosti S, Borelli R, Borgognoni F, Favuzza P, Rizzello C, Tarquini P (2008), 'Study of a dense metal membrane reactor for hydrogen separation from hydroiodic acid decomposition', *International Journal of Hydrogen Energy* **33** (19), 5106-5114.

Trembly JP, Marquez AI, Ohrn TR, Bayless DJ (2006), 'Effects of coal syngas and H2S on the performance of solid oxide fuel cells: Single-cell tests', *Journal of Power Sources* **158** (1), 263-273.

Tsaofang C, Walsh KJ, Fedkiw PS (1991), 'Cyclic voltammetric study of the electrochemical formation of platinum oxide in a Pt/yttria-stabilized zirconia cell', *Solid State Ionics* **47** (3-4), 277-285.

Uchida H, Osada N, Watanabe M (2004), 'High-performance electrode for steam electrolysis: Mixed conducting ceria-based cathode with highly-dispersed Ni electrocatalysts', *Electrochemical and Solid-State Letters* **7** (12), A500-A502.

Ulrich Vogt E, Francois le N, Pierre B, Sune D E IEA/HIA TASK 25: high temperature hydrogen production process. high temperature electrolysis.

Utgikar V, Thiesen T (2006), 'Life cycle assessment of high temperature electrolysis for hydrogen production via nuclear energy', *International Journal of Hydrogen Energy* **31** (7), 939-944.

Verkerk MJ, Middelhuis BJ, Burggraaf AJ (1982), 'Effect of grain boundaries on the conductivity of high-purity ZrO_2-$Y2O_3$ ceramics', *Solid State Ionics* **6** (2), 159-170.

Vernon PDF, Green MLH, Cheetham AK, Ashcroft AT (1990), 'Partial oxidation of methane to synthesis gas', *Catalysis Letters* **6** (2), 181-186.

Veziroglu TN, Barbir F (1992), 'Hydrogen: the wonder fuel', *International Journal of Hydrogen Energy* **17** (6), 391-404.

Veziroglu TN, Sahin S (2008), '21st Century's energy: Hydrogen energy system', *Energy Conversion and Management* **49** (7), 1820-1831.

Vitart X, Carles P, Anzieu P (2008), 'A general survey of the potential and the main issues associated with the sulfur-iodine thermochemical cycle for hydrogen production using nuclear heat', *Progress in Nuclear Energy* **50** (2-6), 402-410.

Vitart X, Le Duigou A, Carles P (2006), 'Hydrogen production using the sulfur-iodine cycle coupled to a VHTR: An overview', *Energy Conversion and Management* **47** (17), 2740-2747.

von Wolfersdorff WDB, Bremen J, Hartmann H (1983), 'The separation of sulfur dioxide and oxygen by absorption', *International Journal of Hydrogen Energy* **8** (2), 97-107.

Wang W, Huang Y, Jung S, Vohs JM, Gorte RJ (2006), 'A comparison of LSM, LSF, and LSCo for solid oxide electrolyzer anodes', *Journal of the Electrochemical Society* **153** (11), A2066-A2070.

West, A. R. (1999), *Basic Solid State Chemistry*, 2nd edn, Wiley.

Wilson JR, Kobsiriphat W, Mendoza R, Chen HY, Hiller JM, Miller DJ, Thornton K, Voorhees PW, Adler SB, Barnett SA (2006), 'Three-dimensional reconstruction of a solid-oxide fuel-cell anode', *Nature Materials* **5** (7), 541-544.

Xin G (1997), 'Effect of DC voltage on the microstructure and electrical properties of stabilized-zirconia', *Solid State Ionics* **99** (1-2), 143-151.

Y. Y. Yao FLH, C. G. Chen, C. J. Chai (1999), *Principle of Chemical Engineering*, Tianjin University, Tianjin.

Yang X, Irvine JTS (2008), '(La0.75Sr0.25)0.95Mn0.5Cr0.5O3 as the cathode of solid oxide electrolysis cells for high temperature hydrogen production from steam', *Journal of Materials Chemistry* **18** (20), 2349-2354.

Yilmaz A, Hindiyarti L, Jensen AD, Glarborg P, Marshall P (2006), 'Thermal Dissociation of SO3 at 1000K-1400 K', *The Journal of Physical Chemistry A* **110** (21), 6654-6659.

Yongning Y (2006), *Material Science and Engineering*, Advanced Education Press, Beijing.

Yoon SP, Nam SW, Kim S-G, Hong S-A, Hyun S-H (2003), 'Characteristics of cathodic polarization at Pt/YSZ interface without the effect of electrode microstructure', *Journal of Power Sources* **115** (1), 27-34.

Zha S, Cheng Z, Liu M (2007), 'Sulfur Poisoning and Regeneration of Ni-Based Anodes in Solid Oxide Fuel Cells', *Journal of the Electrochemical Society* **154** (2), B201-B206.

Zhai Y, Bender G, Dorn S, Rocheleau R (2010), 'The Multiprocess Degradation of PEMFC Performance Due to Sulfur Dioxide Contamination and Its Recovery', *Journal of the Electrochemical Society* **157** (1), b20-b26.

Zhang C, Li C-J, Zhang G, Ning X-J, Li C-X, Liao H, Coddet C (2007), 'Ionic conductivity and its temperature dependence of atmospheric plasma-sprayed yttria stabilized zirconia electrolyte', *Materials Science and Engineering: B* **137** (1-3), 24-30.

Zhang P, Su T, Chen QH, Wang LJ, Chen SZ, Xu JM (2011), 'Catalytic decomposition of sulfuric acid on composite oxides and Pt/SiC', *International Journal of Hydrogen Energy* **In Press, Corrected Proof**

Zhu B, Albinsson I, Andersson C, Borsand K, Nilsson M, Mellander B-E (2006), 'Electrolysis studies based on ceria-based composites', *Electrochemistry Communications* **8** (3), 495-498.

Zhu WZ, Deevi SC (2003), 'A review on the status of anode materials for solid oxide fuel cells', *Materials Science and Engineering: A* **362** (1-2), 228-239.

Zuttel A, Remhof A, Borgschulte A, Friedrichs O (2010), 'Hydrogen: the future energy carrier', *Philosophical Transactions of the Royal Society A: Mathematical, Physical and Engineering Sciences* **368** (1923), 3329-3342.

Appendix A

Heating conclusion of pre-heating quartz tube

For pre-heating tubing of 3 mm outside diameter, the area for heat transfer (A) is

$$A = 2\pi R \times L = 3 \times 3.14 \times 88 \times 3 = 2486.88 mm^2 = 2.49 \times 10^{-3} m^2$$

The overall heat transfer coefficient (U_0) is defined by summing the individual resistances involved in the heat transfer then finding the inverse.

$$\frac{1}{U_0} = \frac{1}{h_0} + \frac{x d_0}{k_{quartz} d_w} + \frac{d_0}{h_i d_i}$$

Where h_0 and h_i are the outside and inside heat convection coefficients respectively, d_o and d_i are the outside and inside wall diameter, d_w is the average wall diameter and k_{quartz} is the thermal conductivity of quartz. The convection coefficients used are the approximate values given for heat transfer to/ from gas with no phase change by Coulson et al. (1999).

Therefore,

$$\frac{1}{U_o} = \frac{1}{20} + \frac{0.001 \times 0.003}{1.3 \times 0.002} + \frac{0.003}{20 \times 0.001} = 0.2012$$

$$U_o = 4.971 \text{ W/m}^2\text{K}$$

The log mean temperature difference (T_m) is calculated as 234.0°C based on approach temperature of 850°C at the inlet end and 25°C at the inlet of the tubing.

$$T_m = \frac{T_A - T_B}{\ln \frac{T_A}{T_B}} = \frac{850 - 25}{\ln \frac{850}{25}} = 234.0 \,^{\circ}C$$

If we were to consider the tube furnace to be non-radiative, the required heat duty for quartz tube can be expressed as:

$$Q1 = U_o \, A \, T_m = 4.971 \text{ x } 2.49 \text{ x } 10^{-3} \text{ x } 294.1 = 2.90 \text{ W}$$

When SO_2 heating was taken as the basis for the calculation as it has the largest

specific heat capacity of gases to be used, a flow rate of 50ml/min at 25°C and 101325Pa) equates to a molar flow rate of 3.406 x 10^{-5} mol/s.

From the graph of gas heat capacity and temperature at 101.33kPa, heat capacity for SO_2 is 44.8 J/(mol K) at 25°C and 55.68 J/(mol K) at 850°C [Figure A1] [Table A1]. The higher value will be used for this calculation.

The required heat duty Q2 for a 850°C temperature rise is:

$$Q2 = mC_p \Delta T = 3.718 \times 10^{-5} \times 55.68 \times 850 = 1.76W$$

The furnace used in this work has a thermal power rating of 1000W, therefore it is not envisaged that there should be any difficulty in maintained the required temperature.

Because,   Q1 > Q2

Then, the pre-heating quartz tubing of 3mm outside diameter, 264mm length should ensure the gas is at the correct temperature before contacting the membrane tube.
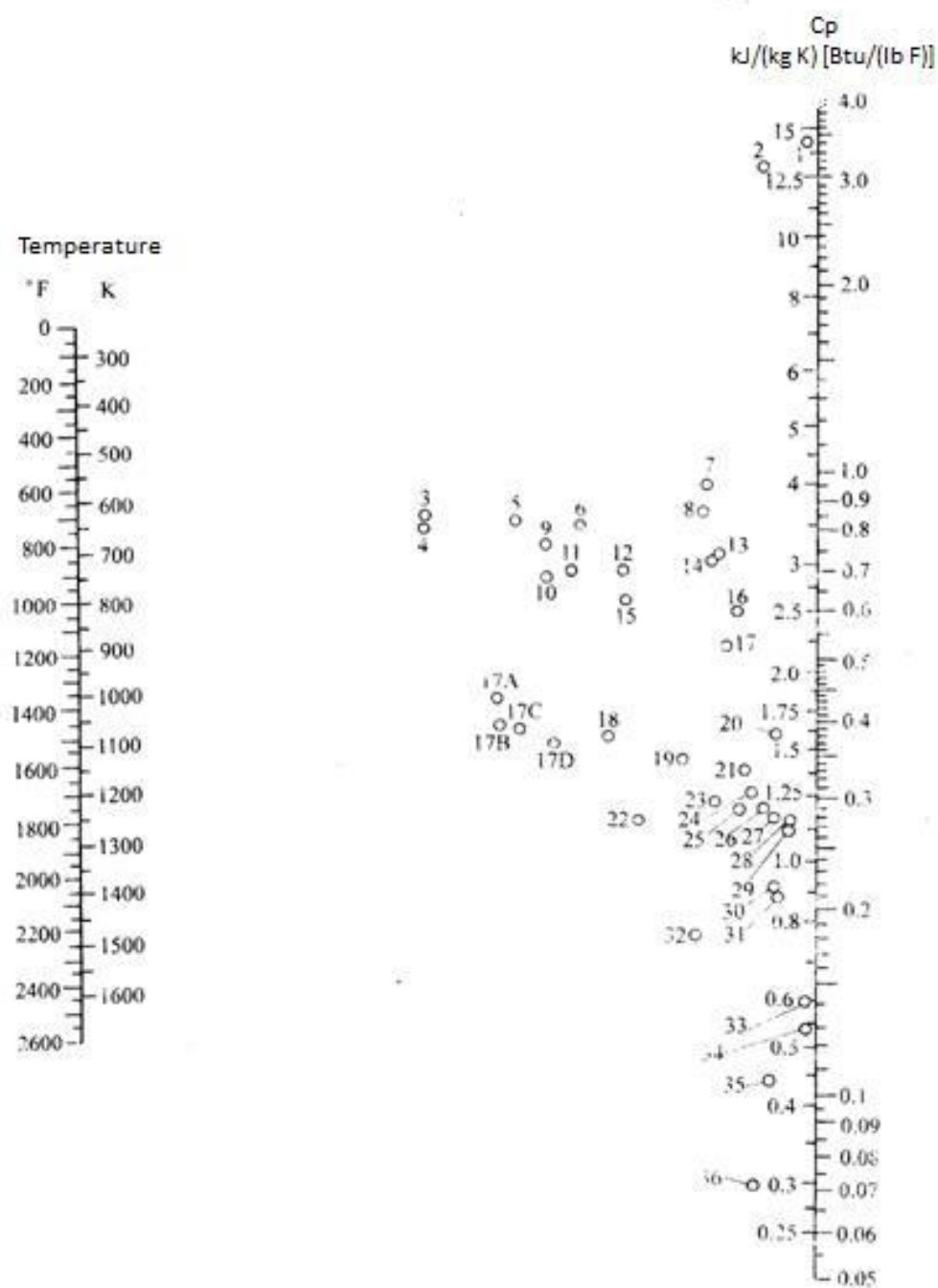
Figure A.1: *Specific heat capacity (Cp) of gases at 101.33kPa (Y. Y. Yao 1999)*

Number	gas	Temperature range, K
10	Acetylene	273 - 473
15	Acetylene	473 - 673
16	Acetylene	673 - 1673
27	Air	273 - 1673
12	Ammonia	273 - 873
14	Ammonia	873 - 1673
18	Carbon dioxide	273 - 673
24	Carbon dioxide	673 - 1673
26	Carbon monoxide	273 - 1673
32	Chlorine	273 - 473
34	Chlorine	473 - 1673
3	Ethane	273 - 473
9	Ethane	473 - 873
8	Ethane	873 - 1673
4	Ethylene	273 - 473
11	Ethylene	473 - 873
13	Ethylene	873 - 1673
17B	Freon-11	273 - 423
17C	Freon-21	273 - 423
17A	Freon-22	278 - 423
17D	Freon-113	273 - 423
1	Hydrogen	273 - 873
2	Hydrogen	873 - 1673
35	Hydrogen bromide	273 - 1673
30	Hydrogen chloride	273 - 1673
20	Hydrogen fluoride	273 - 1673
36	Hydrogen iodide	273 - 1673
19	Hydrogen sulfide	273 - 973
21	Hydrogen sulfide	973 - 1673
5	Methane	273 - 573
6	Methane	573 - 973
7	Methane	973 - 1673
25	Nitric oxide	273 - 973
28	Nitric oxide	973 - 1673
26	Nitrogen	273 - 1673
23	Oxygen	273 - 773
29	Oxygen	773 - 1673
33	Sulfur	573 - 1673
22	Sulfur dioxide	273 - 673
31	Sulfur dioxide	673 - 1673
17	Water	273 - 1673

Table A.1: *The gas number and temperature range (Y. Y. Yao 1999)*

Publications

He G, Elder RH, Sinclair DC, Allen RWK (2012), 'High temperature oxygen separation for the sulphur family of thermochemical cycles - Part II: Sulphur poisoning and membrane performance recovery', *International Journal of Hydrogen Energy* **38** (2), 785-794.

He G, Elder RH, Cumming DJ, Allen RWK (2013), 'Voltage pulsing for performance recovery of yttria-stabilised zirconia oxygen/sulphur dioxide separation membranes' *International Journal of Hydrogen Energy (to be submitted)*

Conference presentations

He G, Elder RH, Allen RWK (2011), 'Performance degradation of Pt/8YSZmembrane in the separation process of He-O_2-SO_2 at high temperature' *in* UK-China Forum 2011: New energy and low carbon economy, University College London, UK

He G (2012), 30 months PhD presentation, Department of Chemical and Biological Engineering, The University of Sheffield, UK

Elder RH, He G, Cumming DJ, Allen RWK (2013), 'Separation of SO_2 and O_2 in thermochemical hydrogen production' *in* AICHE Annual Meeting, San Francisco, USA